Dissertation zur Erlangung des Doktorgrades
der Fakultät für Biologie
der Ludwig-Maximilians-Universität München

Molecular correlates of trait anxiety: expanding biomarker discovery from protein expression to turnover

Yaoyang Zhang

from

Henan, PR China

July, 2010

Erstgutachter: Prof. Dr. Rainer Landgraf

Zweitgutachter: Prof. Dr. Gisela Grupe

Tag der mündlichen Prüfung: 02.12.2010

Contents

1 Abstract

Depression and anxiety disorders affect a great number of people in the world. Although remarkable efforts have been devoted to understanding the clinical and biological basis of these disorders, progress has been relatively slow. Furthermore, no laboratory test currently is available for diagnosis of anxiety and depression. These disorders are mainly diagnosed empirically on the basis of a doctor's personal observations and experiences. Hence, discovery of biomarkers for these psychiatric disorders deserves much scientific attention.

The animal models investigated in the present study represent high, low, and normal anxiety-like phenotypes (HAB, LAB, NAB) and were established by selective inbreeding. To compare the protein expression levels between different animal lines, living animals were metabolically labeled with the ^{15}N stable isotope and then investigated by quantitative mass spectrometry. In addition, metabolomic studies were performed to shed light on pathways affected in the trait anxiety mouse model. A number of proteins and metabolites were found to be significantly altered in their expression levels between the three mouse lines. Both protein and metabolite information was used for *in silico* network analysis to find pathways pertinent to the pathobiology of anxiety disorders.

Another focus of this thesis was the development of new methodologies for the metabolic labeling approach. This includes improved identification of labeled proteins and the analysis of protein turnover. The latter represents another important aspect in the field of proteomics and adds a dynamic dimension to the field. The method allows the detection of protein expression alterations at a much earlier stage. The newly developed *ProTurnyer* (Protein Turnover Analyzer) algorithm is able to calculate in a high throughput manner turnover for individual proteins.

2 Introduction

2.1 Anxiety and depression

2.1.1 Anxiety and depressive disorders

Up to 20% of the world's population suffers from depression or anxiety disorders (Kessler et al., 1994). According to data published by the World Health Organization (WHO), currently depressive disorders are the fourth leading cause of disability in the world and are likely to rise to the second position by 2020. The symptoms of depression and anxiety, such as sadness, hopelessness, feeling of being worthless, diminished interest, anxiety, worry, fear etc., exist in almost everyone's daily life, but in people without mental illness these feelings usually appear to be reasonable and disappear within a couple of hours or days. However, these symptoms are much more persistent and excessive in a person with depression or anxiety or both. Thus, these disorders can interfere severely with patients' lives, the lives of their families, and society in general.

Although remarkable efforts have been devoted to understanding the clinical and biological basis of depression and anxiety, progress has been relatively slow. Epidemiologic studies have demonstrated that heredity factors can contribute roughly 40%-50% to the risk for depression (Fava and Kendler, 2000). In twin studies, 15%-20% heritability was observed for anxiety disorders (Hettema et al., 2001). One promising hypothesis of depression is based on dysregulation of the hypothalamic-pituitary-adrenal (HPA) axis and the relevant components, such as corticotrophin-releasing factor (CRF), adrenocorticotropin (ACTH) and glucocorticoid. Hyperactivity of the HPA axis is observed in approximately half of depressed individuals. A number of factors have been studied and found to be highly relevant for anxiety. For instance, inactivation of the gamma-amino butyric acid (GABA) synthesis enzyme or its receptors resulted in increased anxiety-like behavior (Kash et al., 1999; Low et al., 2000). Similarly, inactivation of the 5-HT1A receptor also increased anxiety-like behavior in mice (Heisler et al., 1998; Parks et al., 1998; Ramboz et al., 1998). In addition, monoamine oxidase A (MAO-A) (Cases et al., 1995), and CRF and its receptors (Bale et al., 2002; Smith et al., 1998a) have been found to regulate anxiety.

Comorbidity is a quite common occurrence in psychiatric disorders. Data have shown that during one year, almost 50% of psychiatric patients have two or more syndromes (Kessler

et al., 2005). Therefore, it is not surprising that depression and anxiety frequently co-occur (Devane et al., 2005; Moffitt et al., 2007; Regier et al., 1998), although they represent distinct phenotypes. The comorbidity between anxiety and depression disorders is as high as 50%-60% (Kaufman and Charney, 2000; Landgraf, 2001). The genetic correlation between major depression and generalized anxiety has been investigated in twin studies (Kendler et al., 2007): correlation scores of 1 and 0.74 were observed in women and men, respectively.

Currently, no laboratory test is available for diagnosis of anxiety and depression. These disorders are mainly diagnosed empirically on the basis of a doctor's personal observations and experiences. The patients' reported symptoms, behavior, way of speaking, and family medical history can all help make the correct diagnosis. The diagnostic criteria also are summarized in the Diagnostic and Statistical Manual of Mental Disorders (DSM-IV-TR), a commonly used classification system. Despite our limited knowledge of anxiety and depression, medication, electroconvulsive seizures (ECS), and psychotherapy are normally effective treatments. Eighty percent of patients with depression benefit from clinical treatment (Holsboer, 2001; Nestler et al., 2002).

2.1.2 Anxiety mouse model

Emotions, cognitions, environmental experience, and individual genetic background vary enormously in human psychiatric disorders, such as anxiety (Blanchard et al., 2001; Gordon and Hen, 2004). To facilitate the study of anxiety, animal models have been introduced to model particular aspects of anxiety-like behavior. There are several advantages to using animals instead of human patients. First, the anxiety-like behavior of the animal models can be very stable. Second, both the genetic and environmental background of the animals can be well controlled via an inbreeding approach and conditioned feeding. Moreover, there is no theoretical limitation to the type and number of specimens, since the animals can be easily bred. In contrast, clinical specimens from patients are always heterogeneous, more difficult to obtain, and limited to body fluids. Despite the above attractive features, the animal phenotype will never be expected fully to mirror the corresponding human phenotype, since it is impossible to know the real emotional status of an animal.

Animal models mainly are established by genetic means or selective breeding. Transgenic mouse models—which may have a gene and its product overexpressed, underexpressed,

lost or wrongly synthesized by adding, deleting, silencing, or mutating a gene—have been created for many neurotransmitters, receptors, messengers, and transporters (Gross et al., 2002; Heisler et al., 1998; Kash et al., 1999). Selective breeding is the process of breeding animals to obtain particular behavioral and genetic traits. Animals with a homogeneous appearance, behavior, and other characteristics are mated and inbred to obtain offspring with a stable phenotype. The characteristic behavior can be maintained steadily after selective breeding for several generations. The behavioral phenotype is the outcome of the integration of all the factors ongoing in both internal and external environments. A single gene change normally does not result in disease occurrence. In this regard, an animal model established on the basis of behavioral selection can be more applicable to simulating the same phenotype in humans.

Behavioral tests normally are used to evaluate the phenotype. The anxiety-like behavioral tests for mice include the elevated plus maze (EPM) (Cook et al., 2001; Handley and Mithani, 1984; Lister, 1987; Pellow et al., 1985) (**Figure 1**), light-dark transitions test (Crawley and Goodwin, 1980), marble burying (Broekkamp et al., 1986; Jacobson et al., 2007), and shock-probe burying (Gasparotto et al., 2007; Sluyter et al., 1996). The tail suspension test (TST) and forced swim test (FST) (Crowley et al., 2005; Cryan et al., 2005; Porsolt et al., 1978; Steru et al., 1985) are the two main tests used to assess depression-like behavior. The EPM test is essential in our animal model development and will be the main focus of the discussion below. EPM has been established on the basis of the fact that anxiety patients avoid exposing themselves to threatening situations and places. In the EPM, the mouse has the opportunity to choose freely between highly elevated, unguarded open arms and unchallenged enclosed arms; the high anxiety level mouse will avoid entering an open arm (**Figure 1**).
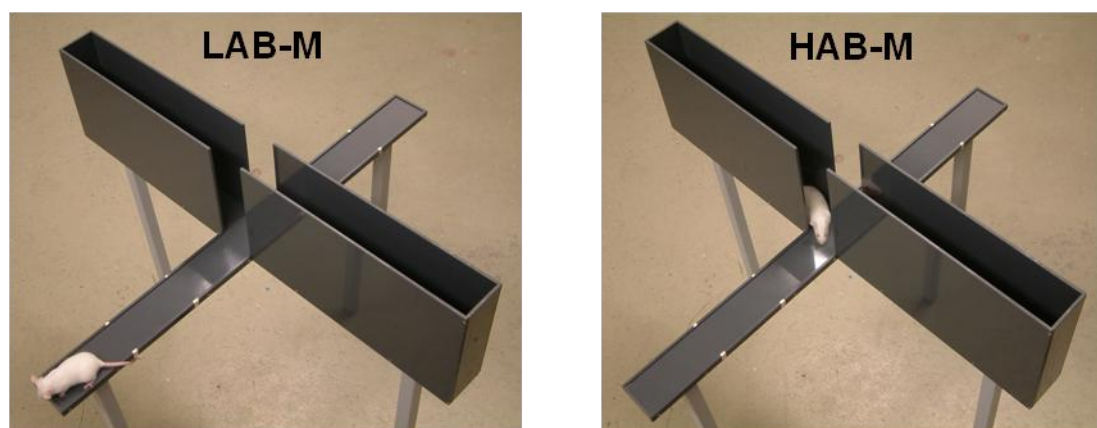
Figure 1. Elevated plus maze set up. Unlike non-anxious LAB-M mice, which explore the aversive open arms of the EPM, the anxious HAB-M mice spend most of the test time in the dimly lit closed arms.

On the basis of EPM behavior, both rats and mice were bred selectively to obtain different animal models with high/low/normal anxiety-related behavior (HAB/LAB/NAB) (Kessler et al., 2007; Kromer et al., 2005; Landgraf et al., 2007; Landgraf and Wigger, 2002; Liebsch et al., 1998a; Liebsch et al., 1998b)(**Figure 1**). HAB mice commonly spend ~10% of time or even less on an open arm; by contrast, LAB mice spend more than 50% of time on an open arm. NAB mice spend ~30% of time on an open arm, which is close to the mean value of outbred mice. These mouse lines have maintained their featured behavior for more than 50 generations. Besides EPM, these animal models were verified by some other anxiety-related and depression-related tests, including the dark-light avoidance test, open-arm exposure test, ultrasound vocalization test, TST and FST (Kromer et al., 2005). The HAB mice also showed a higher passive level of activity in desperate situations during TST and FST.

2.2 Proteomics

Genomics has been used to elucidate the complete sequence of genomes for a number of species (Lander et al., 2001; Venter et al., 2001). Although the whole human genome—with less than 20,325 annotated protein-coding genes—has been fully identified, the function of probably 100,000 of human proteins (Gstaiger and Aebersold, 2009) encoded by those genes remains elusive. Genomic studies are inadequate mainly because: 1) the level of transcription of a gene does not always reflect its level of protein expression; 2) protein post-translational modifications (PTM) play an important role in protein function and activity, but this aspect is undetectable in genomics; 3) a given transcription

can affect more than one protein by altering splicing or PTM or both; and 4) many proteins have bioactivity only when they co-exist with other proteins or RNA molecules.

The study of proteins can complement genomic research because proteins are the bio-functional molecular parts in living organisms, i.e. the actual main components that take part in the physiological mechanisms of biological processes. Moreover, proteins can interact with any other molecular compounds. The word proteome initially came from merging "protein" and "genome" and was created by Wilkins in 1994 (Wilkins et al., 1996). The proteome can be defined as the entire set of proteins expressed by a genome in any organism. The organism can be a cell, tissue, or even whole living body. The term "proteomics" was coined soon after "proteome", in 1997 (James, 1997), in analogy with genomics. Therefore, proteomics can be described as a post-genomic science. Proteomics characterizes the identification and quantification of proteome(s), including protein expression, protein subcellular distribution, protein interaction, protein post-translational modifications, and protein turnover.

2.2.1 Mass spectrometry

2.2.1.1   What is mass spectrometry?

Mass spectrometry (MS) is an analytical approach that measures the mass-to-charge (m/z) ratios of charged compounds. The determined m/z of charged ions or their fragments can be used to interpret the elemental composition of molecules, even the chemical structures. John B Fenn, who received the Nobel Laureate in Chemistry for inventing electrospray ionization, described mass spectrometry as follows: "*Mass spectrometry is the art of measuring atoms and molecules to determine their molecular weight. Such mass or weight information is sometimes sufficient, frequently necessary, and always useful in determining the identity of a species. To practice this art one puts charge on the molecules of interest, i.e., the analyte, then measures how the trajectories of the resulting ions respond in vacuum to various combinations of electric and magnetic fields.*" (Siuzdak, 2006)

A typical mass spectrometer consists of three modules: an ionization source, a mass analyzer, and a detector (**Figure 2**). The ionization source is the mechanical device that allows ionization to occur. This can be achieved by either addition or loss of electrons, protons, cations, anions, and even charged molecules. A mass analyzer measures the ion behaviors in an electric or magnetic field. The ions are separated based on their m/z. The
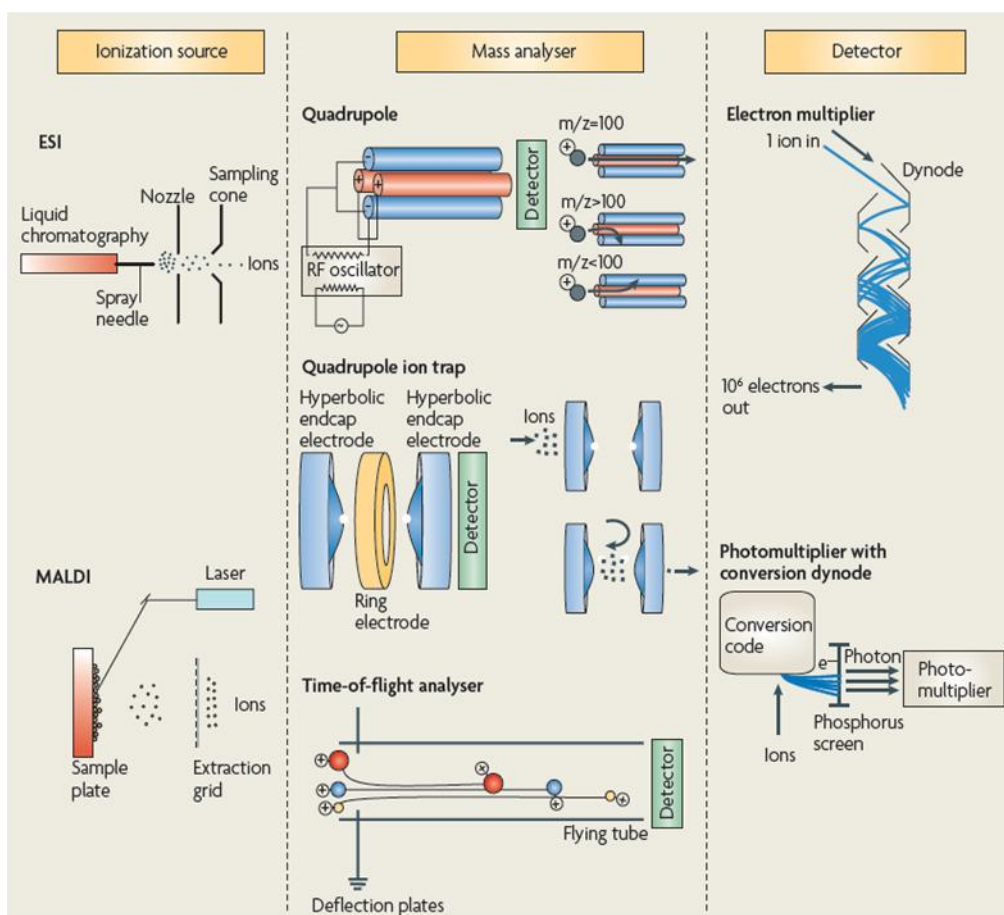
Figure 2. Schematic representation of a mass spectrometer and its constituents. The mass spectrometer has three main modules: an ionization source, a mass analyzer, and a detector. (reproduced with permission from (Bayes and Grant, 2009))

detector records the electric signal of either the charge induced or the current produced when an ion passes by or hits a surface. The value reflects the abundances of each ion present.

Before the development of Matrix-assisted laser desorption/ionization (MALDI) and electrospray ionization (ESI), MS was incapable of measuring large biomolecules whose molecular weights exceeded the limitation of the electron ionization (EI) source. The concept of electrospray was initially described by Dole et al. at the end of the 1960s (Dole et al., 1968). Twenty years later, the well-known breakthrough of ESI occurred when John Fenn of Yale University claimed to have identified polypeptides and proteins with a molecular weight of 130,000 kDa (Fenn et al., 1989). The ESI disperses the liquid containing the analytes of interest into a fine aerosol, which is transferrable to and measureable in a normal MS set-up. The first innovation for application of the laser desorption method to large biomolecules, in which the proteins with m/z up to 100,000

were successfully ionized and detected by mass spectrometry, was reported by Koichi Tanaka in 1988 (Tanaka et al., 1988). MALDI is triggered by a laser beam. The matrix, which consists of crystallized molecules, is used to protect the analytes from being destroyed by the direct laser beam and to facilitate vaporization and ionization.

2.2.1.2   Orbitrap mass analyzer

The ion trap is a robust mass analyzer because of its fast scan rates, MSn ability, easy maintenance, reasonable resolution, sensitivity, and mass accuracy. However, the sensitivity and mass accuracy of the traditional ion trap are relatively low, making it difficult to identify and quantify peptides accurately (Mann and Kelleher, 2008). The Orbitrap mass analyzer initially was developed by Makarov (Makarov, 2000; Makarov et al., 2006a) to overcome these drawbacks. The Orbitrap is a robust instrument with high resolution (150,000 full width at the half height [FWHH]), high mass accuracy (2–5 ppm), a dynamic range (greater than 10^3), an m/z range over 6,000, and high sensitivity (Hu et al., 2005; Makarov et al., 2006b). It is innately capable of very high mass accuracy because the m/z of the ion is the only element affecting the ion axial motion along the central spindle, and there is no impairment by the initial injection condition.

2.2.1.3   Nano HPLC and ESI

High performance liquid chromatography (HPLC) and MS are two important analytical tools in proteomics. Proteomic analytes often are present in biological samples at very low concentrations. To separate and ionize these complex compounds effectively, nano HPLC and nano ESI—in which the HPLC column and ESI emitter are at the micro-/nano-meter level—are frequently employed (Emmett and Caprioli, 1994; Griffina et al., 1991). The internal diameter (ID) of an HPLC column is a critical parameter that influences the detection sensitivity and separation selectivity during chromatographic elution. A smaller ID of the HPLC column can result in a higher sensitivity. Theoretically, the column sensitivity is inversely proportional to the square of the ID of the HPLC column. This means that a change in column ID from a conventional 4.6 mm ID column to a 75 μm column would result in a theoretical sensitivity gain of more than 3,700 fold. Besides the extraordinary sensitivity, nano HPLC is chosen for proteomics studies because of the column loading capacity. The great complexity and extreme dynamic range of biological samples usually make it difficult to purify or enrich the target proteins. Therefore, the quantity of individual analytes is normally very small. The nano HPLC is able to work with minute sample sizes; moreover, nano HPLC—especially the splitless nano HPLC system—is

reasonably priced in terms of consumption of mobile phases. The nano ESI was introduced by Wilm and Mann in 1996 to couple nano HPLC with ESI MS (Wilm and Mann, 1996). The nano ESI emitter is made by pulling laser-heated fused silica into a very fine taper filament, whose orifice is only several microns across. A verified theoretical model predicts a proportionality between the two-thirds power of the flow rate and the size of droplets emitted from the tip of a stable Taylor cone (Wilm and Mann, 1994). A smaller droplet has a higher surface/volume ratio, which makes a larger proportion of analyte molecules available for desorption.

2.2.2 Protein identification by mass spectrometry

MS has become the central technology in proteomics today. To identify a peptide and protein, the mass spectrometer collects both MS and MSn for peptide/protein precursor ions and their fragments. There are three main approaches to identifying peptides through MS data: *de novo* sequencing, spectrum library search, and peptide database search. *De novo* sequencing is the only method that can identify previously unknown peptides or peptides that go against the parameter setting in the search engine. Spectrum library search (Frewen et al., 2006) was developed recently and is based on the establishment of an MS2 spectrum database. Previously identified MS2 data were collected into a reference spectrum library that is used to identify new spectra. With this approach, peptide identification seems to be reliable and faster.

Peptide database search is the most widely used technique in protein identification. For a bottom-up proteomic strategy, the MS actually measures the enzymatic digests, but not intact proteins. Two types of mass spectra are typically obtained: MS spectra containing peptides digested from proteins and MS2 spectra that contain fragments of those peptide precursors. Application of the MS peptide mass fingerprinting (PMF) approach typically requires relatively pure proteins, such as those obtained from two-dimensional gel electrophoresis (2-DE). Thus, proteins can be identified by mapping the peaks in the MS to those of theoretical proteolytic peptides. MS2 is composed of the fragments of a particular precursor peptide, whose m/z is already determined in MS. Ideally, the fragmented ions form a ladder in which each successive fragment contains one additional residue, thus allowing the sequence to be interpreted from the mass shift between the peaks. MS2 can provide information on both the amino acid sequence and the mass of the precursor peptide, resulting in very high confidence identification. Therefore, MS2 is the most preferred technique for peptide identification in current proteomic studies.

Moreover, more than one approach can be employed simultaneously. For example, peptide sequence tag identification (Mann and Wilm, 1994; Mortz et al., 1996) combines *de novo* sequencing and peptide database search.

Since MS2 peptide database search is the most commonly used method, and also the only one performed in the studies presented in this paper, the following description of identification algorithms will cover only this workflow. Several peptide database search engines have been developed to identify peptides in a high throughput manner, such as Mascot (Perkins et al., 1999), SEQUEST (Eng et al., 1994), and X!Tandem (Craig and Beavis, 2004). The overall designs of the different identification algorithms are similar; they all attempt to match experimental spectra with theoretical spectra generated from the sequences in a protein database. Before submitting the data to the search engine, several parameters must be defined, including database, mass accuracy, modification, etc. The algorithm usually has a particular built-in approach to evaluate the match between experimental and theoretical spectra. Users normally can optimize the output on the basis of different filtering thresholds. False discovery rate (FDR) (Balgley et al., 2007; Cargile et al., 2004; Jones et al., 2009; Wang et al., 2009) is usually employed as the criterion for the success rate of the identification. However, the algorithmic difference behind these platforms will not be discussed here; more detailed information can be found in the following informative review articles on this topic (Balgley et al., 2007; Kapp and Schutz, 2007; Martens and Apweiler, 2009; McHugh and Arthur, 2008; Nesvizhskii, 2007; Shadforth et al., 2005).

2.2.3 2-DE based proteomics

To investigate thousands or even more proteins from an organism comprehensively, it is critical to reduce the sample complexity. At the beginning of the proteomic era, 2-DE predominantly was exploited as a tool to separate complex protein mixtures. In a typical 2-DE experiment, the protein mixture is usually loaded onto an immobilized pH gradient (IPG) gel. The proteins move along the gel until they reach their isoelectric points, where the overall charge on the protein is neutral. After the first isoelectric focusing (IEF) separation, the IPG gel saturated with proteins is transferred to a sodium dodecyl sulfate polyacrylamide gel electrophoresis (SDS-PAGE). The proteins with similar isoelectric points can then be further separated on the basis of their molecular weights. 2-DE based quantification is normally performed by comparing the staining densities or patterns of proteins. This provides researchers with a rough idea of the relative quantification.

However, 2-DE has some limitations. First of all, the 2-DE gel has a low resolution, which makes it difficult to resolve all or the majority of the proteome. The incompatibility with hydrophobic proteins means it cannot be used for membrane proteins. 2-DE can handle high abundant proteins but is incapable of analysing low abundant proteins existing in a high dynamic range sample such as plasma, whose dynamic range of protein expression can vary by up to 12 orders of magnitude (Corthals et al., 2000). 2-DE–based quantification detects only extreme differences and inaccurately estimates quantity changes. Furthermore, 2-DE is a low throughput strategy that allows only individual gel spots to be identified.

2.2.4 Shotgun proteomics

The shotgun proteomics approach (Link et al., 1999; Wolters et al., 2001; Yates, 2004), also known as MS-based proteomics (Aebersold and Mann, 2003; Ong et al., 2003; Ong and Mann, 2005), was introduced to obtain large-scale analyses of high-complexity samples (**Figure 3**). It is equivalent to shotgun genomic sequencing. In a typical shotgun proteomics, protein complex mixtures are digested into predictable peptides by a site-specific enzyme, such as trypsin. The peptide mixtures then are separated by an HPLC column and injected directly into a MS system. A number of separating techniques can be used in shotgun proteomics, including SDS gel, one or multiple-dimensional chromatography, IEF, or a combination thereof. Because the amino acid sequence of a peptide is rather unique, the protein can be identified by identifying its peptides.
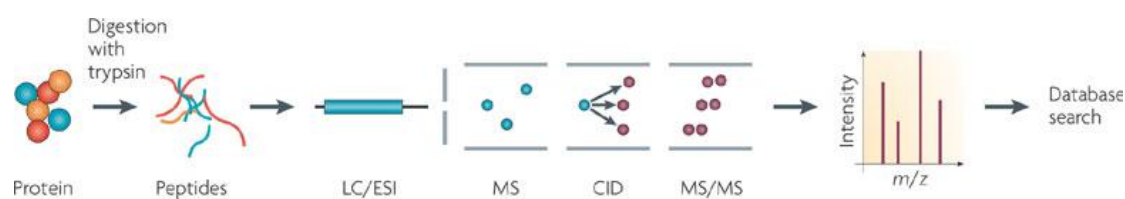
Figure 3. Shotgun proteomics. (reproduced with permission from (Gstaiger and Aebersold, 2009))

2.2.5 Quantitative proteomics

A protein expression map of a certain proteome can now be routinely generated in some depth by the shotgun methods described above (Baerenfaller et al., 2008; Brunner et al., 2007; de Godoy et al., 2008; Schrimpf et al., 2009). The Mann group even demonstrated that MS-based proteomics can cover almost the whole proteome of yeast, with its more

than 4,000 proteins (de Godoy et al., 2008). In its inchoate stage, proteomics was largely aimed at qualitative analysis; however, the expression map normally does not address biological issues efficiently. The absolute or relative quantity change of proteins is probably an important reflection of the disease stage. Altered proteins are possible drug targets and also potential clinical biomarkers for disease diagnosis, even at an early clinical phase. Consequently, quantification has become the essential aspect (Ong and Mann, 2005) by which scientists are attempting to study disease processes. The categorization of the current quantitative approaches is shown in **Figure 4**. As mentioned above, 2-DE-based quantification has inherent weaknesses and is being replaced by MS-based methods. Therefore, the following discussion will cover only the MS-based quantitative strategy. MS-based quantitative data are obtained by either stable isotope labeling or label-free approaches. The isotope labeling approach can be furthermore classified as absolute and relative quantification.
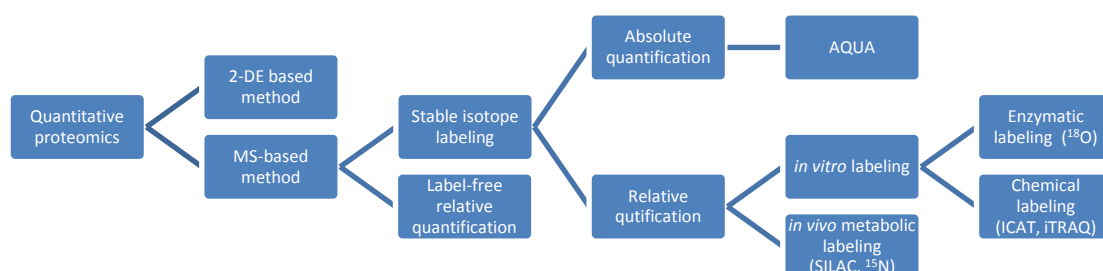
Figure 4. Categorization of current techniques for quantitative proteomics.

The label-free strategy aims to quantify two or more experiments by either comparing the MS ion intensity of peptides (Bondarenko et al., 2002; Chelius and Bondarenko, 2002; Higgs et al., 2008; Wang et al., 2003; Wiener et al., 2004) or using the number of acquired spectra (Gilchrist et al., 2006; Liu et al., 2004; Washburn et al., 2001) matching a peptide/protein as an indicator for their respective amounts in a given sample. The ion intensity is obtained by extracting the chromatographic elution profile of all the

isotoplogues of a given peptide (Ono et al., 2006) for highly resolved MS data. The spectrum-counting approach works because of the fact that more MS2 scans will be triggered when the peptide is present at a higher concentration.

Label-free approaches probably are the least accurate of the MS-based quantification techniques, since both the ion intensity and MS2 count are affected by any systematic or non-systematic alteration. Therefore, variations in sample preparation and chromatographic and electrospraying behavior should be minimized. Despite its poor quantitative accuracy, the label-free method still is considered a powerful quantitative tool in proteomics for several reasons. First, it omits the need for introducing artificially enriched heavy isotope, which can dramatically reduce the complexity of experimental design, and avoids the high cost resulting from stable isotope reagents. Second, an unlimited number of experiments can be compared; in contrast, isotope labeling experiments are limited by the number of isotope reagent patterns. Third, label-free samples result in "pure" spectra, which contain only the peptide with natural isotope composition; these less complex spectra enable a better precursor selection during data acquisition and better peptide identification in the database search.

Stable isotope labeling is the most accurate method in relative quantitative proteomics, and its development has been reviewed in a number of papers (Aebersold and Mann, 2003; Bantscheff et al., 2007; Becker, 2008; Gstaiger and Aebersold, 2009; Guerrera and Kleiner, 2005; Ong et al., 2003; Ong and Mann, 2005; Tao and Aebersold, 2003). A typical stable isotope labeling approach compares two or more physiological states of a biological target. One is labeled with the natural isotope abundance (light/unlabeled) and the other(s) with a stable heavy isotope (heavy/labeled). The labeled and unlabeled samples are mixed and processed together, and the paired peptides behave identically during HPLC separation. The mass difference of the heavy and light peptides or their fragments can be distinguished by mass spectrometry, and the subsequent quantification is achieved by comparing their signal intensities.

Several approaches have been taken to introducing stable isotope tags into proteins/peptides via chemical, enzymatic, or metabolic reactions (**Figure 5**). The first two forms are accomplished *in vitro,* whereas the metabolic labeling is executed *in vivo.*
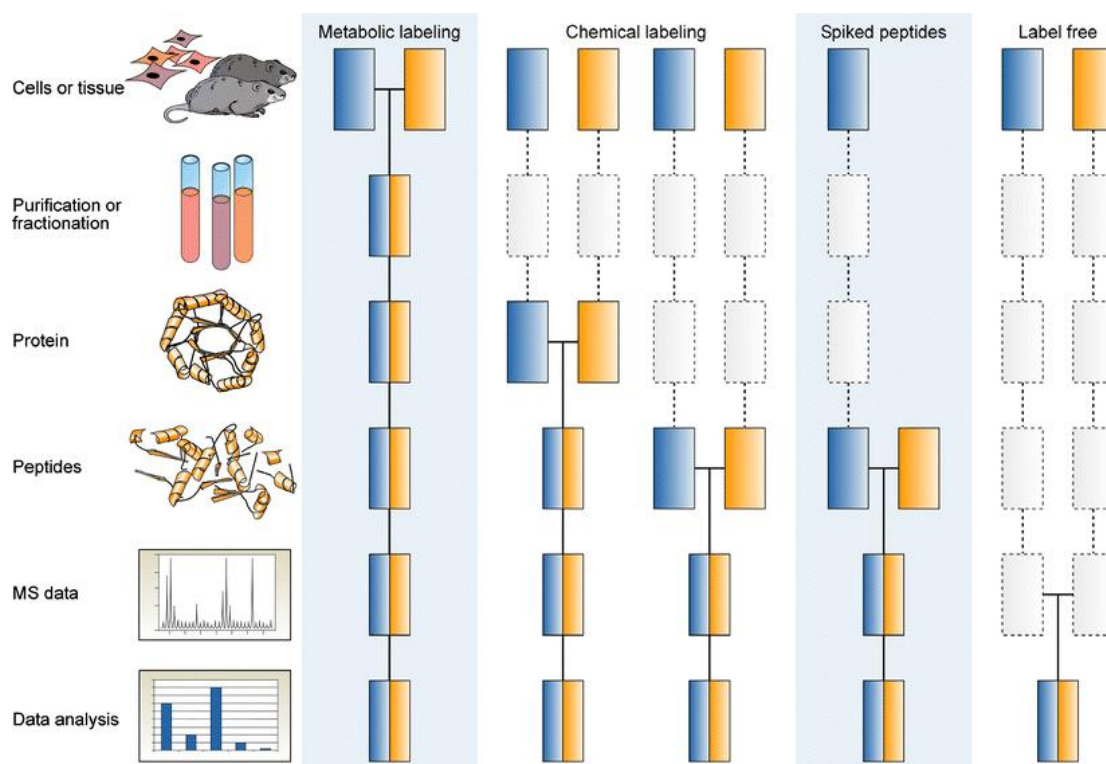
Figure 5. Common quantitative mass spectrometry workflows. Blues and orange boxes represent two experimental conditions. Horizontal lines indicate when samples are combined. Dashed lines indicate points at which experimental variation and thus quantification errors can occur (reproduced with permission from Ref.(Bantscheff et al., 2007))

Enzymatic labeling refers mainly to proteolytic ^{18}O-labeling (Reynolds et al., 2002a; Reynolds et al., 2002b; Yao et al., 2001), which generates ^{16}O/^{18}O isotope-labeled peptides by proteolytic digestion with $H_2^{16}O$ /$H_2^{18}O$ and protease. ^{18}O-labeling is an easily adapted and cost-saving approach; however, the variable incorporation of ^{18}O atoms into peptides (Johnson and Muddiman, 2004; Julka and Regnier, 2004; Ramos-Fernandez et al., 2007) complicates data analysis.

Chemical labeling targets reactive groups on the side chains of amino acids or peptide termini. The first type of chemical labeling methods usually makes use of the reactions between cysteine and isotope-coded tag. The original successful application was the so-called ICAT (isotope-coded affinity tag) procedure (Gygi et al., 1999; Smolka et al., 2001), in which cysteine residues specifically were derivatized with a reagent containing either eight ^{1}H or eight ^{2}H atoms and a biotin group, and the peptide mixture is then subjected to avidin affinity chromatography to purify ICAT coded peptides. Thereafter, the isolated

peptides are analyzed by liquid chromatography-mass spectrometry (LC-MS). As cysteine is not an abundant amino acid, the ICAT technique can reduce significantly the complexity of the peptide mixture, which can be valuable for complex samples. On the other hand, ICAT obviously eliminates all non–cysteine-containing peptides and therefore is not suitable for comprehensive large-scale quantification. Furthermore, a deuterium tag results in a retention time shift between light and heavy peptides in reversed-phase chromatography, which complicates the subsequent data analysis. ICAT has been modified to give several techniques (Hansen et al., 2003; Li et al., 2003; Oda et al., 2003) that are more adaptable for practical applications. Another group of labeling reagents is aimed at the peptide N-terminus and lysine residues, such as isotope-coded protein label (ICPL) (Schmidt et al., 2005), isotope tags for relative and absolute quantification (iTRAQ) (Ross et al., 2004), tandem mass tags (TMT) (Thompson et al., 2003), etc. Of these isotope-coded reagents, iTRAQ, which is compatible with up to eight isobaric mass tags, has become popular and commercially successful. The iTRAQ technique determines the tag ions that are detached from the peptide precursor by MS2 fragmentation. The intensities of these reporter ions enable a relative quantification of the peptides. The most important feature of the iTRAQ strategy is its capability to analyze eight separately labeled pools of protein in a single analysis, improving analytical time significantly. The iTRAQ reagents are undetectable in conventional ion trap instruments because these low-mass reporters are not stable during the activation step, owing to the principle known as the "low mass cut off 1/3 rule" (Louris et al., 1987). A recently developed, new activation method, pulsed q dissociation (PQD)(Cunningham et al., 2006), enables MS/MS reporter ions from isobaric peptide tags such as iTRAQ to be detected in an ion trap mass analyzer. A transformation of chemical isotope labeling is the creation of the labeled peptide/protein from two chemically different tags (Beardsley and Reilly, 2003; Cagney and Emili, 2002) rather than from variant isotope of the same chemical. Although this substitute is much more economical, the labeling reaction, HPLC, and MS behavior may not be identical, which obviously affects the accuracy of the quantification.

Metabolic labeling employs an isotope-enriched medium or diet to culture or feed living systems. The isotopic tracer is incorporated into the whole proteome through protein synthesis during protein turnover and cell multiplication. The labeled peptide has a mass increase that can be detected by a mass spectrometer. When labeled and unlabeled samples are combined, the ratio of peak intensities in the mass spectrum reflects the relative protein abundance. Metabolic labeling is considered to have higher quantitative

accuracy than *in vitro* labeling, since it allows the control and case samples to be mixed prior to any sample preparation, avoiding potential artificial variance (**Figure 5**). However, *in vitro* isotope labeling can be applied universally for any type of sample, which is the major advantage over the *in vivo* metabolic labeling method. In the past, metabolic labeling has been used with radioactive isotopes mainly for metabolite monitoring. By contrast, stable isotope metabolic labeling first was introduced into proteomics by Langen et al. in 1998, who used an ^{15}N- and ^{13}C-labeling approach to compare protein quantities with 2-DE (Langen et al., 1998). Other research groups soon after reported the successful application of ^{15}N metabolic labeling in both yeast (Oda et al., 1999) and a mammalian cell line (Conrads et al., 2001). Nitrogen commonly is chosen rather than carbon, mainly because the isotopic reagent of nitrogen is easier to synthesize. Moreover, there are on average four times as many carbon atoms in a protein than nitrogen atoms. As a result, the ^{13}C-labeled peptide usually results in a broad distribution of the peptide isotopic peak, making data analysis challenging. Up until now, the ^{15}N-labeling technology has been applied successfully to cells in culture (Conrads et al., 2001; Ishihama et al., 2005), plants (Huttlin et al., 2007; Nelson et al., 2007; Palmblad et al., 2007; Schaff et al., 2008), *Drosophila melanogaster* (Krijgsveld et al., 2003), *Caenorhabditis elegans* (Dong et al., 2007; Krijgsveld et al., 2003), and mammals (McClatchy et al., 2007a; Wu et al., 2004). The ^{15}N labeling of mammals also is called stable isotope labeling of amino acids in mammals (SILAM) (Liao et al., 2008; McClatchy et al., 2007b). Another metabolic labeling method, known as stable isotope labeling with amino acids in cell culture (SILAC), was introduced in 2002 (Ong et al., 2002). In a typical SILAC experiment, cells are differentially labeled by growing them in light medium with normal arginine or lysine (e.g. Arg-0 or Lys-0) or labeled medium with heavy arginine or lysine (e.g. Arg-6 or Lys-6). The subsequent trypsin digest cleaves the proteins at arginine and lysine residues. Therefore, every tryptic peptide except for the C-terminal contains one labeled amino acid, which makes the mass increase of the labeled peptide predictable. Conventionally, SILAC is suitable only for cell culture. However, the SILAC approach also has been recently applied to mouse labeling (Kruger et al., 2008) by feeding the mice a $^{13}C_6$-lysine–labeled diet for four generations.

As the two main forms of metabolic labeling, SILAM and SILAC have both strengths and shortcomings (**Table 1**). SILAC and SILAM represent different isotope patterns for labeled peptides in mass spectra. Since only one labeled amino acid can be included for any given tryptic SILAC peptide, the mass difference between the unlabeled and labeled peptide can be predicted, which facilitates data analysis. By contrast, the mass increase of labeled

SILAM peptide depends on the peptide chemical composition as well as on the labeling incorporation rate. This variable mass gain usually makes data analysis more challenging. Moreover, the SILAM and SILAC relative isotope abundance (RIA) ordinarily does not reach 100% because of residual unlabeled atoms in the nutritional source and metabolic amino acid recycling. The SILAM peptide usually contains a number of nitrogen atoms, and these nitrogen atoms are normally more than the labeled number of atoms in SILAC peptide. The incomplete RIA and relatively numerous potentially labeled nitrogen atoms result in a complex and broad isotopic pattern for labeled SILAM peptides. By contrast, SILAC peptides are much easier to handle, since the labeled peptide appears at a certain mass in the spectrum.

Table 1. Comparison of SILAC and SILAM in quantitative proteomics

	SILAC	SILAM
Mass shift for labeled peptide	Predictable	Dependent on both peptide sequence and ^{15}N%
Number of mixed samples	Maximal 3	2
Isotope effect	unknown	reported in a few cases
Identification of labeled peptide	Easy	Challenging
Incorporation requirement	Must be high	Can be relatively low
Cost for mouse labeling	~7,000 EURO/mouse	~1,000 EURO/mouse

SILAC peptides usually appear only in two forms in the MS: labeled and unlabeled. If a protein is only partially labeled, the MS of unlabeled peptide is a mixture composed of two parts: the original unlabeled peptide and the unlabeled peptide resulting from the partial labeling. To avoid this, the labeling incorporation rate of SILAC should be close to 100%. By contrast, as the incorporation rate increases, the labeled MS peaks of SILAM peptide gradually move toward the high mass range. A rather low labeling incorporation rate is sufficient to separate the labeled and unlabeled MS peak envelopes of SILAM peptides. Consequently, partial labeling is also applicable to the SILAM quantitative strategy, reducing the cost and time required for the experiment. Complete labeling usually is

achievable in cell-based experiments because the medium that contains the labeled amino acids can take the place of the whole nutritional source for protein synthesis after the replacement. Moreover, the metabolic rate of cultured cells normally is very high. Mammals such as mouse and rat, which are more relevant for biological research, are not easily labeled fully because of the relatively slow turnover of both proteins and the amino acid pool. Hence, SILAM works better than SILAC for mammal labeling because of its lower incorporation rate compatibility.

In addition, ^{15}N partial labeling can facilitate the determination of protein turnover in mammals. Protein turnover measurement usually tries to calculate the fraction of newly synthesized protein after the isotope tracer has been added. As mentioned above, part of the newly synthesized SILAC peptide will appear in the unlabeled pattern and co-exist with pre-existing peptide, and it is impossible for MS to distinguish between the two. Although the newly synthesized SILAM peptide may appear at a low incorporation rate shortly after the labeling, it is still possible to separate it from the pre-existing unlabeled peptide. The strategy involved will be discussed in depth in the following sections.

The relative quantification methods described above currently dominate the quantitative proteomics field. However, conducting absolute quantification studies is yet another attractive dimension of proteomics. In principle, relative quantification can be incorporated into absolute quantification, since the relative ratios easily can be obtained if the absolute quantities of the proteins are known.

Absolute quantitative proteomics, commonly known as AQUA (absolute quantification of proteins), employs a synthetic stable isotope-labeled peptide at a known concentration (Gerber et al., 2003) as a reference for calculating the concentration of the target peptide. The AQUA method relies on the relative comparison between internal isotope-labeled standard peptide and unlabeled sample digest, in which a chemically identical peptide also is expected. Analysis of the peptide mixture in selected reaction monitoring (SRM) or multiple reaction monitoring (MRM) (Kirkpatrick et al., 2005) modes enables the MS to monitor both the intact peptide mass and one or more specific fragment ions of that peptide over the course of an LC-MS experiment. In combination with the retention time, the AQUA platform can eliminate ambiguities in peptide assignments and extend the quantification range to 4–5 orders of magnitude (Wolf-Yadlin et al., 2007). Unlike the other relatively quantitative approaches, because of the low synthetic efficiency of isotope-labeled peptides AQUA does not measure the protein quantity in a high

throughput manner but determines one or a few specific peptides of interest. The selection of the optimal peptide standard and the amount of the standard to be added to the sample are very important criteria for the AQUA method. Therefore, preliminary experiments are required to determine optimal conditions. However, the degree to which the determined amount in fact reflects the absolute quantity, after the time-consuming sample preparation procedure and physical/chemical treatment of the sample, is still under debate. There is a good probability that it does not reflect the real protein level *in vivo*.

2.3　Metabolomics

Findings concerning DNA (genomics), RNA (transcriptomics), proteins (proteomics), and small molecules (metabolomics) have to be combined to obtain a complete profile of living organisms and to allow a systematic understanding of the occurrence of disease. Metabolite analysis usually is restricted to small molecules, which are the intermediates and products of metabolism. The term metabolome (Oliver et al., 1998) refers to the complete collection of small molecule metabolites, such as metabolic intermediates, hormones, and other signalling molecules, to be found within a biological sample. Metabolomics can be defined as "the quantitative measurement of the dynamic multiparametric response of a living system to pathophysiological stimuli or genetic modification" (Nicholson et al., 2002; Nicholson et al., 1999). The techniques involved should be able to detect, identify, and quantify the global profiling of the metabolome in a high throughput manner. Various platforms are suitable for metabolomic analysis, such as nuclear magnetic resonance (NMR), fourier transform infrared spectroscopy (FT-IR), gas chromatography-mass spectrometry (GC-MS), liquid chromatography-mass spectrometry (LC-MS), ultra performance liquid chromatography-mass spectrometry (UPLC-MS), and capillary electrophoresis-MS (Lenz and Wilson, 2007; Want et al., 2007). This paper focuses on chromatography-MS–based methods.

Two steps typically can be applied to identify metabolites. First, a limited number of possible chemical formulae can be derived from the accurate measurement of the chemical mass. Second, the structure can be deduced from the MS2 fragments of the precursor, which also can be performed by searching an MS/MS library. Moreover, a database can be established, which greatly facilitates identification of the metabolite. If the metabolite has been identified previously, the features of mass, MS/MS, and retention time on the chromatography can be used to identify it again. The signal intensities of MS

are used for the quantification. It should be noted that, like proteomics, metabolomics is still incapable of identifying the entire metabolome.

2.4 Systems biology

The popularity of molecular biology has led scientists toward detailed research at the molecular level, where a specific biomolecule or a few biomolecules are studied. Although millions of –omics data (e.g. from proteomics, metabolomics) have been generated, there is still a long way to go before either a particular molecule or –omics data can be interpreted and eventually applied in therapeutics or as a ''cure'' for diseases. Except for Mendelian diseases, most common human disorders originate from not only one genetic mutation but from the complex interplay between DNAs, proteins, metabolites, and external environmental influences. Therefore, there is a great demand for integrative analysis of data across a wide range of fields; however, this cannot normally be achieved with any independent traditional biological approach. Systems biology thus was introduced to help scientists unravel the organization and interactions of cellular networks between DNAs, RNAs, proteins, and metabolites (Barabasi and Oltvai, 2004; Kitano, 2002) (**Figure 6**). Several technical aims still have to be achieved before these intricate networks can be established on the basis of both validated and predicted interactions (Sauer et al., 2007): 1) identification and quantification of all participants at the –omics level, such as proteomics and metabolomics; 2) experimental identification of physical component interactions; 3) computational deduction of data; and 4) rigorous integration of heterogeneous data.

Obviously, to handle the enormous amount of data in systems biology, computational tools capable of analyzing -omics data from multiple platforms are crucial. A number of algorithmic packages are available, such as KEGG (Kanehisa et al., 2008), PathVisio (van Iersel et al., 2008), pSTIING (Ng et al., 2006), MetaCoret (Ekins et al., 2007), Cytoscape (Shannon et al., 2003), VANTED (Junker et al., 2006), Pathway-Express (Draghici et al., 2007), Systems Biology Markup Language (SBML) (Hucka et al., 2003), and also the commercial tool PathwayStudio® (Sivachenko and Yuryev, 2007) (Ariadne Genomics, Rockville, MD, USA). PathwayStudio, for example, enables a high-throughput, cross-platform analysis of gene, protein, chemical, and disease data. The potential network of any form of interest can be visualized. Although all these tools seem to be highly advanced and powerful enough to uncover the true fundamental physiological

processes, they are still a long way from completely characterizing all the interactions involved in biological events.
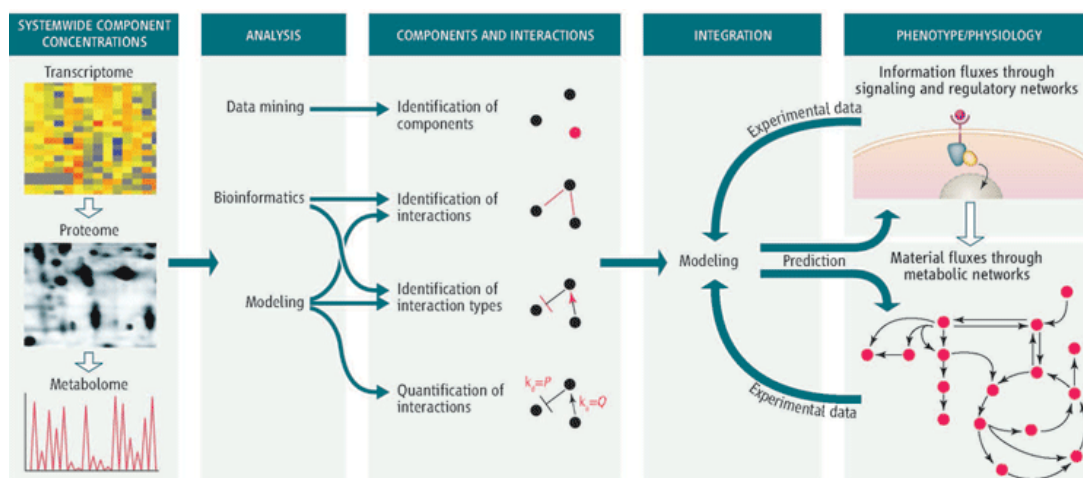
Figure 6. A systems roadmap. (reproduced with permission from (Sauer et al., 2007))

2.5 Biomarkers

According to the North American National Institute of Health (NIH) (http://www.biomarkersconsortium.org/), "Biomarkers are characteristics that are objectively measured and evaluated as indicators of normal biological processes, pathogenic processes, or pharmacologic responses to therapeutic intervention. Biomarkers can be used in clinical practice to identify risk for or diagnose a disease, stratify patients, assess disease severity or progression, predict prognosis, or guide treatment. In drug development biomarkers may be used to help determine how a drug works in the body, to determine a biologically effective dose of a drug, to help assess whether a drug is safe or effective, and to help identify patients most likely to respond to a treatment, or at least likely to suffer an adverse event when treated with a drud. Biomarkers can sometimes be used as part of the approval process for a drug or treatment, to inform regulatory decision-making." As discussed above, biomarkers can be any kind of physical or chemical change between health and disease. Of the potential biomarker targets, proteins are likely the most ubiquitously affected in any cellular process, and protein patterns are more directly related to the phenotype of an organism. In addition, the advances of MS-based proteomics enable the construction of a comprehensive biomarker discovery pipeline. Therefore, protein biomarker discovery is the main focus of this thesis.

The first step is to look for protein biomarker candidates using a quantitative proteomics approach. Afterwards, all or at least a subset of the biomarker candidates require verification. Verification can confirm the MS-based result and provide support for better quantification. A commonly used verification method is the Western blotting technique, which combines one-dimensional gel electrophoresis (1-DE) and antibody immunoreactions. Similarly, enzyme-linked immunosorbent assay (ELISA), which is based on the immune-affinity principle, can be used for verification. Although Western blot is used routinely in every proteomic lab, there are bottlenecks associated with this approach: the method is only semi-quantitative; moreover, the central reagents in Western blot, antibodies, often are of poor specificity, especially those against novel candidate proteins or post-translational modifications.

Alternatively, proteomic data can be verified by SRM or MRM. As described above, together with a standard peptide, MRM enables both the structure and quantity of the analyte to be determined. The final step of the biomarker validation is the clinical evaluation. Despite many efforts and promising biomarker candidates generated from proteomic studies, it remains a formidable, undefined, and expensive task to demonstrate their final clinical usefulness and compliance with regulatory requirements.

Thanks to the great research efforts in the past few decades, a few biomarkers have been validated for complex disorders like diabetes and heart disease; however, currently there are still no biomarkers for psychiatric disorders. Progress in studies of psychiatric disorders is relatively slow because of the limited knowledge of etiology and pathogenesis, the large clinical heterogeneity, uncertain phenotype boundaries, genetic overlap between disorders, and the large influence of non-genetic factors. Despite the existing challenges, MS-based proteomics facilitates the identification of potential biomarkers.

3 Proteomic and metabolomic brain and plasma profiling of a trait anxiety mouse model

3.1 Introduction

As mentioned above, up to 20% of the world's population suffers from depression or anxiety disorders (Kessler et al., 1994), and the number of people is still growing. Although remarkable efforts have been devoted to understanding the clinical and biological basis of depression and anxiety, only relatively slow progress has been made. Currently, no laboratory test is available for diagnosing anxiety and depression. Diagnoses mainly are made empirically, on the basis of a doctor's personal observations.

Emotions, cognitions, environmental experience, and genetic background vary enormously in human psychiatric disorders, such as anxiety (Blanchard et al., 2001; Gordon and Hen, 2004). To make the study of anxiety more realistic, animal models have been introduced to model particular aspects of anxiety-like behavior. The study of animal models has several advantages over the study of humans. First, the anxiety-like behavior of the animal models can be very stable. Second, both the genetic and environmental background of the animals can be well controlled via an inbreeding approach and conditioned feeding. Moreover, there is no theoretical limitation to the type and number of specimens, since the animals can be easily bred. In contrast, clinical samples from patients are always heterogeneous, more difficult to obtain, and limited to body fluids.

On the basis of behaviour on the EPM, both rats and mice have been bred selectively to obtain different animal models with high, low, and normal anxiety-related behavior (HAB, LAB, NAB, respectively) (Kessler et al., 2007; Kromer et al., 2005; Landgraf et al., 2007; Landgraf and Wigger, 2002; Liebsch et al., 1998a; Liebsch et al., 1998b). HAB mice commonly spend ~10% of time or even less on an open arm of the EPM; by contrast, LAB mice spend more than 50% of time on an open arm. NAB mice spend ~30% of time on an open arm, which is close to the mean value of outbred mice. These mouse lines have maintained their featured behavior for more than 50 generations. Besides verfication with the EPM, these animal models were verified by using some other anxiety-related and depression-related tests, including the dark-light avoidance test, open-arm exposure test,

ultrasound vocalization test, TST and FST (Kromer et al., 2005). The HAB mice also showed a higher passive level of activity in desperate situations during the TST and FST.

Stable isotope metabolic labeling of living animals followed by quantitative mass spectrometry is a powerful method for accurately comparing protein expression levels between two or more specimens. Metabolomic studies also can provide additional information and give deeper insights into disease pathobiology. For this purpose, in this study mice were metabolically labeled, starting *in utero*, by feeding a ^{15}N-enriched diet for 56 days. Metabolomic analyses were carried out using a GS-MS platform.

3.2 Material and methods

3.2.1 Materials

The standard rodent diet was purchased from Harlan (Harlan Laboratories, Inc. Indianapolis, IA, USA), and the bacterial protein-based rodent diets were purchased from Silantes (Silantes GmbH, Munich, Germany). Two isotopic forms of bacterial diets were used: natural isotopic (denoted as ^{14}N) and ^{15}N enriched. All the other chemicals were from Sigma-Aldrich (St. Louis, MO, USA), Merck (Darmstadt, Germany), and BioRad (Hercules, CA, USA).

3.2.2 Animal experiments

All the animal experiments were conducted in accordance with the "Guide for the Care and Use of Laboratory Animals of the Government of Bavaria". High (HAB), normal (NAB), and low (LAB) anxiety-related behavior mouse models were established from CD1 mice by using a selective inbreeding approach. The anxiety-related behavior mainly is assessed by the time that the animals spend on the open arm of an EPM device: HAB mice spend approximately 10% of the total time on an open arm, LAB mice > 50% of time, and NAB animals around 30% (Kromer et al., 2005). The animals were bred and housed in the animal facility of Max Planck Institute of Psychiatry. Dams were housed in type 3 macrolone cages, mature animals in groups of four animals in type 2 macrolone cages with 12 h light/dark cycle (lights on at 6 a.m.), room temperature 23±2°C, humidity 60%; tap water and food were available *ad libitum*. All the behavioral tests were performed between 8 a.m. and 1 p.m.

3.2.2.1 Mouse feeding

The ^{15}N/^{14}N feeding started *in utero*. Four to eight female mice from each line were mated one-to-one with an adequate male (i.e. sibling) to increase the pregnancy probability. After 10 days, the pregnancy was detected visually and/or by palpation of the embryos along the backbone, and the males were removed from the cage. To allow them to adapt to the bacterial protein diet, the pregnant females were fed ^{14}N or ^{15}N bacterial diet with standard diet for 4 days. Subsequently, only bacterial diets were provided. All the female pups were sacrificed on postnatal day (PND) 5, 14, and 28. On PND 28, the remaining male pups were weaned and grouped into new cages (2–4 animals per cage) and fed with pure bacterial diets. On PND 56, all the mice were sacrificed for proteomic analysis (**Figure 7**). Blood was taken by cardiac puncture, and plasma was obtained by centrifuging the blood in an EDTA and protease inhibitor cocktail tablet (F. Hoffmann-La Roche Ltd. Basel, Switzerland) pre-added tube at 1,300 × g for 10 min. The pellets were saved as blood cells. The remaining body blood was removed by 0.9% saline perfusion. The brains were divided into four sections: cerebellum, cortex, hippocampus, and amygdale. All the other organs were isolated. The plasma and organs were snap-frozen in liquid nitrogen, and the samples stored at -80°C for further use. The animals did not show any discernible health effects compared with animals fed a standard diet.
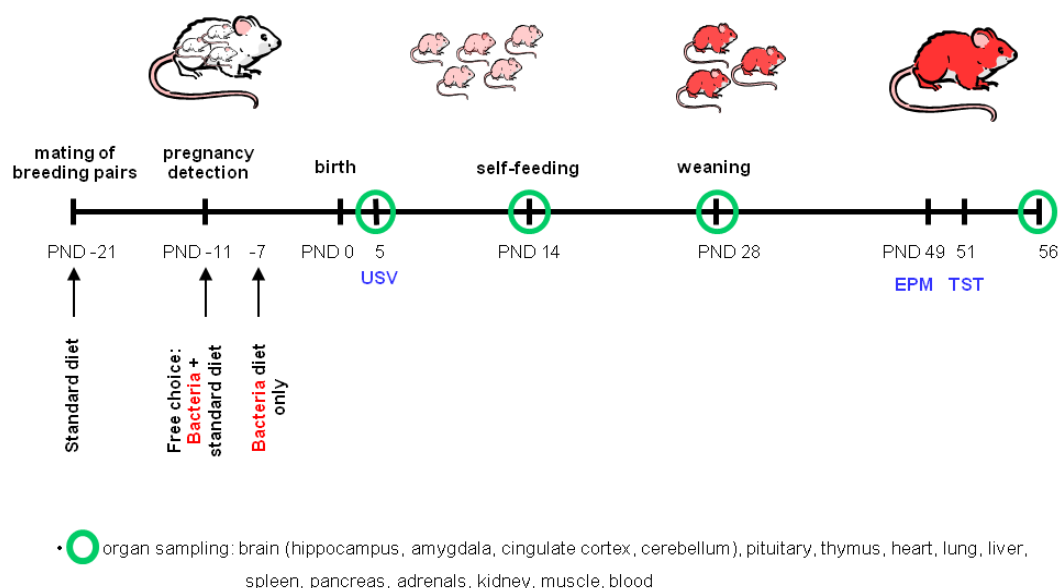
Figure 7. Protocol for feeding mice with the bacteria diet. After pregnancy detection, the animals were given a free choice of standard or bacteria diet for 4 days before being fed the bacteria diet only. Organs were harvested at PND 5, 14, 28 and 56 to determine the ^{15}N incorporation rate and line-specific protein expression pattern.

3.2.2.2   Behavior test

3.2.2.2.1   Ultrasonic vocalization test (USV)

On PND 5, pups were individually separated from their mothers and gently placed on a Petri dish (15 cm diameter) cleaned with 70% ethanol. The temperature was kept constant at 23°C by a water bath underneath the dish. Lines were drawn to divide the dish into 2×2 cm squares. The number of line crossings (two forepaws across the line) was counted during the 5 min test. USV calls were detected and recorded for 5 min with a bat detector (Mini 3 bat-detector, Ultra Sound Advice, U.K.) at 70 kHz.

3.2.2.2.2   Elevated plus maze test (EPM)

The EPM tests were performed on PND 49. The EPM was built of black plastic and consisted of two open arms (30 × 5 cm; 100 lux) and two enclosed arms (30 × 5 × 15 cm; 10 lux). The arms extended from a central platform (5 × 5 cm; 90 lux). The EPM was located 40 cm above the table surface. The whole device was surrounded by a black curtain (Pellow et al., 1985). The mice were put onto the central platform facing a closed arm, and then behavior was recorded for 5 min via a video camera fixed above the maze. The number of entries into the closed and open arms and the percentage of time spent on the open arms were monitored by a trained observer blind to treatment or tracking software. Mice were considered to have entered an open or closed arm when both forepaws and front shoulders were on the arm.

3.2.2.2.3   Tail suspension test (TST)

On PND 51, each mouse was suspended from a bar 35 cm above the floor by affixing the end of its tail to the bar with adhesive scotch tape (Steru et al., 1985). The animals' behavior was videotaped for 6 min and the duration of total immobility scored by a trained observer blind to the treatment.

3.2.3 Quantitative proteomics

3.2.3.1   Determination of ^{15}N incorporation

The development of ^{15}N incorporation rates during the labeling was monitored with the software *QuantiSpec* to determine ^{15}N in both brain and plasma collected on PND 5, 14, 28, and 56 (Haegler et al., 2009a). The ^{14}N and ^{15}N samples were combined at an approximate ratio of 1:1 for cerebella (w/w) and plasma (v/v). The brain and tissue mixtures were put

into an ice-cold 5× buffer of 250mM sucrose, 50mM Tris - HCl (pH 7.4), 5mM MgCl$_2$, 1mM DTT, 25 μg/ml Spermine, 25 μg/ml Spermidine, and a protease inhibitor cocktail tablet (F. Hoffmann-La Roche Ltd. Basel, Switzerland), and then homogenized by using a Teflon-glass dounce homogenizer and an electric drill at 1,200 rpm for 3 min. The homogenates were centrifuged at 20,000 g for 30 min at 4°C and the supernatants collected. The protein mixture was resolved by SDS-PAGE and the gel stained with Coomassie blue. Several selected gel pieces were subjected to in-gel tryptic digestion. Gel pieces were de-stained twice with 100 μL 50mM NH$_4$HCO$_3$ /ACN (1:1, vol/vol) for 30 min, and disulfide bonds reduced with 10mM DTT in 50mM NH$_4$HCO$_3$ at 56°C for 30 min, and then alkylated with 55mM iodoacetamide in 50mM NH$_4$HCO$_3$ in the dark for 30 min. Subsequently, 12.5 ng/μL trypsin in 25mM NH$_4$HCO$_3$ was added to saturate and cover gel slices. The enzymatic reaction was carried out overnight at 37°C. After digestion, the peptides were extracted from the gel pieces by adding 5% formic acid at 37°C for 30 min. The gel pieces were spun down and the liquid collected. The extraction was repeated twice. Finally, the extracted peptide mixture was lyophilized to dryness and dissolved in 10 μL 0.1% trifluoroacetic acid (TFA). The peptide mixtures were then desalted by OMIX tips (Varian, Palo Alto, CA, USA) according to the manufacturer's recommended procedure. The eluted cleaned peptides were spotted with 4-hydroxy-α-cyano-cinnamic acid (HCCA) onto AnchorChip™ targets (Bruker Daltonics, Bremen, Germany) (Schuerenberg et al., 2000). Both peptide mass fingerprinting (PMF) and MS/MS data were acquired by using an Ultraflex mass spectrometer (Bruker Daltonics).

3.2.3.2   QuantiSpec

Both PMF and MS/MS data were subjected to a MASCOT database search. The PMF spectra were exported in DAT format by using the script that was part of the FlexAnalysis 2.4 software (Bruker Daltonics). Furthermore, the Mascot results were exported in XML format via the Mascot server XML-export service. The DAT and XML files were processed by QuantiSpec, written in ActivePerl language. Briefly, on the basis of the theoretical isotopologue distribution of identified peptides with a known amino acid sequence, the ^{15}N incorporation rate was determined by comparing the experimental isotope patterns with a set of theoretical ones. Relative quantitation was accomplished by calculating the signal intensity ratios for each ^{14}N/^{15}N peptide pair.

3.2.3.3   Sample preparation

The hippocampus and plasma of male mice from PND56 were used for quantitative proteomics. The ^{14}N-HAB/^{15}N-HAB comparison was processed by a direct strategy (**Figure 8**), whereas the HAB/LAB comparison was processed by indirect comparison (**Figure 9**).

The plasma samples were first diluted 1:50 with a dilution buffer (10 mM Tris-HCl, pH 7.4, 150 mM NaCl) provided in an IgY-M7 Spin column kit (GenWay Biotech, Inc., CA). The protein concentrations were estimated by Bradford assay, and then the two samples being compared (^{14}N-HAB vs. ^{15}N-HAB, ^{14}N-HAB vs. ^{15}N-NAB, ^{14}N-LAB vs. ^{15}N-NAB) were mixed at a ratio of 1:1, based on their protein content. The protein mixtures were subjected to IgY-M7 Spin column to remove the 7 high abundant proteins (Mouse Serum Albumin, IgG, Fibrinogen, Transferrin, IgM, Haptoglobin, and alpha1-Antitrypsin), according to the manufacturer's guidelines. Briefly, the mixed proteins were first incubated with IgY microbeads, which bound the 7 high abundant proteins with the immobilized specific IgY antibodies. The other unbound proteins were spun down and collected as the flow-through factions, which contained the low abundant proteins. The flow-through fractions were concentrated by ultrafiltration with a centrifugal YM-3, 3 kDa cut-off filter (Millipore, MA). The resulting proteins were ready for SDS-PAGE separation. The bound fractions were eluted out with stripping buffer (0.1M Glycine-HCl, pH 2.5), and the columns regenerated by adding neutralization buffer (0.1M Tris-HCl, pH 8.0).

The blood pellets collected from the plasma preparation were used to extract red blood cell proteins. For red blood cell lysis, the pellets were thawed on ice, and cold water containing 1mM PMSF was added. After the removal of cellular debris, the concentrations of supernatants were measured and ^{14}N-LAB and ^{15}N-HAB samples were mixed at a ratio of 1:1.
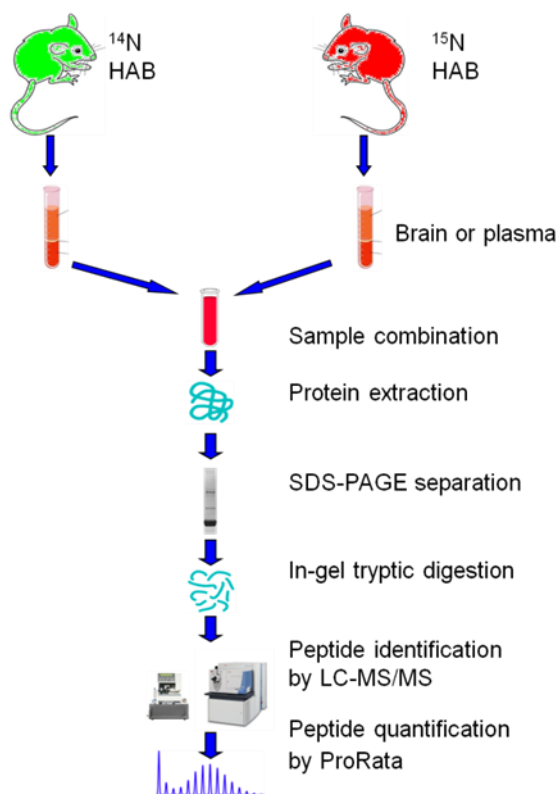
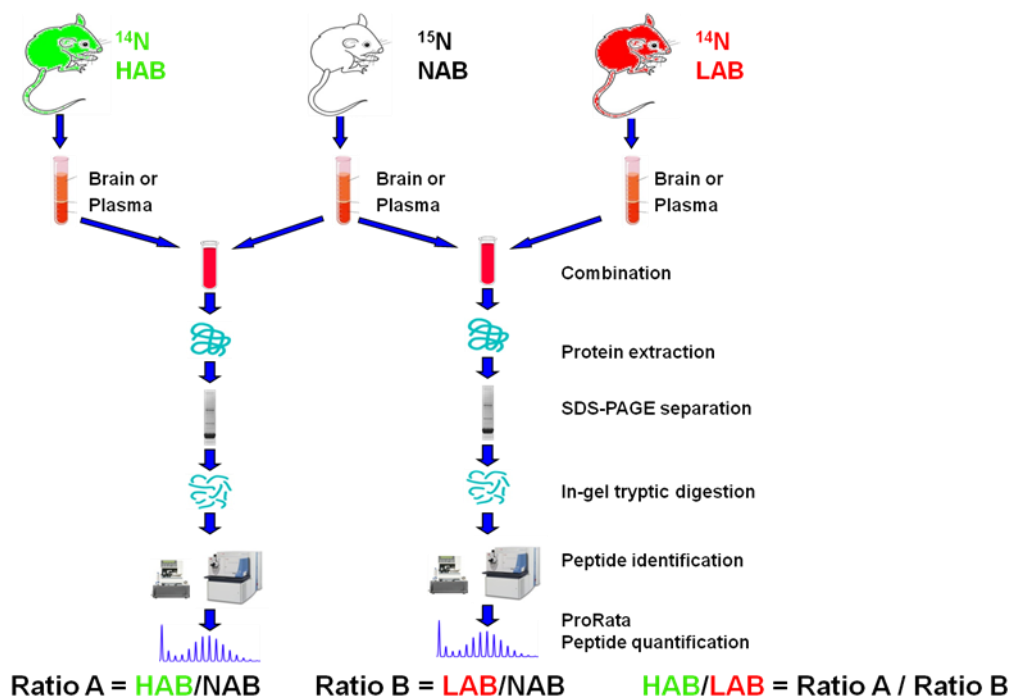**Figure 8. Proteomic direct comparison between two mouse strains**

Figure 9. Proteomic indirect comparison between two mouse strains.

The brain proteins were extracted by using methods slightly modified from earlier ones (Cox and Emili, 2006). The mouse hippocampus was put into an ice-cold 10× buffer of 250mM sucrose, 50mM Tris - HCl (pH 7.4), 5mM $MgCl_2$, 1mM DTT, 25 µg/ml Spermine, 25 µg/ml Spermidine and a protease inhibitor cocktail tablet (F. Hoffmann-La Roche Ltd., Basel, Switzerland) and then homogenized with a Teflon-glass dounce homogenizer and an electric drill at 1,200 rpm for 3 min. The homogenates were then centrifuged at 6,000g for 15 min at 4°C to pellet the nuclei and mitochondria. The supernatants were collected, and the protein concentrations were measured by Bradford assay. The two samples being compared (^{14}N-HAB vs. ^{15}N-HAB, ^{14}N-HAB vs. ^{15}N-NAB, ^{14}N-LAB vs. ^{15}N-NAB) were mixed at a ratio of 1:1, based on their protein content. The protein mixtures were then subjected to an ultracentrifuge for 1 h at 100,000g in a swing bucket at 4°C. The supernatants were collected as the cytosol proteins. The pellets were re-suspended with 0.5 ml of ME buffer (20mM Tris-HCl [pH 7.8], 0.4M NaCl, 15% glycerol, 1mM DTT, protease inhibitor cocktail tablet [F. Hoffmann-La Roche Ltd., Basel, Switzerland], and 1.5% Triton-X-100) and incubated for 1 h with gentle rocking. The supernatants were collected as microsome proteins after a centrifuge at 9,000g, 4°C for 30 min. The protein concentrations of the cytosol and microsome fractions were measured by Bradford assay.

The brain, plasma and blood cell protein mixtures were resolved by Criterion XT Bis-Tris precast gels (Biorad), and the gel stained with Coomassie Brilliant Blue. The gel lane containing the separated proteins was cut into 2 mm wide pieces, and the resulting pieces subjected to in-gel tryptic digestion. Gel pieces were de-stained twice with 100 µL 50mM NH_4HCO_3/ACN (1:1, vol/vol) for 30 min, and disulfide bonds reduced with 10mM DTT in 50mM NH_4HCO_3 at 56°C for 30 min, and then alkylated with 55mM iodoacetamide in 50mM NH_4HCO_3 in the dark for 30 min. Subsequently, 12.5 ng/µL trypsin in 25mM NH_4HCO_3 was added to saturate and cover gel slices. The enzymatic reaction was carried out overnight at 37°C. After digestion, the peptides were extracted from the gel pieces by adding 5% formic acid at 37°C for 30 min. The gel pieces were spun down and the liquid collected. The extraction was repeated twice. Finally, the extracted peptide mixture was lyophilized to dryness and dissolved in 10 µL 0.1% formic acid.

3.2.3.4   HPLC and Mass Spectrometry

The peptide mixtures were analyzed by nanoHPLC (Eksigent Technologies, Inc., Dublin, CA) coupled to an LTQ-Orbitrap (Thermo Fisher Scientific, Bremen, Germany) hybrid mass spectrometer. The C18 reverse-phase columns were made by packing PicoFrit emitters

(New Objective, Inc., Woburn, MA) with a methanol slurry of reverse-phase ReproSil-Pur C18-AQ 3μm resin (Dr. Maisch GmbH, Ammerbuch-Entringen, Germany) under a constant pressure of 100 bar. The packed columns were cut to approximately 15 cm length. Peptides were separated at a 200 nl/min flowrate by using a gradient of 2%-98% solvent B (98% ACN in water, 0.1% FA) over 130 min. The eluates were on-line electrosprayed into the mass spectrometer via a nanoelectrospray ion source (Thermo Fisher Scientific, San Jose, CA).

The LTQ-Orbitrap was running in positive ion, top 5 data-dependent acquisition mode. For full scans in the Orbitrap, the target ion value was 1,000,000, and the maximal injection time was 500 ms at a resolution of r=60,000 at m/z 400. The MS full scan range was 380-1600 m/z. The 5 most intense peaks in the MS scan were fragmented in the LTQ by collision-induced dissociation with a target value of 10,000 ions and an injection time of 250 ms. Former precursor ions selected for MS/MS were dynamically excluded for a period ranging from 30 to 60 s.

The mass spectrometric conditions were: spray voltage, 2.1 kV; no sheath and auxiliary gas flow; ion transfer tube temperature, 200°C; normalized collision energy using wide-band activation mode, 35% for MS2.

3.2.3.5   Data processing

For SEQUEST database analysis, the ORBITRAP raw files were searched against a concatenated forward/reversed IPI-mouse database v 3.46. The ^{14}N database search was performed by using the following parameters: 20 ppm mass tolerance for the MS scan, 1 Da for the MS/MS scan, fixed carbamidomethylation for cysteine, and variable oxidation for methionine. The ^{15}N database search was executed using ^{15}N amino acid masses and an additional -1 Da variable modification for arginine and lysine residues (Zhang et al., 2009). Assembly and removal of redundant proteins based on their accession numbers were performed by using Perl scripts written in-house. The SEQUEST results were filtered by using peptide XCorr >1.9 for 1+ charged ions, >2.7 for 2+ charged ions, >3.5 for 3+ or above charged ions, and DeltaCN >0.08. The false discovery rate (FDR) was then determined by calculating the ratio of the number of peptides identified from decoy to the number identified from forward database searches. Relative quantification of the peptide pair signals was performed with the ProRata software (Pan et al., 2006) on the basis of the SEQUEST identification results. Briefly, the ion chromatograms were extracted for both labeled and unlabeled isotope envelopes according to the identified amino acid sequence.

The m/z window for the natural isotopologue was calculated from the natural isotopic envelope of the peptide. The m/z window for the heavy isotopologue was calculated by using pre-defined ^{15}N% for all nitrogen atoms. The retention time window of the selected ion chromatograms was defined as from 2 min before the identified MS/MS scans to 2 min after the identified MS/MS scans. The ratios of areas of labeled and unlabeled chromatographic peaks were used for peptide quantification.

3.2.4 Corticosterone assay

Corticosterone is the principle glucocorticoid secreted by the adrenal cortices of mice (Shimizu et al., 1983). Glucocorticoid (cortisol in humans and corticosterone in most laboratory rodents) exerts potent actions in the brain, influencing brain function by either shutting off the response of the hypothalamic-pituitary-adrenal (HPA) axis to stress or modulating behavioral states such as mood and emotion and cognitive functions such as learning and memory (Yu et al., 2008). Corticosterone concentrations were measured by radio immunoassay (RIA; DGR Instruments GmbH, Germany). Briefly, 100 µL of unlabeled corticosterone standards at the concentrations 25, 50, 100, 250, 500, and 1000 ng/ml, or 1:200 diluted plasma samples, were mixed with 200 µL ^{125}I-labeled corticosterone. A limited amount of anti-corticosterone was added to react with both labeled and unlabeled corticosterone. As the amount of antigen added increases, the fraction of labeled antigen bound to the antibody decreases correspondingly. After precipitating all antibody-bound antigen, the radioactivity was counted in a gamma counter.

3.2.5 GO and KEGG analysis

Quantified proteins were sorted by $\log_2$ ratio in ascending order and divided into five bins with $\log_2$ ratios of -1.0, -0.5, 0.5, 1.0. The GO analysis (Ashburner et al., 2000) was processed with the methods described previously (Pan et al., 2009) by using R (Team, *2009*) and the GOstats (Falcon and Gentleman, 2007) package. Briefly, for each bin the *P* values for each GO category were calculated with the conditional hypergeometric test by using the quantitative proteome as a background. After obtaining the *P* value for each category and bin, GO categories were filtered on the basis of their *P* values. Categories with no significant enrichment ($P < 0.05$) in any bin were filtered out. Those categories that after filtering did not have a *P* value for a bin were provided a conservative *P* value of 1. Finally, the *P* values were transformed with the equation $x = -\log_{10} P$, and the z-scores were calculated by [x-mean(x)]/sd(x). For the KEGG analysis (Kanehisa et al., 2004), the mouse

proteins were mapped to the KEGG ortholog level. This allows an interspecies comparison for further investigations. Afterwards, the hypergeometric test was calculated by using R. The background of the test was set to all mouse proteins in KEGG with at least one pathway entry (3319). Similar to the GO analysis, the *P* values were transformed into z-scores.

3.2.6 Western blot analysis

MS-based quantitative proteomics has quantified a number of proteins expressed differentially in ^{14}N-HAB/^{15}N-HAB, ^{14}N-HAB/^{15}N-NAB, and ^{14}N-LAB/^{15}N-NAB comparisons. Relative protein levels of several selected proteins were analyzed by Western blot. Protein mixtures with equal protein content (10-30µg) were first resolved by SDS-PAGE. Subsequently, the separated proteins were transferred onto polyvinylidene fluoride (PVDF) membranes. Western blot analysis was performed with several selected antibodies. The membranes were then incubated with HRP-conjugated secondary antibody. ECL system and film were used for membrane visualization. ECL images were quantified by *QuantityOne* software (BioRad).

3.2.7 Metabolomics

The metabolomic analyses shown in this thesis were processed at the 'Metabolomics Core' of the University of California, Davis, CA, USA (Dr. Vladimir Tolstikov).

3.2.7.1 Sample preparation

Six mice from each animal line were employed in metabolic studies.

The plasma samples were prepared by using the method described previously (Fiehn and Kind, 2007). Briefly, the plasma proteins were precipitated, and the metabolite extraction was obtained. An aliquot of plasma extract was dried down, and the other aliquots were frozen for recording purposes. The plasma was derivatized by first adding methoxyamine in an aprotic basic solvent and then adding a trimethylsilylating agent. The derivatized sample was analyzed by direct thermodesorption GC-TOF.

The brain tissue samples were prepared as follows: First, the extraction solution was prepared by mixing acetonitrile, isopropanol, and water in the volume proportion 3:3:2. The pH of acetonitrile and isopropanol (pH7) was checked using wetted pH paper. The extraction solution mix was rinsed with small bubbles of argon for 5 min. The Argon line

was flushed out of air before being used for degassing the extraction solvent solution. The extraction solution was pre-cooled at -18°C to -22°C. Eppendorf tubes with two metal balls (3 mm diameter) containing frozen mouse brain samples were placed in a freezer pre-chilled to -80°C or with liquid nitrogen Eppendorf-holder of the grinder. Immediately afterwards the Eppendorf tubes were put back in liquid nitrogen. 10-50 mg of frozen mouse brain (hippocampus) was homogenized with 500-2.500 µl (or aliquot according to sample aliquot) extraction solution mix for 45 s in 25 ml conical polypropylene tubes in the homogenizer Tissue Master 125. The homogenate was centrifuged at 2500 rpm for 5 min. An aliquoted 250 or 500 µl of supernatant was evaporated in the Labconco Centrivap cold trap concentrator to complete dryness. The dried residue was then re-suspended with 500 µl of acetonitrile : water (1:1 v/v) mixture and centrifuged for 2 min at 14000 rcf in the centrifuge Eppendorf 5415 D. The clear supernatant was for GC-TOF-MS analysis. Samples were dried in the Labconco Centrivap cold trap concentrator to complete dryness and, once dried, stored in darkness under argon. The dried samples were then derivatized for GC/MS profiling. Methyl oxime derivatives were produced by dissolving the dry extracts in 20 µL freshly prepared omethylhydroxylamine·HCl (40 mg/mL in pyridine) and incubated at 30°C for 90 min while being shaken continuously. Subsequent trimethyl silylation was achieved by adding 80 µL of *N*-methyl-*N*-trimethylsilyltrifluoroacetamide (MSTFA), followed by continuous shaking for 30 min at 37°C.

3.2.7.2   GC-MS data acquisition

GC-TOF-MS analysis was performed by using an Agilent 6890 N gas chromatograph (Palo Alto, CA, USA) interfaced to a time-of-flight (TOF) Pegasus III mass spectrometer (Leco, St. Joseph, MI, USA). The mass spectrometer first was tuned according to the manufacturer's manuals to achieve optimal parameters for ion lenses, detector voltage, and other settings. Automated injections were performed with a programmable robotic Gerstel MPS2 multipurpose sampler (Mülheim an der Ruhr, Germany). The gas chromatograph (GC) was fitted with both an Agilent injector and a Gerstel temperature-programmed injector, a cooled injection system (model CIS 4) with a Peltier cooling source. An automated liner exchange (ALEX), designed by Gerstel, was used to eliminate cross-contamination from the sample matrix between sample runs. Multiple baffled liners for the GC inlet were deactivated with 1 µL injections of MSTFA. One microliter of each sample was injected in splitless mode, depending on the metabolite concentrations and eventual signal-to-noise ratios in the GC-MS profiles. The Agilent injector temperature was held constant at 250°C while the Gerstel injector was programmed (initial temperature 50°C, hold 0.1 min,

increased at a rate of 10°C/s to a final temperature of 330°C, hold time 10 min). Injections of 1 μL were made in split (1:5) mode (purge time 120 s, purge flow 40 ml/min). Chromatography was performed on an Rtx-5Sil MS column (30 m × 0.25 mm i.d., 0.25 μm film thickness) with an Integra-Guard column (Restek, Bellefonte, PA, USA). Helium carrier gas was used at a constant flow of 1 mL/min. The GC oven temperature program had an initial temperature of 50°C, with a 1 min hold time, and was ramped at 20°C/min to a final temperature of 330°C with a 5 min hold time. Both the transfer line and source temperatures were 250°C. The Pegasus III TOF (Leco, St. Joseph, MI, USA) mass spectrometer ion source operated at -70 kV filament voltage with ion source. After a solvent delay of 350 s, mass spectra were acquired at 20 scans per second with a mass range of 50 to 500 m/z.

3.2.7.3   Data analysis

The data were processed according to the methods described previously (Zou and Tolstikov, 2008). The Xconvert program included in Xcalibur was used to convert the Xcalibur (*.raw) files to netCDF (*.cdf) format. Automatic peak finding, deconvolution, and alignment were performed using XCMS running on the open statistical platform R. Preliminary data were explored by unsupervised methods such as principle component analysis (PCA) and clustering. For PCA, a scree plot (to show the optimal number of eigenvalues), a score plot (to show the most important principal components and visually detect clusters), and a loading plot (to show positive and negative correlations of components) were included for each analysis by using the R package pcaMethods in the Bioconductor project. Cluster analysis of the PCA scores was performed with partitioning methods such as K-means using the function kmeans() in R package stats; hierarchical agglomerative methods such as Ward's method using the function hclust() in R package stats; multiscale bootstrap resampling using R package pvclust; and the model-based clustering approach using R package mclust, which assumes a variety of data models. Maximum likelihood estimation and Bayes criteria were applied to identify the most likely model and number of clusters.

All calculations were performed in an R integrated development environment (IDE), RKWard, under Kubuntu 7.10, a Debian Linux operating system, on a quad core Dell OptiPlex 755 workstation (4 x 3.0 GHz CPU speed, 2 x 4 MB L2 cache, 8 GB RAM). The current versions of Kubuntu, R, Bioconductor, XCMS, pcaMethods, stats, pvclust, mclust, GALGO, and RKWard are free open source softwares (FOSS).

The MarkerView 1.1 Software (Applied Biosystems/MDS Sciex, Concord, Ontario, Canada) allows data from several samples to be compared so that differences can be identified. Typical applications include metabolomics, biomarker discovery, metabolite identification, impurity profiling, etc. In the current study, this software was used for data analysis in conjunction with the techniques described above. The program uses multivariate analysis techniques to compare samples and provides both supervised and unsupervised methods. Supervised methods use prior knowledge of the sample groups (for example, affected/altered vs. control) to determine the variables that distinguish the groups. In contrast, unsupervised methods allow the structure within the data to be determined and visualized. The two approaches can be combined, i.e. unsupervised methods can be used to determine the groups, and then supervised methods can be used to confirm the important variables.

3.2.8 Pathway analysis

The interactions between protein-protein, protein-metabolite, and metabolite-metabolite were analyzed with the software Pathway Studio (Ariadne Inc., MD). The differentially expressed proteins (>2 fold change, $\geq$2 out of 3 replicates, $\geq$10 peptides) and metabolites ($P < 0.05$) were uploaded and converted to the synonymous names compatible with the software database. The direct interactions among different entities were mapped by Pathway Studio. The confidence of each interaction can be evaluated by the number of references providing evidence. The enrichment of a sub-network can be calculated regarding any functional group. The enrichment of each Gene Ontology category was also obtained. Specific networks were generated for different purposes.

3.3 Results

3.3.1 Animal experiments

3.3.1.1 Bacterial diet feeding

No discernible health effects were observed in the animals fed the bacterial diet compared with those fed a standard diet. After pregnancy detection, 4 days of free-choice feeding between the standard and bacterial diets provided enough time for animals to adapt gradually to the change of diet.

Before weaning, no differences in overall food consumption were observed between dams and the offspring in any mouse line or diet. However, the animals fed bacterial diet showed lower body weights than the animals fed with standard chow (**Figure 10**). The reason for the lower body weight could be the different protein sources and nutritional composition of the two diets.
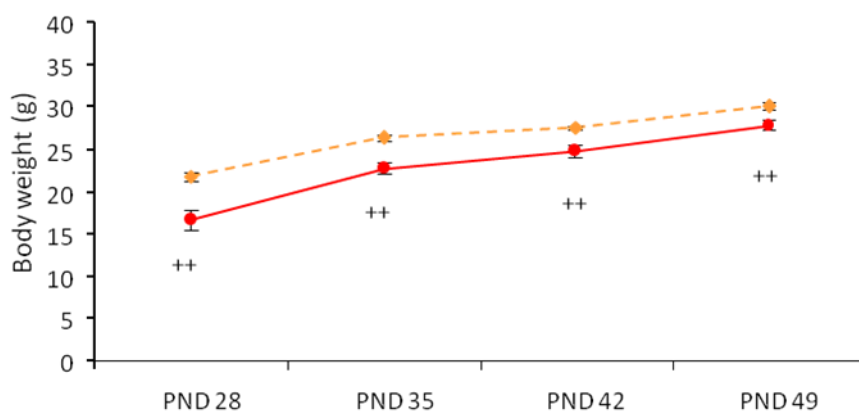
Figure 10. Weight gain after weaning of animals fed with a bacterial or standard diet.
Compared to standard-fed HAB animals (orange dotted line), bacterial-fed animals (red line) had gained less body weight at different developmental time points (++p<0.01 bacterial vs. control).
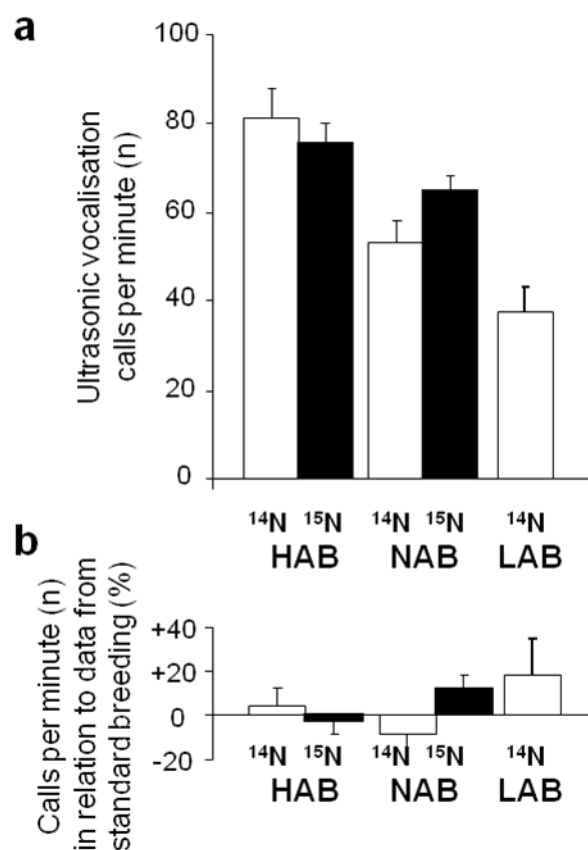
Figure 11. Anxiety-related behavior at post natal day 5 in the ultrasonic vocalization test (USV).

3.3.1.2   Behavior test

3.3.1.2.1   Ultrasonic vocalization (USV)

The ultrasonic vocalization test (UVT) at PND 5 was used to predict the anxiety level at an early developmental stage. The HAB mice emitted significantly more ultrasound vocalization than the LAB mice. The ultrasound vocalization of the NAB mice was between that of the HAB and LAB mice (**Figure 11**). The USV results do not show a significant isotopic effect of the $^{15}N/^{14}N$ bacterial diet on any of the animal lines (**Figure 11**). The ^{15}N-fed NAB mice had a slightly higher USV level than the ^{14}N–NAB mice; however, both were still within the control range. When compared with the USV data acquired from the animals fed the standard diet (**Figure 11 b**), the USV phenotypes of the different anxiety mouse lines did not demonstrate an effect of the bacterial diet.

3.3.1.2.2   Tail suspension test (TST)
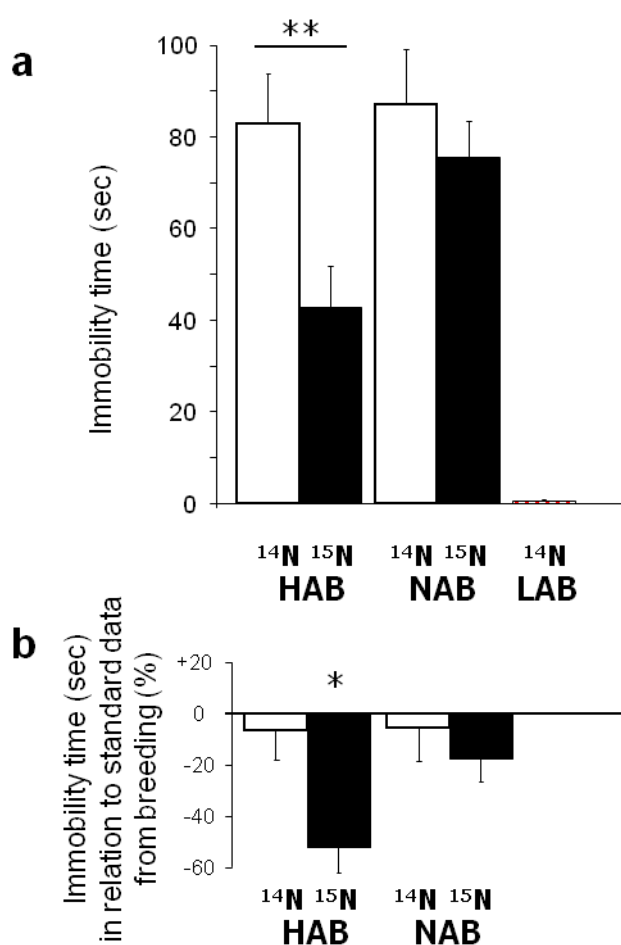
Figure 12. Depression-like behavior in the tail suspension test (TST).

The tail suspension test (TST) evaluates the level of depression-like behavior. Independent of gender (separate data not shown), LAB mice displayed significantly less immobility time than HAB and NAB animals in the TST (**Figure 12**). However, a difference was observed between ^{15}N- and ^{14}N-fed HAB mice. The ^{15}N diet showed an antidepressant-like effect, and HAB mice fed ^{15}N had significantly less immobility time in the TST, implying a lower level of passivity in a hopeless situation. The comparison between the animals fed the standard diet and those fed the bacterial diet indicated that the group of ^{15}N-fed HAB mice was the only one whose TST behavior was affected significantly by ^{15}N feeding (**Figure 12b**), whereas ^{15}N-HAB animals still showed considerably more depression-like behavior than LAB animals. All the other groups demonstrated constant TST behavior, indicating that there were no isotopic or dietary effects. Another ^{15}N-labeled diet based on *Spirulina* protein has shown a similar effect on depression-like behavior in HAB mice (Frank et al., 2009). Therefore, this effect appears to be diet independent. Since the ^{14}N and ^{15}N diets

41

are supposed to have identical ingredients, except for the nitrogen form, the reason for the TST variation between [14]N- and ^{15}N-HAB mice must be related to the ^{15}N isotope. Although the phenotype we observed can involve a combination of different factors, the known factor in this study is the ^{15}N isotope; hence, we assume that an isotope effect exists and that it can affect both animal behavior and protein expression.

In order to avoid this isotope effect, an indirect comparison strategy was employed to analyze the protein expression differences between HAB and LAB mice (**Figure 9**).

3.3.1.2.3   Elevated plus maze (EPM)
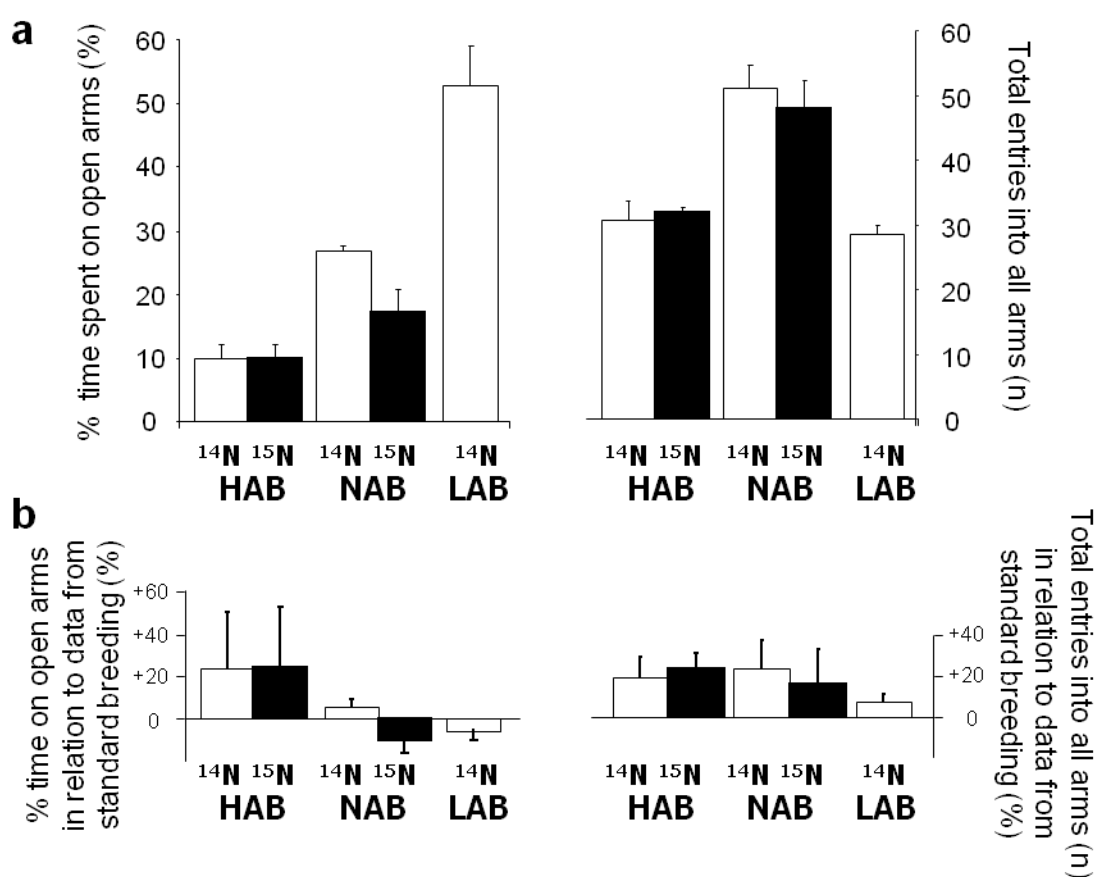
Figure 13. Anxiety-related behavior and locomotion on the elevated plus maze (EPM).

Elevated plus maze (EPM) data (percentage of time spent on the open arms) were used to evaluate the anxiety-like behavior level. As shown in **Figure 13**, the HAB mice spent less than 10% of the total testing time on the open arms of the EPM; by contrast, the LAB mice spent more than 50% of the time on an open arm. The time spent by NAB mice on an open arm was between that of the other two groups. Compared to mice fed the standard

diet, neither the anxiety behavior nor the locomotion of the EPM phenotypes (**Figure 13b**) were affected by either the bacterial diet or ^{15}N isotope.

3.3.2 Quantitative proteomics

3.3.2.1 ^{15}N Incorporation rates

The ^{15}N incorporation rates in brain and plasma were determined on the basis of the peptides and proteins quantified by *QuantiSpc*. **Figure 14** shows how incorporation rates increased during ^{15}N feeding. The peptides mixed 1:1 were analyzed by MALDI-TOF; the mass spectra of tryptic peptides LGEYGFQNAILVR from plasma albumin (**Figure 14a**) and IWHHTFYNELR from brain beta actin (**Figure 14b**) are shown in **Figure 14**. In both cases, the ^{15}N isotopic envelopes moved to the higher mass range during ^{15}N labeling, indicating an increase in the ^{15}N incorporation rate. By PND of sacrifice, day 56, the incorporation rates in both brain and plasma had reached over 90% (**Figure 14c**), which is sufficient for sensitive and accurate quantification by mass spectrometry.
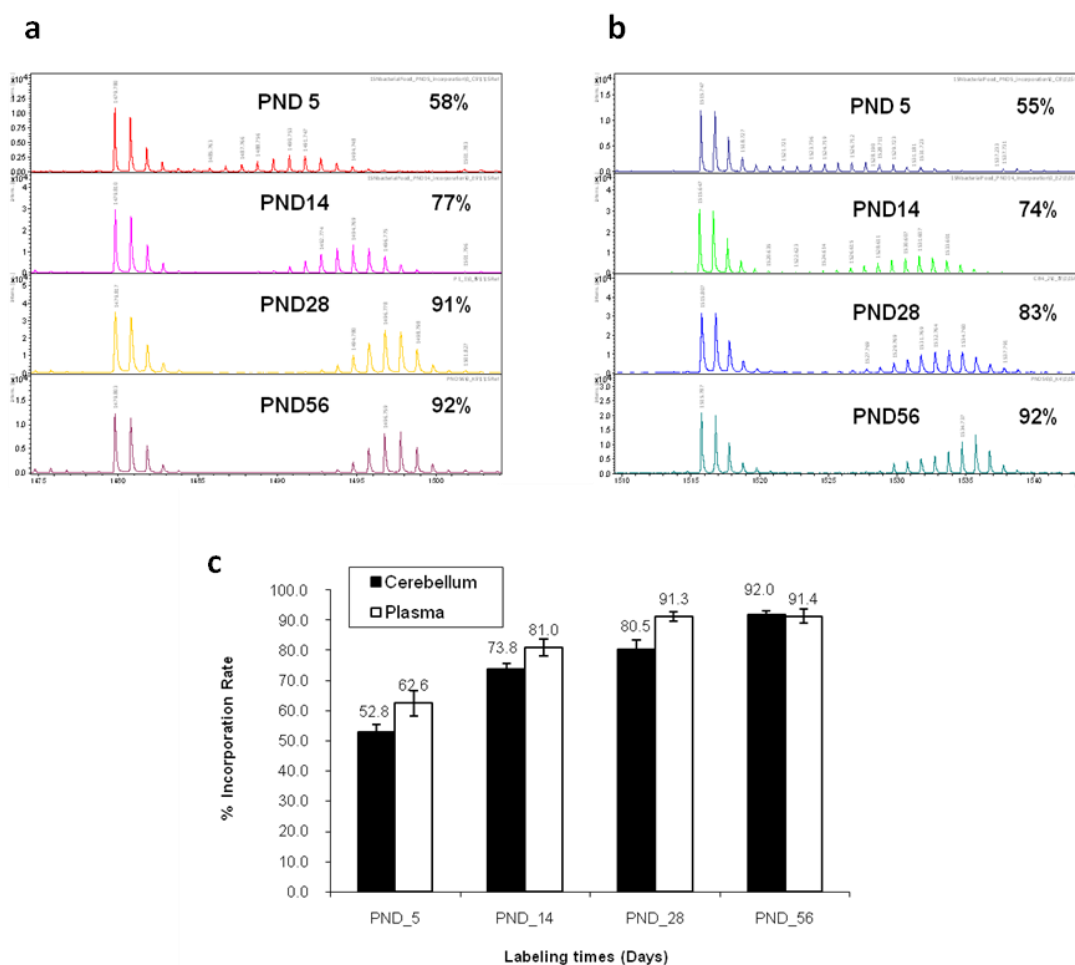
Figure 14. ^{15}N incorporation rate changes during ^{15}N labeling. a: Tryptic peptide LGEYGFQNAILVR derived from mouse plasma albumin; b: Tryptic peptide IWHHTFYNELR derived from brain beta actin; c: The average ^{15}N incorporation rate on different labeling days

3.3.2.2 Glyoxalase-I in blood cells and brain

Glyoxalase-I (Glo1) previously was identified and quantified by two-dimensional gel electrophoresis (2-DE) in both brain and red blood cells as a protein that is expressed differentially between HAB and LAB mice (Kromer et al., 2005) (**Figure 15a**), which was also confirmed by Western blot (**Figure 15b**). However, because of the technical limitations of the 2-DE platform mentioned in the introduction above, Glo1 was one of only a few protein candidates found by 2-DE to be differentially expressed between HAB and LAB.

The SILAM labeling approach has given a much deeper insight into the proteome differences between HAB and LAB. A greater number of proteins were found to have

altered expression levels. Glo 1 was used to evaluate whether SILAM gives the same results as 2-DE. Our ^{14}N-HAB/^{15}N-HAB comparison showed that Glo 1 expression was not influenced by ^{15}N isotopic feeding. Therefore, the ^{15}N-HAB/^{14}N-LAB red blood cells were used for direct comparison of Glo 1 expression, and HAB/LAB hippocampi were compared by using the indirect approach. **Figure 15c** shows the red blood cell Glo 1 tryptic peptide from three different biological replicates. In all instances, the LAB mice have a higher expression level than the HAB mice. **Figure 15d** shows the results of the HAB/LAB indirect comparison for tryptic peptide GLAFIQDPDGYWIEILNPNK. The left panel of **Figure 15d** illustrates that the expression levels of Glo 1 are quite comparable in HAB and NAB mice. However, the NAB and LAB comparison, shown in the right panel, reveals that the LAB mice have a higher expression level of Glo 1. By combining the two comparisons, one can conclude that HAB mice have a lower protein expression level than LAB mice. In summary, SILAM quantification results from both brain and red blood cells closely agree with previous 2-DE experiments.
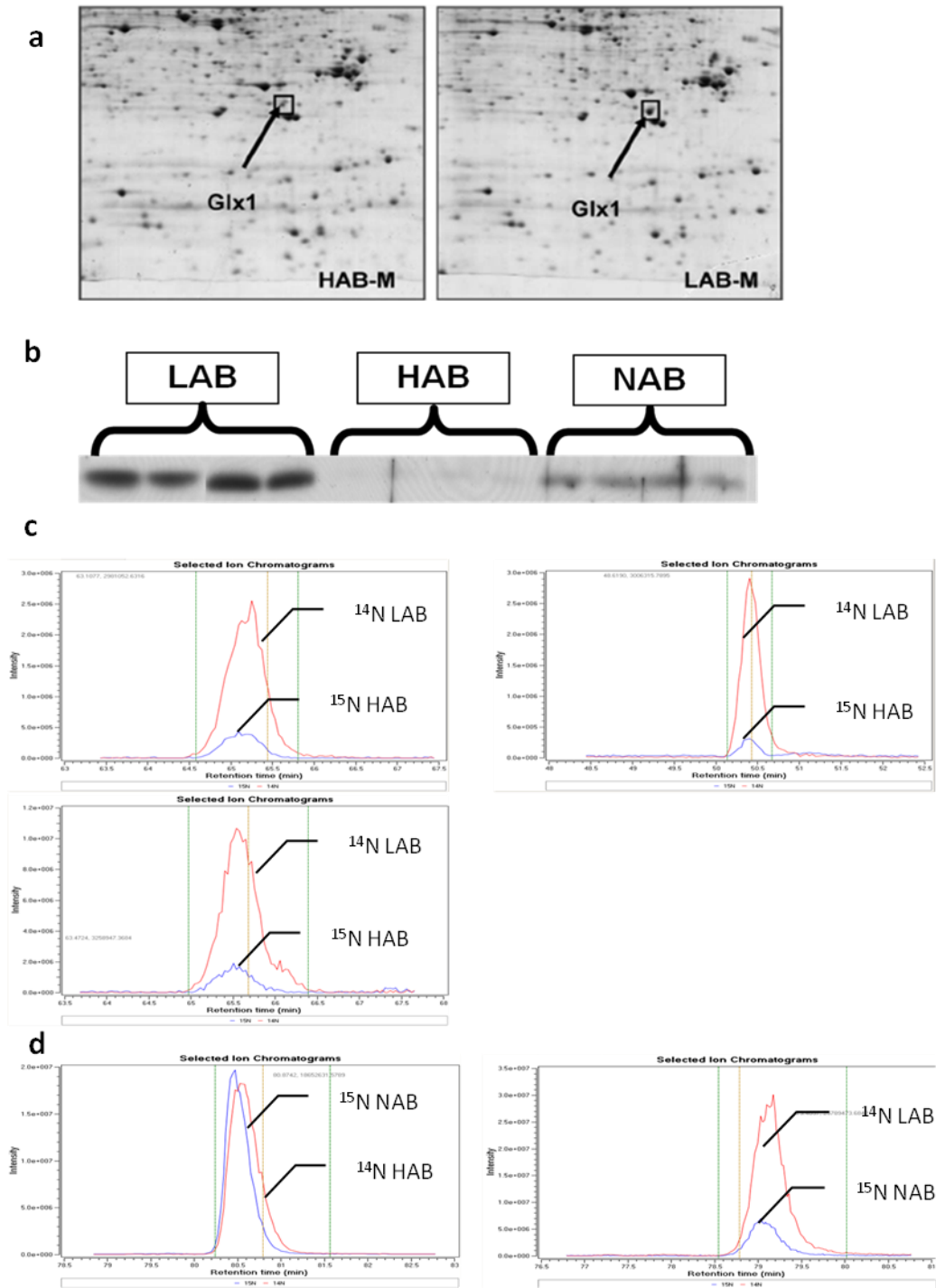
Figure 15. Quantification of glyoxalase-I in red blood cells and brain. a: 2-DE quantification; b: Western blot quantification; c: Direct comparison between HAB and LAB blood cell Glo1; d: Indirect comparison between HAB and LAB hippocampal Glo1.

3.3.2.3 HAB/NAB and LAB/NAB comparison in cytosol and microsomes

HAB/NAB and LAB/NAB hippocampal cytosol comparisons generated quantitative results for 2273 and 1962 proteins, respectively. In total, 2761 proteins were quantified by at least one experiment; 1509 proteins were quantified by both HAB/NAB and LAB/NAB experiments and used for the subsequent HAB/LAB indirect comparison. Of these quantified proteins, 230 were found to be expressed differentially ($\geq$2 fold change, $\geq$2 out of 3 replicates, $\geq$10 peptides) in HAB and LAB hippocampal cytosol (**Supplementary table 1**).

HAB/NAB and LAB/NAB hippocampal microsome comparisons generated quantitative results for 2545 and 1956 proteins, respectively. In total, 3284 proteins were quantified by at least one experiment; 1254 proteins were quantified by both HAB/NAB and LAB/NAB experiments and used for the subsequent HAB/LAB indirect comparison. Of these quantified proteins, 143 were found to be expressed differentially ($\geq$2 fold change, $\geq$2 out of 3 replicates, $\geq$10 peptides) in HAB and LAB hippocampal microsome (**Supplementary table 2**).

The correlation between hippocampal protein regulation and KEGG pathways is shown in **Figure 16**, and between hippocampal protein regulation and GO cellular component in **Figure 17**. The pathways and categories enriched with proteins from the first and fifth bins are of great interest, since they show a change between HAB and LAB. Notably, synapse proteins are enriched in the first bin, implying a role of synapses in psychiatric disorders.

3.3.2.4 HAB/NAB and LAB/NAB comparison in plasma

HAB/NAB and LAB/NAB plasma comparisons generated quantitative results for 640 and 647 proteins, respectively. In total, 974 proteins were quantified by at least one experiment; 355 proteins were quantified by both HAB/NAB and LAB/NAB experiments and used for the subsequent HAB/LAB indirect comparison. Of these quantified proteins, 48 were found to be expressed differentially ($\geq$2 fold change, $\geq$2 out of 3 replicates, $\geq$10 peptides) in HAB and LAB plasma (**Supplementary table 3**).
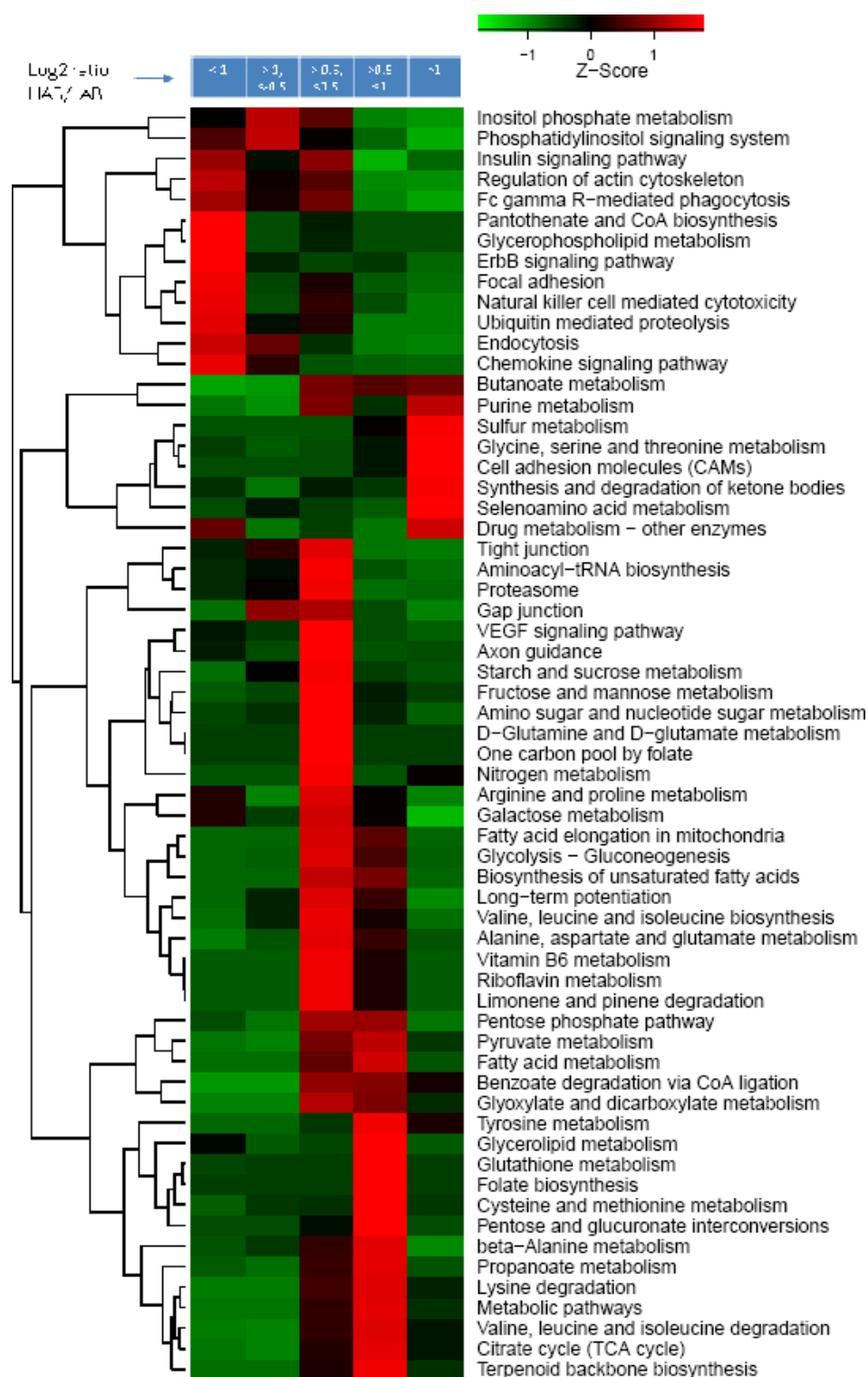
Figure 16. Correlation between hippocampal protein regulation and KEGG pathways. The blue boxes at the top show protein regulation factors between HAB and LAB mouse lines. Proteins were divided into five bins and analyzed with respect to KEGG pathways. *P* values were transformed to z-scores, indicating bin-specific enrichments. (Due to the limited resolution the pathway names on the right are not legible; higher resolution figure is available in electronic file.)
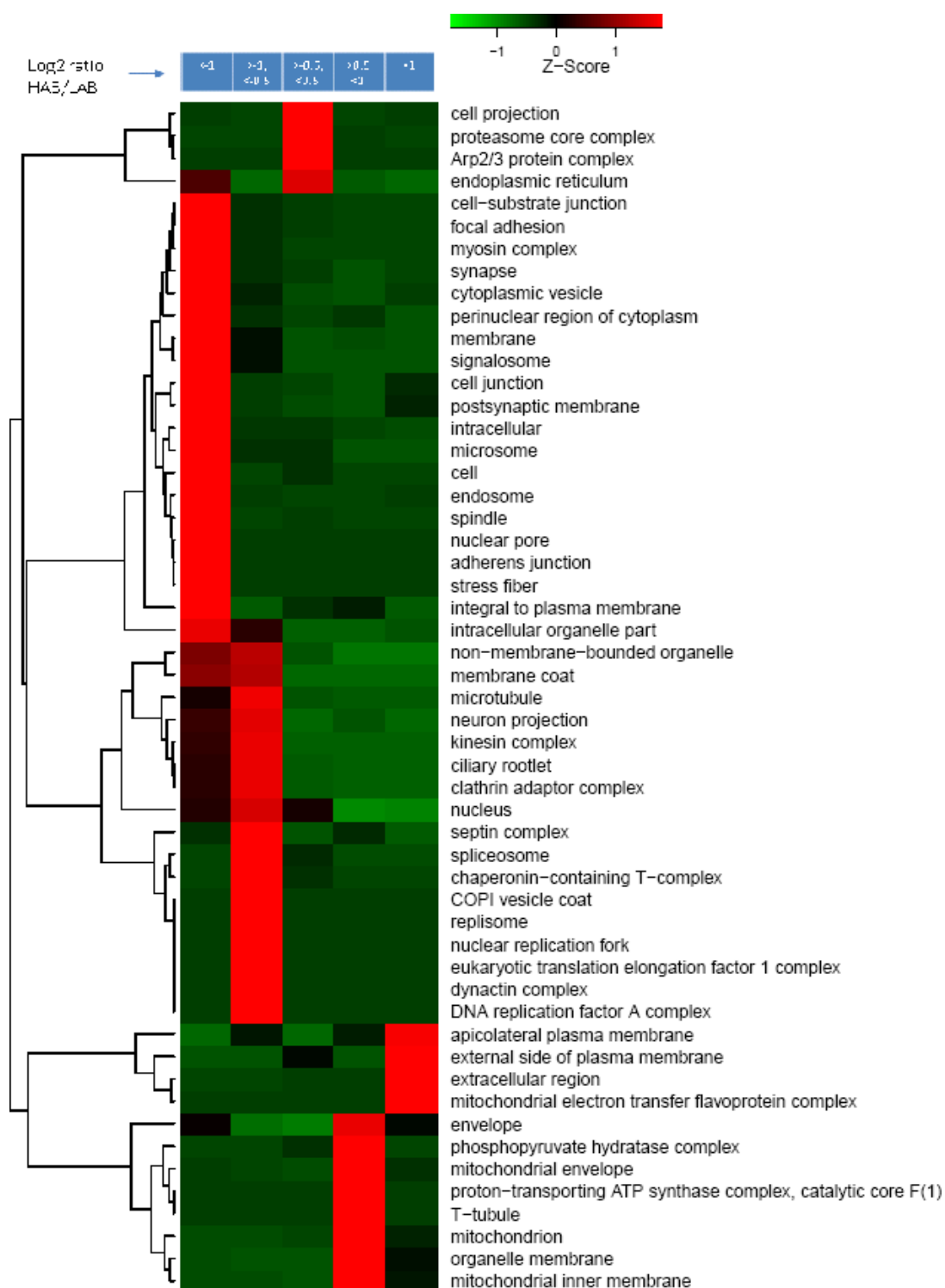
Figure 17. Correlation between hippocampal protein regulation and GO cellular component. The blue boxes at the top show protein regulation factors between HAB and LAB mouse lines. Proteins were divided into five bins and analyzed with respect to GO cellular component categories. *P* values were transformed to z-scores, indicating bin-specific enrichments. (Due to the limited resolution the category names on the right are not legible; higher resolution figure is available in electronic file.)

3.3.2.5 Isotope effects: HAB/HAB comparison in cytosol and plasma

The ^{14}N-HAB/^{15}N-HAB hippocampal cytosol comparison generated quantitative results for 2969 proteins. Of those quantified proteins, 39 were found to be expressed differentially (≥ 2 fold change, ≥ 2 out of 3 replicates, ≥ 10 peptides) in ^{14}N- and ^{15}N-HAB hippocampal cytosol (**Supplementary table 4**).

The correlation between hippocampal protein regulation and KEGG pathways is shown in **Figure 18**. It is clear that most of the protein population enrichments are in the intermediate bin, indicating a consistent expression level between ^{14}N- and ^{15}N-HAB. Notably, the pathway "long–term depression" is enriched with proteins from the second bin, implying differences in this pathway between ^{14}N- and ^{15}N-HAB, which is in accordance with the finding of the isotope effects on depression-like behavior.

A similar analysis was performed for GO cellular component (**Figure 19**). Several categories, such as neurofilament, synaptosome, axon, and myelin sheath—which are highly relevant to psychiatric disorders—were found to be enriched in the fourth bin, indicating a difference between ^{14}N- and ^{15}N-HAB.

The ^{14}N-HAB/^{15}N-HAB plasma comparison generated quantitative results for 788 proteins. Of these quantified proteins, 51 were found to be expressed differentially (≥ 2 fold change, ≥ 2 out of 3 replicates, ≥ 10 peptides) in ^{14}N- and ^{15}N-HAB plasma (**Supplementary table 5**).

3.3.2.6 HAB/NAB indirect comparison in cytosol and plasma

^{14}N-HAB/^{15}N-HAB and ^{14}N-HAB/^{15}N-NAB hippocampal cytosol comparisons generated quantitative results for 2969 and 2273 proteins, respectively. In total, 3376 proteins were quantified by at least one experiment; 1906 proteins were quantified by both HAB/NAB and LAB/NAB experiments and used for the subsequent HAB/LAB indirect comparison. Of these quantified proteins, 132 were found to be expressed differentially (≥ 2 fold change, ≥ 2 out of 3 replicates, ≥ 10 peptides) in HAB and NAB hippocampal cytosol (**Supplementary table 6**).

^{14}N-HAB/^{15}N-HAB and ^{14}N-HAB/^{15}N-NAB plasma comparisons generated quantitative results for 659 and 640 proteins, respectively. In total, 1090 proteins were quantified by at least one experiment; 276 proteins were quantified by both HAB/NAB and LAB/NAB experiments and used for the subsequent HAB/LAB indirect comparison. Of these

quantified proteins, 53 were found to be expressed differentially ($\geq$2 fold change, $\geq$2 out of 3 replicates, $\geq$10 peptides) in HAB and NAB plasma (**Supplementary table 7**).
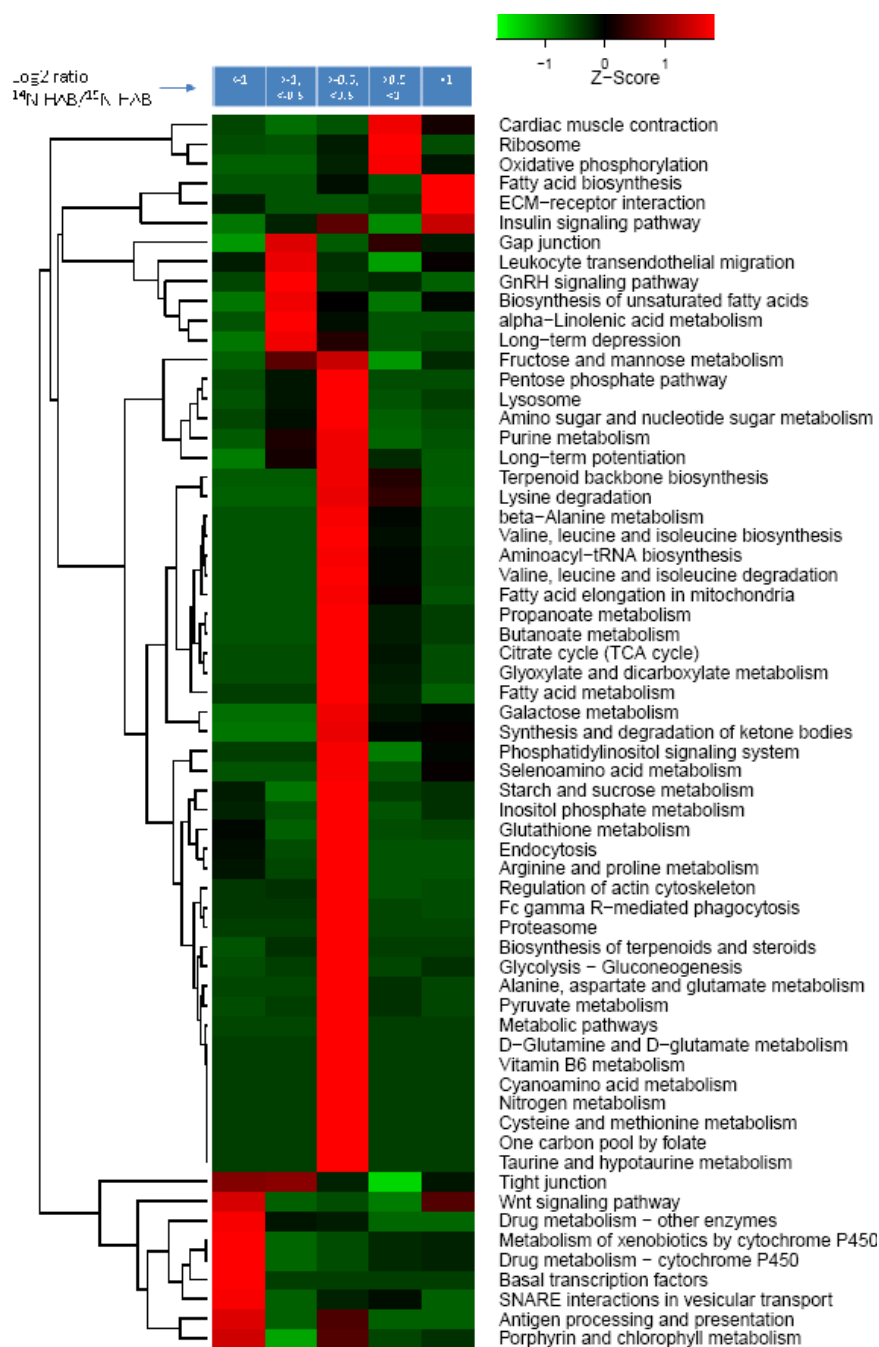

Figure 18. Correlation between hippocampal protein regulation and KEGG pathways. The blue boxes at the top show protein regulation factors between [14]N- and ^{15}N-HAB. Proteins were divided into five bins and analyzed with respect to KEGG pathways. *P* values were transformed to z-scores, indicating bin-specific enrichments. (Due to the limited resolution the pathway names on the right are not legible; higher resolution figure is available in electronic file.)
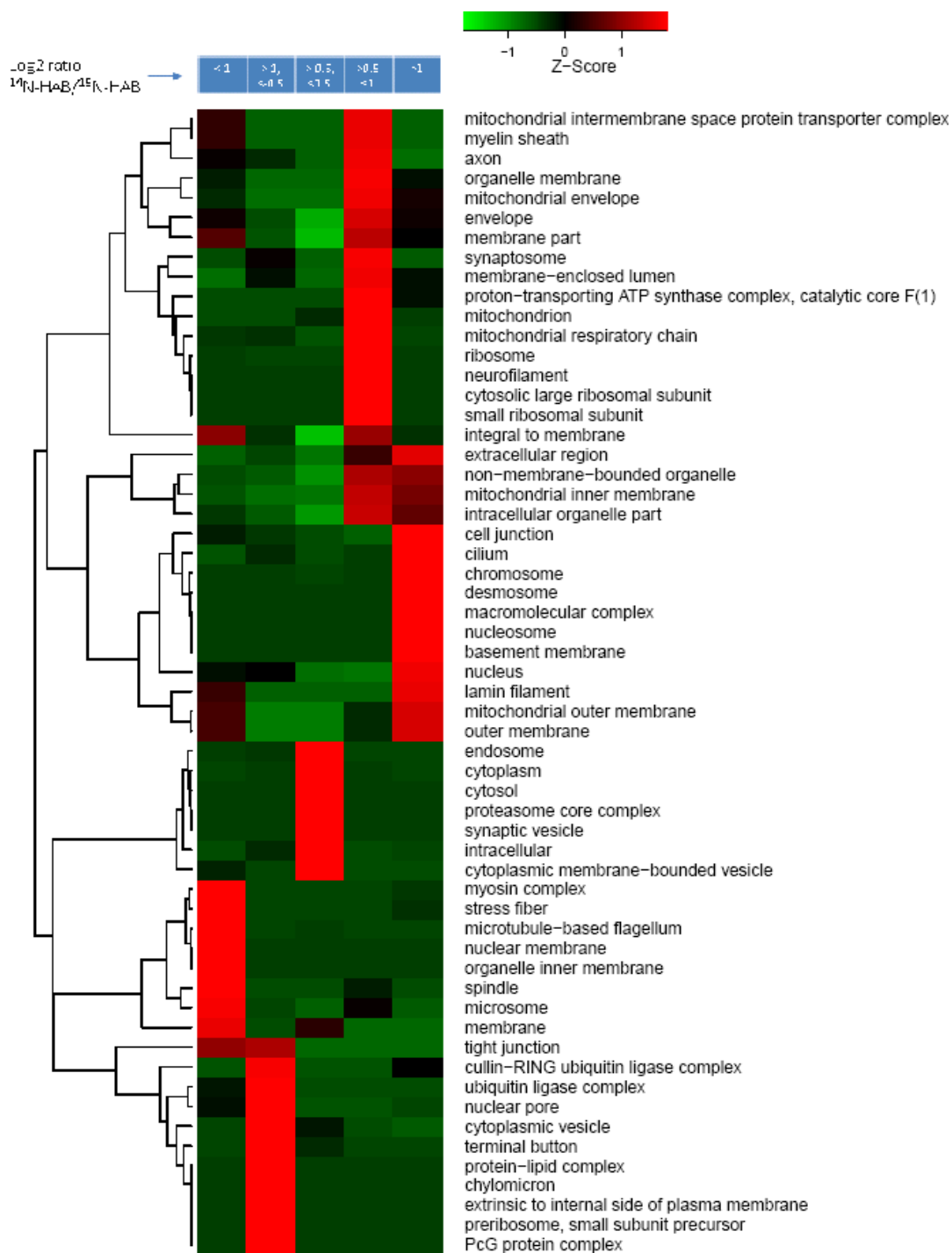
Figure 19. Correlation between hippocampal protein regulation and GO cellular component. The blue boxes at the top show protein regulation factors between [14]N- and ^{15}N-HAB. Proteins were divided into five bins and analyzed with respect to GO cellular component categories. *P* values were transformed to z-scores, indicating bin-specific enrichments. (Due to the limited resolution the category names on the right are not legible; higher resolution figure is available in electronic file.)

3.3.3 Corticosterone assay

The protein corticosteroid-binding globulin (CBG, IPI00116105) showed an expression difference between [14]N- and ^{15}N-HAB in plasma (**Figure 25**). CBG is the major transport protein for glucorticoids and progestins in the blood. Therefore, corticosterone concentrations were investigated in [14]N- and ^{15}N-HAB plasma. The free corticosterone was analyzed after filtering out binding corticosterone by ultrafiltration. The ^{15}N-HAB mice showed significantly higher total corticosterone concentrations (**Figure 20 a**, P = 0.0182) and free corticosterone concentrations (**Figure 20b**, P = 0.0271) than ^{14}N-HAB mice.
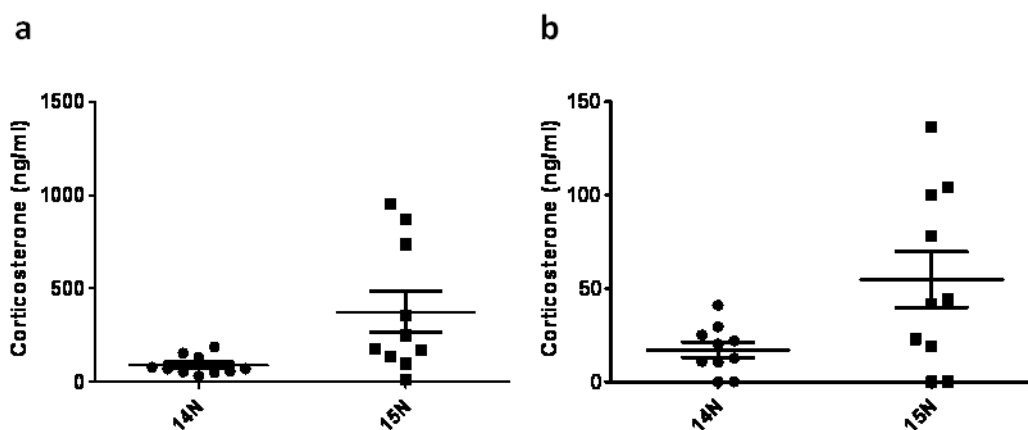
Figure 20. Plasma corticosterone assay. a: Total corticosterone concentrations in [14]N- and ^{15}N-HAB plasma; the ^{15}N mice have a significantly higher level of corticosterone than the ^{14}N mice (P =0.0182); b: Free corticosterone concentrations in [14]N- and ^{15}N-HAB plasma; the ^{15}N mice have a significantly higher level of corticosterone than the ^{14}N mice (P = 0. 0271)

3.3.4 Western blot validation

Western blot analyses were performed for several selected proteins to verify our MS-based quantitative data with a different strategy. Previous discussions (Mann, 2008) and empirical experience have indicated that the sensitivity of Western blot analysis relies largely on the specificity and reactivity of the commercial antibody. Moreover, a large number of experiments have shown that MS-based quantification in general is more sensitive than Western blot. Hence, the success rate of Western blot validation depends on the quality of the antibody, and we did not expect a 100% success rate.

3.3.4.1   ^{14}N-HAB vs. ^{15}N-HAB

3.3.4.1.1 Hippocampus

Neurofascin (IPI00329927) is an axonal member of the L1 subgroup of the immunoglobulin superfamily and is implicated in neurite extension in the course of embryonic development. The MS-based data showed a significant increase in protein expression in ^{14}N-HAB mice (**Figure 21a**). However, the findings could not be validated by Western blot analysis, i.e. the difference between ^{14}N- and ^{15}N-HAB was not found on a global level. However, if we focus only on the individual animals analyzed by mass spectrometry (marked with a star), the ^{14}N-HAB mice showed a tendency towards a higher level of neurofascin (**Figure 21b**). Besides the uncontrolled quality of the antibody, individual biological variance represents another challenge in validating MS results by Western blot.

Neurofilaments, including neurofilament heavy polypeptide (Nefh, IPI00114241), are found specifically in neurons. Some studies have shown that Nefh can impair spatial learning and neuritis (Lalonde and Strazielle, 2003; Liberski et al., 1995). The MS-based data showed a significant protein expression increase in ^{14}N-HAB mice (**Figure 22a**). However, the finding could not be validated by Western blot analysis, i.e. the difference between ^{14}N- and ^{15}N-HAB was not found on a global level. Similar to neurofascin, the individual ^{14}N-HAB animals analyzed by mass spectrometry also demonstrated a tendency towards an elevated expression of Nefh in Western blot analysis compared to the ^{15}N-HAB mice (**Figure 22b**). This protein appears also to show individual biological variance.
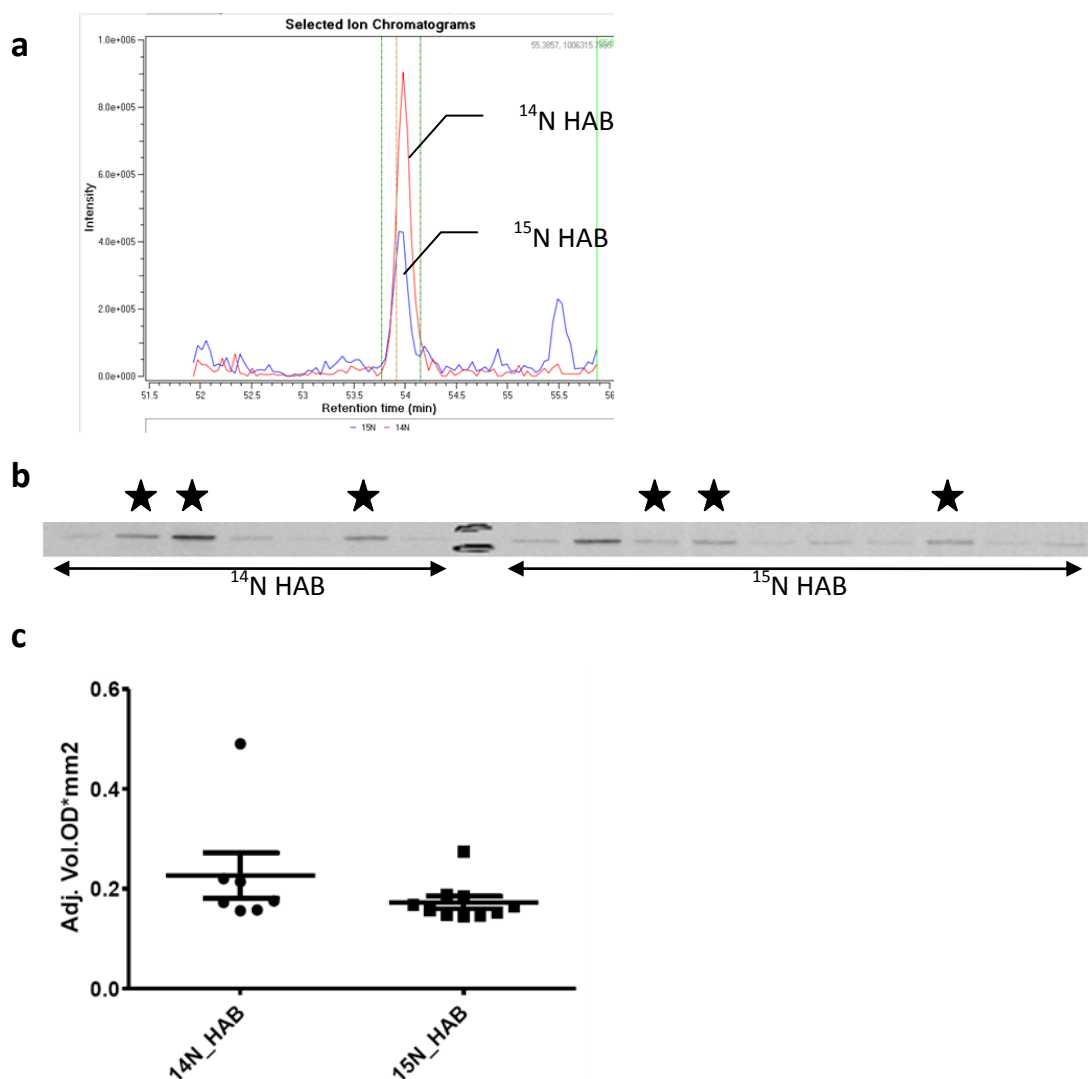
Figure 21. Quantification of ^{14}N-HAB/^{15}N-HAB neurofascin (IPI00329927) by mass spectrometry and Western blot. a: Eluted chromatographic profiles for both ^{14}N and ^{15}N tryptic peptide GPEPDTIIGYSGEDLPSAPR; the peak areas are used for the ^{14}N/^{15}N signal quantification; b: The Western blot analysis of neurofascin for ^{14}N- and ^{15}N-HAB; bands marked with a star are from the animals that were used also for MS analysis; unlabeled bands are from the animals that were analyzed only by Western blot; c: The densities of protein bands from Western blot (b) are shown; a t test was performed to compare the ^{14}N and ^{15}N groups (P = 0.1967).
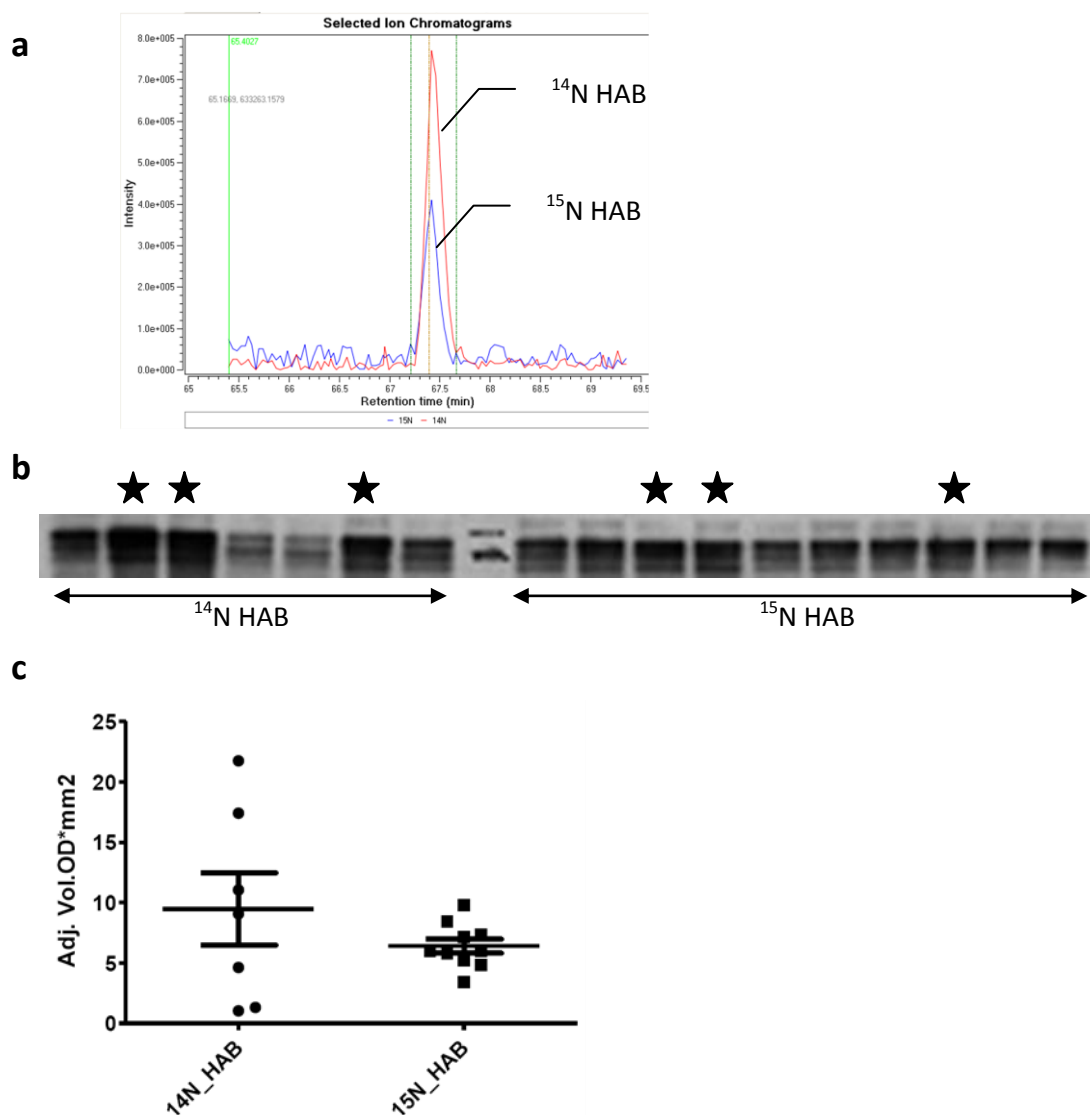
Figure 22. Quantification of ^{14}N-HAB/^{15}N-HAB neurofilament heavy polypeptide (Nefh, IPI00114241) by mass spectrometry and Western blot. a: Eluted chromatographic profiles for both ^{14}N and ^{15}N tryptic peptide HQADIASYQDAIQQLDSELR; the peak areas are used for the ^{14}N/^{15}N signal quantification; b: The Western blot analysis of Nefh for ^{14}N- and ^{15}N-HAB; bands marked with a star are from the animals that were used also for MS analysis; unlabeled bands are from animals that were analyzed only by Western blot; c: The densities of protein bands from Western blot (b) are shown; a *t* test was performed to compare the ^{14}N and ^{15}N groups (*P* = 0.2509).

3.3.4.1.2 Plasma

The endogenous function of major urinary protein 3 (MUP3, IPI00120832) within an animal is still unknown, but may involve regulating energy expenditure. The MS-based data showed a significant protein expression increase in ^{14}N-HAB mouse plasma (**Figure 23a**). The same change was also found by Western blot analysis (**Figure 23b and c**). Some other proteins from the same subfamily have also been quantified by MS and found differentially expressed between ^{14}N- and ^{15}N-HAB (MUP2, MUP4, MUP5).

Complement C5 (C5, IPI00330833) is involved in the complement system, a biochemical cascade that complements the ability of antibodies to clear pathogens from an organism. The complement system has been found to be relevant to many diseases, particularly those of the central nervous system, such as Alzheimer's disease and other neurodegenerative conditions (McGeer and McGeer, 2001; Mukherjee and Pasinetti, 2000). The MS-based data showed a significant protein expression increase in ^{14}N-HAB mouse plasma (**Figure 24a**). The same change also was found in Western blot analysis (**Figure 24b and c**). Some other proteins from the same subfamily also have been quantified by MS as proteins expressed differentially between ^{14}N- and ^{15}N-HAB, including C6, C8, and C9.

Corticosteroid-binding globulin (CBG, IPI00116105) is the major transport protein for glucocorticoids and progestins in the blood of almost all vertebrate species. CBG and glucocorticoids have been found to be relevant to psychiatric diseases (de Kloet et al., 2007; Maes et al., 1996). The MS-based data showed a significant protein expression increase in ^{15}N-HAB mouse plasma (**Figure 25a**). The same change also was found in Western blot analysis (**Figure 25b and c**).

a

b

c
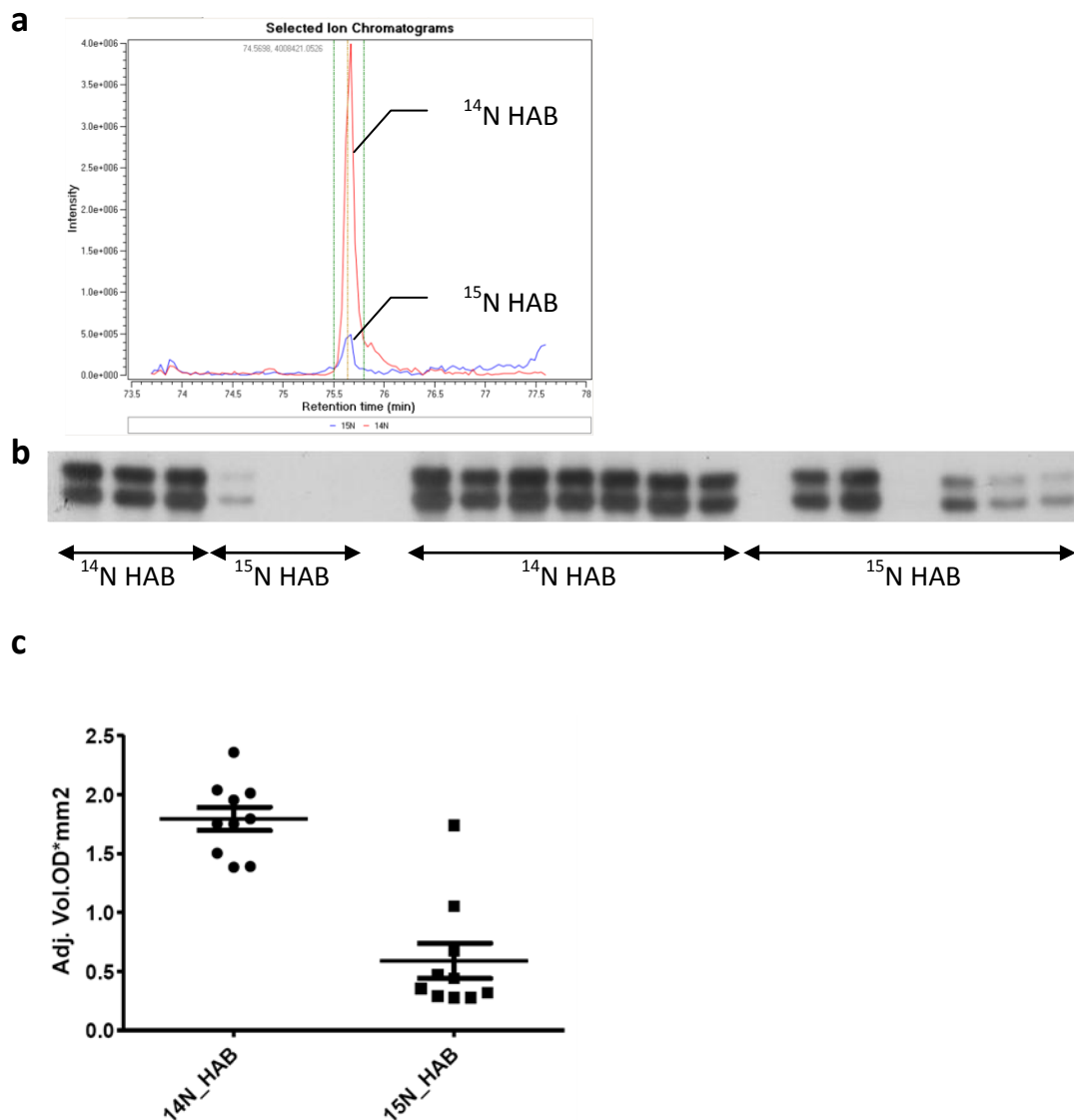
Figure 23. Quantification of ^{14}N-HAB/^{15}N-HAB major urinary protein 3 (MUP3, IPI00120832) by mass spectrometry and Western blot. a: Eluted chromatographic profiles for both ^{14}N and ^{15}N tryptic peptide AGIYYMNYDGFNTFSILK; the peak areas are used for the ^{14}N/^{15}N signal quantification; b: The Western blot analysis of MUP3 for ^{14}N HAB and ^{15}N HAB; c: The densities of protein bands from Western blot (b) are shown; a *t* test was performed between the ^{14}N and ^{15}N groups ($P < 0.0001$).

a

b

c
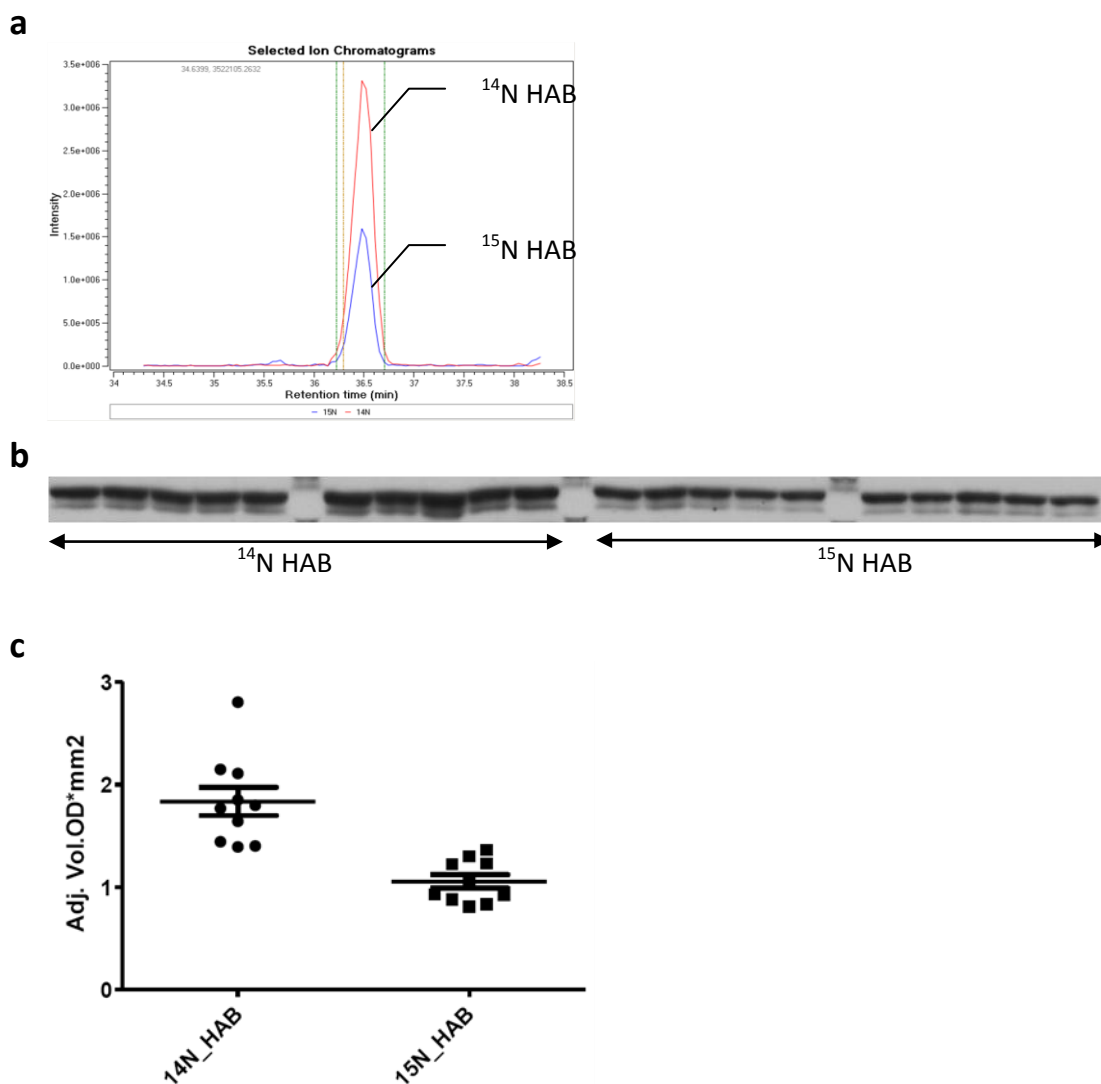
Figure 24. Quantification of ^{14}N-HAB/^{15}N-HAB complement C5 (C5, IPI00330833) by mass spectrometry and Western blot. a: Eluted chromatographic profiles for both ^{14}N and ^{15}N tryptic peptide TDDPELPEENQASK; the peak areas are used for the ^{14}N/^{15}N signal quantification; b: The Western blot analysis of C5 for ^{14}N-HAB and ^{15}N-HAB; c: The densities of protein bands from Western blot (b) are shown; a *t* test was performed between the ^{14}N and ^{15}N groups (*P* < 0.0001).

a

b

c
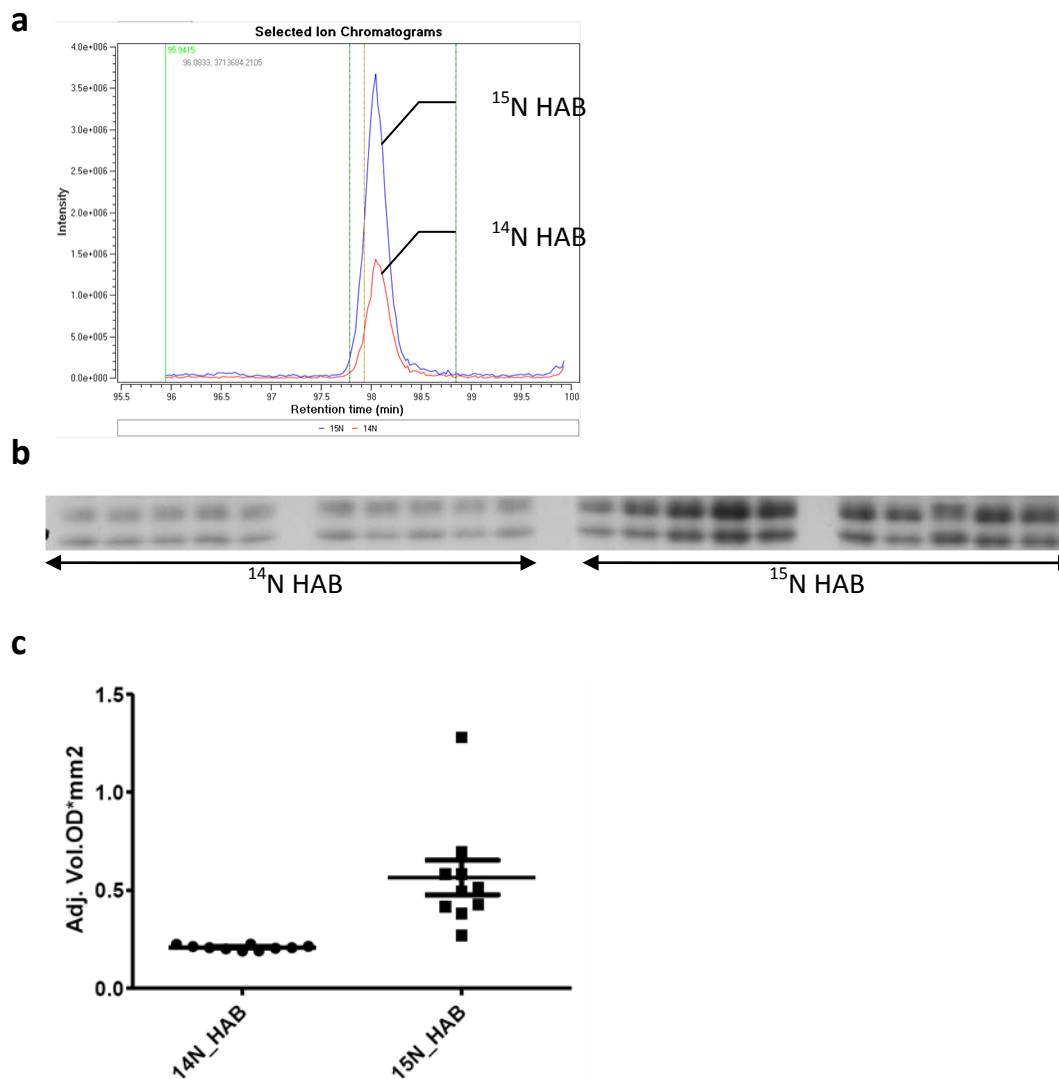
Figure 25. Quantification of ^{14}N-HAB/^{15}N-HAB corticosteroid-binding globulin (CBG, IPI00116105) by using mass spectrometry and Western blot. a: Eluted chromatographic profiles for both ^{14}N and ^{15}N tryptic peptide NTLISPVSISMALAMLSLSTR; the peak areas are used for the ^{14}N/^{15}N signal quantification; b: The Western blot analysis of CBG for ^{14}N-HAB and ^{15}N-HAB; c: The densities of protein bands from Western blot (b) are shown; a t-test was performed between the ^{14}N and ^{15}N groups (P=0.0007).

3.3.4.2   HAB vs. LAB indirect comparison

3.3.4.2.1   Hippocampus

Several proteins (Transthyretin, Myosin, Carbonic anhydrase 2) that showed expression differences in the HAB/LAB hippocampal comparison were chosen for the Western blot analyses.

Transthyretin (TTR, IPI00127560) is a serum and cerebrospinal fluid carrier of the thyroid hormone thyroxine (T4) and retinol. TTR has been reported previously to play important roles in both depressed patients (Sullivan et al., 1999) and suicide attempters (Schultz et al., 2008). In this HAB/LAB indirect comparison using MS data, HAB mice showed a higher expression level of TTR than LAB mice (**Figure 26a and b**). The same difference was found in Western blot analysis (**Figure 26c and d**), confirming the MS-based quantitative result.

Myosin, heavy polypeptide 10 (Myh10, IPI00338604), is a member of the myosin family, a family of mostly motor proteins found in eukaryotic tissues. An earlier study showed that myosin can be controlled indirectly by excess glucocorticoids (Fukumoto et al., 2009), which are one of the main mediators of the stress reaction in the HPA axis. In this HAB/LAB indirect comparison using MS data, HAB mice showed a lower expression level of Myh10 than NAB mice (**Figure 27a and b**). The same difference was found in Western blot analysis (**Figure 27c and d**), confirming the MS-based quantitative result. However, the LAB/NAB comparison could not be validated by Western blot.
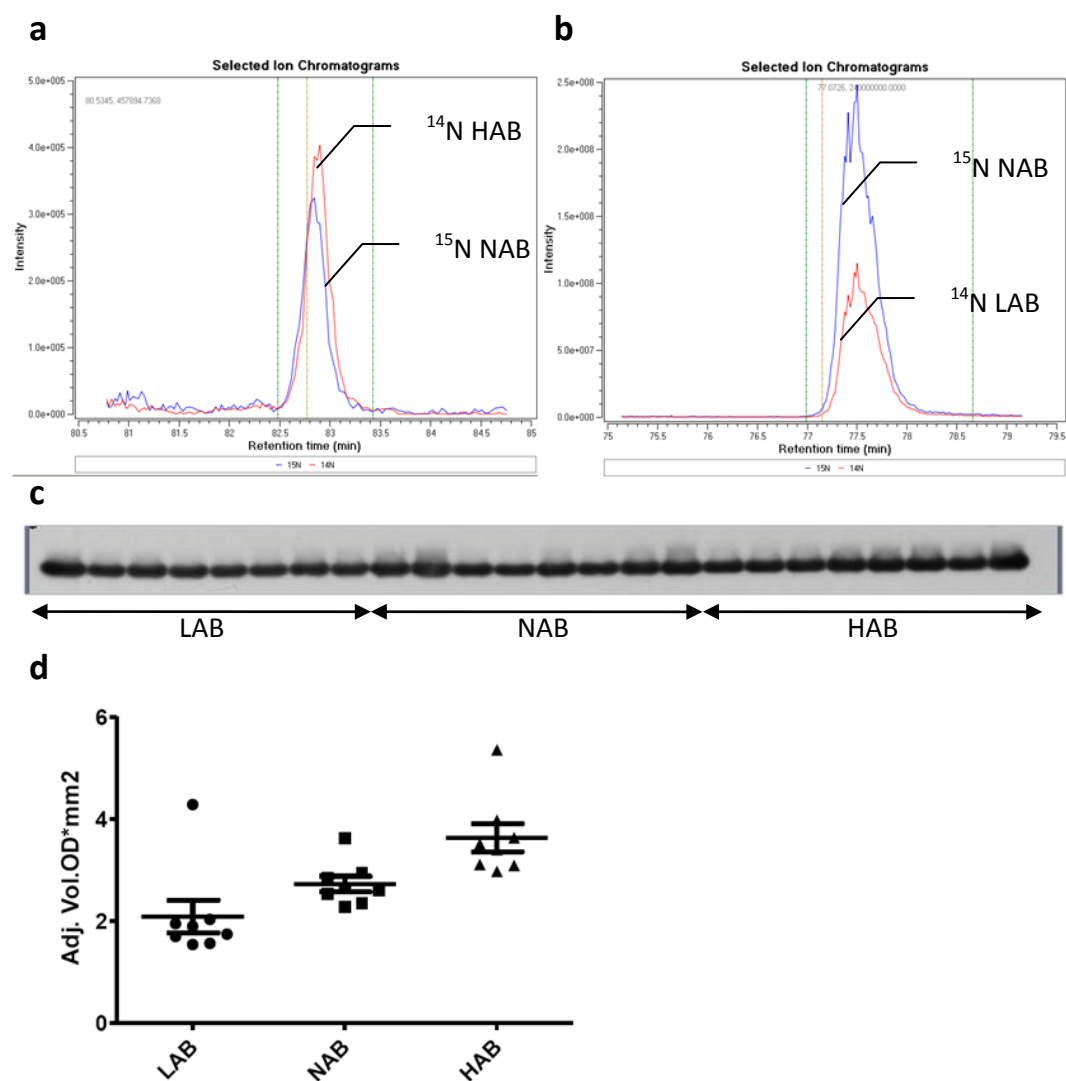
Carbonic anhydrase 2 (CA2, IPI00121534) catalyses the hydration of CO_2 and the hydrolysis of esters. Complete absence of CA2 leads to mild mental retardation, cerebral calcification, osteoporosis, and renal tubular acidosis. For example, the inhibitor of carbonic anhydrase, topiramate, has been used to treat bipolar disorder, and topiramate often is used to augment psychotropics or to counteract the weight gain associated with numerous antidepressants (Arnone, 2005). In this HAB/LAB indirect comparison using MS data, HAB mice showed a higher expression level of CA2 than LAB mice (**Figure 28a and b**). The same difference was found in Western blot analysis (**Figure 28c and d**), confirming the MS-based quantitative result.
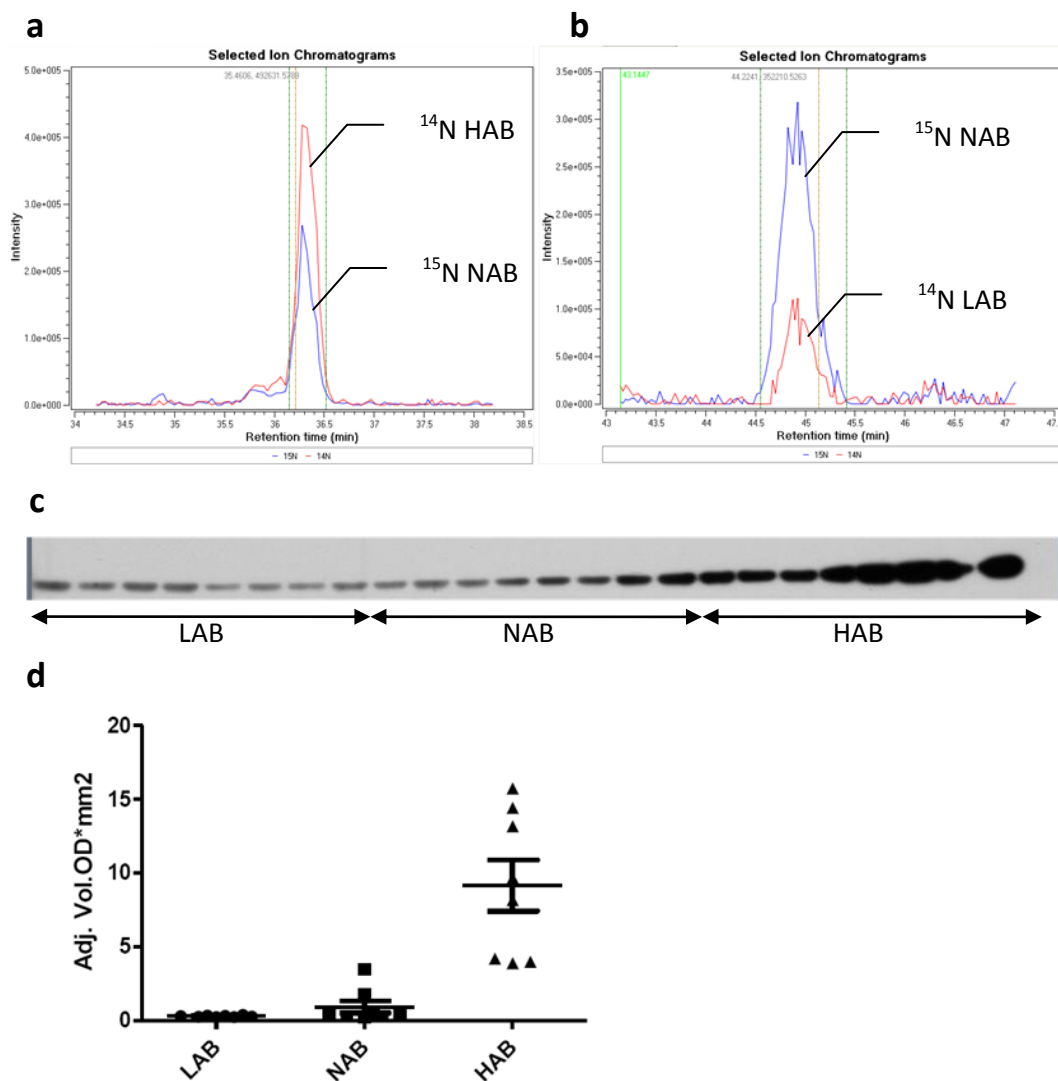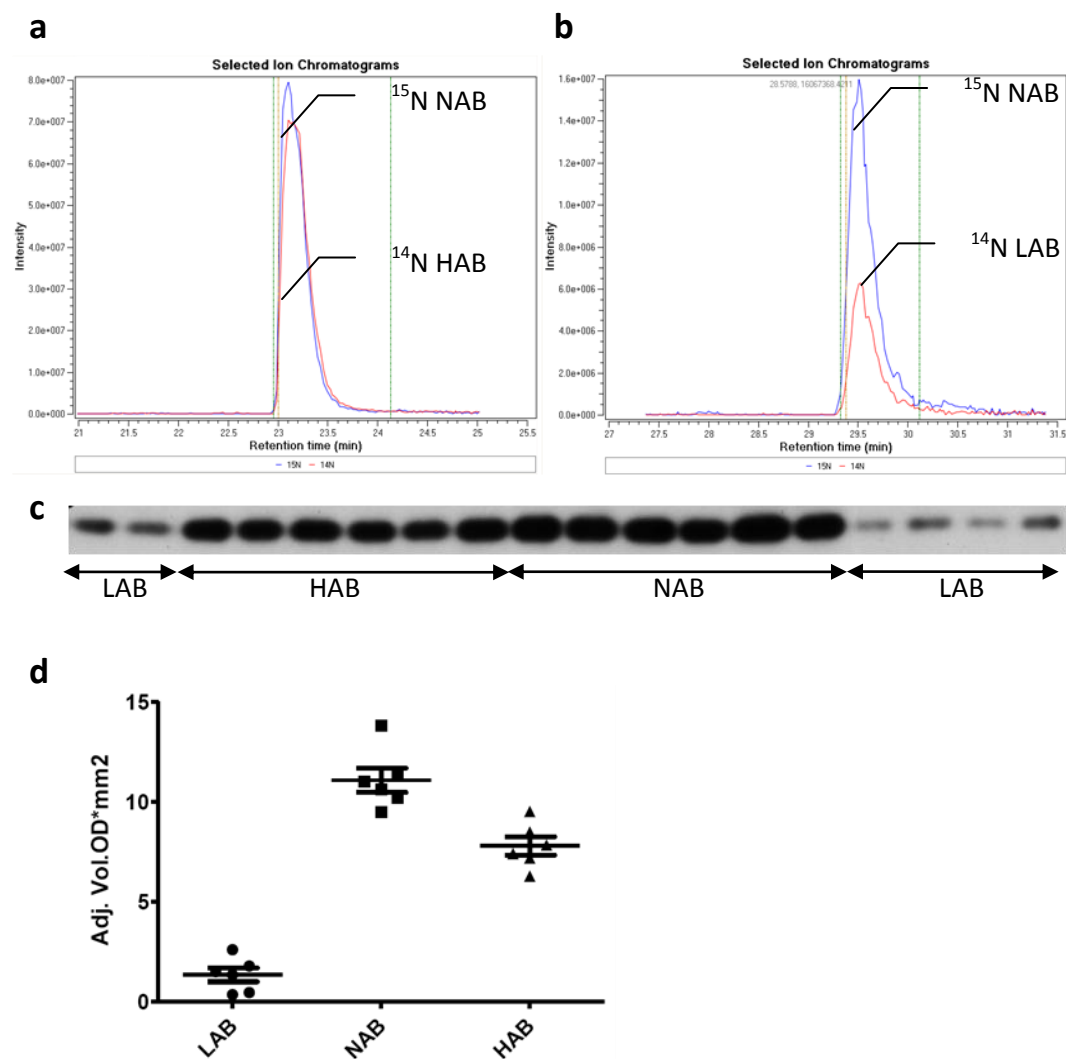
Figure 26. Quantification of HAB/LAB transthyretin (TTR, IPI00127560) by mass spectrometry and Western blot. a: Eluted chromatographic profiles for both ^{14}N-HAB and ^{15}N-NAB tryptic peptide TSEGSWEPFASGK; b: Eluted chromatographic profiles for both ^{14}N-LAB and ^{15}N-NAB tryptic peptide TSEGSWEPFASGK; the peak areas are used for the ^{14}N/^{15}N signal quantification; c: The Western blot analysis of TTR for HAB, LAB, NAB; d: The densities of protein bands from Western blot (c) are shown; a *t* test was performed between groups (LAB vs. HAB: *P* = 0.0002; NAB vs. HAB: *P* = 0.0004)
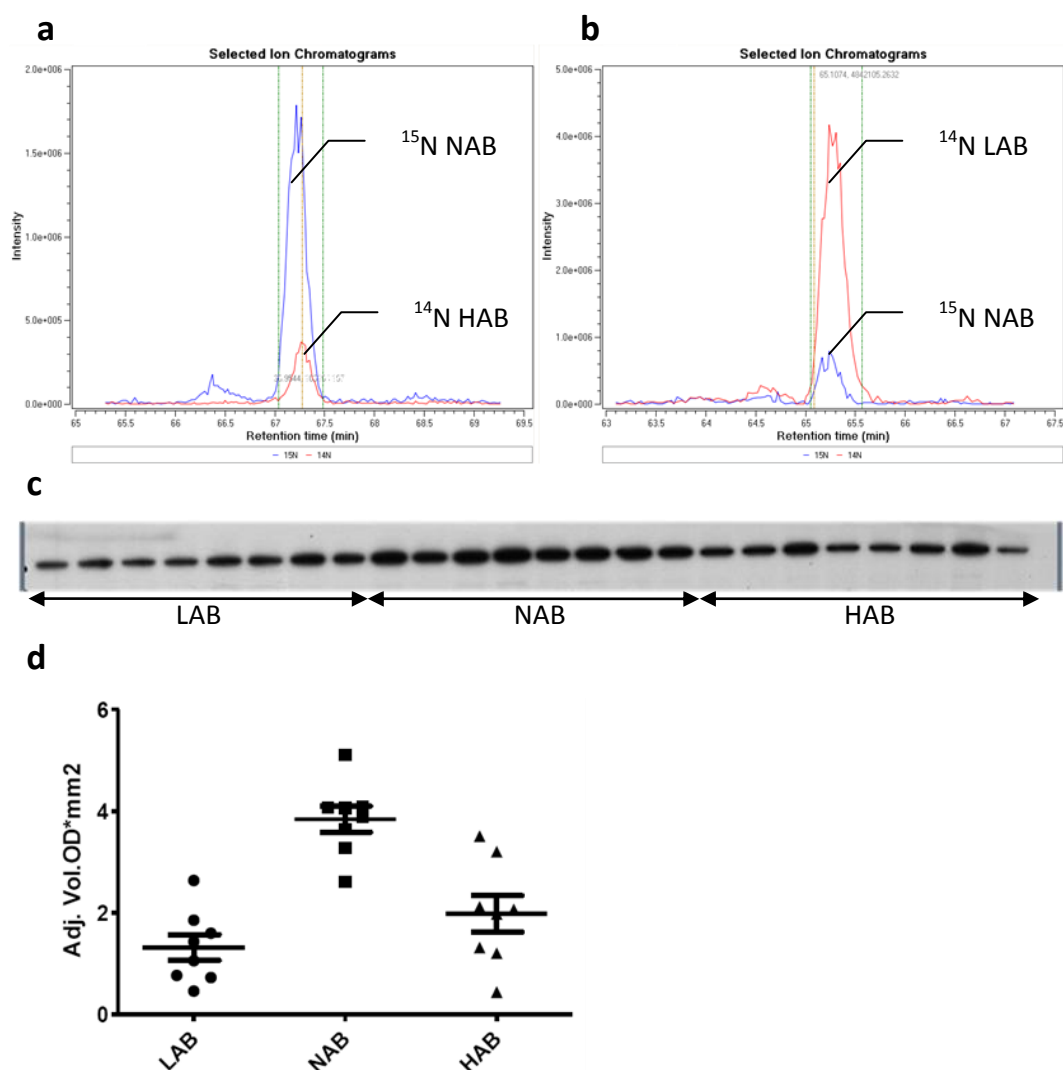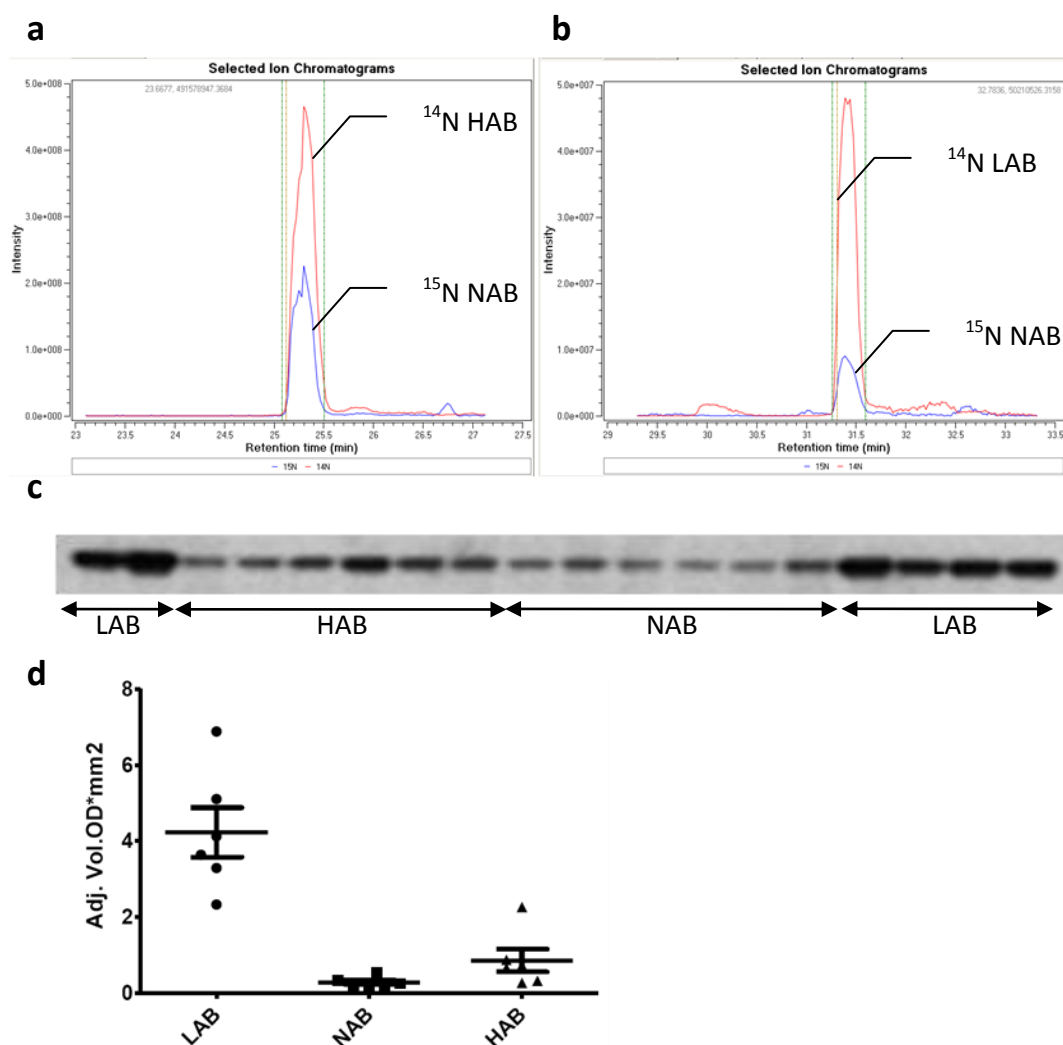
Figure 27. Quantification of HAB/LAB Myosin, heavy polypeptide 10 (Myh10, IPI00338604), by mass spectrometry and Western blot. a: Eluted chromatographic profiles for both ^{14}N-HAB and ^{15}N-NAB tryptic peptide DAAGLESQLQDTQELLQEETR; b: Eluted chromatographic profiles for both ^{14}N-LAB and ^{15}N-NAB tryptic peptide DAAGLESQLQDTQELLQEETR; the peak areas are used for the ^{14}N/^{15}N signal quantification; c: The Western blot analysis of Myh10 for HAB, LAB, NAB; d: The densities of protein bands from Western blot (c) are shown; a *t* test was performed between groups (NAB vs. HAB: *P* = 0.0009).

Figure 28. Quantification of HAB/LAB carbonic anhydrase 2 (CA2, IPI00121534) by mass spectrometry and Western blot. a: Eluted chromatographic profiles for both ^{14}N-HAB and ^{15}N-NAB tryptic peptide AVQQPDGLAVLGIFLK; b: Eluted chromatographic profiles for both ^{14}N-LAB and ^{15}N-NAB tryptic peptide AVQQPDGLAVLGIFLK; the peak areas are used for the ^{14}N/^{15}N signal quantification; c: The Western blot analysis of CA2 for HAB, LAB, NA;. d: The densities of protein bands from Western blot (c) are shown; a *t* test was performed between groups (LAB vs. HAB: $P = 0.0025$; NAB vs. HAB: $P = 0.0114$).

3.3.4.2.2   Plasma

As mentioned above, transthyretin (TTR, IPI00127560) is a serum and cerebrospinal fluid carrier of the thyroid hormone thyroxine (T4) and retinol. TTR is one of a few proteins found to be expressed differentially between HAB and LAB mice in both brain and plasma. In this HAB/LAB indirect comparison using MS data, HAB mice showed a higher expression level of TTR than LAB mice (**Figure 29a and b**). The same difference was found in Western blot analysis (**Figure 29c and d**) confirming the MS-based quantitative result.

Serum amyloid P-component (SAP, IPI00309214) is a normal plasma constituent that has been found to be a biomarker for mild cognitive impairment and Alzheimer's disease (Nishiyama et al., 1996; Verwey et al., 2008; Yasojima et al., 2000). In this HAB/LAB indirect comparison using MS data, LAB mice showed a higher expression level of SAP than HAB mice (**Figure 30a and b**). The same difference was found in Western blot analysis (**Figure 30c and d**), confirming the MS-based quantitative result.

Figure 29. Quantification of HAB/LAB transthyretin (TTR, IPI00127560) by mass spectrometry and Western blot. a: Eluted chromatographic profiles for both ^{14}N-HAB and ^{15}N-NAB peptide tryptic TAESGELHGLTTDEK; b: Eluted chromatographic profiles for both ^{14}N-LAB and ^{15}N-NAB tryptic peptide TAESGELHGLTTDEK; the peak areas are used for the ^{14}N/^{15}N signal quantification; c: The Western blot analysis of TTR for HAB, LAB, NAB; d: The densities of protein bands from Western blot (c) are shown; a *t* test was performed between groups (LAB vs. NAB: *P* < 0.0001; LAB vs. HAB: *P* < 0.0001; NAB vs. HAB: *P* = 0.0015)

Figure 30. Quantification of HAB/LAB Serum amyloid P-component (SAP, IPI00309214) by mass spectrometry and Western blot. a: Eluted chromatographic profiles for both ^{14}N-HAB and ^{15}N-NAB tryptic peptide GRDNELLIYKEK; b: Eluted chromatographic profiles for both ^{14}N-LAB and ^{15}N-NAB tryptic peptide GRDNELLIYKEK; the peak areas are used for the ^{14}N/^{15}N signal quantification; c: The Western blot analysis of SAP for HAB, LAB, NAB; d: The densities of protein bands from Western blot (c) are shown; a *t* test was performed between groups (LAB vs. NAB: *P* = 0.0001; LAB vs. HAB: *P* = 0.0008)

3.3.5 Metabolomics

The data presented in this thesis kindly were analyzed by the 'Metabolomics Core' of the University of California, Davis, CA, USA (Dr. Vladimir Tolstikov). The results concerning the technical platform are presented with permission from Dr. Vladimir Tolstikov.

3.3.5.1 Data processing

GC-TOF-MS data were annotated prior to further analysis (Scholz and Fiehn, 2007). The GC-MS annotation procedure was automated and the data output generated as an Excel table (Scholz and Fiehn, 2007). Initial GC-TOF-MS peak detection and mass spectrum deconvolution were performed with ChromaTOF software (version 2.25, Leco). A reference chromatogram was defined that had a maximum of detected peaks over a signal/noise threshold of 20. This reference chromatogram was used for automated peak identification by means of mass spectral comparison to a standard NIST 05 library and in-house customized mass spectral libraries. Analytes spectra were searched against custom spectrum libraries and identified on the basis of the retention index and spectrum similarity match. A mixture of the retention time standards n-dodecane (RI 1,200), n-pentadecane (RI 1,500), n-nonadecane (RI 1,900), n-docosane (RI 2,200), n-octacosane (RI 2,800), n-dotriacontane (RI 3,200), and n-hexatriacontane (RI 3,600) was included in the final reagent volume (Wagner et al., 2003). Automated assignments of unique fragment ions for each individual metabolite were chosen as quantifiers and corrected manually where necessary. Relative quantification was performed on quantifiers with optimal selectivity. All known artifact peaks caused by column bleeding or phthalates and polysiloxanes derived from MSTFA hydrolysis were identified manually and removed from the results table. Since the purposes of the described studies were mainly clustering, classification, and prediction, metabolite annotation and identification were not required prior to data mining.

GC-TOF-MS datasets were used after annotation. It is very important to search for and eliminate correlated variables introduced during sample preparation or as a result of the analytical methods, or both, especially for values close to the margins of measurements like overload, limits of detection, and background noise levels. Close proximity to these factors easily can generate false positive values characterized by a convincing P value that may not reflect the actual situation but rather the absence of the particular variable, which is not detected in a sample, or group of samples, since its level is below the current lower limit of detection of the instrument or method. When a biological question is

related to the highest variance in a dataset, PCA is a powerful technique to reduce, visualize, and explore dimensionality.

Visualization methods often are the best way to discover interesting grouping information in data, whereas clustering methods provide mathematical rigor. Basically, there are three major categories of clustering methods: partitioning (clusters), hierarchical (trees), or probability model based (models). Partitioning methods map peaks into multiple disjointed clusters using a chosen criterion. K-means is the most popular partitioning method, although it requires the input of an initial clustering number. The K-means clustering algorithm chooses a pre-specified number of cluster centers to minimize the within-class sum of squares from those centers. Hierarchical methods construct a binary tree in which the root is a single cluster containing only one element and the leaves each contain only one element. A divisive tree is built top-down, and an agglomerative tree bottom-up. Recently, with the advances in methods, software, and interpretability of the results, probability model-based clustering methods have become increasingly popular. Probability modeling assumes that the data pool is a mixture with all of the labels lost and tries to find the most probable label for each data point.

3.3.5.2   Plasma

By using the strategy described previously, in mouse plasma 273 metabolites were detected, of which 94 compounds with a known chemical structure were identified. Concentrations of 31 known metabolites differed significantly ($P < 0.05$) between mouse lines (**Table 2**). For instance, the concentration of cholesterol in HAB plasma was much higher than in NAB and LAB plasma (**Figure 31**). Another metabolite that deserves attention is inositol. The HAB mice showed a higher level only for allo-inositol and not for other stereoisomers, such as myo-inositol (**Figure 32**). The PCA plots showed significant clustering and differentiation among groups (**Figure 33**).

Table 2. Metabolite level comparisons ($P < 0.05$) in plasma between three mouse lines

| Metabolites	P values		
	HAB vs. LAB	HAB vs. NAB	LAB vs. NAB
Threonic acid	0.003	0.040	0.968
Pseudo uridine	0.002	0.688	0.001
Malate	0.046	0.817	0.090
Lysine	0.034	0.248	0.397
Inositol myo-	0.002	0.785	0.005

|			
Inositol allo-	0.045	0.079	0.864
Indole-3-lactate	0.026	0.246	0.103
Glutamic acid	0.000	0.299	0.004
Fumaric acid	0.043	0.822	0.066
Cholesterol	0.035	0.000	0.166
Alanine	0.009	0.012	0.544
3-hydroxypropionic acid	0.045	0.008	0.370
3-hydroxy-3-methylglutaric acid	0.042	0.094	0.447
Uric acid	0.180	0.110	0.012
Tocopherol alpha	0.877	0.034	0.018
Ornithine 4TMS	0.085	0.285	0.033
Hydroxycarbamate	0.107	0.684	0.046
Fructose 2	0.118	0.430	0.014
Fructose 1	0.149	0.501	0.026
Arabitol	0.223	0.207	0.023
3,6-anhydrogalactose	0.992	0.057	0.023
Valine	0.515	0.043	0.179
Taurine	0.583	0.041	0.115
Serine	0.357	0.027	0.395
Pelargonic acid	0.516	0.045	0.208
Methionine	0.118	0.003	0.215
Leucine	0.368	0.029	0.192
Isoleucine	0.707	0.037	0.096
Glycine	0.495	0.029	0.098
Ethanolamine	0.698	0.023	0.280
1-monoolein	0.112	0.020	0.880
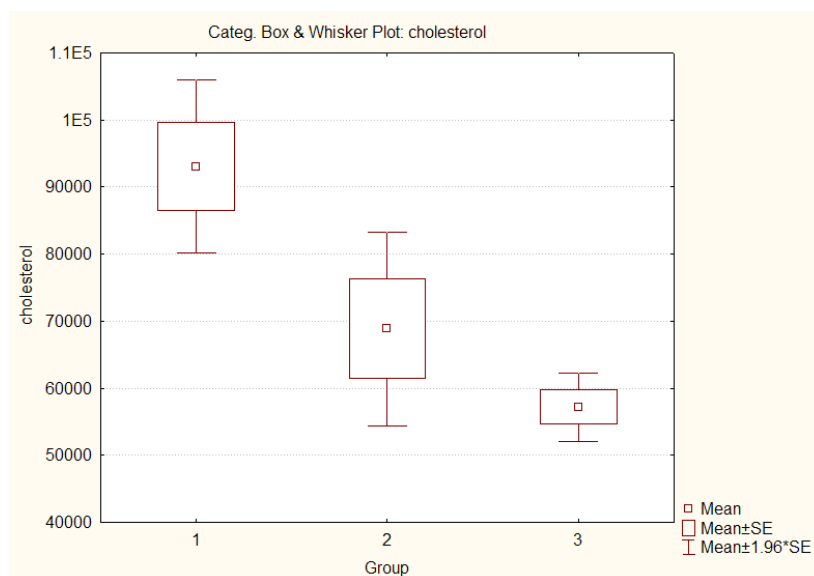
Figure 31. Variation of plasma cholesterol levels in the three mouse lines: 1,HAB; 2,LAB; 3,NAB.

a

b
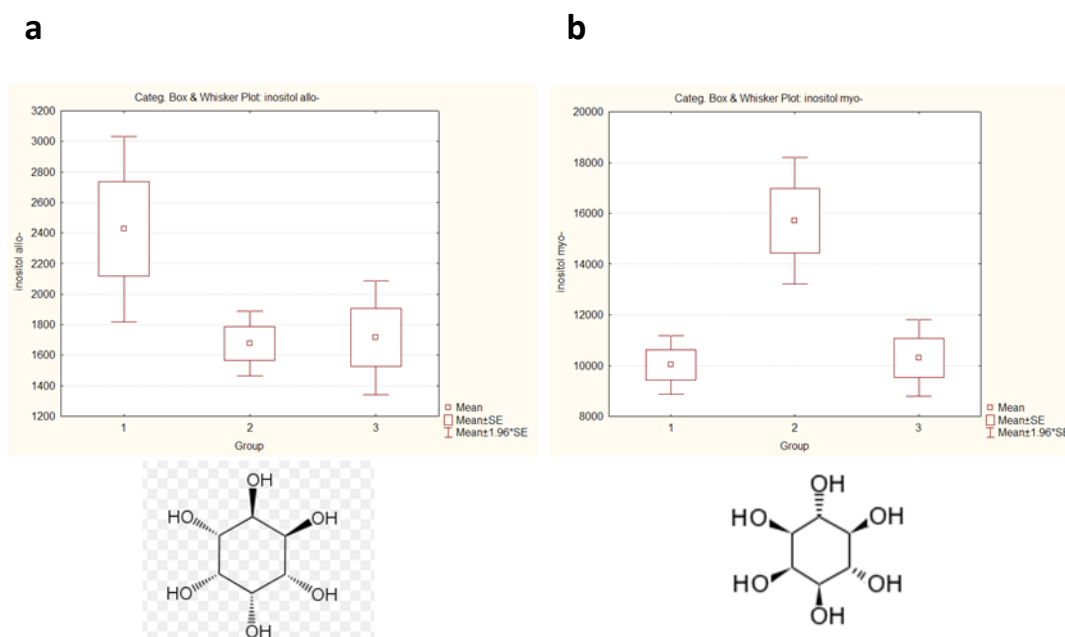
Figure 32. Variation of plasma inositol levels in the three mouse strains: 1,HAB; 2,LAB; 3,NAB. a: allo-inositol stereoisomer; b: myo-inositol stereoisomer
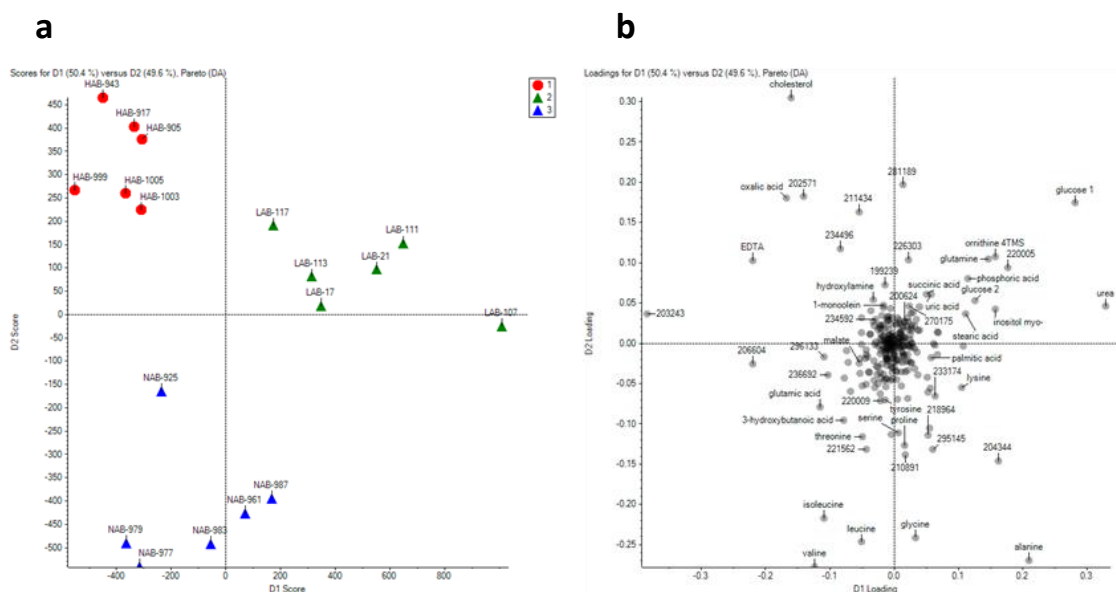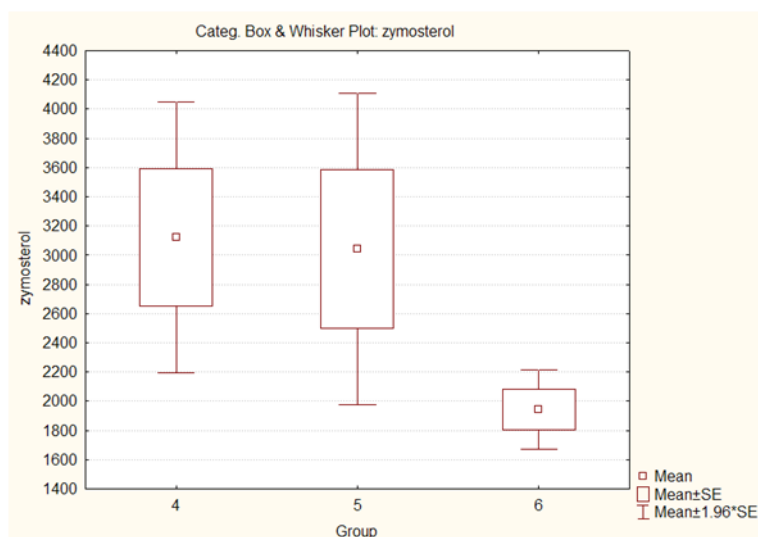
Figure 33. PCA-DA scores and loading plots of the HAB, NAB, and LAB plasma metabolites. GC-TOF-MS data. a: Groups (HAB, NAB, LAB) are color coded as: 1, red: HAB; 2, green: LAB; 3, blue: NAB; the software MarkerView 1.0 was used; b: Loading plot showing resolved metabolites, annotated by BinBase (Scholz and Fiehn, 2007); chemical names are given for known metabolites; unidentified ones are labeled with numbers. (Due to the limited resolution the metabolite names are not legible; higher resolution figure is available in electronic file.)

3.3.5.3   Hippocampus

By applying our strategy to mouse hippocampi, 281 metabolites were detected, 129 of which were identified as having a known chemical structure. Concentrations of 14 known metabolites differed significantly ($P < 0.05$) between mouse lines (**Table 3**). For instance, the concentration of zymosterol, a cholesterol intermediate, was much higher in HAB brain than in LAB brain (**Figure 34**). The PCA plots showed significant clustering and differentiation among groups (**Figure 35**).

Table 3. Metabolite level comparisons ($P < 0.05$) in hippocampi of the three mouse lines

Metabolites	P-values		
	HAB vs. LAB	HAB vs. NAB	LAB vs. NAB
1,2,4-benzenetriol	0.775	0.009	0.274
2-hydroxybutanoic acid	0.032	0.756	0.007
Dehydroascorbate 1	0.123	0.000	0.162
Dehydroascorbate 3	0.132	0.000	0.186
Ethanolamine	0.804	0.010	0.121
FAD	0.128	0.001	0.389
Fucose 1 + rhamnose 2	0.019	0.009	0.217
Glycerol-beta-phosphate	0.365	0.012	0.143
Inosine	0.128	0.556	0.042
Palmitic acid butyl ester NIST	0.653	0.050	0.185
Palmitoleic acid	0.101	0.046	0.573
Threonic acid	0.067	0.048	0.269
Xylose 1	0.297	0.008	0.327
Zymosterol	0.914	0.038	0.079

Figure 34. Variation of hippocampal zymosterol levels in the three mouse strains: 1,HAB; 2,LAB; 3,NAB.
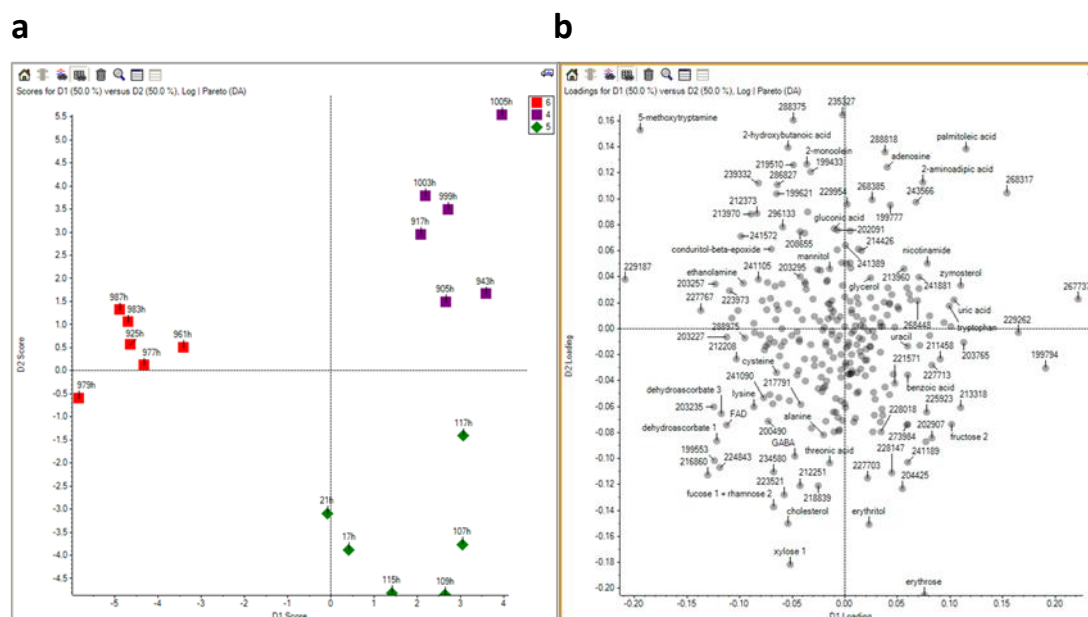
Figure 35. PCA-DA score and loading plots of the HAB, NAB, LAB hippocampal metabolites. GC-TOF-MS data. a: Groups (HAB, NAB, LAB) are color coded as: 4, purple: HAB; 5, green: LAB; 6, red: NAB; the software MarkerView 1.0 was used; b: Loading plot showing resolved metabolites, annotated by BinBase (Scholz and Fiehn, 2007); chemical names are given for known metabolites ; unidentified ones are labeled with numbers. (Due to the limited resolution the metabolite names are not legible; higher resolution figure is available in electronic file.)
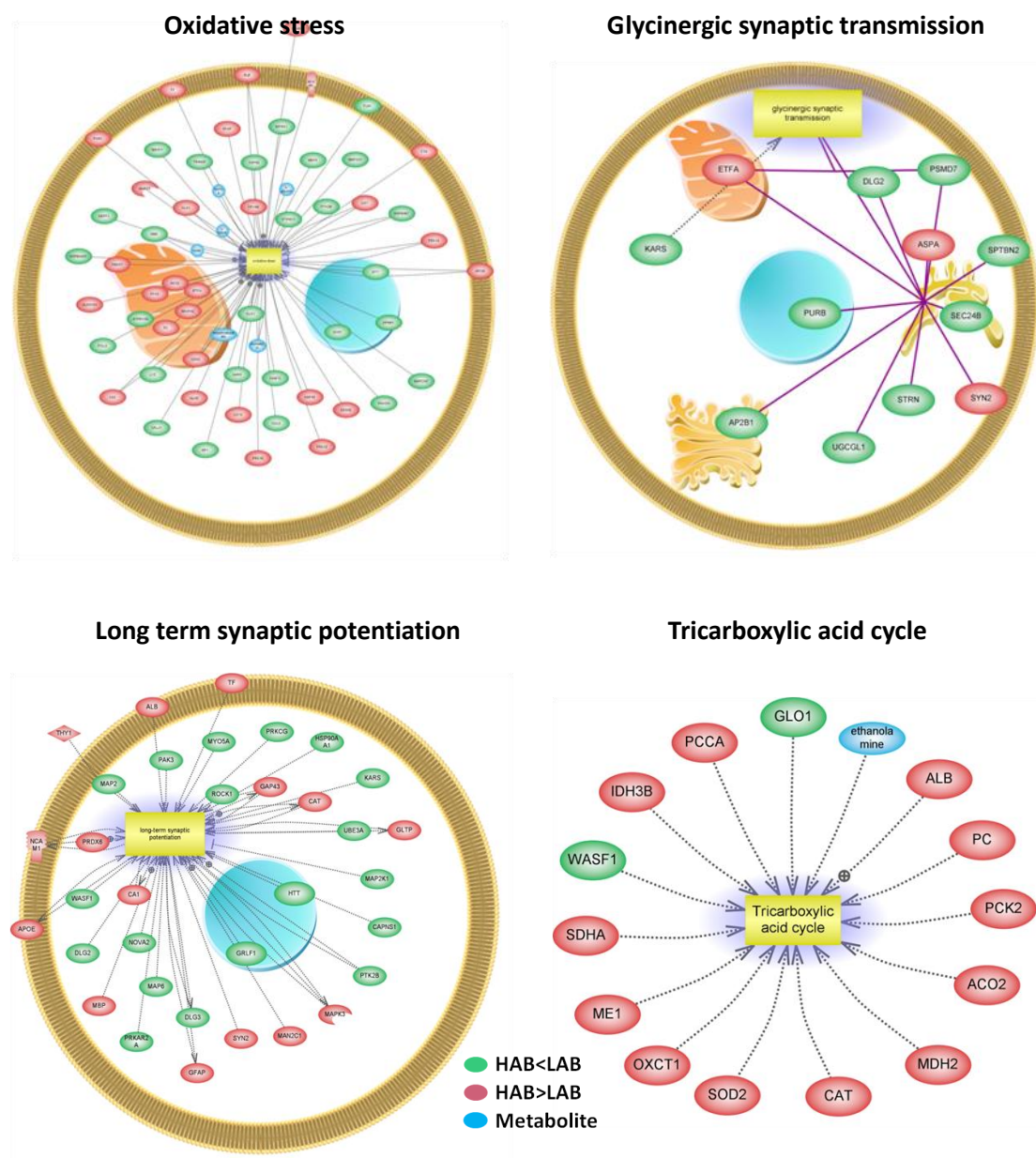
3.3.6 Pathway analysis

The differentially expressed proteins and metabolites quantified from HAB/LAB/NAB mice as biomarker candidates were used to generate interaction maps with the Pathway Studio software. The proteins and metabolites were grouped on the basis of the Ariadne pathways, ontology (software built-in), GO cellular component, molecular function, and biological process. The *P* value of each biological event was calculated to assess the entity enrichment. Furthermore, sub-networks were created on the basis of the different target and interaction types. The enrichments also were assessed for statistical significance. Some of the top enriched categories are listed in **Tables 4-11**. Several well-known biological processes that may contribute to psychiatric disorders demonstrated high entity enrichments, such as oxidative stress, tricarboxylic acid cycle, glycinergic synaptic transmission, and long-term synaptic potentiation (LTP) (**Figure 36**). LTP is a critical neural process that likely underlies learning and memory formation (Bliss and Collingridge, 1993; Cooke and Bliss, 2006) and was another promising finding in this study. LTP has been well

studied in neurodegenerative diseases, such as Alzheimer's disease (Rowan et al., 2003). It also has been found to influence anxiety (Marsch et al., 2007; Walther et al., 1998).

Ariadne pathway and ontology analyses revealed several pathways that are significantly enriched with proteins and metabolites expressed differentially between animal lines (**Table 4-5**). These pathways may provide new insights into disease pathobiology. The tricarboxylic acid cycle (TCA cycle) showed a high entity enrichment in both the Ariadne Metabolic Pathways and ontology (**Table 4-5**) analyses. Twenty-five percent of the total ontology entities involved in the TCA cycle were found to be differentially expressed between the three mouse lines (**Table 5, Figure 36d**), indicating an important role of energy metabolism in anxiety.

The notch pathway resulting from the Ariadne Signaling Pathways demonstrated a high entity enrichment (**Table 6**), implying its potential function in psychiatric disorders. The Notch signaling pathway is a highly conserved cell-signaling system present in most multicellular organisms (Artavanis-Tsakonas et al., 1999) and is very important for cell-cell communication as well as neuronal function (Gaiano and Fishell, 2002) and many diseases (Radtke et al., 2010; Tao et al., 2010). Some other pathways or ontologies, such as axon guidance, also have been found potentially to be involved in anxiety (**Table 6**).

Oxidative stress

Glycinergic synaptic transmission

Long term synaptic potentiation

Tricarboxylic acid cycle

● HAB<LAB
● HAB>LAB
● Metabolite

Figure 36. Pathways enriched with proteins and metabolites. (Due to the limited resolution the protein/metabolite names are not legible; higher resolution figure is available in electronic file)

Table 4. Ariadne metabolic pathways with P < 0.05

Name	Number of Entities	Percent Overlap	P value
Tricarboxylic acid cycle	69	15	8.16E-06
Branched chain amino acids metabolism	127	11	3.68E-05
Serine and glycine metabolism	95	9	2.99E-03
Ser/Gly/Thr/Cys metabolism	183	6	1.29E-02
Folate biosynthesis	73	8	2.85E-02
Bile acids metabolism	104	6	4.80E-02

Table 5. Ariadne ontology with the 15 most significant P values.

Name	Number of Entities	Percent Overlap	P value
Tricarboxylic acid cycle	39	25	1.21E-09
Branced aminoacid metabolism	46	21	6.93E-09
Actin-based cytoskeleton assembly	202	7	3.75E-06
Actomyosin based movement	72	12	5.52E-06
Microtubule sliding	156	7	2.54E-05
ER to Golgi transport	47	12	1.89E-04
ROCK1-2	2	100	3.26E-04
Lipid transport	55	10	4.53E-04
Asp/Lys/Thr/Met/Cys metabolsm	39	12	6.46E-04
PAK	3	66	9.68E-04
Protein folding	88	7	1.06E-03
Aromatic aminoacid metabolism	125	6	1.93E-03
Ubiquitin-dependent protein degradation	166	5	3.20E-03
Microtubule cytoskeleton assembly	148	5	5.45E-03
PP2A	7	28	6.46E-03

Table 6. Ariadne signaling pathways with the 10 most significant P values.

Name	Number of Entities	Percent Overlap	P value
Notch pathway	1486	4	2.61E-06
B-cell activation	1178	4	1.97E-05
Insulin action	905	4	2.38E-05
EphrinR -> actin signaling	216	7	3.21E-05
Actin cytoskeleton regulation	539	5	4.77E-04
T-cell activation	1100	4	5.47E-04
Adipocytokine signaling	780	4	4.05E-03
TNFRSF6 -> HSF1 signaling	15	20	5.96E-03
EctodysplasinR -> AP-1 signaling	19	15	1.18E-02
Axon guidance	1049	3	1.35E-02

The GO biological process analyses revealed a number of categories that are significantly enriched with differentially expressed proteins and metabolites. The TCA cycle also was found as a "top hit" in this study (**Table 7**), confirming another result from Ariadne pathway analysis. Besides the TCA cycle, the fat metabolism-related categories, such as lipid transport (P = 5.65E-08), the cholesterol metabolic process (P = 9.17E-08), phospholipid efflux (P = 2.25E-07), cholesterol efflux (P = 1.66E-06), and the lipoprotein metabolic process (P = 3.56E-06), showed higher enrichments, indicating a potential correlation between fat metabolism and anxiety. Furthermore, proteins involved in oxidation reduction may play an important role in the response to oxidative stress, which is involved in many diseases, including many psychiatric disorders.

Table 7. Gene ontology biological process categories with the 20 most significant *P* values.

Name	Number of Entities	Percent Overlap	*P* value
Metabolic process	858	4	1.43E-14
Transport	1807	2	2.08E-08
Lipid transport	94	10	5.65E-08
Cholesterol metabolic process	75	12	9.17E-08
Tricarboxylic acid cycle	24	25	1.44E-07
Phospholipid efflux	14	35	2.25E-07
Response to oxidative stress	137	8	2.26E-07
Triglyceride metabolic process	33	18	1.09E-06
Cholesterol efflux	20	25	1.66E-06
Response to reactive oxygen species	22	22	2.77E-06
Lipoprotein metabolic process	40	15	3.56E-06
Cell motion	120	7	5.06E-06
Response to axon injury	12	33	5.45E-06
Acute-phase response	43	13	5.51E-06
Protein transport	556	3	7.49E-06
Intracellular protein transport	235	5	7.76E-06
Response to carbohydrate stimulus	13	30	7.81E-06
Anti-apoptosis	198	5	8.43E-06
Interspecies interaction between organisms	239	5	9.21E-06
Oxidation reduction	702	2	1.86E-05

The GO cellular component analyses indicated the localizations of proteins expressed differentially between HAB, NAB, and LAB mice (**Table 8**). Not surprisingly, cytoplasm had the largest number of proteins. The mitochondrial proteins also were more likely to differ between mouse lines; this is in accord with the findings on the TCA cycle because almost all the enzymes of the TCA cycle are located in the mitochondrial matrix. The TCA cycle first oxidizes acetyl-CoA to carbon dioxide and, in the process, produces reduced cofactors (three molecules of NADH and one molecule of $FADH_2$) that are a source of electrons for the electron transport chain and a molecule of GTP that readily can be converted to ATP (Henze and Martin, 2003).

The high-density lipoprotein particle and very-low-density lipoprotein particle were found to be highly enriched with differentially expressed proteins which is in agreement with GO biological process analysis, which found many differences in the expression of proteins related to fat metabolism.

Another relevant group of proteins comes from axons, long, slender projections of a

neuron. Axons conduct electrical impulses away from the neuron's cell body and play a very important role in neuronal signal transmission. Axon dysfucntion previously has been reported to be closely related to schizophrenia (Benes et al., 1987; Eastwood et al., 2003; Pierri et al., 1999), depression (Hatt and Smith, 1976), and other psychiatric disorders.

Table 8. Gene ontology cellular component categories with the 20 most significant *P* values.

Name	Number of Entities	Percent Overlap	*P* value
Cytoplasm	5094	2	5.08E-29
Cytosol	1197	5	8.22E-22
Mitochondrial matrix	171	12	3.96E-16
Mitochondrion	1253	4	1.54E-15
Soluble fraction	428	6	7.67E-12
Cytoskeleton	624	4	7.31E-09
Stress fiber	36	22	1.29E-08
High-density lipoprotein particle	25	28	1.86E-08
Axon	137	9	2.05E-08
Growth cone	61	14	6.92E-08
Microtubule	270	5	3.70E-07
Microtubule-associated complex	80	11	7.51E-07
Perinuclear region of cytoplasm	188	6	8.35E-07
COPII vesicle coat	7	57	8.39E-07
Chylomicron	16	31	1.20E-06
Very-low-density lipoprotein particle	17	29	1.68E-06
Melanosome	88	10	1.69E-06
Proteasome complex	33	18	3.16E-06
ER-Golgi intermediate compartment	36	16	5.39E-06
Protein complex	500	4	6.28E-06

The GO molecular function analyses (**Table 9**) again demonstrated that the energy- and fat-related categories are enriched with proteins. For instance, a large number of proteins involved in ATP and ADP binding were found to be expressed differentially between HAB and LAB. The proteins relevant to phospholipid binding, lipid binding, lipid transporter activity, and cholesterol transporter activity were all highly enriched. Similarly, the oxidation-related proteins in the categories of antioxidant activity and oxidoreductase activity were all found to be highly enriched.

Table 9. Gene ontology molecular function categories with the 20 most significant *P* values.

Name	Number of	Percent	*P* value

	Entities	Overlap	
Protein binding	7274	2	2.29E-20
Catalytic activity	871	4	6.12E-14
Motor activity	157	10	7.09E-11
Nucleotide binding	2057	2	5.56E-10
ATP binding	1750	2	8.58E-10
Eukaryotic cell surface binding	23	30	6.54E-09
Binding	1151	3	1.32E-07
Hydrolase activity	1657	2	1.89E-07
Microtubule binding	84	10	7.14E-07
Phospholipid binding	64	12	9.07E-07
Microtubule motor activity	99	9	2.87E-06
Antioxidant activity	20	25	3.08E-06
Actin binding	352	4	5.65E-06
Lipid binding	169	6	6.15E-06
Unfolded protein binding	146	6	1.04E-05
ADP binding	26	19	1.23E-05
Calmodulin binding	152	6	1.48E-05
Lipid transporter activity	29	17	2.16E-05
Oxidoreductase activity	730	3	2.44E-05
Cholesterol transporter activity	16	25	3.19E-05

The sub-network analyses were performed with two different methods. The interaction type of the first analysis was based exclusively on protein-protein or protein-metabolite binding. The second interaction map used all the other interaction methods, such as regulation, expression, etc. The sub-network analyses identified central proteins, metabolites, or even biological events and their interacting neighbor entities. The presence of a high enrichment of input proteins and metabolites in a particular network may indicate a potential correlation with the disease.

The non-binding analyses demonstrated a number of networks that are highly enriched with proteins and metabolites expressed differentially between HAB and LAB (**Table 10**). The 20 networks with the most significant *P* values are shown in **Table 10.**

Table 10. Sub-networks (connected by non-binding) with the 20 most significant *P* values.

Central Entity	Total Number of Neighbors	Percent Overlap	*P* value
PD 98,059	23	66	2.39E-25
Genistein	16	76	4.40E-22
Dexamethasone	23	58	4.16E-21
Cisplatin	10	90	1.11E-18
Calcimycin	13	71	9.80E-17
Nicotine	14	66	2.91E-16
Wortmannin	11	75	1.75E-15

Cycloheximide	43	29	7.05E-15
Okadaic acid	19	50	1.69E-14
Rapamycin	10	72	1.05E-13
Actinomycin D	10	72	1.05E-13
Trichostatin A	10	72	1.05E-13
Staurosporine	16	52	1.83E-13
U0126	7	87	4.17E-13
Diethylstilbestrol	165	11	5.01E-13
Cilastatin sodium	8	77	1.85E-12
Cyclosporine	9	70	6.11E-12
Edetic acid	9	70	6.11E-12
C.I. 77491	15	50	7.76E-12
D-glucose	1518	3	8.27E-12

Figure 37. Network of Ras/Raf/MEK/ERK pathway inhibition. The proteins shown in this figure interact with the metabolites that inhibit the Ras/Raf/MEK/ERK pathway. (Due to the limited resolution the protein/metabolite names are not legible; higher resolution figure is available in electronic file.)

Figure 38. Quantification of MEK and phosphorylated MEK by Western blot analysis. a: The Western blot analysis of MEK and p-MEK for HAB, LAB, and NAB; b: The densities of protein bands from Western blot (a) are shown; a *t* test was performed between groups (MEK comparisons: LAB vs. NAB: $P < 0.0001$; HAB vs. NAB: $P = 0.0009$; p-MEK comparisons: LAB vs. HAB: $P = 0.0059$; HAB vs. NAB: $P = 0.0329$)

One notable pathway that deserves much attention is the signal transduction Ras/Raf/MEK/ERK(MAPK) pathway. Ras is a protein subfamily of small GTPases; Raf, MEK, and MAPK are all serine/threonine protein kinases. Activated Ras activates the protein kinase activity of Raf kinase; Raf kinase phosphorylates and activates MEK; and MEK phosphorylates and activates a mitogen-activated protein kinase (MAPK). A significant number of central entities, shown in **Table 10**, have been used to inhibit the Ras/Raf/MEK/ERK pathway, including but not limited to PD 98059 (Alessi et al., 1995; Dudley et al., 1995; Lazar et al., 1995; Pang et al., 1995), genistein (Akiyama et al., 1987), wortmannin (Ferby et al., 1996; Wymann et al., 1996), okadaic acid (Fujiki and Suganuma, 2009; Garcia et al., 2003), staurosporine (Karaman et al., 2008), U0126 (Duncia et al., 1998; Favata et al., 1998), and SB 203580 (Cuenda et al., 1995) (**Figure 37**). To verify the involvement of this pathway in our anxiety mouse model, MEK and phosphorylated MEK (p-MEK) were quantified by Western blot (**Figure 38**). The results show that the NAB mice have a higher expression level of MEK than both HAB and LAB, and that the HAB and LAB mice have quite comparable MEK expression levels. However, the HAB mice showed a higher expression level of p-MEK than the LAB and NAB mice (**Figure 38**).

The Ras/Raf/MEK/ERK pathway transfers extracellular stimuli to the nucleus, resulting in diverse cellular responses such as proliferation, growth, differentiation, and apoptosis. The cascade pathways have been found to be relevant in different types of diseases, particularly cancers (Hoshino et al., 1999; Karreth and Tuveson, 2009; Sebolt-Leopold, 2008). However, more recently, correlations between the Ras/Raf/MEK/ERK(MAPK) pathway and psychiatric disorders, such as depression, increasingly have become the focus of many studies, indicating that this pathway may be involved in the neuronal modulation of psychiatric disorders (Dwivedi et al., 2001; Feng et al., 2003; Gourley et al., 2008; Qi et al., 2008; Qi et al., 2009; Tiraboschi et al., 2004; Todorovic et al., 2009). Since a large number of Ras/Raf/MEK/ERK-related sub-networks were found in this analysis, another interaction map derived from the Ras/Raf/MEK/ERK pathway is shown below (**Figure 39**); all the entities in this map are part of the pathway and also have different levels of expression between the mouse lines.
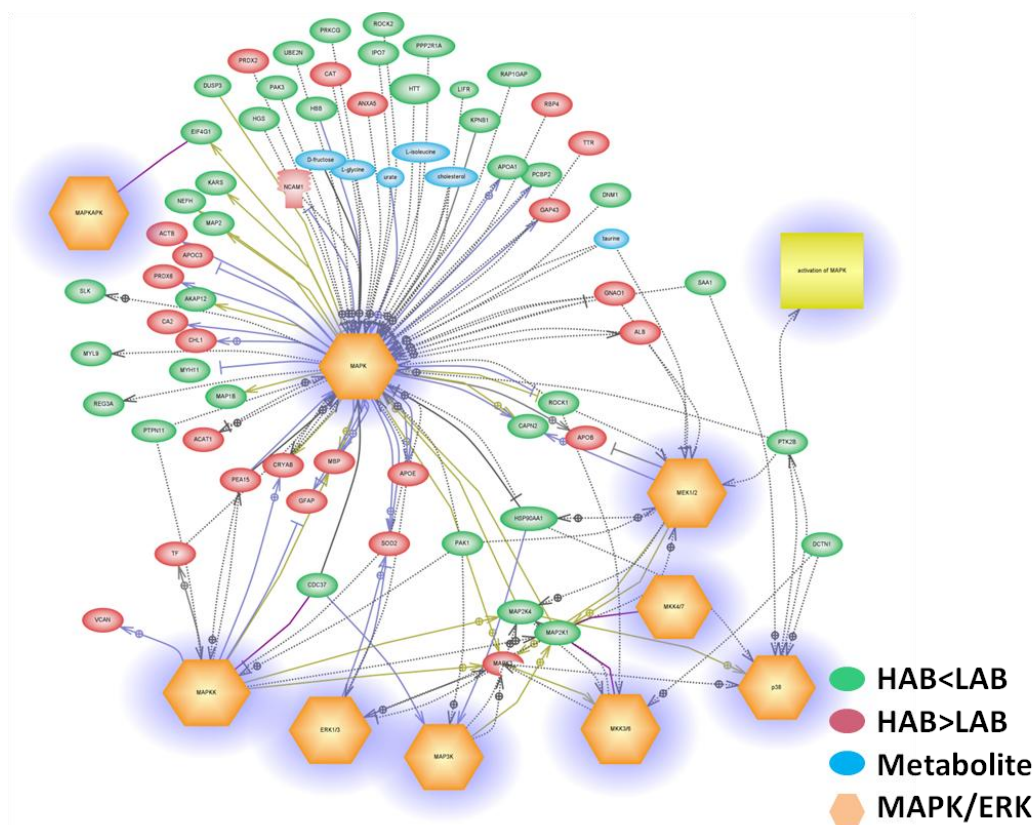
Figure 39. Network of the Ras/Raf/MEK/ERK pathway. (Due to the limited resolution the protein/metabolite names are not legible; higher resolution figure is available in electronic file.)

Another important finding is that dexamethasone (*P* = 4.16E-21) and the neighbors which it interacts with are highly enriched with proteins and metabolites expressed differentially between the animal lines (**Table 10, Figure 40**). Dexamethasone is a synthetic cortisol that acts as an anti-inflammatory and immunosuppressant and is used in cancer chemotherapy. Many studies have indicated that dysfunction of the HPA axis may lead to a depressive situation. Blood cortisol, which is secreted by the adrenal glands, can be used to assess the level of HPA axis activity. In depression patients, cortisol is secreted continuously, even though blood levels are already high. Therefore, the cortisol level is elevated in depression; the high levels usually decrease to a normal level once the depression disappears (Handwerger, 2009; Muller and Holsboer, 2006; Strohle and Holsboer, 2003; Yu et al., 2008).
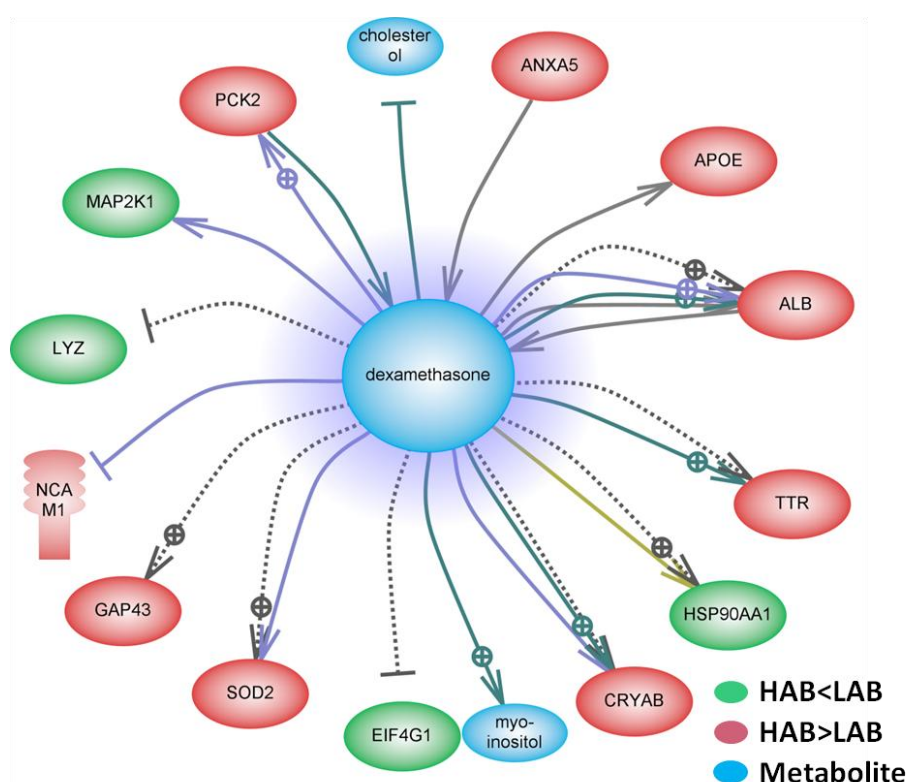
Figure 40. Dexamethasone network. Proteins and metabolites shown in this figure interact with dexamethasone. (Due to the limited resolution the protein/metabolite names are not legible; higher resolution figure is available in electronic file.)

Cortisol levels can be tested using the dexamethasone suppression test (DST). An individual is given a dose of dexamethasone before going to sleep at night, and blood cortisol levels are measured at different times on the following day. In a healthy person, the cortisol level drops at first but then returns to normal as the HPA axis compensates for

the dexamethasone in the blood. In depressed patients, cortisol secretion may not be reduced by the HPA axis or there may be no change at all after receiving dexamethasone.

The sub-networks surrounding nicotine and rapamycin also were found to be enriched with proteins and metabolites expressed differentially between HAB, LAB, and NAB mice (**Table 10**). Nicotine is an alkaloid found in tobacco. Despite its toxicity and addictive properties, nicotine actually has demonstrated potential benefits in Alzheimer's and Parkinson's disease, as well as some mental disorders (Baron, 1996; Dome et al., 2009; Fagerstrom and Aubin, 2009; Quik et al., 2009). Rapamycin is an immunosuppressant drug used to prevent rejection in organ transplantation. It is the key element in the mammalian target of rapamycin (mTOR) pathway, which can influence neuronal development and plasticity (Jaworski and Sheng, 2006), resulting in the development of psychiatric disorders (Ehninger et al., 2009; Lang et al., 2009).

The analyses of binding interactions also revealed a number of sub-networks of great significance and biological interest (**Table 11**). An obvious important one is glycinergic synaptic transmission (**Table 11, Figure 36**). Glycine is a major inhibitory neurotransmitter in, but not restricted to, the spinal cord and brainstem and has been shown to have a key function in the regulation of locomotor behavior (Kirsch, 2006; Legendre, 2001; Xu and Gong, 2010; Zafra et al., 1997). Several decades ago, glycine was found to be beneficial in depression treatment (Weinberg and Pittsburg, 1945).

Table 11. Sub-networks (connected by binding) with the 20 most significant *P* values

Central Entity	Total Number of Neighbors	Percent Overlap	*P* value
UGCGL1	10	100	9.07E-19
Glycinergic synaptic transmission	10	90	4.35E-16
ETFA	14	73	1.14E-15
PSMD7	15	68	3.57E-15
Reduction of virulence	9	90	1.76E-14
Myelin maintenance	9	90	1.76E-14
Microsporogenesis	9	90	1.76E-14
AP2B1	19	55	1.26E-13
SEC24B	26	44	2.58E-13
ASPA	23	45	1.73E-12
STRN	27	39	1.37E-11
SYN2	27	39	1.37E-11
PURB	28	37	2.16E-11
Toluene catabolism	7	87	2.73E-11
Carbon dioxide transport	7	87	2.73E-11

Spermine transport	7	87	2.73E-11
Nav channel clustering	7	87	2.73E-11
Humoral defense mechanism	7	87	2.73E-11
Delayed-type hypersensitivity	7	87	2.73E-11
SPTBN2	29	36	3.34E-11

An additional analysis was performed to investigate the interaction between proteins and psychiatric disorders, with a focus on anxiety and depression. The correlation was built up on the basis of previous studies of depression and anxiety-related disorders. All the proteins shown in **Figure 41** showed different expression levels between mouse lines on the basis of our MS-based data; their important roles in these psychiatric disorders have been the subject of much published resarch. For instance, a possible correlation with the anxiety phenotype previously was reported for both Glo1 and ApoE and was confirmed by the present study.
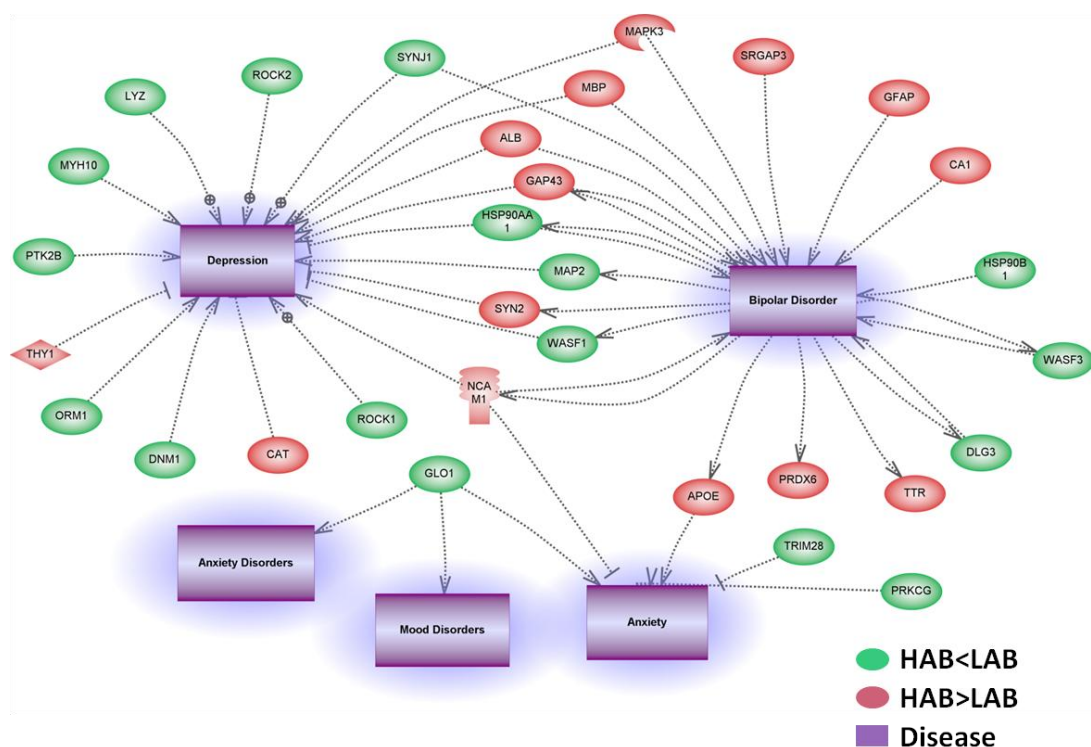
Figure 41. Network of psychiatric disorders. The proteins shown in this figure are expressed differentially between HAB and LAB mice. These proteins have been reported previously to be relevant to psychiatric disorders. (Due to the limited resolution the protein/metabolite names are not legible; higher resolution figure is available in electronic file.)

3.4   Discussion

By using the SILAM approach, we were able to identify and quantify a large number of proteins in a high throughput mode. As mentioned above, metabolic labeling enables us to mix the samples being compared at the earliest possible stage, reducing the potential variance generated during sample preparation. This study identified a lot more potential new biomarker candidates than had been found with the traditional 2-DE gel platform and thus helps improve our understanding of the anxiety mouse models as well as of the disorder as a whole.

The stable isotope-labeled diet increased the costs of the whole experiment. However, labeling the whole animal allows all tissues to be harvested, and the labeled tissues are commonly used as the reference for mixing with case samples. Therefore, one labeled mouse enabled us to run numerous experiments on different tissues, making this approach actually relatively economical.

3.4.1 Isotope effect

As shown in this study, the ^{15}N- and ^{14}N-fed mice showed differences in both depression-like behavior and protein expression. The ingredients of the ^{14}N and ^{15}N diets are identical except for the nitrogen forms, and the only apparent difference between the two diets is the nitrogen source of the media used for bacterial culture. Although the observed effect can result from multiple factors, the isotope is the only known one; therefore, this effect is referred to as the isotope effect in this thesis.

The underlying explanations for this isotope effect are still uncertain. One hypothesis is that the introduction of ^{15}N may change the stability and synthesis rate of some proteins. Protein synthesis and degradation involve breaking and forming covalent peptide bonds, which are generated by the reaction between carboxyl and amine groups from two molecules. Two different types of isotope effects can be observed: the primary isotope effect happens at a chemical bond that is broken or formed, such a peptide bond, where it affects the reaction rate; the secondary isotope effect results from isotope substitution involved in the side chain (Cassano et al., 2004; Cleland, 2003, 2005).

In the SILAM approach, all the ^{14}N atoms in an amine group are replaced by ^{15}N. Furthermore, the nitrogen atoms at the side chains also are labeled with ^{15}N. Heavier atoms normally result in more stable chemical bonds or lower vibration frequencies.

Therefore, more energy is required to break the ^{15}N peptide bond. Since every peptide bond is modified during the SILAM experiment, this effect seems to be very pronounced. Actually, the vibrational frequencies of the affected bonds are highly dependent on the relative mass change. For instance, changing a hydrogen (H) atom to deuterium (D) results in a 100% increase in mass, whereas replacing ^{14}N with ^{15}N increases the mass by only 7%. The absolute mass increase of both H to D and ^{14}N to ^{15}N is 1 Dalton; however, the rate of a reaction involving a C-H bond is typically 6 to 10 times faster than the rate of a reaction involving a C-D bond, whereas an ^{14}N reaction is only slightly faster than the corresponding ^{15}N reaction.

As discussed above, ^{15}N labeling may lead to a slight change in protein stability and protein synthesis and degradation rates. The influence of the ^{15}N isotope may be amplified if the protein synthesis rate is the rate-limiting step in a biological process or if the activities of some enzymes are sensitive to their stabilities, resulting in biological responses. However, there is no evidence yet to support our hypothesis.

Despite the unclear explanations for the isotope effects on the animals' behavior and protein expression, a finding of interest is that the ^{15}N diet showed an antidepressant-like effect in the HAB mice. Therefore, the differentially expressed proteins may be related to depression-like behavior, which may provide some hints for depression research. The pathobiology of this disorder will be discussed in the following sections.

Even though the isotope influences protein expression to some degree, this is irrelevant when using ^{15}N labeling tissue for quantitative proteomics. A typical approach—called indirect comparison in this study—is to use the ^{15}N labeled material as the reference and to mix it with either case or control samples. These two proteomic experiments are then used to compare case and control samples. The biggest benefit of this approach is that any kind of dietary or isotopic effect can be avoided. Another benefit is that standard healthy animals can be used for labeling; furthermore, all the labeled tissues can be used in many different studies. By contrast, a labeled case animal may be used exclusively in only one study. However, a shortcoming of indirect comparison is that the number of overlapping proteins between two experiments is reduced, and the final protein quantification can employ only those overlapping proteins, leading to a smaller proteome coverage for quantification. However, the situation is improved by using multiple biological or technical replicates, or both.

3.4.2 Pathobiology of the anxiety phenotype

Although the detailed pathogenesis of psychiatric disorders remains elusive, there is growing evidence for the involvment of several neural circuits and pathways in the brain. A single genetic, physiological or environmental lesion may not result in a psychiatric phenotype. Hence, systems biological analyses were performed in this study with both proteomic and metabolic data from trait anxiety mouse models. The strategies used enabled us to identify and quantify a great number of proteins and metabolites that are differentially expressed in HAB, LAB, and NAB mice. The interaction maps of protein and metabolite candidates were developed on the basis of various types of interaction. The results found several significant biological processes or pathways that showed high enrichment for candidate entities. These pathways help increase our understanding of anxiety. Some of the significant biological processes and pathways are highly related to psychiatric disorders (see further discussion below).

3.4.2.1 Oxidative stress

It is well known that the oxygen redox reaction is essential to and found everywhere in aerobic organisms. However, a disturbance in this normal redox state can have toxic effects through the production of peroxides and free radicals (molecules with unpaired electrons on an open shell configuration), leading to a higher chemical reactivity. Free radicals can damage all components of the cell, including proteins, lipids, and DNA (Davies, 1995; Filomeni and Ciriolo, 2006).

Oxidative stress has been thought to play an important role in the pathogenesis of various diseases, including psychiatric disorders. The brain is highly vulnerable to oxidative damage for the following reasons: first, the O_2 consumption is high and hence more free radicals can be generated; and second, the antioxidant defense is modest, and third, a lipid-rich constitution provides a larger amount of substrates for oxidation (Halliwell, 2006; Valko et al., 2007).

Oxidative stress has been found to be highly relevant to a number of neurological diseases, including Alzheimer's disease, Parkinson's disease, multiple sclerosis, and stroke (Kaur and Ling, 2008). Moreover, oxidative stress also has been associated with several psychiatric disorders, such as schizophrenia, bipolar disorder, and depression (Adibhatla and Hatcher, 2009; Andreazza et al., 2008; Bouayed et al., 2009; Do et al., 2009; Ng et al., 2008; Tylec et al., 2007; Wood et al., 2009). In the present study, both ^{14}N-HAB/^{15}N-HAB and HAB/LAB

comparisons indicated a significant number of proteins responsible for responding to oxidative stress, and these proteins demonstrated expression differences between the mouse groups. Glo1 is an enzyme that modulates the level of oxidative stress and has been reported to be highly relevant to anxiety disorder by our research group as well as that of Hovatta (Hambsch et al., 2010; Hovatta et al., 2005; Kromer et al., 2005). However, the results of the two independent research groups are inconsistent: we found that Glo1 was expressed at a higher level in low anxiety mice, while Hovatta found that overexpression of Glo1 resulted in an increase of anxiety-like behavior. The contradiction may partly be explained by the differences in the genotypes of the animals, but may not be limited to this explanation. Both results support the presence of abnormal Glo1 in anxiety-like behavior. Our finding is in accordance with that of another study focusing on mood disorder (which has a high comorbidity rate with anxiety disorders); this study also found that expression of Glo1 was lower in major depression and bipolar disorder patients than in healthy control subjects (Fujimoto et al., 2008).

Further support for the involvement of oxidative stress in anxiety comes from the phospholipid transfer protein (PLTP) and alpha-tocopherol, the main isomer of vitamin E. Vitamin E is transferred by PLTP and is an antioxidant widely used in clinical therapies (Desrumaux et al., 2005). Complete PLTP deficiency is accompanied in mice by increased anxiety, as shown by fewer entries into and less time spent in the open arms of an elevated plus maze. Bouayed et al. found a positive relationship between peripheral oxidative status and level of anxiety in mice (Bouayed et al., 2007).

Human studies on anxiety disorders, such as panic disorder and obsessive-compulsive disorder (OCD), also have indicated a correlation between oxidative stress and anxiety. Ersan et al. showed a significant relationship between OCD and oxidative stress and, consequently, an involvement of free radicals and of antioxidant defense (Ersan et al., 2006). Kuloglu et al. reported that both panic disorder and OCD were associated with free radicals (Kuloglu et al., 2002a; Kuloglu et al., 2002b).

There is a lot more evidence to support the correlation between oxidative stress and neuropsychiatric disorders (Bouayed et al., 2009; Masood et al., 2008; Rammal et al., 2008a, b). Oxidative stress, like many other emotional stresses, also has a strong influence on anxiety behavior (Gingrich, 2005). All the published multi-dimensional data, including the OMICS data presented in this thesis, demonstrate that there is a link between oxidative stress and anxiety. These data imply that oxidative mechanisms play a key role in

pathogenic pathways in psychiatric disorders and antioxidants can be used as therapeutic targets for these diseases.

3.4.2.2   HPA axis and hormones

The role of the HPA axis in depression has been well studied for several decades (Pariante and Lightman, 2008). HPA axis activity is governed by the secretion of corticotropin-releasing factor (CRF), and vasopressin from the paraventricular nucleus of hypothalamus. CRF and vasopressin can in turn stimulate and regulate the secretion of adrenocorticotrophic hormone (ACTH) from the pituitary. ACTH further stimulates the secretion of the glucocorticoids (cortisol in humans and corticosterone in rodents) from the adrenal gland. Glucocorticoids then not only interact with their receptors in multiple target tissues but also act on the HPA axis (to suppress CRH and ACTH production) in a negative feedback cycle (**Figure 42**) (Herbert et al., 2006; Keck and Holsboer, 2001). The glucocorticoids, including synthetic forms such as dexamethasone, suppress CRF and ACTH synthesis and release. In this manner, glucocorticoids inhibit their own synthesis. Besides their peripheral functions, such as regulation of glucose metabolism, and their role in the immune system, the HPA axis and glucocorticoids also regulate neuronal survival, neurogenesis, memory, and emotions (Herbert et al., 2006). Excess glucocorticoids may impair or even damage the hippocampus, which may initiate and maintain a hypercortisolemic state, as found in some cases of depression (Nestler et al., 2002). A number of studies have shown that in depressed people the HPA axis is not suppressed by an oral dose of synthetic glucocorticoid dexamethasone; by contrast, in non-depressed people a small dose of dexamethasone can result in a reduced cortisol level, indicating a negative feedback inhibition of the HPA axis (Pariante and Lightman, 2008).

The HPA axis mainly has been studied in depressive disorders. However, anxiety and depressive disorders are often comorbid and also commonly co-occur with other psychiatric disorders (Aina and Susman, 2006). Possible reasons for this comorbidity may relate to factors such as overlapping of symptoms, environment, and biology. Furthermore, anxiety also is a stress-related illness, and obviously stress can greatly affect the HPA axis. Therefore, HPA dysfunction also has been associated with anxiety by a number of studies (Cameron, 2006; Young et al., 2004).

The ^{15}N-labeled diet used in this study showed an antidepressant-like effect in HAB mice. Although we do not have a clear idea how the ^{15}N diet reduces depression-like behavior, we consider it to be an antidepressant. Our finding is in good agreement with that of an

earlier study in which the effects of acute and subchronic treatment with different antidepressants (amitriptyline, fluoxetine, mirtazapine, St John's wort extract) on the brain/plasma distribution of corticosterone were investigated in mice (Weber et al., 2006). Significantly elevated plasma and brain corticosterone levels were found after one single oral treatment with fluoxetine, mirtazapine, or St John's wort extract. However, in subchronic treatment, only fluoxetine and St John's wort extract significantly elevated plasma and brain corticosterone levels. Mirtazapine and amitriptyline showed no effects. However, earlier studies showed inconsistent results concerning the effect of fluoxetine on plasma corticosterone (Stout et al., 2002). A possible explanation for the observation in our study is that the antidepressant may increase cortisol secretion by enhancing serotoninergic and noradrenergic neurotransmission (Schule et al., 2004). Furthermore, the levels of corticosteroid-binding globulin (CBG), which is responsible for binding and transferring corticosteroid, were found to be higher in ^{15}N-fed mice than in ^{14}N-fed mice. In other words, the ^{15}N antidepressant-like effect can result in both increased corticosterone and CBG. Although it is unclear whether increased CBG is a result of increased corticosterone or another cause, this finding is in accordance with that of a previous study in which positive associations were observed between CBG and cortisol levels following the Trier Social Stress Test (TSST) (Kumsta et al., 2007).
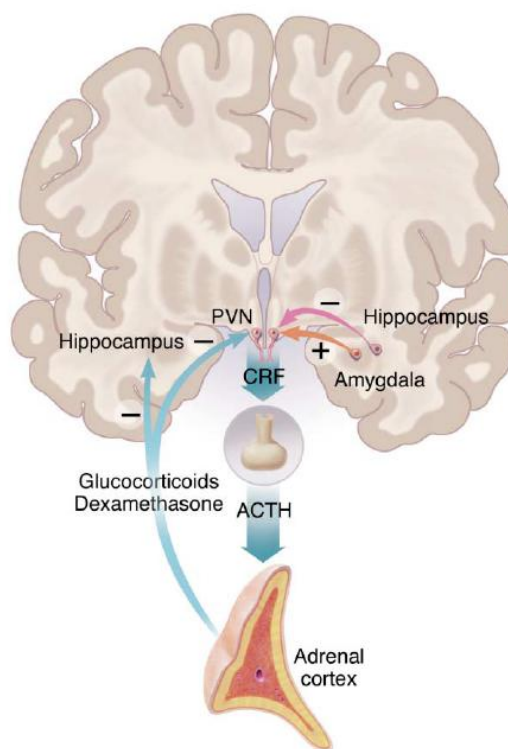
Figure 42. Regulation of the Hypothalamic-Pituitary-Adrenal Axis. (Reproduced from (Nestler et al., 2002)).

3.4.2.3 Neurotransmission

Neurotransmission is an electrical movement across synapses caused by the propagation of nerve impulses by a neurotransmitter. Anxiety disorders may involve decreased inhibitory signaling by gamma amino butyric acid (GABA) or increased excitatory signaling by glutamate (Martin et al., 2009). Currently, the mainstays of anxiety therapies are benzodiazepines and selective serotonin reuptake inhibitors (SSRIs) (Gingrich, 2005), both of which are targeted at neurotransmitter pathways. Benzodiazepines interact with the receptor A of gamma amino butyric acid (GABA), an inhibitory neurotransmitter in the mammalian central nervous system that plays a role in regulating neuronal excitability. SSRIs increase the extracellular level of the neurotransmitter serotonin, also known as 5-hydroxytryptamine (5-HT), by inhibiting its reuptake into the presynaptic cell and thus increasing the level of serotonin available to bind to the postsynaptic receptor. This implies that neurotransmission plays an essential role in anxiety disorders.

The two principal subtypes of postsynaptic GABA receptor complexes, the ionotropic GABA-A and metabotropic GABA-B receptors, play important roles in the brain and are a target for a variety of endogenous and exogenous modulators (Kalueff and Nutt, 2007;

Mombereau et al., 2004; Nutt and Malizia, 2001). GABA-A receptors are ligand-gated ion channels, and activated GABA-A could hyperpolarize the neuronal membrane, reducing neuron excitability and leading to inhibitory actions of GABA. GABA-B receptors may be involved in modulating the generation of excitatory postsynaptic potential and long-term potentiation (Chang et al., 2003). Both GABA-A and -B receptors have been shown to be involved in the regulation of neuronal excitability and rapid changes in fear arousal, such as sleep, anxiety, panic, and the acute stress response (Brambilla et al., 2003; Kalueff and Nutt, 2007).

Our study identified a number of candidate proteins associated with GABAergic neurotransmission. Moreover, glycinergic synaptic transmission was found to be enriched with proteins and metabolites expressed differentially between mouse lines. Both glycine and GABA are two essential inhibitory neurotransmitters in the central nervous system. Although glycine's involvement in psychiatric disorders is less understood than GABA's, co-localization and release of GABA and glycine is widespread in inhibitory neurons of the brain and spinal cord, and GABA even acts as a co-agonist to modify the response of glycine receptors (Lu et al., 2008). Furthermore, glycine is a requisite co-agonist of glutamate, the most abundant excitatory neurotransmitter in the vertebrate nervous system (Laube et al., 1993; Lester et al., 1993). Therefore, it is reasonable to assume an important role of glycinergic transmission in psychiatric disorders. Indeed, studies have found that glycine exerts inhibitory effects in certain areas of the brain, resulting in significant anxiety relief (Chojnacka-Wojcik et al., 2001; Young et al., 1974).

3.4.2.4   Ras/Raf/MEK/ERK pathway

The Ras/Raf/MEK/ERK pathway is a signal transduction pathway involved in metazoan development; it controls many biological processes, including metabolic processes, the cell cycle, cell migration, and cell shape as well as cell proliferation and differentiation (Schlessinger, 2000).

The receptor tyrosine kinases (RTKs), such as the EGF receptor, first stimulate the exchange of GTP for GDP on the small G protein Ras, which is activated by the Grb2/Sos complex. Then, the Ras interacts with Raf to stimulate intracellular processes. Activated Raf stimulates MAP-kinase-kinase (MAPKK, MEK) by phosphorylating a key Ser residue. MAPKK then phosphorylates and activates MAPK (ERK). Activated MAPK phosphorylates a variety of cytoplasmic- and membrane-linked substrates. In addition, MAPK is transferred

rapidly into the nucleus, where it phosphorylates and activates transcription factors (**Figure 43**).

The Ras/Raf/MEK/ERK pathway has been found to be highly related to diverse diseases, especially cancers (Dhillon et al., 2007; Hoshino et al., 1999; Roberts and Der, 2007). Raf has attracted much attention since the Raf gene was found to be mutated in a large percentage of malignant tumors (Wan et al., 2004). Furthermore, Ras, Raf, and MEK have been used as drug targets in cancer for many years (Kohno and Pouyssegur, 2006). In contrast to its relevance in cancer, the importance of the Ras/Raf/MEK/ERK pathway in psychiatric disorders is relatively poorly understood; however, it is increasingly becoming a focus of research in psychiatry.

As discussed above, the HPA axis and the hormones it controls are of great importance in psychiatric disorders, including depression and anxiety. One hypothesis is that CRF acts as a ligand that can bind to and phosphorylate the CRF receptor and eventually may activate the Ras/Raf/MEK/ERK pathway (Hauger et al., 2006; Hillhouse and Grammatopoulos, 2006; Sananbenesi et al., 2003).

In this study, a number of enriched sub-networks were found to be relevant to the Ras/Raf/MEK/ERK pathway. Western blot results showed that activated MEK is expressed at a higher level in high anxiety mice, which is in accordance with the findings of a previous study in which mice deficient in CRF_2 displayed an increased anxiety level and also an increased hippocampal level of activated MEK (Todorovic et al., 2009). Furthermore, inhibition of the Ras/Raf/MEK/ERK pathway by the MEK inhibitor U0126 was found to decrease dramatically the depression-like behavior in both wild-type and mutant mice, indicating an involvement of this pathway in psychiatric disorders (Todorovic et al., 2009). Some inconsistent findings were that activation of ERK may result in depression or anxiety-like behavior (Qi et al., 2008; Qi et al., 2006; Qi et al., 2009). This contradiction can be partly explained by the finding that region-specific manipulation of the Ras/Raf/MEK/ERK pathways may generate quite different behavioral phenotypes (Todorovic et al., 2009).
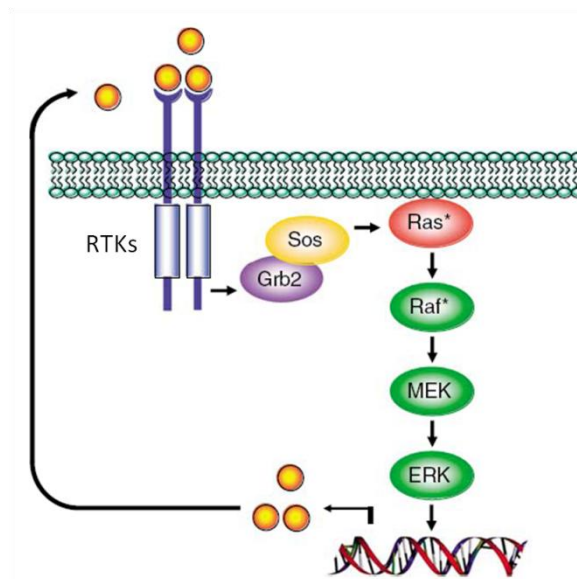
Figure 43. Schematic representation of the Ras/Raf/MEK/ERK signaling cascade. (Reproduced from (Roberts and Der, 2007))

In summary, the pathology of psychiatric disorders is not yet fully understood. However, it is well accepted that psychiatric disorders probably arise from a combination of factors, including genetic vulnerabilities and environmental stressors. A typical biological study focusing on a particular protein or pathway is normally insufficient to deepen the understanding of the pathophysiology of a disease. On the basis of our OMCIS data, we have found a number of proteins and metabolites that are involved in some important pathways and that could provide a new approach in psychiatric disorder research. As demonstrated in this thesis, anxiety probably is caused by several pathways. A simple hypothesis could be that oxidative stress damages the brain and neurotransmission and also stimulates the HPA axis and hormone excretion. CRF also may be involved in the Ras/Raf/MEK/ERK signaling cascade. Any dysregulation in this complex network may contribute to anxiety disorders.

4 Technology development

The previous section has demonstrated that methods involving stable isotope metabolic labeling result in high quantitative accuracy, since they allow the combination of two or more samples before workup. Unfortunately, stable isotope incorporation rates in metabolic labeling experiments using mammalian organisms usually do not reach 100%. As a consequence, protein identifications in ^{15}N database searches with mass spectrometry data have poor success rates. In this section, we report on a strategy that significantly improves the number of ^{15}N-labeled protein identifications and results in a more comprehensive and accurate relative peptide quantification workflow.

At present most quantitative proteomics investigations are restricted to the analysis of protein expression differences between two or more sample specimens. With each analysis a static snapshot of a cellular state is captured with regard to protein expression. However, any information on protein turnover cannot be obtained using classic methodologies. Protein turnover, the result of protein synthesis and degradation, represents a dynamic process, which is of equal importance to understanding physiological processes. Therefore a protein turnover analysis method was developed using the ^{15}N-labeled diet as an isotopic tracer. Unlike the ^{15}N complete labeling strategy used for relative quantitation, adult mice were fed with the labeled diet for limited time periods and the resulting partially labeled proteins digested and subjected to tandem mass spectrometry. Results are presented reflecting the dynamics for a great number of proteins from mouse brain and plasma.

4.1 A mass spectrometry data search method for improved ^{15}N-labeled protein identification

4.1.1 Introduction

Modern quantitative proteomics greatly benefits from both high resolving mass spectrometers and stable isotope labeling. In this regard global metabolic labeling with ^{15}N, as well as 'Stable Isotope Labeling with Amino Acids in Cell Culture' (SILAC) (Kruger et al., 2008; Ong et al., 2002), are the gold standards in terms of accuracy since the control and case samples are combined prior to any sample preparation. This avoids the risk of introducing artificial variance due to inconsistent sample preparation. The ^{15}N labeling

technology has been applied successfully to cells in culture (Conrads et al., 2001; Ishihama et al., 2005), plants (Huttlin et al., 2007; Nelson et al., 2007; Palmblad et al., 2007; Schaff et al., 2008), *Drosophila melanogaster* (Krijgsveld et al., 2003), *Caenorhabditis elegans* (Dong et al., 2007; Krijgsveld et al., 2003), and mammals (McClatchy et al., 2007a; Wu et al., 2004).

Proteins are labeled with ^{15}N during their synthesis. However, the ^{15}N incorporation rates typically do not reach 100% due to residual ^{14}N that is left in the diet and/or organism. Incomplete ^{15}N labeling will result in a rather complex peptide isotopologue distribution during mass spectrometry analysis, which affects both peptide identification and quantification. Therefore, a modified method for ^{15}N-labeled protein identification was considered in the present study.

4.1.2 Material and methods

4.1.2.1 Methods

For protein identification using mass spectrometry data, the expected and measured monoisotopic peptide peak values need to coincide during the first step of the database search. Hence, during mass spectrometry data acquisition the instrument needs to select the correct ^{15}N monoisotopic peak for subsequent fragmentation and MS/MS analysis. For incompletely labeled peptides the ^{15}N isotopologue envelope is different from the natural ^{14}N envelope. If the ^{15}N monoisotopic peak does not represent the most intense signal, it is typically not chosen as precursor ion for fragmentation. Instead the most intense peak that is not made up of only the ^{15}N isotope is selected for fragmentation. For ^{15}N incorporation rates of approximately 90% the mass of the most intense peak is generally 1 Da smaller than that of the fully labeled ^{15}N monoisotopic peak (**Figure 44**). This deviation results in a low success rate for ^{15}N protein identification using default search parameters and a ^{15}N protein database.
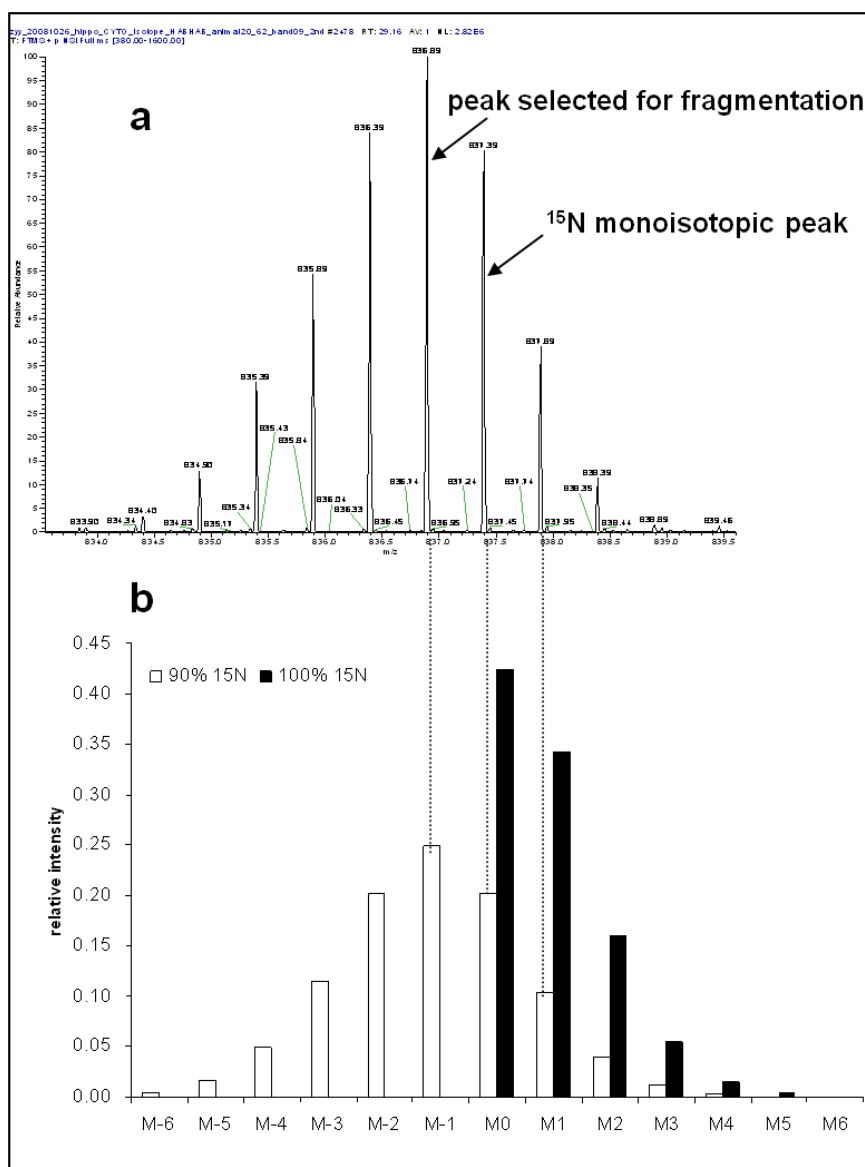
Figure 44. Isotopologue distributions of ^{15}N labeled peptide TFTTQETITNAETAK, $C_{70}H_{114}N_{18}O_{28}$. a: observed isotopologue distribution, in which the most intense peak is 1 Da smaller than the ^{15}N monoisotopic peak and therefore subjected to fragmentation during MS/MS analysis. b: theoretical isotopogue distributions of the same peptide with 90% and 100% ^{15}N enrichment. The mass of the most intense peak for 90% ^{15}N incorporation is 1Da smaller than that for 100% incorporation.

In a tryptic protein digest every identified peptide contains at least one arginine or lysine residue with the exception of the C-terminal peptide. Here we introduce a hypothetical -0.997035 Da ($\Delta mass = {}^{14}N - {}^{15}N$), simplified as -1 Da, variable modification for arginine and lysine residues to correct for non-monoisotopic peak selection in MS/MS analysis during mass spectrometry data acquisition. Amino acid modifications can be easily included in

MASCOT (Perkins et al., 1999) or SEQUEST (Eng et al., 1994) database searches. By introducing the -1 Da variable modification for arginine and lysine residues, both the all ^{15}N and n-1 ^{15}N signals will be considered in the database search. For the MS/MS fragment ions no modification edits are necessary, since all isotopologue peaks in close proximity to the selected precursor ion will be included during fragmentation.

4.1.2.2   Experiments

The animal studies were conducted in accordance with the "Guide for the Care and Use of Laboratory Animals of the Government of Bavaria". CD1 mice were fed for 56 days starting *in utero* with either U-15N-SILAM-Mouse or U-14N-SILAM-Mouse diets (Silantes GmbH, Munich, Germany) (McClatchy et al., 2007a; Wu et al., 2004). The ^{15}N incorporation rates determined by MALDI-TOF analysis and the in-house software *QuantiSpec* (Haegler et al., 2009b) were approximately 90% and 98% for brain and plasma proteins, respectively. ^{15}N and ^{14}N mouse hippocampal protein extracts were mixed at a ratio of 1:1 based on Bradford assay quantification. The protein mixture was resolved by SDS-PAGE (4-12%) and the gel stained with Coomassie blue. The gel lane containing the separated proteins was cut into 2 mm-wide pieces and each piece subjected to in-gel tryptic digestion (Shevchenko et al., 2006). Gel pieces were destained twice with 100 µL 50 mM NH_4HCO_3/acetonitrile (1:1, vol/vol) for 30 min, and disulfide bonds reduced with 10 mM DTT in 50 mM NH_4HCO_3 at 56°C for 30 min, and then alkylated with 55 mM iodoacetamide in 50 mM NH_4HCO_3 in the dark for 30 min. Subsequently, 12.5ng/µl trypsin in 25 mM NH_4HCO_3 was added to saturate and cover gel slices. The enzymatic reaction was carried out at 37°C overnight. After the digestion, the peptides were extracted from the gel pieces by adding 5% formic acid at 37°C for 30 min. The gel pieces were spun down and the liquid collected. The extraction was repeated twice. Finally, the extracted digest peptide mixture was lyophilized to dryness, dissolved in 10 µL 0.1% formic acid and then analyzed by LC-MS/MS with an ORBITRAP (Thermo Fisher Scientific, Bremen, Germany) analyzer. In addition, ^{15}N and ^{14}N mouse plasma proteins were mixed at a 1:1 ratio, and seven high abundant proteins were immunodepleted using the IgY-M7 cartridge (GenWay Biotech Inc., San Diego, CA) according to the product manual. The flow-through fraction was processed using the same workflow as for the brain samples.

4.1.2.3   Data process

For SEQUEST database analysis the ORBITRAP Raw files were searched against a concatenated forward / reversed IPI-mouse database v 3.46. The Raw files were also

converted to mzData files with Bioworks 3.3.1 SP1 (Thermo Fisher Scientific Inc., Waltham, MA), and then searched against forward IPI-mouse database v 3.46 with activation of the *Decoy* checkbox in MASCOT v 2.2. The ^{14}N database search was performed by using the following parameters: 20 ppm mass tolerance for the MS scan, 1 Da for the MS/MS scan, fixed carbamidomethylation for cysteine and variable oxidation for methionine, one miscleavage. The ^{15}N database search was executed twice using two different sets of parameters. The first search was done with the same parameters as for the ^{14}N search but using ^{15}N amino acid masses. The second search employed an additional -1 Da variable modification for arginine and lysine residues. Assembly and removal of redundant proteins based on their accession numbers were performed by in-house written Perl scripts. The SEQUEST results were filtered using peptide XCorr >1.9 for 1+ charged ions, >2.7 for 2+ charged ions, >3.5 for 3+ or above charged ions, and DeltaCN >0.08 . MASCOT results were filtered using a fixed significance threshold of $p<0.01$, and MASCOT score > 20. The False Discovery Rate (FDR) was then determined by calculating the ratio of the number of peptides identified from decoy and forward database searches (Wang et al., 2009). Relative quantification of the peptide pair signals was performed with the ProRata software (Pan et al., 2006) based on the SEQUEST identification results. Briefly, the ion chromatograms were extracted for both labeled and unlabeled isotope envelopes according to the identified amino acid sequence, and the ratio of areas of labeled and unlabeled chromatographic peaks were used for peptide quantification.

4.1.3 Results

The above mass spectrometry data search strategy significantly improves ^{15}N protein identification success for the brain protein mass spectrometry dataset, with the number of proteins approaching those of the ^{14}N database search results (**Table 12**). The conventional SEQUEST search parameters and a ^{15}N database resulted in 798 identified peptides corresponding to 525 proteins. When using the modified search method, we identified 10525 peptides corresponding to 1586 proteins, 1203 of which were only identified by the latter method. The FDR also greatly improved due to the modified database search method. Together with ^{14}N search results the total number of identified proteins for the brain mass spectrometry dataset is 2681 with the modified method; 1294 proteins were identified by both ^{14}N and ^{15}N database searches. The ^{15}N/^{14}N database search results overlap is only 283 proteins when the conventional method is used. Moreover, the average number of identified peptides for a given protein also increases with our method (**Table**

12). The MASCOT search results also demonstrate the advantage of the modified ^{15}N database search method, with an increase of the identified ^{15}N peptide number from 3892 to 22713, and a decrease of the FDR from 8.42% to 2.02% (**Table 12**).

Table 12. Number of peptides and proteins identified by different search methods

search mode	SEQUEST			MASCOT		
	peptides[a]	proteins[b]	peptide FDR	peptides[c]	proteins[b]	peptide FDR[d]
Brain						
^{14}N and ^{15}N unmodified	32102	2631	-	42685	3205	-
^{14}N and ^{15}N modified	41829	2681	-	61506	3353	-
^{14}N	31304	2389	0.40%	38793	3083	3.57%
unmodified ^{15}N	798	525	45.74%	3892	948	8.42%
modified ^{15}N	10525	1586	10.92%	22713	1616	2.02%
Plasma						
^{14}N and ^{15}N unmodified	25209	873	-	37372	1145	-
^{14}N and ^{15}N modified	26514	892	-	37225	1093	-
^{14}N	13414	663	0.19%	19346	896	6.08%
unmodified ^{15}N	11795	702	1.66%	18026	741	3.34%
modified ^{15}N	13100	725	2.41%	17879	662	2.37%

a) Number of redundant peptides with SEQUEST XCorr >1.9 for charge state 1+, >2.7 for charge state 2+, >3.5 for charge state 3+ or above, and DeltaCN >0.08
b) Number of non-redundant proteins
c) Number of redundant peptides with MASCOT significance threshold p<0.01, MASCOT score > 20
d) FDR based on the peptide matches above identity threshold calculated by MASCOT

The proteins in plasma show higher ^{15}N incorporation rates, which is a reflection of their higher metabolic turnover rates compared to brain proteins. The almost 100% ^{15}N incorporation rates resulted in a greater success rate for monoisotopic peak selection. Therefore, the plasma ^{15}N protein identification numbers using the modified database search method did not improve as much as it did for the brain proteins. However, there were still 1305 peptides and 25 proteins exclusively identified by SEQUEST with the modified ^{15}N database search method. The majority of large peptides could only be identified by the new database search method, since their isotopologue distributions are more affected by small amounts of residual ^{14}N. Using SEQUEST the modified method identified 408 peptides > 3 kDa, whereas the conventional method resulted in only 23 peptides. Similarly, 969 peptides and 252 peptides, respectively, were found to be > 2.5 kDa with the modified and conventional search methods. MASCOT results show no significant advantage of our modified method for highly labeled plasma proteins.
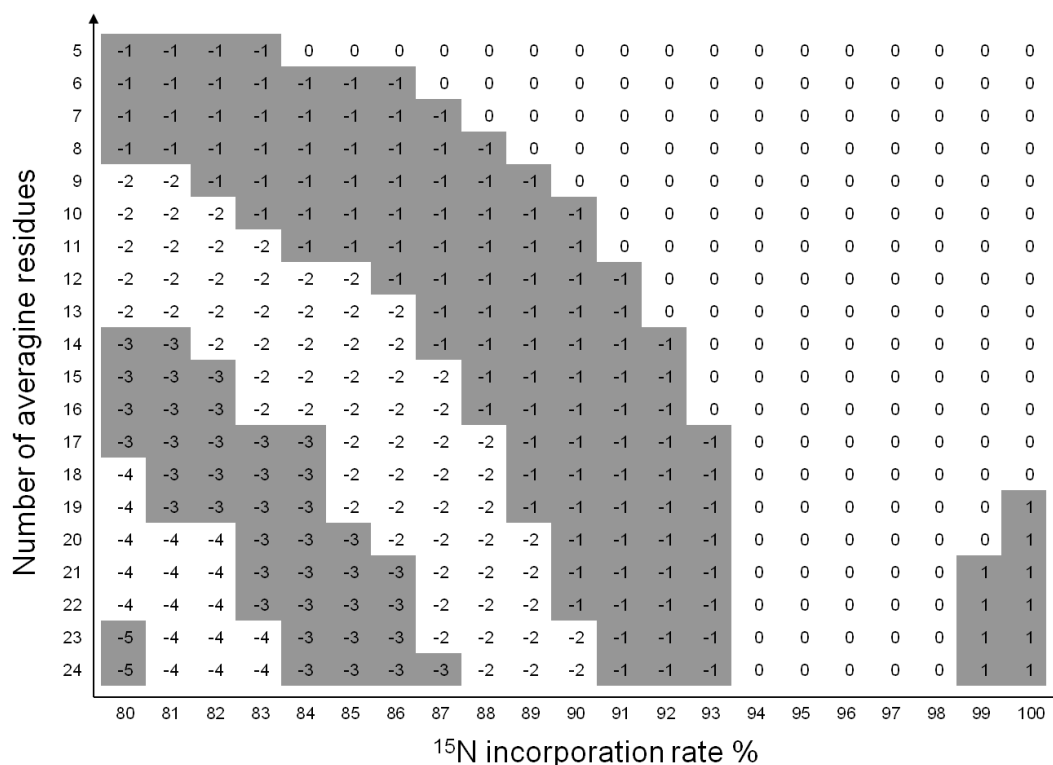
4.1.4 Discussion

As has been reported by others (Balgley et al., 2007; Elias et al., 2005; Kapp et al., 2005) the number of identified peptides depends on the search engine and score threshold. For a given search engine, be it SEQUEST or MASCOT, a ^{15}N database search benefits from the presented modified method in terms of peptide identification number, when the labeling percentage is not close to 100%. The observed FDR for ^{15}N identifications using the conventional method appears to be relatively high, a finding that has been reported by others (Nelson et al., 2007). This is probably due to the increased complexity of the ^{15}N isotopomer and isotopologue patterns, making the correct monoisotopic peak selection during data acquisition and peak mapping during database search less likely. Furthermore, for a 1:1 ^{14}N/^{15}N protein mixture, the ratio of MS/MS spectra from ^{14}N and ^{15}N precursors should also be approximately 1:1. As a consequence, a great number of ^{15}N peptide-derived data submitted to either ^{14}N or ^{15}N database searches will result in a significant number of false positive identifications. This situation gets worse the lower the ^{15}N incorporation rates are since the spectra get even more complex. For our 98% labeled plasma dataset, the ^{15}N FDR for SEQUEST and MASCOT searches is low. However, for 90% labeled brain proteins our modified search method using SEQUEST or MASCOT decreases the ^{15}N FDR by approximately 75% compared to the conventional search method. The ^{15}N search continues to show a much higher FDR than a ^{14}N search for SEQUEST if a fixed threshold filtering is applied. The difference between SEQUEST and MASCOT searches are most likely due to decoy search and threshold filtering methods. MASCOT shows a higher compatibility with lower % ^{15}N incorporation data.

The modified search method also facilitates relative protein quantification. Although existing algorithms like Census (Park et al., 2008) or ProRata (Pan et al., 2006) are able to quantify the paired ^{14}N and ^{15}N peptides from either ^{14}N or ^{15}N search results, a greater number of identified peptides and proteins provide better statistical quantification values. With the conventional search method, peptide and protein quantification is predominantly based on the identified ^{14}N peptides since the number of ^{15}N identifications is low. This results in a loss of information in cases where the ^{15}N signal has a higher intensity than the corresponding ^{14}N signal, the latter thus not being subjected to fragmentation. As a result, peptide signal comparison and quantification are not possible in those cases. With the present method, the greater number of identified and quantified ^{14}N and ^{15}N peptide pairs from the same protein results in increased accuracy, especially in cases where only a few peptides are identified for a protein.

Gouw and colleagues have introduced another method for dealing with ^{15}N-labeled mass spectrometry data (Gouw et al., 2008). In this case precursor selection was corrected. However, this leads to a doubling of database search time and post-search alignment is required. Our method can be performed with a single database search and no post-alignment is necessary since the -1 Da correction can be introduced at the database search step.

We should also emphasize that the deviation between the most intense peak and ^{15}N monoisotopic peak varies not only with the rate of ^{15}N incorporation but also peptide length, both of them affecting isotopologue distribution. This becomes evident from a theoretical simulation of both parameters (**Figure 45**). Averagine is an imaginary average amino acid with the molecular formula $C_{4.9384}H_{7.7583}N_{1.3577}O_{1.4773}S_{0.0417}$, which represents the statistical occurrence of the 20 common amino acids in the Protein Identification Resource (PIR) protein database (Senko et al., 1995). Peptides with different averagine residue numbers and ^{15}N incorporation rates result in isotopologue patterns with varying mass deviations between the ^{15}N monoisotopic peak and the most intense peak. These mass deviations can be calculated for every hypothetical peptide. If the ^{15}N monoisotopic peak and most intense peak coincide this difference is zero. A mass correction in the database search becomes necessary for all the peptides with negative deviation shown in Fig. 2. When the ^{15}N incorporation rate is equal or greater than 90%, the -1Da variable modification works well, and extended modifications, such as -2 Da, do not generate more peptide identifications (data not shown). The modification can be adjusted (e.g. -2 Da) in cases of lower ^{15}N incorporation rates. Searches with more than one modification can also be performed in parallel if necessary. The presented method can also be applied to other global metabolic labeling techniques, including ^{13}C and ^{2}H isotopes, when the incorporation rates are less than 100%. Alternatively, the hypothetical -1 Da variable modification can also be used for peptide C- or N-termini. One advantage of choosing arginine and lysine residues for the variable modification is that the mass shift of long peptides resulting from missed cleavage will be automatically adjusted to -2 Da or greater.

Number of averagine residues	80	81	82	83	84	85	86	87	88	89	90	91	92	93	94	95	96	97	98	99	100
5	-1	-1	-1	-1	0	0	0	0	0	0	0	0	0	0	0	0	0	0	0	0	0
6	-1	-1	-1	-1	-1	-1	-1	0	0	0	0	0	0	0	0	0	0	0	0	0	0
7	-1	-1	-1	-1	-1	-1	-1	-1	0	0	0	0	0	0	0	0	0	0	0	0	0
8	-1	-1	-1	-1	-1	-1	-1	-1	0	0	0	0	0	0	0	0	0	0	0	0	0
9	-2	-2	-1	-1	-1	-1	-1	-1	-1	0	0	0	0	0	0	0	0	0	0	0	0
10	-2	-2	-2	-1	-1	-1	-1	-1	-1	-1	-1	0	0	0	0	0	0	0	0	0	0
11	-2	-2	-2	-2	-1	-1	-1	-1	-1	-1	-1	0	0	0	0	0	0	0	0	0	0
12	-2	-2	-2	-2	-2	-2	-1	-1	-1	-1	-1	-1	0	0	0	0	0	0	0	0	0
13	-2	-2	-2	-2	-2	-2	-2	-1	-1	-1	-1	-1	0	0	0	0	0	0	0	0	0
14	-3	-3	-2	-2	-2	-2	-2	-1	-1	-1	-1	-1	-1	0	0	0	0	0	0	0	0
15	-3	-3	-3	-2	-2	-2	-2	-2	-1	-1	-1	-1	-1	0	0	0	0	0	0	0	0
16	-3	-3	-3	-2	-2	-2	-2	-2	-1	-1	-1	-1	-1	0	0	0	0	0	0	0	0
17	-3	-3	-3	-3	-3	-2	-2	-2	-2	-1	-1	-1	-1	-1	0	0	0	0	0	0	0
18	-4	-3	-3	-3	-3	-2	-2	-2	-2	-1	-1	-1	-1	-1	0	0	0	0	0	0	0
19	-4	-3	-3	-3	-3	-2	-2	-2	-2	-1	-1	-1	-1	-1	0	0	0	0	0	0	1
20	-4	-4	-4	-3	-3	-3	-2	-2	-2	-2	-1	-1	-1	-1	0	0	0	0	0	0	1
21	-4	-4	-4	-3	-3	-3	-3	-2	-2	-2	-1	-1	-1	-1	0	0	0	0	0	1	1
22	-4	-4	-4	-3	-3	-3	-3	-2	-2	-2	-1	-1	-1	-1	0	0	0	0	0	1	1
23	-5	-4	-4	-4	-3	-3	-3	-2	-2	-2	-2	-1	-1	-1	0	0	0	0	0	1	1
24	-5	-4	-4	-4	-3	-3	-3	-3	-2	-2	-2	-1	-1	-1	0	0	0	0	0	1	1

^{15}N incorporation rate %

Figure 45. The mass shift between the most intense peak and ^{15}N monoisotopic peak. The peptides illustrated are hypothetical and consist of a different number of averagine residues. Averagine has the molecular formula $C_{4.9384}H_{7.7583}N_{1.3577}O_{1.4773}S_{0.0417}$, which is based on the statistical occurrence of the 20 common amino acids in the PIR protein database.

4.2 Proteome scale turnover analysis in living animals using stable isotope metabolic labeling

4.2.1 Introduction

Proteomics continues to generate valuable protein identification and quantitation information for many cell types and species. A particular focus of current proteomics efforts is the quantitative assessment of relative as well as absolute protein expression levels. Methods based on stable isotope labeling and label free approaches are employed using mass spectrometers of high resolving power and accuracy (Aebersold and Mann, 2003; Ong and Mann, 2005). Although these studies provide valuable protein identification and quantitation information they only represent "snapshot" pictures of a cellular state that capture the proteomic state of affairs at a given time. However, the proteome is a highly dynamic and tightly regulated entity that is constantly changing and

adapting to its environment. The protein amount represents the final outcome of the protein synthesis and degradation process resulting in expanded, contracted or unchanged protein pools.

Previous studies have found only weak correlations between mRNA and protein levels (Chen et al., 2002; Griffin et al., 2002; Ideker et al., 2001). A potential reason for these discrepancies is differential protein turnover that impacts on the overall protein levels in the cell. Since the overall amount of a protein depends on its synthesis and degradation upcoming changes in protein levels are apparent at a much earlier time point using turnover analysis when those changes are not yet reflected by the total protein amount. This paradigm has great significance for biomarker discovery since it would allow the detection of upcoming protein changes at a much earlier time point. Several reports confirm this hypothesis. Rao *et al.* have found that 5 proteins were upregulated in *Mycobacterium tuberculosis* bacteria grown in high iron medium. However, higher turnover rates were found for 24 proteins in the same experiment (Rao et al., 2008). In another study, Pupim *et al.* found that in chronic hemodialysis patients, nutritional interventions do not or only slightly affect the concentration of serum albumin, whereas turnover of the protein was significantly changed (Pupim et al., 2004).

Protein turnover analysis is typically performed by administering either radiolabeled or stable isotope labeled tracers, mostly amino acids, which are incorporated into proteins during synthesis. The rate of the gain or loss of a tracer provides a measure of protein dynamics. Among other disadvantages the primary shortcoming of turnover determination with the help of radioisotopes is that these methods are restricted to the assessment of whole-body protein. Individual protein dynamics can only be achieved after protein purification rendering this method inefficient for high throughput analyses (Afify, 2002; Marshall et al., 2005; Rechinger et al., 2000). For this and also safety reasons the stable isotope tracer method is now preferred for protein turnover studies, and has become feasible with the availability of mass spectrometers that have high resolution and accuracy.

Studying protein dynamics in cultured cells is a rather straightforward process. In this case, after changing the cell culture media the precursor pool is rapidly converted from an unlabeled to a labeled state or vice versa, so that the media relative isotope abundance (RIA) of the tracer represents the precursor RIA in the cell. Hence the newly synthesized protein will be labeled with a known RIA, and no RIA calculations are required (Pratt et al., 2002).

An RIA of 1, however, can only be achieved in cell culture experiments and is difficult to realize in living animals due to the presence of internal unlabeled amino acids resulting from the degradation of pre-existing proteins. Living animals can be labeled by intravenously injecting the isotope tracer by either continuous infusion (Caso et al., 2001; Walrand et al., 2004) or a flooding dose (Bregendahl et al., 2004). In both cases, however, measuring protein turnover of individual proteins in a high throughput manner is not possible (Doherty and Beynon, 2006a). Furthermore, the sudden intake of the isotope tracer by intravenous injection may alter protein synthesis and lead to artificial protein turnover data (Smith et al., 1998b). Alternatively, the isotope tracer can be administered orally with the diet (Doherty et al., 2005) or water (Rachdaoui et al., 2009) resulting in a more natural labeling of the animals.

All the current methods for protein dynamics measurement require data on precursor RIA, which especially in living animals is difficult to measure precisely. We have developed a new approach which enables monitoring individual protein turnover rates in complex mixtures. A diet, in which all the 20 amino acids are fully ^{15}N-labeled was used as the tracer. This is in contrast to other methods that either use single labeled amino acids as tracers or heavy water where mainly labeled nonessential amino acids are generated. In both instances only low overall RIAs are achieved. The all amino acid labeled diet that we have used significantly amplifies protein labeling efficiency and results in greater data accuracy. Even early on during the labeling process when the precursor RIA is still relatively low, peptides derived from newly synthesized proteins will rarely consist of only unlabeled amino acids.

The mass spectrometry signal of a labeled peptide derived from a newly synthesized protein overlaps with the peptide signal from pre-existing unlabeled protein. To distinguish the labeled/newly synthesized from the unlabeled/pre-existing peptide populations we developed the algorithm *ProTurnyzer* (Protein Turnover Analyzer). The algorithm is based on the hypothesis that the monoisotopic (all ^{14}N) peptide only originates from the pre-existing protein population and hence the knowledge of precursor RIA is not required for protein turnover analysis. Here we present protein turnover data from bacteria and mice that demonstrate the validity of the method.

4.2.2 Material and methods

4.2.2.1   Material

Standard rodent diet (Harlan Laboratories, Inc., Indianapolis, IN) and bacterial protein-based rodent diet (Silantes GmbH, Munich, Germany) were used for all experiments. Two isotopic forms of the bacterial diet were used: natural isotope ^{14}N and ^{15}N-enriched. Media for *E. coli* culture were ^{14}N (Spectra 9-U) and ^{15}N-enriched (Spectra 9-N, >98%) (Cambridge Isotope Laboratories, Inc., Andover, MA). All other chemicals were from Sigma-Aldrich (St. Louis, MO), Merck (Darmstadt, Germany) and BioRad (Hercules, CA).

4.2.2.2   Animal experiments

Twelve 8-week old DBA/2 male mice were divided into 6 groups. For adaptation to the bacterial protein diet the animals were first fed ^{14}N bacterial diet for 4 days. Two mice only fed with the ^{14}N bacterial diet were then sacrificed. Blood was taken by cardiac puncture, and the plasma was obtained by centrifuging the blood in an EDTA pre-added tube at 1,300 × g for 10 min. The remaining body blood was removed by 0.9% saline perfusion. The plasma and organs were snap-frozen in liquid nitrogen and the samples stored at -80°C for further usage. The food supply for the remaining mice was switched to ^{15}N-labeled bacterial diet and 2 mice each were sacrificed after 1, 2, 4, 7, and 14 days of feeding with the labeled diet (**Figure 46**). Organs and blood were isolated. The animals did not show any discernible health effects compared to animals fed with a standard diet.
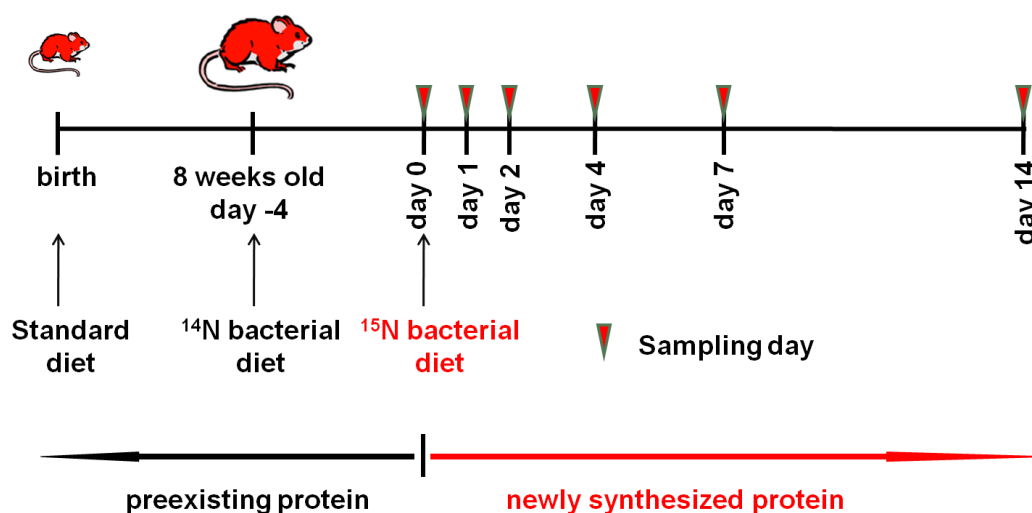

Figure 46. ^{15}N feeding protocol for DBA/2 mice.

4.2.2.3   *E.coli* experiments

[14]N (Spectra 9-U) and ^{15}N-enriched (Spectra 9-N, >98%) media were used for bacterial cultures. 20%, 40%, and 60% ^{15}N-labeled media were generated by mixing the ^{14}N and ^{15}N media at 80 : 20, 60 : 40, and 40 : 60 ratios, respectively. Single *E. coli* clones were pre-cultured in 2 ml of natural, 20%, 40%, or 60% ^{15}N-labeled media for 6 h at 37°C with shaking at 220 rpm. Then the bacteria were expanded into 100 ml of the same media containing 100 μg / ml ampicillin and incubated overnight at 37°C with shaking at 220 rpm. The bacterial pellets were obtained by centrifuging the cultures at 5,000 rpm for 15 min at 4°C.

4.2.2.4   Sample preparation

Mouse plasma protein concentrations from days 0, 1, 2, 4, 7 were measured by Bradford assay. Mouse cerebella from days 0, 2, 4, 7, 14 were put into ice-cold 5× buffer of 250 mM sucrose, 50 mM Tris - HCl (pH 7.4), 5 mM $MgCl_2$, 1 mM DTT, 25 μg / ml Spermine, 25 μg / ml Spermidine and protease inhibitor cocktail tablet (F. Hoffmann-La Roche Ltd., Basel, Switzerland), and then homogenized with a Teflon-glass dounce homogenizer and an electric drill at 1,200 rpm for 3 min. The homogenates were centrifuged at 20,000 g for 30 min at 4°C and the supernatants collected. The protein concentrations were estimated by Bradford assay.

The *E. coli* pellets were sonicated in lysis buffer consisting of 100 mM Tris-HCl (pH 8), 150 mM NaCl, 1 mM EDTA to break the bacterial cells. The lysates were then centrifuged at 13,000 rpm for 12 min and the supernatants containing the soluble proteins were collected. The protein concentrations were estimated by Bradford assay. The [14]N- and differently ^{15}N-labeled *E. coli* populations were mixed to obtain defined *E. coli* mixtures with different labeled/unlabeled ratios according to their protein concentrations (**Table 13**). The labeled protein fractions consisted of 3 populations with different ^{15}N incorporations in order to simulate newly synthesized proteins exposed to different ^{15}N amounts.

The mouse brain, mouse plasma, and *E. coli* protein mixtures were resolved by SDS-PAGE and the gel stained with Coomassie Brilliant Blue. The gel lane containing the separated proteins was cut into 2 mm-wide pieces, and several selected pieces subjected to in-gel tryptic digestion. Gel pieces were destained twice with 100 μL 50 mM NH_4HCO_3 / ACN (1 : 1, vol / vol) for 30 min, and disulfide bonds reduced with 10 mM DTT in 50 mM NH_4HCO_3 at 56°C for 30 min, and then alkylated with 55 mM iodoacetamide in 50 mM NH_4HCO_3 in the dark for 30 min. Subsequently, 12.5 ng / μL trypsin in 25 mM NH_4HCO_3 was added to saturate and cover gel slices. The enzymatic reaction was carried out at 37°C overnight.

After digestion, the peptides were extracted from the gel pieces by adding 5% formic acid at 37°C for 30 min. The gel pieces were spun down and the liquid collected. The extraction was repeated twice. Finally, the extracted peptide mixture was lyophilized to dryness and dissolved in 10 μL 0.1% formic acid.

4.2.2.5   HPLC and mass spectrometry

The peptide mixtures were analyzed by nanoHPLC (Eksigent Technologies, Inc., Dublin, CA) coupled to an LTQ-Orbitrap (Thermo Fisher Scientific, Bremen, Germany) hybrid mass spectrometer. The C18 reverse-phase columns were made by packing PicoFrit emitters (New Objective, Inc., Woburn, MA) using a methanol slurry of reverse-phase ReproSil-Pur C18-AQ 3μm resin (Dr. Maisch GmbH, Ammerbuch-Entringen, Germany) under a constant 100 bar pressure. The packed columns were cut to approximately 15 cm length. Peptides were separated at a 200 nl/min flowrate using a gradient of 2-98% solvent B (98% ACN in water, 0.1% FA) over 130 min. The eluates were on-line electrosprayed into the mass spectrometer via a nanoelectrospray ion source (Thermo Fisher Scientific, San Jose, CA).

The LTQ-Orbitrap was running in positive ion, top 5 data-dependent acquisition mode. For full scans in the Orbitrap, the target ion value was 1,000,000 and the maximal injection time was 500 ms at a resolution of r=60,000 at m/z 400. The MS full scan range was 380-1600 m/z. The 5 most intense peaks in the MS scan were fragmented in the LTQ by collision-induced dissociation with a target value of 10,000 ions and injection time of 250 ms. Former precursor ions selected for MS/MS were dynamically excluded for a period ranging from 30 to 60 s.

The mass spectrometric conditions were: spray voltage, 2.1 kV; no sheath and auxiliary gas flow; ion transfer tube temperature, 200°C; normalized collision energy using wide-band activation mode, 35% for MS2.

4.2.2.6   Free amino acid analysis

We analyzed tissue free amino acids to investigate the enrichment of the precursor pool for protein synthesis. Although aminoacyl-tRNA is the actual precursor (Caso et al., 2002; Johnson et al., 1999; Martini et al., 2004), previous studies have shown that the tissue free amino acid pool is a valid surrogate for measuring the enrichment, while being accessible much more easily (Davis et al., 1999). Mouse plasma and brain extract were prepared using a cation-exchange extraction and derivatization with propyl chloroformate using the EZfaast amino acid analysis kit (Phenomenex, Torrance, CA). Prior to extraction the

samples were spiked with a mixture of internal standards homoarginine, methionine d3, and homophenylalanine supplied with the kit. Extraction and derivatization were performed according to the manufacturer's manual. Derivatized amino acids were separated in 15 min in gradient mode using a reversed phase Kinetex 2.1 x 150 mm 1.7 um C18 column (Phenomenex) at 0.25 mL/min flow rate on an ACQUITY UPLC system (Waters, Milford, MA). The column was thermostated at 40°C. Mobile phase A was 10 mM ammonium formate in water, mobile phase B was 10 mM ammonium formate in 99.5% methanol. The following gradient program was used: 0 min – 40% B, 10 min – 75% B, 12 min – 75% B with subsequent equilibration at 40% B for 3 min. The amino acid samples were held in an autosampler at 15°C. Injection volume was 5 µL and each sample was injected twice. The UPLC was coupled to an Exactive benchtop Orbitrap mass spectrometer (Thermo Fisher Scientific). The mass spectrometer operated in positive electrospray ionization mode at 50,000 FWHM resolution (2 scans/s), 250 ms maximum inject time and balanced AGC target (10e6 ions) scanning in m/z 195-505 mass range. The following tune parameters were used: 3.5 kV spray voltage, 275°C capillary temperature, 40, 8 and 1 arbitrary units of sheath, auxiliary and sweep gas (nitrogen), 60 V capillary voltage, 100 V tube lens voltage, 20 V skimmer voltage. The data analysis was performed using LCquan software (Thermo Fisher). Theoretical masses of natural and ^{15}N labeled derivatized amino acids were calculated using Xcalibur software and a 2 mmu window was used to ensure selective detection. Eight level calibration curve was built at concentration levels 6 nM, 20 nM, 60 nM, 2,00 nM, 600 nM, 2,000 nM, 6,000 nM, and 20,000 nM with 1/X weighting factor. Calibration curve was linear with R^2 at least 0.95. Calibrators were spiked with internal standards at the same level as the samples. Therefore a response factor (area ratio of analyte peak to internal standard peak) was calibrated to concentration levels. Calibration standards of natural amino acids were supplied with the kit. The samples were 10 fold diluted compared to the calibration standard to avoid column and detector saturation problems for abundant amino acids. Concentration of ^{15}N-labeled amino acids was calculated under the assumption that the response factor is the same for natural and ^{15}N-labeled amino acids.

4.2.2.7 Data processing

The LTQ-Orbitrap raw files were converted to universal mzXML format using ReAdW (http://tools.proteomecenter.org/software.php). The raw MSn data were converted to mzData files with Bioworks 3.3.1 SP1 (Thermo Fisher Scientific, Waltham, MA), and then searched against IPI-mouse database v 3.57 (20 ppm mass tolerance for the MS scan, 0.8

Da for the MS/MS scan, fixed carbamidomethylation for cysteine, and variable oxidation for methionine) or SwissProt15.3 *E.Coli* database (20 ppm mass tolerance for the MS scan, 1 Da for the MS/MS scan, fixed carbamidomethylation for cysteine, and variable oxidation for methionine) with activation of the *Decoy* checkbox using MASCOT v 2.2 (Perkins et al., 1999). MASCOT results were exported as xml files with a filtering threshold of p<0.001 and score>20. MASCOT xml and mzXML files were subsequently used for *ProTurnyzer* analysis.

4.2.2.8   ProTurnyzer

The in-house developed software *ProTurnyzer* was written in Java. All peptide IDs are read from the MASCOT files and for each ID the sequence and identification scan (MS/MS scan) are stored. The expected isotopologue distributions (masses and frequencies) of the peptides are calculated based on the respective sequence and natural frequencies of the isotopes. For each peptide, additional theoretical masses are calculated to account for additional peaks of isotope enriched (labeled) molecules. For each mass extracted ion chromatograms (XICs) were created by extracting peak intensities from the raw data from scans within an elution time window of 60 s before and after the corresponding MS/MS scan. The chromatographic peak of the peptide was determined by local minima of the XIC of the monoiostopic ion. In general there is no need for de-noising and smoothing before peak extraction on modern mass spectrometers such as the LTQ Orbitrap due to their high resolution and accuracy.

The following equations formally describe the algorithm to estimate the fractional synthesis rate of an identified peptide.

Let m_p be the theoretical mass of the *p*th isotopic peak and $p \in \{0,\dots,N,\dots,M\}$. The first *N + 1* masses are calculated based on natural isotope abundances comprising all natural isotopologues, whose frequency is at least 10%. The remaining *M − N* masses correspond to additional theoretical masses of all peaks that might arise from isotopic enrichments in a given range. These additional masses are defined by

$$m_p = m_{p-1} + d \text{ for } p \in \{N+1,\dots,M\}, \tag{1}$$

where *d* is the constant mass difference between the ^{15}N and the ^{14}N isotopes. In other words, the additional masses arise by replacing a ^{14}N atom with a ^{15}N atom until the percentage of heavy nitrogen atoms reaches a user defined maximum.

Let i_p be the total measured intensities of the pth isotopic peak, which is derived by summing up all extracted ion intensities for that particular mass across the chromatographic peak of the peptide. Simple summation results in a weighted average of the relative isotopologue intensities. Based on ion statistics, the most intense scans (highest weight) should also most accurately reflect the true relative intensities. The total peptide intensity T is then simply the sum of all intensities arising from both natural and labeled molecules, denoted by T^{nat} and T^{lab}, respectively

$$T = T^{nat} + T^{lab} \tag{2}$$

From the extracted data the amount of total unlabeled signal can be calculated by

$$T^{nat} = \frac{i_0}{f_0} \tag{3}$$

where i_0 and f_0 are the extracted intensity and calculated theoretical fractional frequency of the monoisotopic peak, respectively. The labeled peptide fraction LPF is then defined as the proportion of the labeled peptide signal to the total peptide signal, i.e.

$$LPF = \frac{T^{lab}}{T} = \frac{T - T^{nat}}{T} = 1 - \frac{T^{nat}}{T} \tag{4}$$

In order to determine actual rates, protein degradation has to be taken into account as well. Assuming steady state conditions (amount of synthesis = amount of degradation), the labeled peptide fraction measured after labeling duration t, LPF_t, can be described by an exponential equation

$$LPF_t = 1 - e^{-\lambda t} \tag{5}$$

Where λ is the degradation/synthesis rate constant. Rearranging yields the final equation to estimate the FSR, which is independent of the labeling duration

$$FSR = \lambda = \frac{-\ln(1 - LPF_t)}{t} \tag{6}$$

For further analysis, in case the required conditions are met, the LPF values can be converted into fractional synthesis rates using equation (6). However, even if steady state cannot be assumed, relative differences in protein turnover between two states can be readily derived from the LPF.

4.2.2.9   Western blot

Relative protein levels of α-tubulin from 14 d labeled brain, and liver carboxylesterase 1 from 1 d labeled plasma were analyzed by Western blot. Protein mixtures with equal protein content (10 µg) were first resolved by SDS-PAGE. Each sample was loaded three times. Subsequently, the separated proteins were transferred onto polyvinylidene fluoride membranes. Western blot analysis was then performed with anti-α-tubulin (1:5000, CP06**,** Oncogene Research Products, La Jolla, CA) and anti-liver carboxylesterase 1 (1:500, ab52941, Abcam plc., Cambridge, UK) antibodies, respectively. The membranes were then incubated with HRP-conjugated secondary antibody. ECL system and film were used for membrane visualization. Quantification of ECL images was done using *Quantity One* software (BioRad).

4.2.2.10   Gene ontology and pathway analysis

Brain proteins derived from 7 day labeled mice were sorted by FSR in ascending order and divided into four equal bins. The GO (Ashburner et al., 2000) analysis was performed using the methods described previously (Pan et al., 2009) using R (Team, *2009*) and the GOstats (Falcon and Gentleman, 2007) package. Briefly, for each bin the p-values for each GO category were calculated by the conditional hypergeometric test using the quantitative proteome as a background. After obtaining the p-value for each category and bin, GO categories were filtered based on their p-values. Categories with no significant enrichment (p<0.05) in any bin were filtered out. Those categories which did not have a p-value for a bin after filtering were provided a conservative p-value of 1. Finally, the p-values were transformed with the equation $x = -\log_{10} p$, and the z-scores were calculated by [x-mean(x)]/sd(x). For the KEGG (Kanehisa et al., 2004) analysis the mouse proteins were mapped to the KEGG ortholog level. This allows an interspecies comparison for further investigations. Afterwards the hypergeometric test was calculated using R. The background of the test was set to all mouse proteins in KEGG with at least one pathway entry (3319). Similar to the GO analysis the p-values were transformed into z-scores.

4.2.3 Results

4.2.3.1   ProTurnyzer

The determination of protein turnover with the newly developed *ProTurnyzer* algorithm is based on the assumption that for peptides derived from co-existing labeled and unlabeled proteins, the monoisotopic peptide population almost exclusively originates from the

pre-existing protein fraction. This is evident from the following calculations. The probability of observing monoisotopic tryptic peptides is influenced by the total number of atoms N of each element and its corresponding heavy isotope percentage in the precursor pool p during protein synthesis. The greater N and/or p are, the lower is their contribution to the monoisotopic fraction. For example, for a hypothetical peptide consisting of 10 averagines (Senko et al., 1995) that is synthesized under unlabeled conditions, the probability of generating a monoisotopic peptide is 53.4% (**Figure 47a**). In contrast, if the precursor pool is labeled with 10% ^{15}N, the probability of synthesizing a monoisotopic peptide is reduced to 13.6% (**Figure 47b**). In case of a 20% ^{15}N-labeled precursor pool, the monoisotopic peptide level decreases to only 3% (**Figure 47c**). Although an *in silico* tryptic digestion of all proteins from a typical protein database results in a relatively large number of small peptides (Elias and Gygi, 2007), only very few peptides smaller than 10 amino acids in sequence are typically identified during a shotgun mass spectrometry experiment. Commonly identified tryptic peptides have an average length of approximately 15 amino acids (Wang et al., 2010) and the newly synthesized labeled peptides are mainly non-monoisotopic in nature. For instance, a 15 averagine peptide only contains 0.4% monoisotopic signal when labeled with 20% ^{15}N (**Figure 47g**). In summary, unless a peptide has a very short sequence and a low ^{15}N% incorporation, the newly synthesized fraction is mainly made up of the non-monoisotopic species. Thus, for the majority of commonly identified peptides, the newly synthesized fraction will have a negligible monoisotopic signal (**Figure 47d, h**).
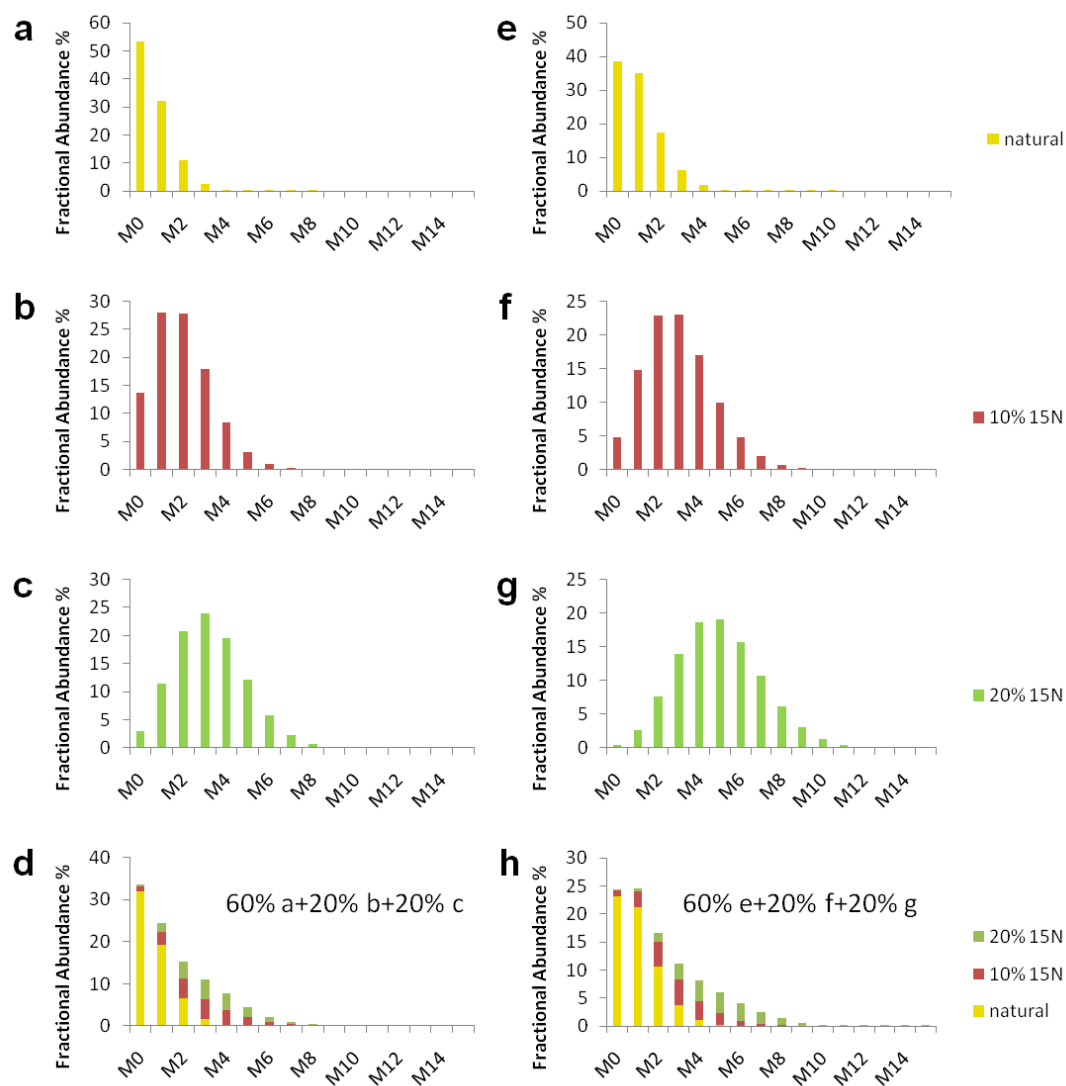
Figure 47. Theoretical isotopologue distributions for peptides consisting of 10 (a,b,c,d) or 15 (e,f,g,h) averagine residues with natural (a,e), 10% (b,f) and 20% [15]N (c,g) content. The monoisotopic peptide signal disappears rapidly with increasing peptide length and/or ^{15}N incorporation. Spectra d and h show mixed peptide populations, consisting of natural, 10% [15]N, 20% [15]N populations at a ratio of 60:20:20. The example demonstrates that the monoisotopic peptide signal mainly represents the natural protein population. M_0 represents the monoisotopic peptide. Mx the peptides containing x heavy isotopes.
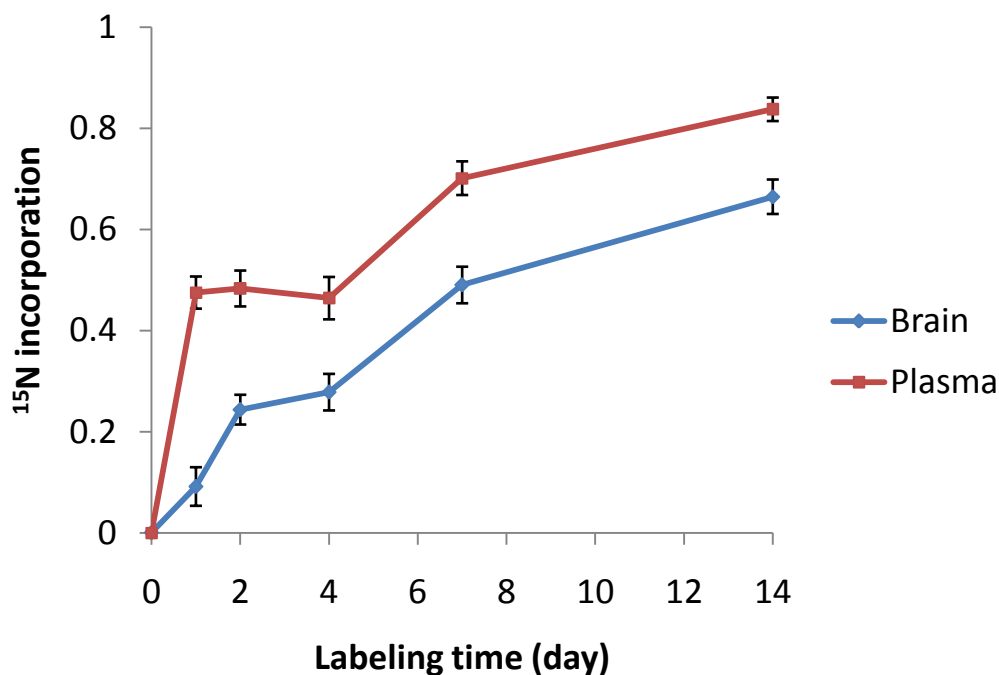
Figure 48. The free amino acid relative isotopic abundance in mouse brain and plasma during ^{15}N labeling. A rapid increase of the ^{15}N label is observed in plasma whereas in brain tissue the ^{15}N incorporation is somewhat delayed.

To verify the above assumption we analyzed free amino acids in tissue and plasma for ^{15}N enrichment of the precursor pool in living mice. Prior to feeding the animals with the ^{15}N-labeled diet only ^{14}N amino acid signals were detectable. After feeding the ^{15}N-labeled diet for 14 days, the ^{15}N amino acid signal increased from 0% to 66% in brain tissue and from 0% to 84% in plasma (**Figure 48**). Since diet-based amino acids can get into plasma more rapidly, the ^{15}N amino acid quantity increased at a relatively high rate at the beginning of labeling (47% on day 1). The plasma proteins which are mostly synthesized in the liver incorporate labeled amino acids without much delay resulting in mainly non-monoisotopic signals for almost all tryptic peptides. Previous studies have shown that brain has lower amino acid concentrations since free amino acids cannot enter it directly due to the blood brain barrier (Hawkins et al., 2006). This is the reason for the low ^{15}N increase in brain compared to plasma. On day 1 the free ^{15}N amino acid levels were approximately 10% and increased to 66% on day 14 (**Figure 48**). Since essential amino acids cannot be synthesized *de novo* by the organism, they must be obtained from the diet. Therefore, the essential amino acid ^{15}N% should increase at a faster rate than the one for non-essential amino acids. This was indeed the case for the plasma samples on days 1, 2 and 4 whereas in the brain samples the difference was insignificant (data not shown).
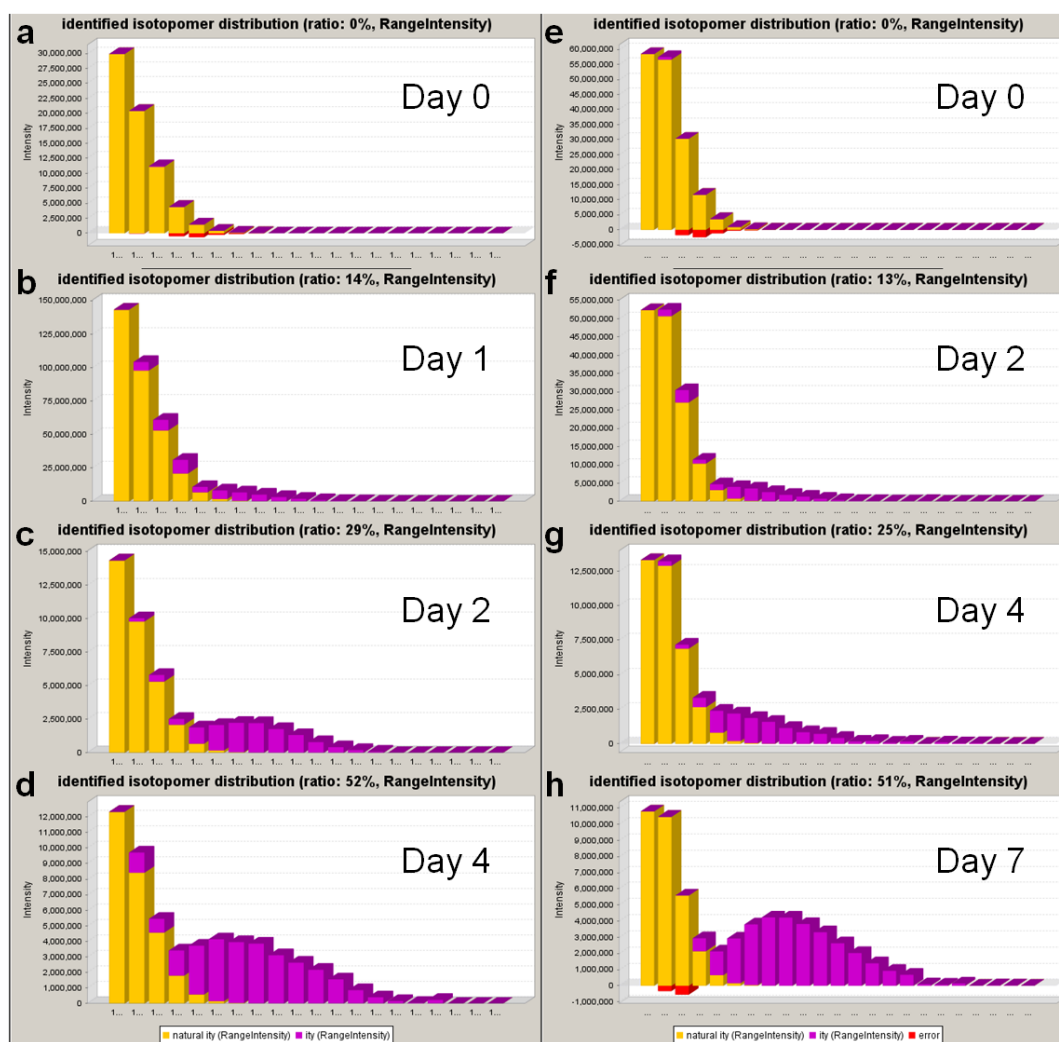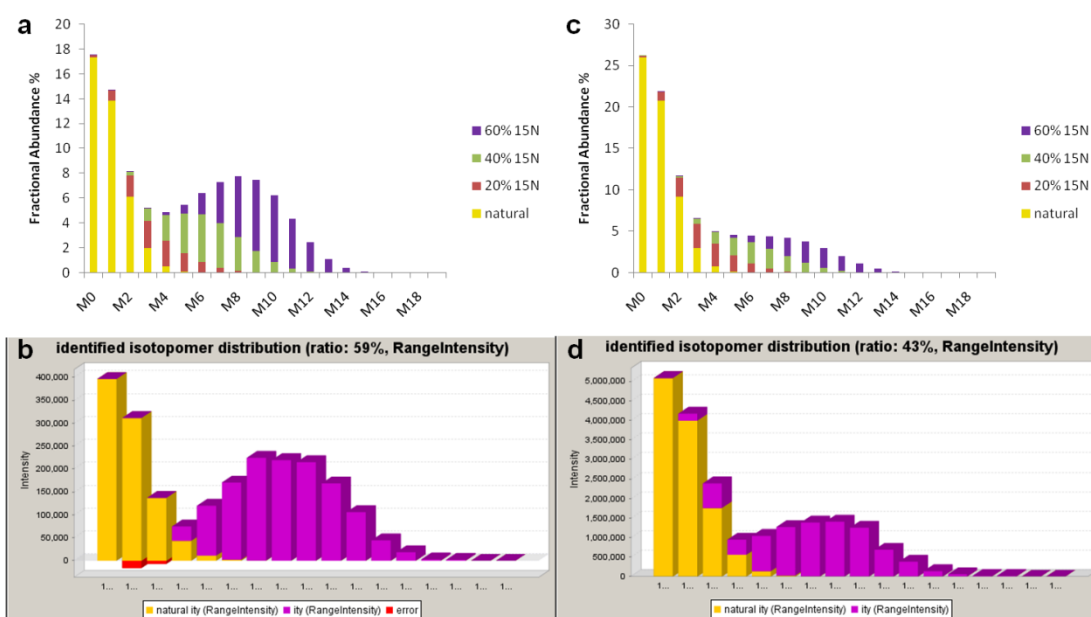
Figure 49. Isotopologue distributions of plasma albumin peptide TCVADESAANCDK (a, b, c, d) and brain heat shock protein 70kDa peptide LDKSQIHDIVLVGGSTR (e, f, g, h) at different labeling times as determined by mass spectrometry followed by *ProTurnyzer* analysis. The yellow part of the bars represents the peptide derived from pre-existing protein, and the purple part the peptide derived from newly synthesized protein. With increasing labeling time the newly synthesized protein fraction steadily increases whereas the pre-existing protein fraction disappears. The average mass of the peptide derived from newly synthesized protein increases along with the precursor pool RIA.

Table 13. *E.Coli* protein mixtures labeled to different extents with ^{15}N.

	^{15}N content	Proportion (%) in mixture	Theoretical ^{15}N labeled fraction (%)	Measured ^{15}N labeled fraction (mean±S.E. %)
Mixture 1	Natural	40	60	61.18±1.34

|			
	20%	10	(n=82)
	40%	20	
	60%	30	
Mixture 2	Natural	60	
	20%	13.3	38.92±1.09
	40%	13.3	40 (n=116)
	60%	13.3	

Figure 50. Mass spectra of *E.Coli* protein carbamoyl-phosphate synthase peptide ELLIDESLIGWK. a, c: theoretical isotopologue distributions of the peptide in mixtures 1 (a) and 2 (c) (see **Table** 13 for compositions). b, d: observed mass spectra of the peptide following *ProTurnyzer* analysis. The yellow part of the bars represents the natural peptide and the purple part the labeled peptide fractions.

In order to validate the *ProTurnyzer* algorithm for calculating the protein fractional synthesis rate (FSR), we performed experiments with predefined ^{15}N-labeled protein mixtures derived from *E.coli* cultures (**Table 13**). The objective here was to distinguish labeled and unlabeled peptide populations based on the mass spectrometry isotopologue patterns. In the example, the observed isotopologue distribution of *E.Coli* carbamoyl-phosphate synthase tryptic peptide ELLIDESLIGWK is close to the predicted isotopologue distribution calculated based on the differentially labeled protein mixtures (**Figure 50**). The *ProTurnyzer* algorithm is able to distinguish the labeled and unlabeled fractions (**Figure 50b, d**) and the average % of labeled peptide in mixtures 1 and 2 was

calculated to be 61.18±1.34% and 38.92±1.09%, respectively (**Table 13**), which is in good agreement with the expected values (60% and 40%, respectively). These data demonstrate that *ProTurnyzer* succeeds in capturing the labeled fraction of an isotopologue pattern from labeled and unlabeled peptide mixtures without prior knowledge of the precursor pool RIA.

4.2.3.2   Protein turnover analysis in living mice

Mice were fed a ^{15}N-labeled diet for several days to analyze brain tissue and plasma protein turnover. **Figure 49** shows tryptic peptide isotopologue distributions for plasma albumin and brain heat shock protein 70 kDa at different labeling times. The yellow part of the bars represents the unlabeled peptide fraction derived from pre-existing protein. The purple part represents the peptide fraction that is newly synthesized from ^{15}N-labeled amino acids in the precursor pool. The gain of purple and loss of yellow signals reflect the protein turnover progress. The average peptide mass of the purple signal increases over the course of ^{15}N labeling, reflecting an increased ^{15}N amino acid incorporation into the precursor pool. At an early labeling time the newly synthesized proteins have a low ^{15}N content and the tryptic peptide isotopologue signal overlaps with the one from the pre-existing protein. Despite this low ^{15}N content *ProTurnyzer* is still able to distinguish the mixed peptide populations. Our data show that the FSR calculated for the albumin peptide TCVADESAANCDK is approximately 15%/day, which is in good agreement with the 4.96%/8h value reported using the $H_2^{18}O$ labeling method (Rachdaoui et al., 2009).
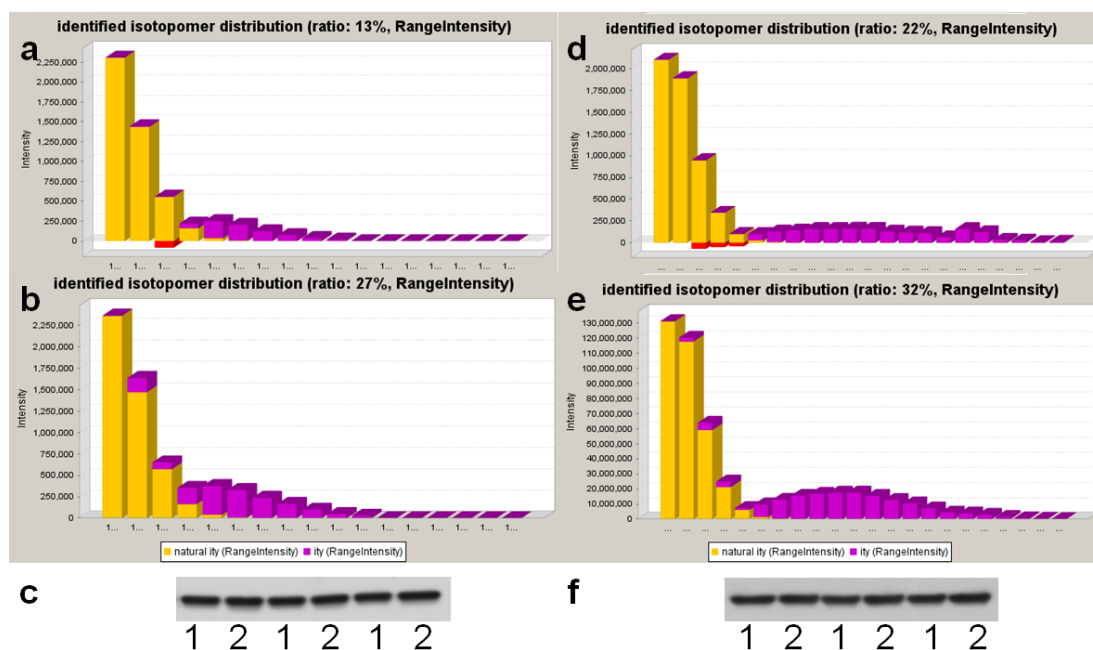
Figure 51. Liver carboxylesterase (a,b,c) and alpha-tubulin (d,e,f) *ProTurnyzer*(a,b,d,e) and Western blot analyses (c,f) in two mice of the same strain. a, b: *ProTurnyzer* analysis results for carboxylesterase peptide EGASEEETNLSK from 1-day labeled mouse plasma. d, e: *ProTurnyzer* results for alpha-tubulin peptide NLDIERPTYTNLNR from 14-day labeled mouse brains. The purple part of the bars represents peptide derived from newly synthesized protein. In both cases, mouse 2 (corresponding to spectra b and e) shows a faster turnover rate than mouse 1 (corresponding to spectra a and d). No difference in protein amount is detected by western blot (c, f) between the two animals (analyzed in triplicate).

In another set of studies we investigated the correlation between protein turnover and quantity. Liver carboxylesterase N (IPI00138342) from 1-day labeled plasma and tubulin alpha (IPI00117350) from 14-day labeled brain tissue showed different turnover rates between two animals (**Figure 51a, b, d, e**). At the same time western immunoblots showed no detectable change in the two proteins' expression levels (**Figure 51c, f**) implying that protein synthesis can vary without an obvious change in overall protein expression. It also demonstrates that protein turnover is a more sensitive measure for detecting biological variability.
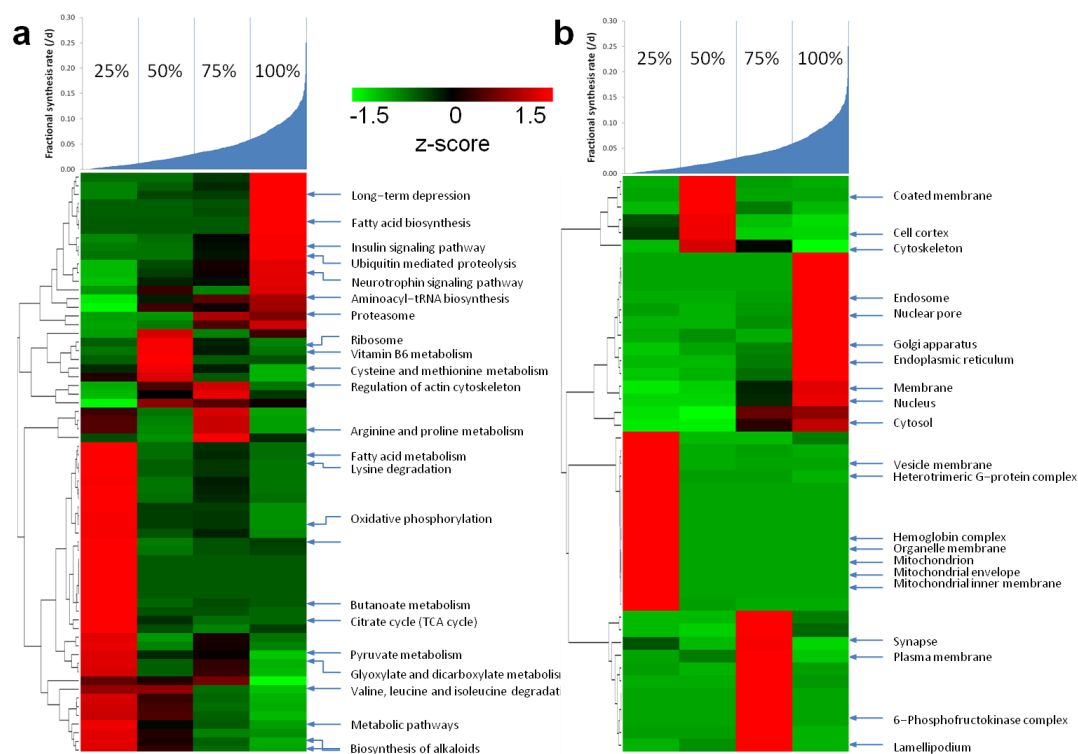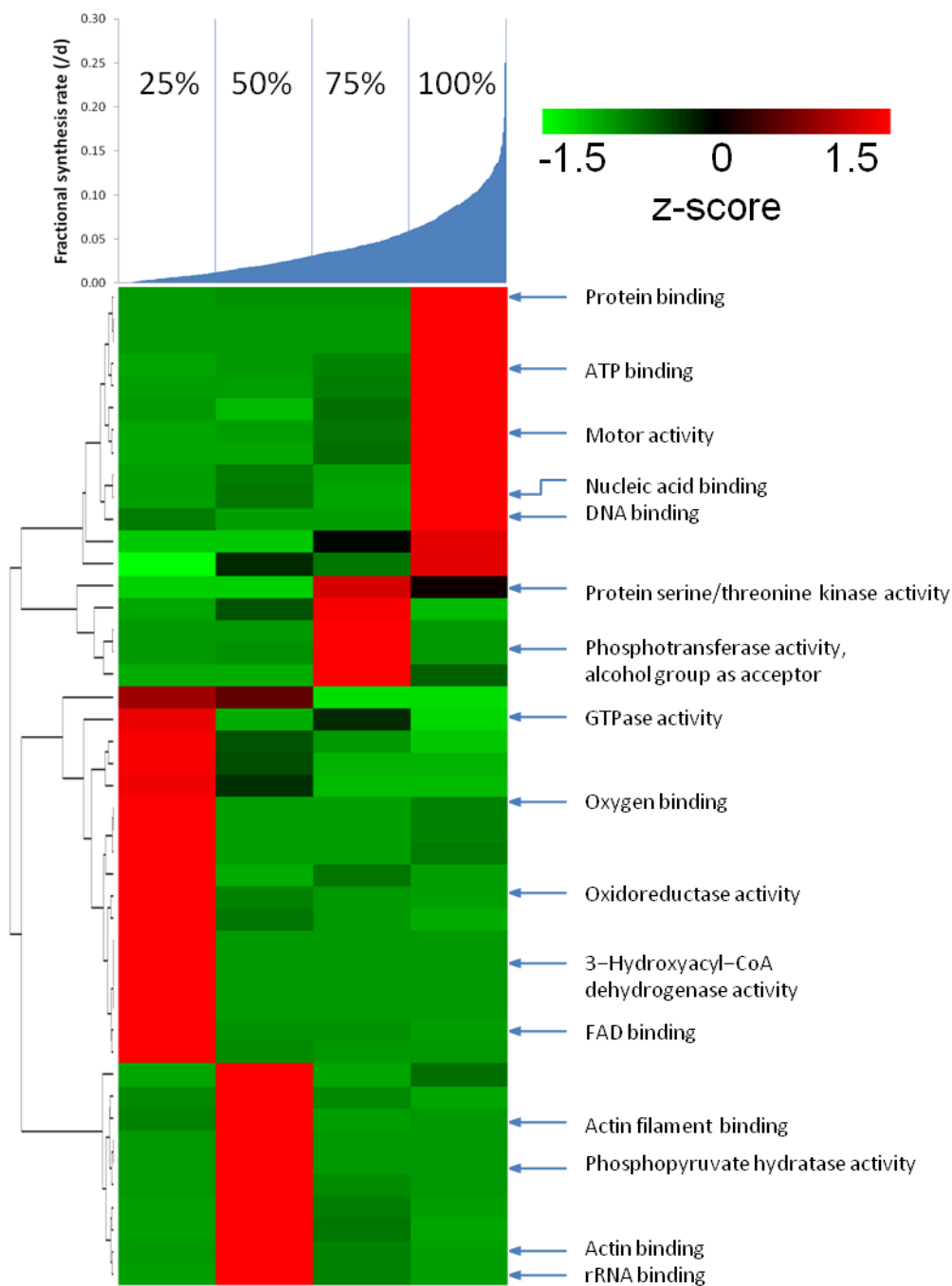
Figure 52. Correlation between brain protein turnover and KEGG pathway (a) and gene ontology cellular component (b). The blue graph on top displays protein FSR distribution from 7-day labeled brain tissue. Proteins were divided into four equal bins and analyzed with respect to KEGG pathways and GO categories. P-values were transformed to z-scores indicating bin specific enrichments (Due to the limited resolution the pathway and category names on the right are not legible; higher resolution figure is available in electronic file.).

Based on their FSRs brain proteins from 7-day labeled brain tissue were divided into equal four bins. Proteins in each bin were analyzed independently with respect to enrichment in GO categories cellular component, molecular function, biological process, as well as KEGG pathways. Only categories with at least one bin of statistical significance larger than 95% (p-value<0.05) are shown. KEGG pathway analyses (**Figure 52a**) reveal that pathways citrate cycle (TCA cycle) (p=7.6E-17), valine, leucine and isoleucine degradation (p=5.8E-15) and butanoate metabolism (p=2.5E-12) are enriched with proteins from the first bin with low FSRs. In contrast, proteasome (*p*=1.7E-5), fatty acid biosynthesis (*p*=3.9E-4) and aminoacyl-tRNA biosynthesis (*p*=5.0E-4) are enriched with proteins from the fourth bin, implying high turnover rates. The GO analysis on cellular components (**Figure 52b**) demonstrates that proteins in the mitochondrion (*p*=7.1E-15), mitochondrial inner membrane (*p*=6.3E-12), mitochondrial envelope (*p*=8.3E-11), and organelle membrane

(p=4.2E-9) are enriched in the first bin, and proteins in the nucleus (p=2.0E-5) and endoplasmic reticulum (p=7.0E-4) are enriched in the fourth bin. Our results are in agreement with a previous study (Takizawa and Yamashita, 1989) that also found shorter biological half lives for nuclear compared to mitochondrial proteins. GO biological process and molecular function analyses also demonstrate differences in protein turnover. Proteins relevant to oxidation/reduction (p=3.4E-5), acetyl-CoA metabolic process (p=4.7E-5), and hyaluronic acid binding (p=0.001) and oxidoreductase activity (p=0.004) are enriched in the first bin, indicating slow turnover rates. The proteins relevant to protein metabolic process (p=2.7E-4), cellular biopolymer metabolic process (p=8.3E-4), and protein binding (p=1.7E-4), DNA binding (p=4.7E-4), unfolded protein binding (p=6.7E-4) and ATP binding (p=7.9E-4) are enriched in the fast turnover bin (**Figure 53, 54**).
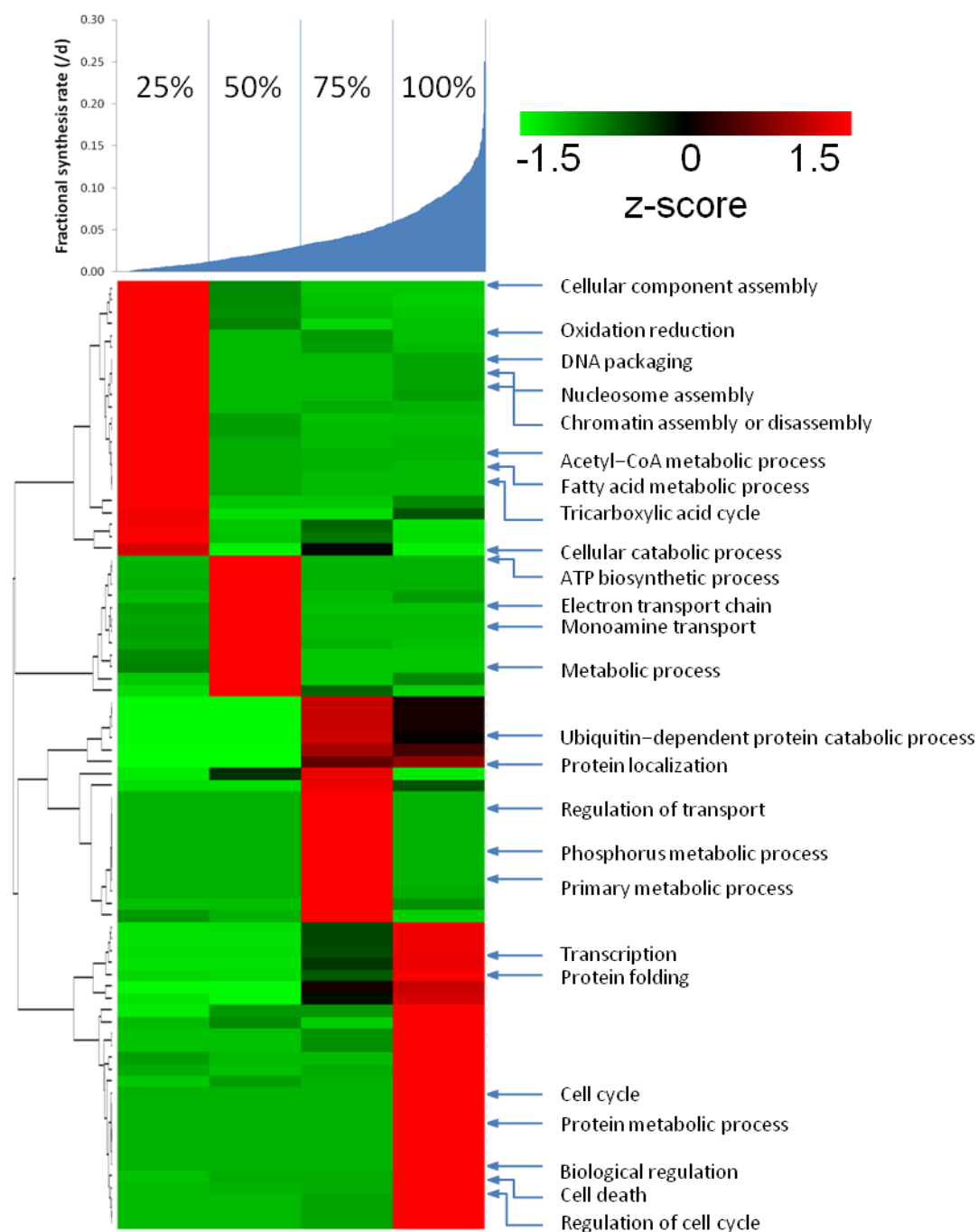
Figure 53. Correlation between brain protein turnover and gene ontology biological process. The blue graph on top displays protein FSR distribution from 7-day labeled brain tissue. Proteins were divided into four equal bins and analyzed with respect to KEGG pathways and GO categories. P-values were transformed to z-scores indicating bin specific enrichments.

Figure 54. Correlation between brain protein turnover and gene ontology molecular function. The blue graph on top displays protein FSR distribution from 7-day labeled brain tissue. Proteins were divided into four equal bins and analyzed with respect to KEGG pathways and GO categories. P-values were transformed to z-scores indicating bin specific enrichments.

4.2.4 Discussion

We introduce a new straightforward method for the global analysis of individual protein turnover in live organisms that unlike other protein turnover analysis methods (Doherty and Beynon, 2006b) does not require precursor pool RIA knowledge. Our method is based on the hypothesis that tryptic peptides derived from newly synthesized proteins are essentially devoid of any monoisotopic peptides. This is attributable to the fully ^{15}N labeled dietary tracer, which significantly increases labeling efficiency. We show that for an average sized tryptic peptide with a low ^{15}N incorporation the monoisotopic peptide signal is mostly derived from the pre-existing protein population (**Figure 47h**). We also demonstrate that the free amino acid RIA increases rapidly for plasma proteins, and somewhat slower in the brain. As a consequence the newly synthesized protein fraction can be distinguished from the pre-existing fraction already early on in the labeling process (**Figure 49**).

Other methods for protein turnover analysis in live organisms that rely on RIA knowledge have been developed previously. One such method is mass isotopomer distribution analysis (MIDA) (Hellerstein and Neese, 1992, 1999). After labeling an organism with a single labeled amino acid tracer, the precursor RIA can be calculated based on the ratio between the intensities of singly and doubly labeled peptide populations. However, adapting the MIDA method to precursor pools whose RIA is changing is not straightforward, since proteins synthesized over the course of the labeling process are exposed to non-homogeneous precursor RIAs. The second limitation of the MIDA approach is that only tracer amino acid-containing peptides are amenable to turnover analysis. In one MIDA-based study chicken were labeled with valine as a tracer (Doherty et al., 2005). Using this approach protein turnover can only be calculated for valine-containing peptides after determining the precursor RIA. The chicken was chosen in this study because of its continuous diet intake which leads to a quick increase and plateauing of precursor RIA that subsequently remains constant. However, this method is not applicable to other mammals including mice.

In an alternative approach, stable isotope labeled water, ^2H_2O or $H_2^{18}O$, has been orally administered to determine protein dynamics (Rachdaoui et al., 2009). In this case the labeled water is utilized by the animal for the synthesis of amino acids and proteins (Foster et al., 1938). The assumption of this strategy is that a fast equilibration can be achieved between body water and free amino acid. Isotopologue analysis is used to determine the protein turnover. However, the small change in isotopologue distribution resulting from

low tracer incorporation makes the analysis of slow turnover and low abundant proteins difficult. Moreover, the hydrogen/deuterium exchange is reversible and can result in a back-exchange from deuterium to hydrogen during sample preparation in aqueous solvents (Kipping and Schierhorn, 2003; Mandell et al., 1998).

Stable isotope labeling with amino acids in cell culture (SILAC) (Ong et al., 2002) was originally introduced to relatively quantify two or more proteomes from different physiological cellular states. More recently, the SILAC method has also been adapted for the determination of protein dynamics in cultured cell systems (Doherty et al., 2009). In HeLa cells the effect of microRNAs on protein synthesis was investigated by the pulsed SILAC (pSILAC) approach (Selbach et al., 2008). However, for incomplete precursor RIA the SILAC peptides derived from newly synthesized protein can only have two patterns: labeled or unlabeled. The peptide signals derived from the unlabeled newly synthesized protein overlaps with the one from unlabeled pre-existing protein. In case of a low precursor RIA the majority of the peptide signal derived from newly synthesized protein shows up in its unlabeled form. Hence the knowledge of the amino acid precursor RIA is mandatory if one wants to apply the pSILAC approach to living animals. Since the SILAC tryptic peptides only contain one labeled tracer amino acid (unless proteins are cleaved incompletely) and the precursor RIA in living animals is continuously changing after tracer administration, calculation of the precursor RIA with the MIDA method cannot be performed. In a recent report pSILAC was also applied to living mice (58th ASMS Conference on Mass Spectrometry and Allied Topics poster "Proteome wide determination of true turnover rates in mice" by Ruhs *et al.*). Here the precursor RIA was calculated by fitting an exponential function to proteins with the highest incorporation rates. However, data from multiple labeling time points had to be acquired. Furthermore, the calculated precursor RIA resulting from the labeled fractions of a few proteins with a fast turnover may not correspond to the real-time RIA when the animal is sacrificed. Hence, if the precursor RIA for different proteins is not homogeneous, the method is prone to error.

The major advantage of the protein turnover analysis method we are presenting here is that precursor RIA determination is not required. The accuracy of our method depends on the match between measured and theoretical isotopologue distributions. Deviations between the two are more pronounced for peptides derived from low abundant proteins due to poor mass spectrometry ion statistics (Xu et al., 2010) and the variable decay rates for different isotopic species in certain mass spectrometer detectors (Bresson et al., 1998).

However, using a weighted average isotopologue distribution of all spectra across the entire elution time of a peptide improves this situation.

[15]N labeling periods for brain and plasma of 7 days and 2 days, respectively, resulted in the determination of FSRs for a great number of proteins, typically showing ratios between labeled and unlabeled protein fractions neither too low nor too high. This results in a small overlap of the mass spectrometry signals from the two peptide populations that the *ProTurnyzer* software can easily deal with.

Our data indicate that protein FSRs differ from each other to a significant extent. For an in-depth analysis, two labeling time points can be applied in order to capture proteins covering a wide range of FSRs. For instance, a 1-day labeling period is sufficient for the plasma protein plasminogen (FSR > 50%/day). In this case longer labeling times would result in the disappearance of the pre-existing natural protein fraction which makes FSR determination difficult. Brain heat shock protein 70kDa FSR was much lower than that of plasminogen. Here longer labeling times can reduce the error caused by the monoisotopic peptide signal derived from proteins that are newly synthesized shortly after onset of labeling while precursor RIA is still low. Using proper labeling times our method succeeds in measuring individual protein dynamics. Based on our data the labeling time window is reasonably wide and results in comparable FSRs even when different labeling times are used.

As mentioned in the 'Introduction' mRNA and its corresponding protein levels do not always correlate. Protein turnover is one important aspect of translatomics since it reflects the rate of protein translation and serves as an important link between mRNA and protein. Methods able to determine protein turnover in a high throughput manner, especially in living animals, are critical to obtain a better understanding of the poor correlation between mRNA and protein quantities. We have been able to analyze FSRs for a great number of proteins, and the KEGG pathway and GO analyses have shown that protein turnover correlates with biological processes and organelle protein distribution.

In the medical sciences protein turnover analysis can deliver important information for biomarker research that is more sensitive than simple protein quantitation. Particularly in the blood where proteins are rapidly turned over standard analyses for protein expression levels may not be able to catch subtle differences between healthy and diseased states and FSR analysis could provide a more sensitive platform for protein biomarker assays.

This becomes especially relevant in the case of low abundant proteins. Even in cases where protein expression levels are detectable the analysis of protein turnover may sense these upcoming changes at a much earlier time point, which is critical for the early detection of disease.

5 Perspectives

The presented studies have demonstrated that a combination of proteomics and metabolomics is able to identify molecular pathways pertinent for the anxiety phenotype in a mouse model. The identified proteins and metabolites allow the elucidation of biological networks, which provide a global view of disease pathobiology. Based on the presented findings on the anxiety mouse model two lines of future research can be considered. On one hand an investigation of the possibility of translating the results from the mouse model to the clinic should be performed. After successful clinical validation of a candidate biomarker, the latter can serve to indicate the anxiety phenotype in case / control studies and to monitor treatment response. Even without knowing a biomarker's role in modulating anxiety disorders, it still can assist the psychiatrist to get a better diagnosis for patients. The second level of studies is related to preclinical research. Although several pathways that are relevant to psychiatric disorders are suggested in the present study, the ultimate disease cause is still not understood. The current study opens several directions for psychiatric disease research. Among others the identified pathways can be used for drug development efforts by the pharmaceutical industry.

Besides protein expression quantification, the ^{15}N metabolic labeling technology enables us to detect the protein turnover rate, whose alteration is thought to be more sensitive than protein expression. The protein turnover information opens another venue for biomarker discovery efforts, as changes in protein levels are apparent at a much earlier time point using turnover analysis and those changes are not yet reflected by the total protein amount. Moreover, protein turnover studies may help us to get a better understanding of the poor correlation between mRNA and protein quantities.

Another focus when it comes to technology development is the analysis of clinical samples. Disease specific signature proteins and metabolites should be

quantified by an assay procedure in a standard and fast manner. The current -omics platforms are relatively time consuming. There is a need to improve the shotgun proteomics workflow to analyze low abundant biomarkers in a targeted fashion precisely and fast.

6 References

Adibhatla, R.M., and Hatcher, J.F. (2009). Lipid oxidation and peroxidation in CNS health and disease: from molecular mechanisms to therapeutic opportunities. Antioxid Redox Signal *12*, 125-169.

Aebersold, R., and Mann, M. (2003). Mass spectrometry-based proteomics. Nature *422*, 198-207.

Afify, E.A. (2002). Turnover of mu-opioid receptors in neuroblastoma cells. Brain Res Mol Brain Res *106*, 83-87.

Aina, Y., and Susman, J.L. (2006). Understanding comorbidity with depression and anxiety disorders. J Am Osteopath Assoc *106*, S9-14.

Akiyama, T., Ishida, J., Nakagawa, S., Ogawara, H., Watanabe, S., Itoh, N., Shibuya, M., and Fukami, Y. (1987). Genistein, a specific inhibitor of tyrosine-specific protein kinases. J Biol Chem *262*, 5592-5595.

Alessi, D.R., Cuenda, A., Cohen, P., Dudley, D.T., and Saltiel, A.R. (1995). Pd-098059 Is a Specific Inhibitor of the Activation of Mitogen-Activated Protein-Kinase Kinase in-Vitro and in-Vivo. Journal of Biological Chemistry *270*, 27489-27494.

Andreazza, A.C., Kauer-Sant'anna, M., Frey, B.N., Bond, D.J., Kapczinski, F., Young, L.T., and Yatham, L.N. (2008). Oxidative stress markers in bipolar disorder: a meta-analysis. J Affect Disord *111*, 135-144.

Arnone, D. (2005). Review of the use of Topiramate for treatment of psychiatric disorders. Ann Gen Psychiatry *4*, 5.

Artavanis-Tsakonas, S., Rand, M.D., and Lake, R.J. (1999). Notch signaling: cell fate control and signal integration in development. Science *284*, 770-776.

Ashburner, M., Ball, C.A., Blake, J.A., Botstein, D., Butler, H., Cherry, J.M., Davis, A.P., Dolinski, K., Dwight, S.S., Eppig, J.T.*, et al.* (2000). Gene ontology: tool for the unification of biology. The Gene Ontology Consortium. Nat Genet *25*, 25-29.

Baerenfaller, K., Grossmann, J., Grobei, M.A., Hull, R., Hirsch-Hoffmann, M., Yalovsky, S., Zimmermann, P., Grossniklaus, U., Gruissem, W., and Baginsky, S. (2008). Genome-scale proteomics reveals Arabidopsis thaliana gene models and proteome dynamics. Science *320*, 938-941.

Bale, T.L., Picetti, R., Contarino, A., Koob, G.F., Vale, W.W., and Lee, K.F. (2002). Mice deficient for both corticotropin-releasing factor receptor 1 (CRFR1) and CRFR2 have an impaired stress response and display sexually dichotomous anxiety-like behavior. J Neurosci *22*, 193-199.

Balgley, B.M., Laudeman, T., Yang, L., Song, T., and Lee, C.S. (2007). Comparative evaluation of tandem MS search algorithms using a target-decoy search strategy. Mol Cell Proteomics *6*, 1599-1608.

Bantscheff, M., Schirle, M., Sweetman, G., Rick, J., and Kuster, B. (2007). Quantitative mass spectrometry in proteomics: a critical review. Anal Bioanal Chem *389*, 1017-1031.

Barabasi, A.L., and Oltvai, Z.N. (2004). Network biology: understanding the cell's functional organization. Nat Rev Genet *5*, 101-113.

Baron, J.A. (1996). Beneficial effects of nicotine and cigarette smoking: the real, the possible and the spurious. Br Med Bull *52*, 58-73.

Bayes, A., and Grant, S.G. (2009). Neuroproteomics: understanding the molecular organization and complexity of the brain. Nat Rev Neurosci *10*, 635-646.

Beardsley, R.L., and Reilly, J.P. (2003). Quantitation using enhanced signal tags: a technique for comparative proteomics. J Proteome Res *2*, 15-21.

Becker, G.W. (2008). Stable isotopic labeling of proteins for quantitative proteomic applications. Brief Funct Genomic Proteomic *7*, 371-382.

Benes, F.M., Majocha, R., Bird, E.D., and Marotta, C.A. (1987). Increased vertical axon numbers in cingulate cortex of schizophrenics. Arch Gen Psychiatry *44*, 1017-1021.

Blanchard, D.C., Griebel, G., and Blanchard, R.J. (2001). Mouse defensive behaviors: pharmacological and behavioral assays for anxiety and panic. Neurosci Biobehav Rev *25*, 205-218.

Bliss, T.V., and Collingridge, G.L. (1993). A synaptic model of memory: long-term potentiation in the hippocampus. Nature *361*, 31-39.

Bondarenko, P.V., Chelius, D., and Shaler, T.A. (2002). Identification and relative quantitation of protein mixtures by enzymatic digestion followed by capillary reversed-phase liquid chromatography-tandem mass spectrometry. Anal Chem *74*, 4741-4749.

Bouayed, J., Rammal, H., and Soulimani, R. (2009). Oxidative stress and anxiety: Relationship and cellular pathways. Oxid Med Cell Longev *2*, 63-67.

Bouayed, J., Rammal, H., Younos, C., and Soulimani, R. (2007). Positive correlation between peripheral blood granulocyte oxidative status and level of anxiety in mice. Eur J Pharmacol *564*, 146-149.

Brambilla, P., Perez, J., Barale, F., Schettini, G., and Soares, J.C. (2003). GABAergic dysfunction in mood disorders. Mol Psychiatry *8*, 721-737, 715.

Bregendahl, K., Liu, L., Cant, J.P., Bayley, H.S., McBride, B.W., Milligan, L.P., Yen, J.T., and Fan, M.Z. (2004). Fractional protein synthesis rates measured by an intraperitoneal injection of a flooding dose of L-[ring-2H5]phenylalanine in pigs. J Nutr *134*, 2722-2728.

Bresson, J.A., Anderson, G.A., Bruce, J.E., and Smith, R.D. (1998). Improved isotopic abundance measurements for high resolution Fourier transform ion cyclotron resonance mass spectra via time-domain data extraction. Journal of the American Society for Mass Spectrometry *9*, 799-804.

Broekkamp, C.L., Rijk, H.W., Joly-Gelouin, D., and Lloyd, K.L. (1986). Major tranquillizers can be distinguished from minor tranquillizers on the basis of effects on marble burying and swim-induced grooming in mice. Eur J Pharmacol *126*, 223-229.

Brunner, E., Ahrens, C.H., Mohanty, S., Baetschmann, H., Loevenich, S., Potthast, F., Deutsch, E.W., Panse, C., de Lichtenberg, U., Rinner, O.*, et al.* (2007). A high-quality catalog of the Drosophila melanogaster proteome. Nat Biotechnol *25*, 576-583.

Cagney, G., and Emili, A. (2002). De novo peptide sequencing and quantitative profiling of complex protein mixtures using mass-coded abundance tagging. Nat Biotechnol *20*, 163-170.

Cameron, O.G. (2006). Anxious-depressive comorbidity: effects on HPA axis and CNS noradrenergic functions. Essent Psychopharmacol *7*, 24-34.

Cargile, B.J., Bundy, J.L., and Stephenson, J.L., Jr. (2004). Potential for false positive identifications from large databases through tandem mass spectrometry. J Proteome Res *3*, 1082-1085.

Cases, O., Seif, I., Grimsby, J., Gaspar, P., Chen, K., Pournin, S., Muller, U., Aguet, M., Babinet, C., Shih, J.C.*, et al.* (1995). Aggressive behavior and altered amounts of brain serotonin and norepinephrine in mice lacking MAOA. Science *268*, 1763-1766.

Caso, G., Ford, G.C., Nair, K.S., Garlick, P.J., and McNurlan, M.A. (2002). Aminoacyl-tRNA enrichment after a flood of labeled phenylalanine: insulin effect on muscle protein synthesis. Am J Physiol Endocrinol Metab *282*, E1029-1038.

Caso, G., Ford, G.C., Nair, K.S., Vosswinkel, J.A., Garlick, P.J., and McNurlan, M.A. (2001). Increased concentration of tracee affects estimates of muscle protein synthesis. Am J Physiol Endocrinol Metab *280*, E937-946.

Cassano, A.G., Anderson, V.E., and Harris, M.E. (2004). Understanding the transition states of phosphodiester bond cleavage: insights from heavy atom isotope effects. Biopolymers *73*, 110-129.

Chang, L., Cloak, C.C., and Ernst, T. (2003). Magnetic resonance spectroscopy studies of GABA in neuropsychiatric disorders. J Clin Psychiatry *64 Suppl 3*, 7-14.

Chelius, D., and Bondarenko, P.V. (2002). Quantitative profiling of proteins in complex mixtures using liquid chromatography and mass spectrometry. J Proteome Res *1*, 317-323.

Chen, G., Gharib, T.G., Huang, C.C., Taylor, J.M., Misek, D.E., Kardia, S.L., Giordano, T.J., Iannettoni, M.D., Orringer, M.B., Hanash, S.M.*, et al.* (2002). Discordant protein and mRNA expression in lung adenocarcinomas. Mol Cell Proteomics *1*, 304-313.

Chojnacka-Wojcik, E., Klodzinska, A., and Pilc, A. (2001). Glutamate receptor ligands as anxiolytics. Curr Opin Investig Drugs *2*, 1112-1119.

Cleland, W.W. (2003). The use of isotope effects to determine enzyme mechanisms. J Biol Chem *278*, 51975-51984.

Cleland, W.W. (2005). The use of isotope effects to determine enzyme mechanisms. Arch Biochem Biophys *433*, 2-12.

Conrads, T.P., Alving, K., Veenstra, T.D., Belov, M.E., Anderson, G.A., Anderson, D.J., Lipton, M.S., Pasa-Tolic, L., Udseth, H.R., Chrisler, W.B.*, et al.* (2001). Quantitative analysis of bacterial and mammalian proteomes using a combination of cysteine affinity tags and 15N-metabolic labeling. Anal Chem *73*, 2132-2139.

Cook, M.N., Williams, R.W., and Flaherty, L. (2001). Anxiety-related behaviors in the elevated zero-maze are affected by genetic factors and retinal degeneration. Behav Neurosci *115*, 468-476.

Cooke, S.F., and Bliss, T.V. (2006). Plasticity in the human central nervous system. Brain *129*, 1659-1673.

Corthals, G.L., Wasinger, V.C., Hochstrasser, D.F., and Sanchez, J.C. (2000). The dynamic range of protein expression: a challenge for proteomic research. Electrophoresis *21*, 1104-1115.

Cox, B., and Emili, A. (2006). Tissue subcellular fractionation and protein extraction for use in mass-spectrometry-based proteomics. Nat Protoc *1*, 1872-1878.

Craig, R., and Beavis, R.C. (2004). TANDEM: matching proteins with tandem mass spectra. Bioinformatics *20*, 1466-1467.

Crawley, J., and Goodwin, F.K. (1980). Preliminary report of a simple animal behavior model for the anxiolytic effects of benzodiazepines. Pharmacol Biochem Behav *13*, 167-170.

Crowley, J.J., Blendy, J.A., and Lucki, I. (2005). Strain-dependent antidepressant-like effects of citalopram in the mouse tail suspension test. Psychopharmacology (Berl) *183*, 257-264.

Cryan, J.F., Mombereau, C., and Vassout, A. (2005). The tail suspension test as a model for assessing antidepressant activity: review of pharmacological and genetic studies in mice. Neurosci Biobehav Rev *29*, 571-625.

Cuenda, A., Rouse, J., Doza, Y.N., Meier, R., Cohen, P., Gallagher, T.F., Young, P.R., and Lee, J.C. (1995). SB 203580 is a specific inhibitor of a MAP kinase homologue which is stimulated by cellular stresses and interleukin-1. FEBS Lett *364*, 229-233.

Cunningham, C., Glish, G.L., and Burinsky, D.J. (2006). High amplitude short time excitation: A method to form and detect low mass product ions in a quadrupole ion trap mass spectrometer. Journal of the American Society for Mass Spectrometry *17*, 81-84.

Davies, K.J. (1995). Oxidative stress: the paradox of aerobic life. Biochem Soc Symp *61*, 1-31.

Davis, T.A., Fiorotto, M.L., Nguyen, H.V., and Burrin, D.G. (1999). Aminoacyl-tRNA and tissue free amino acid pools are equilibrated after a flooding dose of phenylalanine. Am J Physiol *277*, E103-109.

de Godoy, L.M., Olsen, J.V., Cox, J., Nielsen, M.L., Hubner, N.C., Frohlich, F., Walther, T.C., and Mann, M. (2008). Comprehensive mass-spectrometry-based proteome quantification of haploid versus diploid yeast. Nature *455*, 1251-1254.

de Kloet, C.S., Vermetten, E., Heijnen, C.J., Geuze, E., Lentjes, E.G., and Westenberg, H.G. (2007). Enhanced cortisol suppression in response to dexamethasone administration in traumatized veterans with and without posttraumatic stress disorder. Psychoneuroendocrinology *32*, 215-226.

Desrumaux, C., Risold, P.Y., Schroeder, H., Deckert, V., Masson, D., Athias, A., Laplanche, H., Le Guern, N., Blache, D., Jiang, X.C.*, et al.* (2005). Phospholipid transfer protein (PLTP) deficiency reduces brain vitamin E content and increases anxiety in mice. FASEB J *19*, 296-297.

Devane, C.L., Chiao, E., Franklin, M., and Kruep, E.J. (2005). Anxiety disorders in the 21st century: status, challenges, opportunities, and comorbidity with depression. Am J Manag Care *11*, S344-353.

Dhillon, A.S., Hagan, S., Rath, O., and Kolch, W. (2007). MAP kinase signalling pathways in cancer. Oncogene *26*, 3279-3290.

Do, K.Q., Cabungcal, J.H., Frank, A., Steullet, P., and Cuenod, M. (2009). Redox dysregulation, neurodevelopment, and schizophrenia. Curr Opin Neurobiol *19*, 220-230.

Doherty, M.K., and Beynon, R.J. (2006a). Protein turnover on the scale of the proteome. Expert Review of Proteomics *3*, 97-110.

Doherty, M.K., and Beynon, R.J. (2006b). Protein turnover on the scale of the proteome. Expert Rev Proteomics *3*, 97-110.

Doherty, M.K., Hammond, D.E., Clague, M.J., Gaskell, S.J., and Beynon, R.J. (2009). Turnover of the human proteome: determination of protein intracellular stability by dynamic SILAC. J Proteome Res *8*, 104-112.

Doherty, M.K., Whitehead, C., McCormack, H., Gaskell, S.J., and Beynon, R.J. (2005). Proteome dynamics in complex organisms: using stable isotopes to monitor individual protein turnover rates. Proteomics *5*, 522-533.

Dole, M., Mack, L.L., and Hines, R.L. (1968). Molecular Beams of Macroions. Journal of Chemical Physics *49*, 2240-&.

Dome, P., Lazary, J., Kalapos, M.P., and Rihmer, Z. (2009). Smoking, nicotine and neuropsychiatric disorders. Neurosci Biobehav Rev *34*, 295-342.

Dong, M.Q., Venable, J.D., Au, N., Xu, T., Park, S.K., Cociorva, D., Johnson, J.R., Dillin, A., and Yates, J.R., 3rd (2007). Quantitative mass spectrometry identifies insulin signaling targets in C. elegans. Science *317*, 660-663.

Draghici, S., Khatri, P., Tarca, A.L., Amin, K., Done, A., Voichita, C., Georgescu, C., and Romero, R. (2007). A systems biology approach for pathway level analysis. Genome Res *17*, 1537-1545.

Dudley, D.T., Pang, L., Decker, S.J., Bridges, A.J., and Saltiel, A.R. (1995). A Synthetic Inhibitor of the Mitogen-Activated Protein-Kinase Cascade. Proceedings of the National Academy of Sciences of the United States of America *92*, 7686-7689.

Duncia, J.V., Santella, J.B., Higley, C.A., Pitts, W.J., Wityak, J., Frietze, W.E., Rankin, F.W., Sun, J.H., Earl, R.A., Tabaka, A.C.*, et al.* (1998). MEK inhibitors: The chemistry and biological activity of U0126, its analogs, and cyclization products. Bioorganic & Medicinal Chemistry Letters *8*, 2839-2844.

Dwivedi, Y., Rizavi, H.S., Roberts, R.C., Conley, R.C., Tamminga, C.A., and Pandey, G.N. (2001). Reduced activation and expression of ERK1/2 MAP kinase in the post-mortem brain of depressed suicide subjects. J Neurochem *77*, 916-928.

Eastwood, S.L., Law, A.J., Everall, I.P., and Harrison, P.J. (2003). The axonal chemorepellant semaphorin 3A is increased in the cerebellum in schizophrenia and may contribute to its synaptic pathology. Mol Psychiatry *8*, 148-155.

Ehninger, D., de Vries, P.J., and Silva, A.J. (2009). From mTOR to cognition: molecular and cellular mechanisms of cognitive impairments in tuberous sclerosis. J Intellect Disabil Res *53*, 838-851.

Ekins, S., Nikolsky, Y., Bugrim, A., Kirillov, E., and Nikolskaya, T. (2007). Pathway mapping tools for analysis of high content data. Methods Mol Biol *356*, 319-350.

Elias, J.E., and Gygi, S.P. (2007). Target-decoy search strategy for increased confidence in large-scale protein identifications by mass spectrometry. Nat Methods *4*, 207-214.

Elias, J.E., Haas, W., Faherty, B.K., and Gygi, S.P. (2005). Comparative evaluation of mass spectrometry platforms used in large-scale proteomics investigations. Nat Methods *2*, 667-675.

Emmett, M., and Caprioli, R. (1994). Micro-electrospray mass spectrometry: ultra-high-sensitivity analysis of peptides and proteins. . J Am Soc Mass Spectrom *5*, 605-613.

Eng, J.K., Mccormack, A.L., and Yates, J.R. (1994). An Approach to Correlate Tandem Mass-Spectral Data of Peptides with Amino-Acid-Sequences in a Protein Database. Journal of the American Society for Mass Spectrometry *5*, 976-989.

Ersan, S., Bakir, S., Erdal Ersan, E., and Dogan, O. (2006). Examination of free radical metabolism and antioxidant defence system elements in patients with obsessive-compulsive disorder. Prog Neuropsychopharmacol Biol Psychiatry *30*, 1039-1042.

Fagerstrom, K., and Aubin, H.J. (2009). Management of smoking cessation in patients with psychiatric disorders. Curr Med Res Opin *25*, 511-518.

Falcon, S., and Gentleman, R. (2007). Using GOstats to test gene lists for GO term association. Bioinformatics *23*, 257-258.

Fava, M., and Kendler, K.S. (2000). Major depressive disorder. Neuron *28*, 335-341.

Favata, M.F., Horiuchi, K.Y., Manos, E.J., Daulerio, A.J., Stradley, D.A., Feeser, W.S., Van Dyk, D.E., Pitts, W.J., Earl, R.A., Hobbs, F.*, et al.* (1998). Identification of a novel inhibitor of mitogen-activated protein kinase kinase. Journal of Biological Chemistry *273*, 18623-18632.

Feng, P., Guan, Z., Yang, X., and Fang, J. (2003). Impairments of ERK signal transduction in the brain in a rat model of depression induced by neonatal exposure of clomipramine. Brain Res *991*, 195-205.

Fenn, J.B., Mann, M., Meng, C.K., Wong, S.F., and Whitehouse, C.M. (1989). Electrospray ionization for mass spectrometry of large biomolecules. Science *246*, 64-71.

Ferby, I., Waga, I., Kume, K., Sakanaka, C., and Shimizu, T. (1996). PAF-induced MAPK activation is inhibited by Wortmannin in neutrophils and macrophages. Platelet-Activating Factor and Related Lipid Mediators 2 *416*, 321-326

Fiehn, O., and Kind, T. (2007). Metabolite profiling in blood plasma. Methods Mol Biol *358*, 3-17.

Filomeni, G., and Ciriolo, M.R. (2006). Redox control of apoptosis: an update. Antioxid Redox Signal *8*, 2187-2192.

Foster, G.L., Rittenberg, D., and Schoenheimer, R. (1938). J Biol Chem *125*.

Frank, E., Kessler, M.S., Filiou, M.D., Zhang, Y., Maccarrone, G., Reckow, S., Bunck, M., Heumann, H., Turck, C.W., Landgraf, R.*, et al.* (2009). Stable isotope metabolic labeling

with a novel N-enriched bacteria diet for improved proteomic analyses of mouse models for psychopathologies. PLoS ONE *4*, e7821.

Frewen, B.E., Merrihew, G.E., Wu, C.C., Noble, W.S., and MacCoss, M.J. (2006). Analysis of peptide MS/MS spectra from large-scale proteomics experiments using spectrum libraries. Anal Chem *78*, 5678-5684.

Fujiki, H., and Suganuma, M. (2009). Carcinogenic aspects of protein phosphatase 1 and 2A inhibitors. Prog Mol Subcell Biol *46*, 221-254.

Fujimoto, M., Uchida, S., Watanuki, T., Wakabayashi, Y., Otsuki, K., Matsubara, T., Suetsugi, M., Funato, H., and Watanabe, Y. (2008). Reduced expression of glyoxalase-1 mRNA in mood disorder patients. Neurosci Lett *438*, 196-199.

Fukumoto, K., Morita, T., Mayanagi, T., Tanokashira, D., Yoshida, T., Sakai, A., and Sobue, K. (2009). Detrimental effects of glucocorticoids on neuronal migration during brain development. Mol Psychiatry *14*, 1119-1131.

Gaiano, N., and Fishell, G. (2002). The role of notch in promoting glial and neural stem cell fates. Annu Rev Neurosci *25*, 471-490.

Garcia, A., Cayla, X., Guergnon, J., Dessauge, F., Hospital, V., Rebollo, M.P., Fleischer, A., and Rebollo, A. (2003). Serine/threonine protein phosphatases PP1 and PP2A are key players in apoptosis. Biochimie *85*, 721-726.

Gasparotto, O.C., Carobrez, S.G., and Bohus, B.G. (2007). Effects of LPS on the behavioural stress response of genetically selected aggressive and nonaggressive wild house mice. Behav Brain Res *183*, 52-59.

Gerber, S.A., Rush, J., Stemman, O., Kirschner, M.W., and Gygi, S.P. (2003). Absolute quantification of proteins and phosphoproteins from cell lysates by tandem MS. Proc Natl Acad Sci U S A *100*, 6940-6945.

Gilchrist, A., Au, C.E., Hiding, J., Bell, A.W., Fernandez-Rodriguez, J., Lesimple, S., Nagaya, H., Roy, L., Gosline, S.J., Hallett, M.*, et al.* (2006). Quantitative proteomics analysis of the secretory pathway. Cell *127*, 1265-1281.

Gingrich, J.A. (2005). Oxidative stress is the new stress. Nat Med *11*, 1281-1282.

Gordon, J.A., and Hen, R. (2004). Genetic approaches to the study of anxiety. Annu Rev Neurosci *27*, 193-222.

Gourley, S.L., Wu, F.J., Kiraly, D.D., Ploski, J.E., Kedves, A.T., Duman, R.S., and Taylor, J.R. (2008). Regionally specific regulation of ERK MAP kinase in a model of antidepressant-sensitive chronic depression. Biol Psychiatry *63*, 353-359.

Gouw, J.W., Tops, B.B., Mortensen, P., Heck, A.J., and Krijgsveld, J. (2008). Optimizing identification and quantitation of 15N-labeled proteins in comparative proteomics. Anal Chem *80*, 7796-7803.

Griffin, T.J., Gygi, S.P., Ideker, T., Rist, B., Eng, J., Hood, L., and Aebersold, R. (2002). Complementary profiling of gene expression at the transcriptome and proteome levels in Saccharomyces cerevisiae. Mol Cell Proteomics *1*, 323-333.

Griffina, P.R., Coffmana, J.A., Hooda, L.E., and Yates III, J.R. (1991). Structural analysis of proteins by capillary HPLC electrospray tandem mass spectrometry International Journal of Mass Spectrometry and Ion Processes *111*, 131-149.

Gross, C., Zhuang, X., Stark, K., Ramboz, S., Oosting, R., Kirby, L., Santarelli, L., Beck, S., and Hen, R. (2002). Serotonin1A receptor acts during development to establish normal anxiety-like behaviour in the adult. Nature *416*, 396-400.

Gstaiger, M., and Aebersold, R. (2009). Applying mass spectrometry-based proteomics to genetics, genomics and network biology. Nat Rev Genet *10*, 617-627.

Guerrera, I.C., and Kleiner, O. (2005). Application of mass spectrometry in proteomics. Biosci Rep *25*, 71-93.

Gygi, S.P., Rist, B., Gerber, S.A., Turecek, F., Gelb, M.H., and Aebersold, R. (1999). Quantitative analysis of complex protein mixtures using isotope-coded affinity tags. Nat Biotechnol *17*, 994-999.

Haegler, K., Mueller, N.S., Maccarrone, G., Hunyadi-Gulyas, E., Webhofer, C., Filiou, M.D., Zhang, Y., and Turck, C.W. (2009a). QuantiSpec--Quantitative mass spectrometry data analysis of (15)N-metabolically labeled proteins. J Proteomics *71*, 601-608.

Haegler, K., Mueller, N.S., Maccarrone, G., Hunyadi-Gulyas, E., Webhofer, C., Filiou, M.D., Zhang, Y., and Turck, C.W. (2009b). QuantiSpec - Quantitative mass spectrometry data analysis of (15)N-metabolically labeled proteins. J Proteomics *71*, 601-608.

Halliwell, B. (2006). Oxidative stress and neurodegeneration: where are we now? J Neurochem *97*, 1634-1658.

Hambsch, B., Chen, B.G., Brenndorfer, J., Meyer, M., Avrabos, C., Maccarrone, G., Liu, R.H., Eder, M., Turck, C.W., and Landgraf, R. (2010). Methylglyoxal-mediated anxiolysis involves increased protein modification and elevated expression of glyoxalase 1 in the brain. J Neurochem *113*, 1240-1251.

Handley, S.L., and Mithani, S. (1984). Effects of alpha-adrenoceptor agonists and antagonists in a maze-exploration model of 'fear'-motivated behaviour. Naunyn Schmiedebergs Arch Pharmacol *327*, 1-5.

Handwerger, K. (2009). Differential patterns of HPA activity and reactivity in adult posttraumatic stress disorder and major depressive disorder. Harv Rev Psychiatry *17*, 184-205.

Hansen, K.C., Schmitt-Ulms, G., Chalkley, R.J., Hirsch, J., Baldwin, M.A., and Burlingame, A.L. (2003). Mass spectrometric analysis of protein mixtures at low levels using cleavable 13C-isotope-coded affinity tag and multidimensional chromatography. Mol Cell Proteomics *2*, 299-314.

Hatt, H., and Smith, D.O. (1976). Synaptic depression related to presynaptic axon conduction block. J Physiol *259*, 367-393.

Hauger, R.L., Risbrough, V., Brauns, O., and Dautzenberg, F.M. (2006). Corticotropin releasing factor (CRF) receptor signaling in the central nervous system: new molecular targets. CNS Neurol Disord Drug Targets *5*, 453-479.

Hawkins, R.A., O'Kane, R.L., Simpson, I.A., and Vina, J.R. (2006). Structure of the blood-brain barrier and its role in the transport of amino acids. J Nutr *136*, 218S-226S.

Heisler, L.K., Chu, H.M., Brennan, T.J., Danao, J.A., Bajwa, P., Parsons, L.H., and Tecott, L.H. (1998). Elevated anxiety and antidepressant-like responses in serotonin 5-HT1A receptor mutant mice. Proc Natl Acad Sci U S A *95*, 15049-15054.

Hellerstein, M.K., and Neese, R.A. (1992). Mass isotopomer distribution analysis: a technique for measuring biosynthesis and turnover of polymers. Am J Physiol *263*, E988-1001.

Hellerstein, M.K., and Neese, R.A. (1999). Mass isotopomer distribution analysis at eight years: theoretical, analytic, and experimental considerations. Am J Physiol *276*, E1146-1170.

Henze, K., and Martin, W. (2003). Evolutionary biology: essence of mitochondria. Nature *426*, 127-128.

Herbert, J., Goodyer, I.M., Grossman, A.B., Hastings, M.H., de Kloet, E.R., Lightman, S.L., Lupien, S.J., Roozendaal, B., and Seckl, J.R. (2006). Do corticosteroids damage the brain? J Neuroendocrinol *18*, 393-411.

Hettema, J.M., Prescott, C.A., and Kendler, K.S. (2001). A population-based twin study of generalized anxiety disorder in men and women. J Nerv Ment Dis *189*, 413-420.

Higgs, R.E., Knierman, M.D., Gelfanova, V., Butler, J.P., and Hale, J.E. (2008). Label-free LC-MS method for the identification of biomarkers. Methods Mol Biol *428*, 209-230.

Hillhouse, E.W., and Grammatopoulos, D.K. (2006). The molecular mechanisms underlying the regulation of the biological activity of corticotropin-releasing hormone receptors: implications for physiology and pathophysiology. Endocr Rev *27*, 260-286.

Holsboer, F. (2001). Stress, hypercortisolism and corticosteroid receptors in depression: implications for therapy. J Affect Disord *62*, 77-91.

Hoshino, R., Chatani, Y., Yamori, T., Tsuruo, T., Oka, H., Yoshida, O., Shimada, Y., Ari-i, S., Wada, H., Fujimoto, J.*, et al.* (1999). Constitutive activation of the 41-/43-kDa mitogen-activated protein kinase signaling pathway in human tumors. Oncogene *18*, 813-822.

Hovatta, I., Tennant, R.S., Helton, R., Marr, R.A., Singer, O., Redwine, J.M., Ellison, J.A., Schadt, E.E., Verma, I.M., Lockhart, D.J.*, et al.* (2005). Glyoxalase 1 and glutathione reductase 1 regulate anxiety in mice. Nature *438*, 662-666.

Hu, Q., Noll, R.J., Li, H., Makarov, A., Hardman, M., and Graham Cooks, R. (2005). The Orbitrap: a new mass spectrometer. J Mass Spectrom *40*, 430-443.

Hucka, M., Finney, A., Sauro, H.M., Bolouri, H., Doyle, J.C., Kitano, H., Arkin, A.P., Bornstein, B.J., Bray, D., Cornish-Bowden, A.*, et al.* (2003). The systems biology markup language (SBML): a medium for representation and exchange of biochemical network models. Bioinformatics *19*, 524-531.

Huttlin, E.L., Hegeman, A.D., Harms, A.C., and Sussman, M.R. (2007). Comparison of full versus partial metabolic labeling for quantitative proteomics analysis in Arabidopsis thaliana. Mol Cell Proteomics *6*, 860-881.

Ideker, T., Thorsson, V., Ranish, J.A., Christmas, R., Buhler, J., Eng, J.K., Bumgarner, R., Goodlett, D.R., Aebersold, R., and Hood, L. (2001). Integrated genomic and proteomic analyses of a systematically perturbed metabolic network. Science *292*, 929-934.

Ishihama, Y., Sato, T., Tabata, T., Miyamoto, N., Sagane, K., Nagasu, T., and Oda, Y. (2005). Quantitative mouse brain proteomics using culture-derived isotope tags as internal standards. Nat Biotechnol *23*, 617-621.

Jacobson, L.H., Bettler, B., Kaupmann, K., and Cryan, J.F. (2007). Behavioral evaluation of mice deficient in GABA(B(1)) receptor isoforms in tests of unconditioned anxiety. Psychopharmacology (Berl) *190*, 541-553.

James, P. (1997). Protein identification in the post-genome era: the rapid rise of proteomics. Q Rev Biophys *30*, 279-331.

Jaworski, J., and Sheng, M. (2006). The growing role of mTOR in neuronal development and plasticity. Mol Neurobiol *34*, 205-219.

Johnson, H.A., Baldwin, R.L., France, J., and Calvert, C.C. (1999). A model of whole-body protein turnover based on leucine kinetics in rodents. J Nutr *129*, 728-739.

Johnson, K.L., and Muddiman, D.C. (2004). A method for calculating 16O/18O peptide ion ratios for the relative quantification of proteomes. J Am Soc Mass Spectrom *15*, 437-445.

Jones, A.R., Siepen, J.A., Hubbard, S.J., and Paton, N.W. (2009). Improving sensitivity in proteome studies by analysis of false discovery rates for multiple search engines. Proteomics *9*, 1220-1229.

Julka, S., and Regnier, F. (2004). Quantification in proteomics through stable isotope coding: a review. J Proteome Res *3*, 350-363.

Junker, B.H., Klukas, C., and Schreiber, F. (2006). VANTED: a system for advanced data analysis and visualization in the context of biological networks. BMC Bioinformatics *7*, 109.

Kalueff, A.V., and Nutt, D.J. (2007). Role of GABA in anxiety and depression. Depress Anxiety *24*, 495-517.

Kanehisa, M., Araki, M., Goto, S., Hattori, M., Hirakawa, M., Itoh, M., Katayama, T., Kawashima, S., Okuda, S., Tokimatsu, T.*, et al.* (2008). KEGG for linking genomes to life and the environment. Nucleic Acids Res *36*, D480-484.

Kanehisa, M., Goto, S., Kawashima, S., Okuno, Y., and Hattori, M. (2004). The KEGG resource for deciphering the genome. Nucleic Acids Res *32*, D277-280.

Kapp, E., and Schutz, F. (2007). Overview of tandem mass spectrometry (MS/MS) database search algorithms. Curr Protoc Protein Sci *Chapter 25*, Unit25 22.

Kapp, E.A., Schutz, F., Connolly, L.M., Chakel, J.A., Meza, J.E., Miller, C.A., Fenyo, D., Eng, J.K., Adkins, J.N., Omenn, G.S.*, et al.* (2005). An evaluation, comparison, and accurate benchmarking of several publicly available MS/MS search algorithms: sensitivity and specificity analysis. Proteomics *5*, 3475-3490.

Karaman, M.W., Herrgard, S., Treiber, D.K., Gallant, P., Atteridge, C.E., Campbell, B.T., Chan, K.W., Ciceri, P., Davis, M.I., Edeen, P.T.*, et al.* (2008). A quantitative analysis of kinase inhibitor selectivity. Nat Biotechnol *26*, 127-132.

Karreth, F.A., and Tuveson, D.A. (2009). Modelling oncogenic Ras/Raf signalling in the mouse. Curr Opin Genet Dev *19*, 4-11.

Kash, S.F., Tecott, L.H., Hodge, C., and Baekkeskov, S. (1999). Increased anxiety and altered responses to anxiolytics in mice deficient in the 65-kDa isoform of glutamic acid decarboxylase. Proc Natl Acad Sci U S A *96*, 1698-1703.

Kaufman, J., and Charney, D. (2000). Comorbidity of mood and anxiety disorders. Depress Anxiety *12 Suppl 1*, 69-76.

Kaur, C., and Ling, E.A. (2008). Antioxidants and neuroprotection in the adult and developing central nervous system. Curr Med Chem *15*, 3068-3080.

Keck, M.E., and Holsboer, F. (2001). Hyperactivity of CRH neuronal circuits as a target for therapeutic interventions in affective disorders. Peptides *22*, 835-844.

Kendler, K.S., Gardner, C.O., Gatz, M., and Pedersen, N.L. (2007). The sources of co-morbidity between major depression and generalized anxiety disorder in a Swedish national twin sample. Psychol Med *37*, 453-462.

Kessler, M.S., Murgatroyd, C., Bunck, M., Czibere, L., Frank, E., Jacob, W., Horvath, C., Muigg, P., Holsboer, F., Singewald, N.*, et al.* (2007). Diabetes insipidus and, partially, low anxiety-related behaviour are linked to a SNP-associated vasopressin deficit in LAB mice. Eur J Neurosci *26*, 2857-2864.

Kessler, R.C., Chiu, W.T., Demler, O., Merikangas, K.R., and Walters, E.E. (2005). Prevalence, severity, and comorbidity of 12-month DSM-IV disorders in the National Comorbidity Survey Replication. Arch Gen Psychiatry *62*, 617-627.

Kessler, R.C., McGonagle, K.A., Zhao, S., Nelson, C.B., Hughes, M., Eshleman, S., Wittchen, H.U., and Kendler, K.S. (1994). Lifetime and 12-month prevalence of DSM-III-R psychiatric disorders in the United States. Results from the National Comorbidity Survey. Arch Gen Psychiatry *51*, 8-19.

Kipping, M., and Schierhorn, A. (2003). Improving hydrogen/deuterium exchange mass spectrometry by reduction of the back-exchange effect. J Mass Spectrom *38*, 271-276.

Kirkpatrick, D.S., Gerber, S.A., and Gygi, S.P. (2005). The absolute quantification strategy: a general procedure for the quantification of proteins and post-translational modifications. Methods *35*, 265-273.

Kirsch, J. (2006). Glycinergic transmission. Cell Tissue Res *326*, 535-540.

Kitano, H. (2002). Systems biology: a brief overview. Science *295*, 1662-1664.

Kohno, M., and Pouyssegur, J. (2006). Targeting the ERK signaling pathway in cancer therapy. Ann Med *38*, 200-211.

Krijgsveld, J., Ketting, R.F., Mahmoudi, T., Johansen, J., Artal-Sanz, M., Verrijzer, C.P., Plasterk, R.H., and Heck, A.J. (2003). Metabolic labeling of C. elegans and D. melanogaster for quantitative proteomics. Nat Biotechnol *21*, 927-931.

Kromer, S.A., Kessler, M.S., Milfay, D., Birg, I.N., Bunck, M., Czibere, L., Panhuysen, M., Putz, B., Deussing, J.M., Holsboer, F*., et al.* (2005). Identification of glyoxalase-I as a protein marker in a mouse model of extremes in trait anxiety. J Neurosci *25*, 4375-4384.

Kruger, M., Moser, M., Ussar, S., Thievessen, I., Luber, C.A., Forner, F., Schmidt, S., Zanivan, S., Fassler, R., and Mann, M. (2008). SILAC mouse for quantitative proteomics uncovers kindlin-3 as an essential factor for red blood cell function. Cell *134*, 353-364.

Kuloglu, M., Atmaca, M., Tezcan, E., Gecici, O., Tunckol, H., and Ustundag, B. (2002a). Antioxidant enzyme activities and malondialdehyde levels in patients with obsessive-compulsive disorder. Neuropsychobiology *46*, 27-32.

Kuloglu, M., Atmaca, M., Tezcan, E., Ustundag, B., and Bulut, S. (2002b). Antioxidant enzyme and malondialdehyde levels in patients with panic disorder. Neuropsychobiology *46*, 186-189.

Kumsta, R., Entringer, S., Hellhammer, D.H., and Wust, S. (2007). Cortisol and ACTH responses to psychosocial stress are modulated by corticosteroid binding globulin levels. Psychoneuroendocrinology *32*, 1153-1157.

Lalonde, R., and Strazielle, C. (2003). Neurobehavioral characteristics of mice with modified intermediate filament genes. Rev Neurosci *14*, 369-385.

Lander, E.S., Linton, L.M., Birren, B., Nusbaum, C., Zody, M.C., Baldwin, J., Devon, K., Dewar, K., Doyle, M., FitzHugh, W*., et al.* (2001). Initial sequencing and analysis of the human genome. Nature *409*, 860-921.

Landgraf, R. (2001). Neuropeptides and anxiety-related behavior. Endocr J *48*, 517-533.

Landgraf, R., Kessler, M.S., Bunck, M., Murgatroyd, C., Spengler, D., Zimbelmann, M., Nussbaumer, M., Czibere, L., Turck, C.W., Singewald, N*., et al.* (2007). Candidate genes of anxiety-related behavior in HAB/LAB rats and mice: focus on vasopressin and glyoxalase-I. Neurosci Biobehav Rev *31*, 89-102.

Landgraf, R., and Wigger, A. (2002). High vs low anxiety-related behavior rats: an animal model of extremes in trait anxiety. Behav Genet *32*, 301-314.

Lang, U.E., Heger, J., Willbring, M., Domula, M., Matschke, K., and Tugtekin, S.M. (2009). Immunosuppression using the mammalian target of rapamycin (mTOR) inhibitor everolimus: pilot study shows significant cognitive and affective improvement. Transplant Proc *41*, 4285-4288.

Langen, H., Fountoulakis, M., Evers, S., Wipf, B., and Berndt, P. (1998). From Genome to Proteome, 3rd Siena 2D Electrophoresis Meeting *Wiley-VCH*, Germany, Siena.

Laube, B., Kuryatov, A., Kuhse, J., and Betz, H. (1993). Glycine-glutamate interactions at the NMDA receptor: role of cysteine residues. FEBS Lett *335*, 331-334.

Lazar, D.F., Wiese, R.J., Brady, M.J., Mastick, C.C., Waters, S.B., Yamauchi, K., Pessin, J.E., Cuatrecasas, P., and Saltiel, A.R. (1995). Mitogen-Activated Protein-Kinase Kinase Inhibition Does Not Block the Stimulation of Glucose-Utilization by Insulin. Journal of Biological Chemistry *270*, 20801-20807.

Legendre, P. (2001). The glycinergic inhibitory synapse. Cell Mol Life Sci *58*, 760-793.

Lenz, E.M., and Wilson, I.D. (2007). Analytical strategies in metabonomics. J Proteome Res *6*, 443-458.

Lester, R.A., Tong, G., and Jahr, C.E. (1993). Interactions between the glycine and glutamate binding sites of the NMDA receptor. J Neurosci *13*, 1088-1096.

Li, J., Steen, H., and Gygi, S.P. (2003). Protein profiling with cleavable isotope-coded affinity tag (cICAT) reagents: the yeast salinity stress response. Mol Cell Proteomics *2*, 1198-1204.

Liao, L., McClatchy, D.B., Park, S.K., Xu, T., Lu, B., and Yates, J.R., 3rd (2008). Quantitative analysis of brain nuclear phosphoproteins identifies developmentally regulated phosphorylation events. J Proteome Res *7*, 4743-4755.

Liberski, P.P., Budka, H., Yanagihara, R., and Gajdusek, D.C. (1995). Neuroaxonal dystrophy in experimental Creutzfeldt-Jakob disease: electron microscopical and immunohistochemical demonstration of neurofilament accumulations within affected neurites. J Comp Pathol *112*, 243-255.

Liebsch, G., Linthorst, A.C., Neumann, I.D., Reul, J.M., Holsboer, F., and Landgraf, R. (1998a). Behavioral, physiological, and neuroendocrine stress responses and differential sensitivity to diazepam in two Wistar rat lines selectively bred for high- and low-anxiety-related behavior. Neuropsychopharmacology *19*, 381-396.

Liebsch, G., Montkowski, A., Holsboer, F., and Landgraf, R. (1998b). Behavioural profiles of two Wistar rat lines selectively bred for high or low anxiety-related behaviour. Behav Brain Res *94*, 301-310.

Link, A.J., Eng, J., Schieltz, D.M., Carmack, E., Mize, G.J., Morris, D.R., Garvik, B.M., and Yates, J.R., 3rd (1999). Direct analysis of protein complexes using mass spectrometry. Nat Biotechnol *17*, 676-682.

Lister, R.G. (1987). The use of a plus-maze to measure anxiety in the mouse. Psychopharmacology (Berl) *92*, 180-185.

Liu, H., Sadygov, R.G., and Yates, J.R., 3rd (2004). A model for random sampling and estimation of relative protein abundance in shotgun proteomics. Anal Chem *76*, 4193-4201.

Louris, J.N., Cooks, R.G., Syka, J.E.P., Kelley, P.E., Stafford, G.C., and Todd, J.F.J. (1987). Instrumentation, Applications, and Energy Deposition in Quadrupole Ion-Trap Tandem Mass-Spectrometry. Analytical Chemistry *59*, 1677-1685.

Low, K., Crestani, F., Keist, R., Benke, D., Brunig, I., Benson, J.A., Fritschy, J.M., Rulicke, T., Bluethmann, H., Mohler, H.*, et al.* (2000). Molecular and neuronal substrate for the selective attenuation of anxiety. Science *290*, 131-134.

Lu, T., Rubio, M.E., and Trussell, L.O. (2008). Glycinergic transmission shaped by the corelease of GABA in a mammalian auditory synapse. Neuron *57*, 524-535.

Maes, M., Van Gastel, A., Blockx, P., Martin, M., Cosyns, P., Scharpe, S., Ranjan, R., and Desnyder, R. (1996). Lower serum transcortin (CBG) in major depressed females: relationships with baseline and postdexamethasone cortisol values. J Affect Disord *38*, 47-56.

Makarov, A. (2000). Electrostatic axially harmonic orbital trapping: a high-performance technique of mass analysis. Anal Chem *72*, 1156-1162.

Makarov, A., Denisov, E., Kholomeev, A., Balschun, W., Lange, O., Strupat, K., and Horning, S. (2006a). Performance evaluation of a hybrid linear ion trap/orbitrap mass spectrometer. Anal Chem *78*, 2113-2120.

Makarov, A., Denisov, E., Lange, O., and Horning, S. (2006b). Dynamic range of mass accuracy in LTQ Orbitrap hybrid mass spectrometer. J Am Soc Mass Spectrom *17*, 977-982.

Mandell, J.G., Falick, A.M., and Komives, E.A. (1998). Measurement of amide hydrogen exchange by MALDI-TOF mass spectrometry. Anal Chem *70*, 3987-3995.

Mann, M. (2008). Can proteomics retire the western blot? J Proteome Res *7*, 3065.

Mann, M., and Kelleher, N.L. (2008). Precision proteomics: the case for high resolution and high mass accuracy. Proc Natl Acad Sci U S A *105*, 18132-18138.

Mann, M., and Wilm, M. (1994). Error-tolerant identification of peptides in sequence databases by peptide sequence tags. Anal Chem *66*, 4390-4399.

Marsch, R., Foeller, E., Rammes, G., Bunck, M., Kossl, M., Holsboer, F., Zieglgansberger, W., Landgraf, R., Lutz, B., and Wotjak, C.T. (2007). Reduced anxiety, conditioned fear, and hippocampal long-term potentiation in transient receptor potential vanilloid type 1 receptor-deficient mice. J Neurosci *27*, 832-839.

Marshall, S., Okuyama, R., and Rumberger, J.M. (2005). Turnover and characterization of UDP-N-acetylglucosaminyl transferase in a stably transfected HeLa cell line. Biochem Biophys Res Commun *332*, 263-270.

Martens, L., and Apweiler, R. (2009). Algorithms and databases. Methods Mol Biol *564*, 245-259.

Martin, E.I., Ressler, K.J., Binder, E., and Nemeroff, C.B. (2009). The neurobiology of anxiety disorders: brain imaging, genetics, and psychoneuroendocrinology. Psychiatr Clin North Am *32*, 549-575.

Martini, W.Z., Chinkes, D.L., and Wolfe, R.R. (2004). The intracellular free amino acid pool represents tracer precursor enrichment for calculation of protein synthesis in cultured fibroblasts and myocytes. J Nutr *134*, 1546-1550.

Masood, A., Nadeem, A., Mustafa, S.J., and O'Donnell, J.M. (2008). Reversal of oxidative stress-induced anxiety by inhibition of phosphodiesterase-2 in mice. J Pharmacol Exp Ther *326*, 369-379.

McClatchy, D.B., Dong, M.Q., Wu, C.C., Venable, J.D., and Yates, J.R. (2007a). N-15 metabolic labeling of mammalian tissue with slow protein turnover. Journal of Proteome Research *6*, 2005-2010.

McClatchy, D.B., Liao, L., Park, S.K., Venable, J.D., and Yates, J.R. (2007b). Quantification of the synaptosomal proteome of the rat cerebellum during post-natal development. Genome Res *17*, 1378-1388.

McGeer, E.G., and McGeer, P.L. (2001). Innate immunity in Alzheimer's disease: a model for local inflammatory reactions. Mol Interv *1*, 22-29.

McHugh, L., and Arthur, J.W. (2008). Computational methods for protein identification from mass spectrometry data. PLoS Comput Biol *4*, e12.

Moffitt, T.E., Harrington, H., Caspi, A., Kim-Cohen, J., Goldberg, D., Gregory, A.M., and Poulton, R. (2007). Depression and generalized anxiety disorder: cumulative and sequential comorbidity in a birth cohort followed prospectively to age 32 years. Arch Gen Psychiatry *64*, 651-660.

Mombereau, C., Kaupmann, K., Froestl, W., Sansig, G., van der Putten, H., and Cryan, J.F. (2004). Genetic and pharmacological evidence of a role for GABA(B) receptors in the modulation of anxiety- and antidepressant-like behavior. Neuropsychopharmacology *29*, 1050-1062.

Mortz, E., O'Connor, P.B., Roepstorff, P., Kelleher, N.L., Wood, T.D., McLafferty, F.W., and Mann, M. (1996). Sequence tag identification of intact proteins by matching tanden mass spectral data against sequence data bases. Proc Natl Acad Sci U S A *93*, 8264-8267.

Mukherjee, P., and Pasinetti, G.M. (2000). The role of complement anaphylatoxin C5a in neurodegeneration: implications in Alzheimer's disease. J Neuroimmunol *105*, 124-130.

Muller, M.B., and Holsboer, F. (2006). Mice with mutations in the HPA-system as models for symptoms of depression. Biol Psychiatry *59*, 1104-1115.

Nelson, C.J., Huttlin, E.L., Hegeman, A.D., Harms, A.C., and Sussman, M.R. (2007). Implications of 15N-metabolic labeling for automated peptide identification in Arabidopsis thaliana. Proteomics *7*, 1279-1292.

Nestler, E.J., Barrot, M., DiLeone, R.J., Eisch, A.J., Gold, S.J., and Monteggia, L.M. (2002). Neurobiology of depression. Neuron *34*, 13-25.

Nesvizhskii, A.I. (2007). Protein identification by tandem mass spectrometry and sequence database searching. Methods Mol Biol *367*, 87-119.

Ng, A., Bursteinas, B., Gao, Q., Mollison, E., and Zvelebil, M. (2006). pSTIING: a 'systems' approach towards integrating signalling pathways, interaction and transcriptional regulatory networks in inflammation and cancer. Nucleic Acids Res *34*, D527-534.

Ng, F., Berk, M., Dean, O., and Bush, A.I. (2008). Oxidative stress in psychiatric disorders: evidence base and therapeutic implications. Int J Neuropsychopharmacol *11*, 851-876.

Nicholson, J.K., Connelly, J., Lindon, J.C., and Holmes, E. (2002). Metabonomics: a platform for studying drug toxicity and gene function. Nature Reviews Drug Discovery *1*, 153-161.

Nicholson, J.K., Lindon, J.C., and Holmes, E. (1999). 'Metabonomics': understanding the metabolic responses of living systems to pathophysiological stimuli via multivariate statistical analysis of biological NMR spectroscopic data. Xenobiotica *29*, 1181-1189.

Nishiyama, E., Iwamoto, N., Kimura, M., and Arai, H. (1996). Serum amyloid P component level in Alzheimer's disease. Dementia *7*, 256-259.

Nutt, D.J., and Malizia, A.L. (2001). New insights into the role of the GABA(A)-benzodiazepine receptor in psychiatric disorder. Br J Psychiatry *179*, 390-396.

Oda, Y., Huang, K., Cross, F.R., Cowburn, D., and Chait, B.T. (1999). Accurate quantitation of protein expression and site-specific phosphorylation. Proc Natl Acad Sci U S A *96*, 6591-6596.

Oda, Y., Owa, T., Sato, T., Boucher, B., Daniels, S., Yamanaka, H., Shinohara, Y., Yokoi, A., Kuromitsu, J., and Nagasu, T. (2003). Quantitative chemical proteomics for identifying candidate drug targets. Anal Chem *75*, 2159-2165.

Oliver, S.G., Winson, M.K., Kell, D.B., and Baganz, F. (1998). Systematic functional analysis of the yeast genome. Trends Biotechnol *16*, 373-378.

Ong, S.E., Blagoev, B., Kratchmarova, I., Kristensen, D.B., Steen, H., Pandey, A., and Mann, M. (2002). Stable isotope labeling by amino acids in cell culture, SILAC, as a simple and accurate approach to expression proteomics. Mol Cell Proteomics *1*, 376-386.

Ong, S.E., Foster, L.J., and Mann, M. (2003). Mass spectrometric-based approaches in quantitative proteomics. Methods *29*, 124-130.

Ong, S.E., and Mann, M. (2005). Mass spectrometry-based proteomics turns quantitative. Nat Chem Biol *1*, 252-262.

Ono, M., Shitashige, M., Honda, K., Isobe, T., Kuwabara, H., Matsuzuki, H., Hirohashi, S., and Yamada, T. (2006). Label-free quantitative proteomics using large peptide data sets generated by nanoflow liquid chromatography and mass spectrometry. Mol Cell Proteomics *5*, 1338-1347.

Palmblad, M., Bindschedler, L.V., and Cramer, R. (2007). Quantitative proteomics using uniform (15)N-labeling, MASCOT, and the trans-proteomic pipeline. Proteomics *7*, 3462-3469.

Pan, C., Kora, G., McDonald, W.H., Tabb, D.L., VerBerkmoes, N.C., Hurst, G.B., Pelletier, D.A., Samatova, N.F., and Hettich, R.L. (2006). ProRata: A quantitative proteomics program for accurate protein abundance ratio estimation with confidence interval evaluation. Anal Chem *78*, 7121-7131.

Pan, C., Kumar, C., Bohl, S., Klingmueller, U., and Mann, M. (2009). Comparative proteomic phenotyping of cell lines and primary cells to assess preservation of cell type-specific functions. Mol Cell Proteomics *8*, 443-450.

Pang, L., Sawada, T., Decker, S.J., and Saltiel, A.R. (1995). Inhibition of Map Kinase Kinase Blocks the Differentiation of Pc-12 Cells Induced by Nerve Growth-Factor. Journal of Biological Chemistry *270*, 13585-13588.

Pariante, C.M., and Lightman, S.L. (2008). The HPA axis in major depression: classical theories and new developments. Trends Neurosci *31*, 464-468.

Park, S.K., Venable, J.D., Xu, T., and Yates, J.R., 3rd (2008). A quantitative analysis software tool for mass spectrometry-based proteomics. Nat Methods *5*, 319-322.

Parks, C.L., Robinson, P.S., Sibille, E., Shenk, T., and Toth, M. (1998). Increased anxiety of mice lacking the serotonin1A receptor. Proc Natl Acad Sci U S A *95*, 10734-10739.

Pellow, S., Chopin, P., File, S.E., and Briley, M. (1985). Validation of open:closed arm entries in an elevated plus-maze as a measure of anxiety in the rat. J Neurosci Methods *14*, 149-167.

Perkins, D.N., Pappin, D.J., Creasy, D.M., and Cottrell, J.S. (1999). Probability-based protein identification by searching sequence databases using mass spectrometry data. Electrophoresis *20*, 3551-3567.

Pierri, J.N., Chaudry, A.S., Woo, T.U., and Lewis, D.A. (1999). Alterations in chandelier neuron axon terminals in the prefrontal cortex of schizophrenic subjects. Am J Psychiatry *156*, 1709-1719.

Porsolt, R.D., Anton, G., Blavet, N., and Jalfre, M. (1978). Behavioural despair in rats: a new model sensitive to antidepressant treatments. Eur J Pharmacol *47*, 379-391.

Pratt, J.M., Petty, J., Riba-Garcia, I., Robertson, D.H., Gaskell, S.J., Oliver, S.G., and Beynon, R.J. (2002). Dynamics of protein turnover, a missing dimension in proteomics. Mol Cell Proteomics *1*, 579-591.

Pupim, L.B., Flakoll, P.J., and Ikizler, T.A. (2004). Nutritional supplementation acutely increases albumin fractional synthetic rate in chronic hemodialysis patients. J Am Soc Nephrol *15*, 1920-1926.

Qi, X., Lin, W., Li, J., Li, H., Wang, W., Wang, D., and Sun, M. (2008). Fluoxetine increases the activity of the ERK-CREB signal system and alleviates the depressive-like behavior in rats exposed to chronic forced swim stress. Neurobiol Dis *31*, 278-285.

Qi, X., Lin, W., Li, J., Pan, Y., and Wang, W. (2006). The depressive-like behaviors are correlated with decreased phosphorylation of mitogen-activated protein kinases in rat brain following chronic forced swim stress. Behav Brain Res *175*, 233-240.

Qi, X., Lin, W., Wang, D., Pan, Y., Wang, W., and Sun, M. (2009). A role for the extracellular signal-regulated kinase signal pathway in depressive-like behavior. Behav Brain Res *199*, 203-209.

Quik, M., Huang, L.Z., Parameswaran, N., Bordia, T., Campos, C., and Perez, X.A. (2009). Multiple roles for nicotine in Parkinson's disease. Biochem Pharmacol *78*, 677-685.

Rachdaoui, N., Austin, L., Kramer, E., Previs, M.J., Anderson, V.E., Kasumov, T., and Previs, S.F. (2009). Measuring proteome dynamics in vivo: as easy as adding water? Mol Cell Proteomics *8*, 2653-2663.

Radtke, F., Fasnacht, N., and Macdonald, H.R. (2010). Notch signaling in the immune system. Immunity *32*, 14-27.

Ramboz, S., Oosting, R., Amara, D.A., Kung, H.F., Blier, P., Mendelsohn, M., Mann, J.J., Brunner, D., and Hen, R. (1998). Serotonin receptor 1A knockout: an animal model of anxiety-related disorder. Proc Natl Acad Sci U S A *95*, 14476-14481.

Rammal, H., Bouayed, J., Younos, C., and Soulimani, R. (2008a). Evidence that oxidative stress is linked to anxiety-related behaviour in mice. Brain Behav Immun *22*, 1156-1159.

Rammal, H., Bouayed, J., Younos, C., and Soulimani, R. (2008b). The impact of high anxiety level on the oxidative status of mouse peripheral blood lymphocytes, granulocytes and monocytes. Eur J Pharmacol *589*, 173-175.

Ramos-Fernandez, A., Lopez-Ferrer, D., and Vazquez, J. (2007). Improved method for differential expression proteomics using trypsin-catalyzed 18O labeling with a correction for labeling efficiency. Mol Cell Proteomics *6*, 1274-1286.

Rao, P.K., Rodriguez, G.M., Smith, I., and Li, Q. (2008). Protein dynamics in iron-starved Mycobacterium tuberculosis revealed by turnover and abundance measurement using hybrid-linear ion trap-Fourier transform mass spectrometry. Anal Chem *80*, 6860-6869.

Rechinger, K.B., Siegumfeldt, H., Svendsen, I., and Jakobsen, M. (2000). "Early" protein synthesis of Lactobacillus delbrueckii ssp. bulgaricus in milk revealed by [35S] methionine labeling and two-dimensional gel electrophoresis. Electrophoresis *21*, 2660-2669.

Regier, D., Rae, D., Narrow, W., Kaebler, C., and Schatzberg, A. (1998). Prevalence of anxiety disorders and their comorbidity with mood and addictive disorders. British Journal of Psychiatry *173* 24-28.

Reynolds, K.J., Yao, X., and Fenselau, C. (2002a). Proteolytic 18O labeling for comparative proteomics: evaluation of endoprotease Glu-C as the catalytic agent. J Proteome Res *1*, 27-33.

Reynolds, K.J., Yao, X.D., and Fenselau, C. (2002b). Proteolytic O-18 labeling for comparative proteomics: Evaluation of endoprotease Glu-C as the catalytic agent. Journal of Proteome Research *1*, 27-33.

Roberts, P.J., and Der, C.J. (2007). Targeting the Raf-MEK-ERK mitogen-activated protein kinase cascade for the treatment of cancer. Oncogene *26*, 3291-3310.

Ross, P.L., Huang, Y.N., Marchese, J.N., Williamson, B., Parker, K., Hattan, S., Khainovski, N., Pillai, S., Dey, S., Daniels, S.*, et al.* (2004). Multiplexed protein quantitation in Saccharomyces cerevisiae using amine-reactive isobaric tagging reagents. Mol Cell Proteomics *3*, 1154-1169.

Rowan, M.J., Klyubin, I., Cullen, W.K., and Anwyl, R. (2003). Synaptic plasticity in animal models of early Alzheimer's disease. Philos Trans R Soc Lond B Biol Sci *358*, 821-828.

Sananbenesi, F., Fischer, A., Schrick, C., Spiess, J., and Radulovic, J. (2003). Mitogen-activated protein kinase signaling in the hippocampus and its modulation by corticotropin-releasing factor receptor 2: a possible link between stress and fear memory. J Neurosci *23*, 11436-11443.

Sauer, U., Heinemann, M., and Zamboni, N. (2007). Genetics. Getting closer to the whole picture. Science *316*, 550-551.

Schaff, J.E., Mbeunkui, F., Blackburn, K., Bird, D.M., and Goshe, M.B. (2008). SILIP: a novel stable isotope labeling method for in planta quantitative proteomic analysis. Plant J *56*, 840-854.

Schlessinger, J. (2000). Cell signaling by receptor tyrosine kinases. Cell *103*, 211-225.

Schmidt, A., Kellermann, J., and Lottspeich, F. (2005). A novel strategy for quantitative proteomics using isotope-coded protein labels. Proteomics *5*, 4-15.

Scholz, M., and Fiehn, O. (2007). SetupX--a public study design database for metabolomic projects. Pac Symp Biocomput, 169-180.

Schrimpf, S.P., Weiss, M., Reiter, L., Ahrens, C.H., Jovanovic, M., Malmstrom, J., Brunner, E., Mohanty, S., Lercher, M.J., Hunziker, P.E.*, et al.* (2009). Comparative functional analysis of the Caenorhabditis elegans and Drosophila melanogaster proteomes. PLoS Biol *7*, e48.

Schuerenberg, M., Luebbert, C., Eickhoff, H., Kalkum, M., Lehrach, H., and Nordhoff, E. (2000). Prestructured MALDI-MS sample supports. Anal Chem *72*, 3436-3442.

Schule, C., Baghai, T., Schmidbauer, S., Bidlingmaier, M., Strasburger, C.J., and Laakmann, G. (2004). Reboxetine acutely stimulates cortisol, ACTH, growth hormone and prolactin secretion in healthy male subjects. Psychoneuroendocrinology *29*, 185-200.

Schultz, K., Traskman-Bendz, L., and Petersen, A. (2008). Transthyretin in cerebrospinal fluid from suicide attempters. J Affect Disord *109*, 205-208.

Sebolt-Leopold, J.S. (2008). Advances in the development of cancer therapeutics directed against the RAS-mitogen-activated protein kinase pathway. Clin Cancer Res *14*, 3651-3656.

Selbach, M., Schwanhausser, B., Thierfelder, N., Fang, Z., Khanin, R., and Rajewsky, N. (2008). Widespread changes in protein synthesis induced by microRNAs. Nature *455*, 58-63.

Senko, M.W., Beu, S.C., and Mclafferty, F.W. (1995). Determination of Monoisotopic Masses and Ion Populations for Large Biomolecules from Resolved Isotopic Distributions. Journal of the American Society for Mass Spectrometry *6*, 229-233.

Shadforth, I., Crowther, D., and Bessant, C. (2005). Protein and peptide identification algorithms using MS for use in high-throughput, automated pipelines. Proteomics *5*, 4082-4095.

Shannon, P., Markiel, A., Ozier, O., Baliga, N.S., Wang, J.T., Ramage, D., Amin, N., Schwikowski, B., and Ideker, T. (2003). Cytoscape: a software environment for integrated models of biomolecular interaction networks. Genome Res *13*, 2498-2504.

Shevchenko, A., Tomas, H., Havlis, J., Olsen, J.V., and Mann, M. (2006). In-gel digestion for mass spectrometric characterization of proteins and proteomes. Nat Protoc *1*, 2856-2860.

Shimizu, K., Amagaya, S., and Ogihara, Y. (1983). Analysis of corticosterone in the serum of mice and rats using high-performance liquid chromatography. J Chromatogr *272*, 170-175.

Siuzdak, G. (2006). The Expanding Role of Mass Spectrometry in Biotechnology, Second Edition (MCC Press).

Sivachenko, A.Y., and Yuryev, A. (2007). Pathway analysis software as a tool for drug target selection, prioritization and validation of drug mechanism. Expert Opin Ther Targets *11*, 411-421.

Sluyter, F., Korte, S.M., Bohus, B., and Van Oortmerssen, G.A. (1996). Behavioral stress response of genetically selected aggressive and nonaggressive wild house mice in the shock-probe/defensive burying test. Pharmacol Biochem Behav *54*, 113-116.

Smith, G.W., Aubry, J.M., Dellu, F., Contarino, A., Bilezikjian, L.M., Gold, L.H., Chen, R., Marchuk, Y., Hauser, C., Bentley, C.A.*, et al.* (1998a). Corticotropin releasing factor receptor 1-deficient mice display decreased anxiety, impaired stress response, and aberrant neuroendocrine development. Neuron *20*, 1093-1102.

Smith, K., Reynolds, N., Downie, S., Patel, A., and Rennie, M.J. (1998b). Effects of flooding amino acids on incorporation of labeled amino acids into human muscle protein. Am J Physiol *275*, E73-78.

Smolka, M.B., Zhou, H., Purkayastha, S., and Aebersold, R. (2001). Optimization of the isotope-coded affinity tag-labeling procedure for quantitative proteome analysis. Anal Biochem *297*, 25-31.

Steru, L., Chermat, R., Thierry, B., and Simon, P. (1985). The tail suspension test: a new method for screening antidepressants in mice. Psychopharmacology (Berl) *85*, 367-370.

Stout, S.C., Owens, M.J., and Nemeroff, C.B. (2002). Regulation of corticotropin-releasing factor neuronal systems and hypothalamic-pituitary-adrenal axis activity by stress and chronic antidepressant treatment. J Pharmacol Exp Ther *300*, 1085-1092.

Strohle, A., and Holsboer, F. (2003). Stress responsive neurohormones in depression and anxiety. Pharmacopsychiatry *36 Suppl 3*, S207-214.

Sullivan, G.M., Hatterer, J.A., Herbert, J., Chen, X., Roose, S.P., Attia, E., Mann, J.J., Marangell, L.B., Goetz, R.R., and Gorman, J.M. (1999). Low levels of transthyretin in the CSF of depressed patients. Am J Psychiatry *156*, 710-715.

Takizawa, Y., and Yamashita, J. (1989). Metabolism of tritiated water in the cell nucleus and intracellular substances of the rat. Radiat Res *117*, 523-530.

Tanaka, K., Waki, H., Ido, Y., Akita, S., Yoshida, Y., Yoshida, T., and Matsuo, T. (1988). Protein and polymer analyses up to m/z 100 000 by laser ionization time-of-flight mass spectrometry. Rapid Communications in Mass Spectrometry *2*, 151-153.

Tao, J., Chen, S., and Lee, B. (2010). Alteration of Notch signaling in skeletal development and disease. Ann N Y Acad Sci *1192*, 257-268.

Tao, W.A., and Aebersold, R. (2003). Advances in quantitative proteomics via stable isotope tagging and mass spectrometry. Curr Opin Biotechnol *14*, 110-118.

Team, R.D.C. (2009). R: a language and environment for statistical computing. R Foundation for Statistical Computing, Vienna, Austria.

Thompson, A., Schafer, J., Kuhn, K., Kienle, S., Schwarz, J., Schmidt, G., Neumann, T., Johnstone, R., Mohammed, A.K., and Hamon, C. (2003). Tandem mass tags: a novel quantification strategy for comparative analysis of complex protein mixtures by MS/MS. Anal Chem *75*, 1895-1904.

Tiraboschi, E., Tardito, D., Kasahara, J., Moraschi, S., Pruneri, P., Gennarelli, M., Racagni, G., and Popoli, M. (2004). Selective phosphorylation of nuclear CREB by fluoxetine is linked to activation of CaM kinase IV and MAP kinase cascades. Neuropsychopharmacology *29*, 1831-1840.

Todorovic, C., Sherrin, T., Pitts, M., Hippel, C., Rayner, M., and Spiess, J. (2009). Suppression of the MEK/ERK signaling pathway reverses depression-like behaviors of CRF2-deficient mice. Neuropsychopharmacology *34*, 1416-1426.

Tylec, A., Jarzab, A., Stryjecka-Zimmer, M., and Wojcicka, A. (2007). [Stress oxidative in schizophrenia]. Pol Merkur Lekarski *23*, 74-77.

Valko, M., Leibfritz, D., Moncol, J., Cronin, M.T., Mazur, M., and Telser, J. (2007). Free radicals and antioxidants in normal physiological functions and human disease. Int J Biochem Cell Biol *39*, 44-84.

van Iersel, M.P., Kelder, T., Pico, A.R., Hanspers, K., Coort, S., Conklin, B.R., and Evelo, C. (2008). Presenting and exploring biological pathways with PathVisio. BMC Bioinformatics *9*, 399.

Venter, J.C., Adams, M.D., Myers, E.W., Li, P.W., Mural, R.J., Sutton, G.G., Smith, H.O., Yandell, M., Evans, C.A., Holt, R.A.*, et al.* (2001). The sequence of the human genome. Science *291*, 1304-1351.

Verwey, N.A., Schuitemaker, A., van der Flier, W.M., Mulder, S.D., Mulder, C., Hack, C.E., Scheltens, P., Blankenstein, M.A., and Veerhuis, R. (2008). Serum amyloid p component as a biomarker in mild cognitive impairment and Alzheimer's disease. Dement Geriatr Cogn Disord *26*, 522-527.

Wagner, C., Sefkow, M., and Kopka, J. (2003). Construction and application of a mass spectral and retention time index database generated from plant GC/EI-TOF-MS metabolite profiles. Phytochemistry *62*, 887-900.

Walrand, S., Guillet, C., Gachon, P., Rousset, P., Giraudet, C., Vasson, M.P., and Boirie, Y. (2004). Protein synthesis rates of human PBMC and PMN can be determined simultaneously in vivo by using small blood samples. Am J Physiol Cell Physiol *286*, C1474-1478.

Walther, T., Balschun, D., Voigt, J.P., Fink, H., Zuschratter, W., Birchmeier, C., Ganten, D., and Bader, M. (1998). Sustained long term potentiation and anxiety in mice lacking the Mas protooncogene. Journal of Biological Chemistry *273*, 11867-11873.

Wan, P.T., Garnett, M.J., Roe, S.M., Lee, S., Niculescu-Duvaz, D., Good, V.M., Jones, C.M., Marshall, C.J., Springer, C.J., Barford, D.*, et al.* (2004). Mechanism of activation of the RAF-ERK signaling pathway by oncogenic mutations of B-RAF. Cell *116*, 855-867.

Wang, B., Valentine, S., Plasencia, M., Raghuraman, S., and Zhang, X. (2010). Artificial neural networks for the prediction of peptide drift time in ion mobility mass spectrometry. BMC Bioinformatics *11*, 182.

Wang, G., Wu, W.W., Zhang, Z., Masilamani, S., and Shen, R.F. (2009). Decoy methods for assessing false positives and false discovery rates in shotgun proteomics. Anal Chem *81*, 146-159.

Wang, W., Zhou, H., Lin, H., Roy, S., Shaler, T.A., Hill, L.R., Norton, S., Kumar, P., Anderle, M., and Becker, C.H. (2003). Quantification of proteins and metabolites by mass spectrometry without isotopic labeling or spiked standards. Anal Chem *75*, 4818-4826.

Want, E.J., Nordstrom, A., Morita, H., and Siuzdak, G. (2007). From exogenous to endogenous: the inevitable imprint of mass spectrometry in metabolomics. J Proteome Res *6*, 459-468.

Washburn, M.P., Wolters, D., and Yates, J.R., 3rd (2001). Large-scale analysis of the yeast proteome by multidimensional protein identification technology. Nat Biotechnol *19*, 242-247.

Weber, C.C., Eckert, G.P., and Muller, W.E. (2006). Effects of antidepressants on the brain/plasma distribution of corticosterone. Neuropsychopharmacology *31*, 2443-2448.

Weinberg, M.H., and Pittsburg, P. (1945). Aminoacetic Acid (Glycine) in the Treatment of Depression. Journal of Nervous & Mental Disease *102* 601-610.

Wiener, M.C., Sachs, J.R., Deyanova, E.G., and Yates, N.A. (2004). Differential mass spectrometry: a label-free LC-MS method for finding significant differences in complex peptide and protein mixtures. Anal Chem *76*, 6085-6096.

Wilkins, M.R., Pasquali, C., Appel, R.D., Ou, K., Golaz, O., Sanchez, J.C., Yan, J.X., Gooley, A.A., Hughes, G., Humphery-Smith, I*., et al.* (1996). From proteins to proteomes: large scale protein identification by two-dimensional electrophoresis and amino acid analysis. Biotechnology (N Y) *14*, 61-65.

Wilm, M., and Mann, M. (1996). Analytical properties of the nanoelectrospray ion source. Anal Chem *68*, 1-8.

Wilm, M.S., and Mann, M. (1994). Electrospray and Taylor-Cone theory, Dole's beam of macromolecules at last? Int J Mass Spectrom Ion Proc *136*, 167-180.

Wolf-Yadlin, A., Hautaniemi, S., Lauffenburger, D.A., and White, F.M. (2007). Multiple reaction monitoring for robust quantitative proteomic analysis of cellular signaling networks. Proc Natl Acad Sci U S A *104*, 5860-5865.

Wolters, D.A., Washburn, M.P., and Yates, J.R., 3rd (2001). An automated multidimensional protein identification technology for shotgun proteomics. Anal Chem *73*, 5683-5690.

Wood, S.J., Yucel, M., Pantelis, C., and Berk, M. (2009). Neurobiology of schizophrenia spectrum disorders: the role of oxidative stress. Ann Acad Med Singapore *38*, 396-396.

Wu, C.C., MacCoss, M.J., Howell, K.E., Matthews, D.E., and Yates, J.R., 3rd (2004). Metabolic labeling of mammalian organisms with stable isotopes for quantitative proteomic analysis. Anal Chem *76*, 4951-4959.

Wymann, M.P., BulgarelliLeva, G., Zvelebil, M.J., Pirola, L., Vanhaesebroeck, B., Waterfield, M.D., and Panayotou, G. (1996). Wortmannin inactivates phosphoinositide 3-kinase by covalent modification of Lys-802, a residue involved in the phosphate transfer reaction. Molecular and Cellular Biology *16*, 1722-1733.

Xu, T.L., and Gong, N. (2010). Glycine and glycine receptor signaling in hippocampal neurons: Diversity, function and regulation. Prog Neurobiol.

Xu, Y., Heilier, J.F., Madalinski, G., Genin, E., Ezan, E., Tabet, J.C., and Junot, C. (2010). Evaluation of Accurate Mass and Relative Isotopic Abundance Measurements in the LTQ-Orbitrap Mass Spectrometer for Further Metabolomics Database Building. Anal Chem.

Yao, X., Freas, A., Ramirez, J., Demirev, P.A., and Fenselau, C. (2001). Proteolytic 18O labeling for comparative proteomics: model studies with two serotypes of adenovirus. Anal Chem *73*, 2836-2842.

Yasojima, K., Schwab, C., McGeer, E.G., and McGeer, P.L. (2000). Human neurons generate C-reactive protein and amyloid P: upregulation in Alzheimer's disease. Brain Res *887*, 80-89.

Yates, J.R., 3rd (2004). Mass spectral analysis in proteomics. Annu Rev Biophys Biomol Struct *33*, 297-316.

Young, A.B., Zukin, S.R., and Snyder, S.H. (1974). Interaction of benzodiazepines with central nervous glycine receptors: possible mechanism of action. Proc Natl Acad Sci U S A *71*, 2246-2250.

Young, E.A., Abelson, J.L., and Cameron, O.G. (2004). Effect of comorbid anxiety disorders on the hypothalamic-pituitary-adrenal axis response to a social stressor in major depression. Biol Psychiatry *56*, 113-120.

Yu, S., Holsboer, F., and Almeida, O.F. (2008). Neuronal actions of glucocorticoids: focus on depression. J Steroid Biochem Mol Biol *108*, 300-309.

Zafra, F., Aragon, C., and Gimenez, C. (1997). Molecular biology of glycinergic neurotransmission. Mol Neurobiol *14*, 117-142.

Zhang, Y., Webhofer, C., Reckow, S., Filiou, M.D., Maccarrone, G., and Turck, C.W. (2009). A MS data search method for improved 15N-labeled protein identification. Proteomics *9*, 4265-4270.

Zou, W., and Tolstikov, V.V. (2008). Probing genetic algorithms for feature selection in comprehensive metabolic profiling approach. Rapid Commun Mass Spectrom *22*, 1312-1324.

7 Supplementary tables

Supplementary table 1. Proteins expressed differentially between HAB/LAB hippocampal cytosol (indirect comparison)

Accession	Gene symbol	Log2 Ratio	Peptide number
IPI00271166.4	Htt	-7.2	28
IPI00128071.7	Uso1	-4.1	14
IPI00320831.3	Nbea	-3.9	107
IPI00652358.5	Arsb	-3.6	13
IPI00377455.3	Gcc2	-3.4	12
IPI00336281.1	Golga3	-3	39
IPI00115663.2	Dctn1	-3	50
IPI00228222.1	Ubr3	-3	13
IPI00788324.1	Myh9	-2.9	11
IPI00331299.9	Ncdn	-2.9	173
IPI00112001.1	Cap2	-2.8	22
IPI00466610.5	Map2k1	-2.7	10
IPI00453996.1	Myh14	-2.7	16
IPI00114894.1	Myh11	-2.7	116
IPI00421179.1	Eif4g1	-2.6	28
IPI00308938.6	Capn2	-2.6	14
IPI00123181.3	Myh9	-2.5	352
IPI00400432.2	Eif4a2	-2.4	16
IPI00621417.1	Hbb-b1	-2.4	231
IPI00467383.2	Cul3	-2.3	41
IPI00225961.5	Phgdh	-2.3	21

IPI00130390.5	Kif1b	-2.2	31
IPI00221817.5	Loh11cr2a	-2.2	23
IPI00453613.3	Huwe1	-2.2	89
IPI00761751.2	Kif13b	-2.2	12
IPI00480321.2	Grlf1	-2.1	27
IPI00338604.5	Myh10	-2.1	558
IPI00331444.7	Ipo7	-2.1	58
IPI00123709.1	Akap12	-2	36
IPI00123465.1	Cops7a	-2	23
IPI00118120.1	Myo5a	-2	94
IPI00128341.1	Wasf3	-2	12
IPI00453615.3	Huwe1	-2	21
IPI00420562.5	Cand1	-2	281
IPI00119762.4	Dclk1	-2	26
IPI00453803.5	Ube2o	-2	93
IPI00114667.1	Psmd7	-1.9	14
IPI00116752.7	Sec23ip	-1.9	22
IPI00115833.2	Mtap6	-1.9	165
IPI00319320.4	Nckap1	-1.9	94
IPI00407835.2	Ubap2l	-1.9	30
IPI00229483.3	Sec24c	-1.9	28
IPI00262114.1	Pak3	-1.9	12
IPI00117929.1	Oxr1	-1.9	238
IPI00377609.2	Vcpip1	-1.9	25
IPI00464181.4	BC067047	-1.8	11
IPI00224151.5	Ap1g1	-1.8	14
IPI00118676.3	Eif4a1	-1.8	17
IPI00377592.7	Sec31a	-1.8	137
IPI00554992.2	Kif1a	-1.8	63

IPI00132762.1	Trap1	-1.8	83
IPI00129350.1	Aldh18a1	-1.7	12
IPI00270877.5	Usp14	-1.7	11
IPI00136350.3	Dlg3	-1.7	36
IPI00108388.1	Usp9x	-1.7	131
IPI00407144.1	Kif1b	-1.7	18
IPI00405625.9	Cyfip2	-1.7	134
IPI00187356.1	Ankfy1	-1.7	22
IPI00626501.3	Kif1a	-1.7	58
IPI00124614.1	Epm2aip1	-1.7	36
IPI00399840.2	Ube3a	-1.7	21
IPI00343557.1	Mapre3	-1.7	31
IPI00321646.3	AI314180	-1.7	21
IPI00881540.2	Synj1	-1.7	11
IPI00115824.1	Nipsnap1	-1.7	43
IPI00108150.1	Rock2	-1.7	172
IPI00221769.5	Ak3	-1.7	14
IPI00229080.7	Hsp90ab1	-1.7	883
IPI00172221.2	Dnm1l	-1.7	60
IPI00133132.1	Ptk2b	-1.6	54
IPI00132080.1	Pgls	-1.6	51
IPI00321734.7	Glo1	-1.6	207
IPI00125135.1	Ube2d2	-1.6	41
IPI00465648.3	Dnm1	-1.6	31
IPI00331016.1	Sec24b	-1.6	37
IPI00312128.3	Trim28	-1.6	52
IPI00227236.2	Cadps2	-1.5	28
IPI00109044.8	2900073G15Rik	-1.5	12
IPI00330476.3	Cyfip1	-1.5	202

IPI00459745.3	Rap1gap	-1.5	39	IPI00469103.1	Kars	-1.3	23	IPI00169448.1	Ube2m	-1.1	26
IPI00229647.5	Tln2	-1.5	62	IPI00112335.1	Map2k4	-1.3	24	IPI00187407.4	Cops8	-1.1	36
IPI00123624.8	2610301G19Rik	-1.5	53	IPI00381019.1	Smarcc2	-1.3	21	IPI00119876.1	Dync1h1	-1.1	1143
				IPI00123379.1	Hdlbp	-1.3	16	IPI00165854.3	Ube2n	-1.1	65
IPI00352986.2	Strn	-1.5	38	IPI00221723.1	Wasf2	-1.2	12	IPI00381365.1	Abr	-1.1	64
IPI00129526.1	Hsp90b1	-1.5	337	IPI00123518.1	Lypla2	-1.2	18	IPI00224128.7	Nmt1	-1	15
IPI00808550.1	B230112C05Rik	-1.5	18	IPI00261627.1	Sucla2	-1.2	59	IPI00130992.1	Capns1	-1	11
				IPI00850983.1	Synj1	-1.2	665	IPI00420385.4	11-Sep	-1	17
IPI00458854.2	Sart3	-1.5	30	IPI00351252.4	Gmps	-1.2	78	IPI00127176.3	6720456B07Rik	-1	24
IPI00117087.1	Cdc37	-1.4	12	IPI00468516.3	D6Wsu116e	-1.2	23				
IPI00116546.2	Prkar2a	-1.4	10					IPI00471372.2	Wasf1	-1	54
IPI00129282.1	Dlg2	-1.4	31	IPI00123292.5	Fubp1	-1.2	59	IPI00668903.1	Cadps	-1	14
IPI00311461.1	Atp6v1h	-1.4	25	IPI00225231.1	Ank2	-1.2	20	IPI00134344.6	Spnb3	-1	606
IPI00758170.2	Synj1	-1.4	116	IPI00312076.4	Kif3a	-1.2	10	IPI00853823.2	Rapgef2	-1	134
IPI00222496.3	Pdia6	-1.4	18	IPI00108147.1	Rock1	-1.1	25	IPI00127492.1	Smap1	-1	29
IPI00123349.2	Sec23a	-1.4	42	IPI00415908.4	Ppme1	-1.1	23	IPI00310131.5	Ap2a2	-1	76
IPI00120076.2	Ckmt2	-1.4	41	IPI00128127.1	Dgkg	-1.1	15	IPI00114241.2	Nefh	-1	43
IPI00331076.4	Slk	-1.4	169	IPI00132278.1	Cplx1	-1.1	12	IPI00405227.3	Vcl	-1	214
IPI00137331.6	Cap1	-1.4	109	IPI00226602.3	6-Sep	-1.1	22	IPI00347394.7	1300001I01Rik	-1	48
IPI00314439.3	Psmd3	-1.4	19	IPI00762897.2	Ugcgl1	-1.1	208				
IPI00113214.1	Usp5	-1.4	373	IPI00330163.4	Cadps	-1.1	203	IPI00124787.3	Arl3	-1	36
IPI00331568.7	Hgs	-1.4	23	IPI00116554.2	Ptpn11	-1.1	37	IPI00876559.1	Khsrp	-1	20
IPI00310091.8	Ppp2r1a	-1.4	75	IPI00118075.1	Mtap2	-1.1	3147	IPI00110990.1	Dusp3	-1	123
IPI00330804.4	Hsp90aa1	-1.4	614	IPI00420870.4	Ogt	-1.1	114	IPI00128867.3	Purb	-1	21
IPI00465786.3	Tln1	-1.3	41	IPI00119689.1	Ap2b1	-1.1	159	IPI00894724.1	Mtap2	-1	43
IPI00323483.3	Pdcd6ip	-1.3	50	IPI00555125.1	Kif5b	-1.1	27	IPI00308446.2	Ahcyl2	-1	16
IPI00406624.2	Mgea5	-1.3	41	IPI00329843.4	Ankfy1	-1.1	40	IPI00127172.3	Ddx1	-1	42
IPI00132993.1	Pak1	-1.3	64	IPI00154004.1	LOC100046081	-1.1	86	IPI00849505.1	LOC100043998	-1	138
IPI00127707.1	Pcbp2	-1.3	14								
IPI00131692.7	Rabep1	-1.3	62	IPI00222306.5	Ppp2r1b	-1.1	68	IPI00379625.2	Nova2	-1	15
IPI00323881.1	Kpnb1	-1.3	100	IPI00109420.2	Kif5a	-1.1	120	IPI00228113.5	Mthfd1l	-1	32

Accession	Gene symbol	Log2 Ratio	Peptide number
IPI00453849.3	Rnmt	-1	10
IPI00553419.3	Dsp	1	40
IPI00229598.4	Cnp	1	19
IPI00129519.3	Basp1	1	94
IPI00130280.1	Atp5a1	1	124
IPI00468481.2	Atp5b	1	132
IPI00330523.1	Pcca	1	109
IPI00308976.1	Me3	1	249
IPI00223216.5	Tst	1	78
IPI00272401.4	Acyp2	1	114
IPI00126172.1	4931406C07Rik	1	17
IPI00317309.5	Anxa5	1	139
IPI00336881.1	Ddah2	1	31
IPI00114710.2	Pcx	1	637
IPI00127450.1	Man2c1	1	82
IPI00110351.1	2310007H09Rik	1	16
IPI00459279.2	Qdpr	1	138
IPI00459326.1	Uncharacterized	1	23
IPI00626662.3	Aldh1a1	1.1	11
IPI00118011.6	Manba	1.1	27
IPI00121440.4	Etfb	1.1	63
IPI00109169.1	Idh3g	1.1	93
IPI00116753.4	Etfa	1.1	187
IPI00230351.1	Sdha	1.1	121
IPI00329927.4	Nfasc	1.1	127
IPI00380195.1	1700012G19Rik	1.1	69
IPI00109109.1	Sod2	1.1	360
IPI00108980.2	Cpne4	1.1	14
IPI00123744.1	Cst3	1.1	128
IPI00130344.3	Clic1	1.1	20
IPI00170307.1	Apoa1bp	1.1	156
IPI00228253.2	Acat2	1.1	80
IPI00131830.1	Serpina3k	1.1	56
IPI00469548.2	Syn2	1.2	10
IPI00132653.1	Oxct1	1.2	354
IPI00122971.1	Ncam1	1.2	80
IPI00315452.5	Pnp1	1.2	25
IPI00120030.1	Crym	1.2	423
IPI00315302.5	Ndufa2	1.2	18
IPI00123014.1	Padi2	1.2	69
IPI00310035.3	Fah	1.2	33
IPI00133557.1	Tppp3	1.2	61
IPI00139788.2	Trf	1.2	219
IPI00223060.1	Pck2	1.3	96
IPI00653664.2	Enoph1	1.3	26
IPI00137736.1	Rps28	1.3	19
IPI00127267.4	Gldc	1.3	26
IPI00331094.3	Aspa	1.3	11
IPI00471246.2	Ivd	1.5	58
IPI00670735.1	LOC677317	1.5	24
IPI00117042.3	Gfap	1.6	75
IPI00121038.2	Vcan	1.6	50
IPI00115240.1	Mbp	1.7	12
IPI00312058.5	Cat	1.7	22
IPI00121534.11	Car2	1.7	267
IPI00229475.1	Jup	1.9	39
IPI00133034.3	Hint2	1.9	47
IPI00112719.1	Alad	1.9	55
IPI00138274.1	Cryab	2	10
IPI00130640.5	Hrsp12	2.2	242
IPI00127560.1	Ttr	2.5	54
IPI00131695.3	Alb	3.2	412
IPI00222228.5	4732456N10Rik	3.5	33
IPI00762198.2	Hbb-b1	5.3	233
IPI00330039.3	Srgap3	8.1	14

Supplementary table 2. Proteins expressed differentially between HAB/LAB hippocampal microsome (indirect comparison)

Accession	Gene symbol	Log2 Ratio	Peptide number
IPI00116222.1	Hibadh	-5.1	41
IPI00135915.1	Glb1	-5	10

155

IPI00466610.5	Map2k1	-2.7	60	IPI00420562.5	Cand1	-1.3	288	IPI00225533.1	Necap1	-1	34
IPI00464166.2	Ptpn23	-2.4	24	IPI00377609.2	Vcpip1	-1.2	21	IPI00626501.3	Kif1a	-1	42
IPI00116331.1	Sgta	-2.3	27	IPI00222496.3	Pdia6	-1.2	38	IPI00117929.1	Oxr1	-1	173
IPI00378557.3	Pfdn4	-2.2	12	IPI00115097.1	Copb2	-1.2	26	IPI00114667.1	Psmd7	-1	73
IPI00114894.1	Myh11	-2.1	95	IPI00122069.1	Prkcc	-1.2	153	IPI00270877.5	Usp14	-1	17
IPI00421179.1	Eif4g1	-2	41	IPI00132993.1	Pak1	-1.2	12	IPI00320831.3	Nbea	-1	78
IPI00331299.9	Ncdn	-1.9	267	IPI00377592.7	Sec31a	-1.2	77	IPI00133428.3	Psmc1	-1	30
IPI00453615.3	Huwe1	-1.8	18	IPI00117063.1	Fus	-1.2	17	IPI00115546.4	Gnao1	1	319
IPI00119762.4	Dclk1	-1.7	36	IPI00112001.1	Cap2	-1.2	50	IPI00109727.1	Thy1	1	141
IPI00453996.1	Myh14	-1.7	23	IPI00462934.2	Khsrp	-1.2	68	IPI00230277.3	Mapk3	1	12
IPI00336281.1	Golga3	-1.7	22	IPI00119876.1	Dync1h1	-1.2	1527	IPI00154054.1	Acat1	1	246
IPI00123181.3	Myh9	-1.7	320	IPI00312128.3	Trim28	-1.2	52	IPI00331745.2	Lxn	1	36
IPI00282957.4	Mtap7d1	-1.7	16	IPI00461469.3	Mars	-1.1	42	IPI00117312.1	Got2	1	719
IPI00115663.2	Dctn1	-1.7	141	IPI00115833.2	Mtap6	-1.1	157	IPI00126635.1	Idh3b	1	124
IPI00123624.8	2610301G19Rik	-1.7	85	IPI00108147.1	Rock1	-1.1	17	IPI00468653.3	Pccb	1	53
				IPI00319320.4	Nckap1	-1.1	114	IPI00110827.1	Acta1	1	814
IPI00752390.4	Sbf1	-1.6	87	IPI00120076.2	Ckmt2	-1.1	79	IPI00110850.1	Actb	1	1062
IPI00453613.3	Huwe1	-1.6	99	IPI00139795.2	Rplp2	-1.1	66	IPI00226430.2	Acaa2	1	38
IPI00172221.2	Dnm1l	-1.6	176	IPI00458854.2	Sart3	-1.1	32	IPI00380195.1	1700012G19Rik	1	48
IPI00788324.1	Myh9	-1.5	19	IPI00321646.3	AI314180	-1.1	105				
IPI00118120.1	Myo5a	-1.5	242	IPI00896700.1	Mtap1b	-1.1	40	IPI00115679.1	Ganab	1	159
IPI00338604.5	Myh10	-1.5	573	IPI00124223.3	Psme1	-1	23	IPI00269481.7	Capzb	1	164
IPI00118676.3	Eif4a1	-1.4	41	IPI00127176.3	6720456B07Rik	-1	10	IPI00116120.3	Pdcd5	1	24
IPI00467383.2	Cul3	-1.4	38					IPI00128857.1	Me1	1	94
IPI00321734.7	Glo1	-1.4	146	IPI00114801.2	Inpp1	-1	17	IPI00126940.1	Adk	1	19
IPI00407835.2	Ubap2l	-1.4	43	IPI00123465.1	Cops7a	-1	52	IPI00317309.5	Anxa5	1	106
IPI00128296.1	Ckmt1	-1.4	307	IPI00553419.3	Dsp	-1	28	IPI00471246.2	Ivd	1	37
IPI00321922.2	Pacs1	-1.3	17	IPI00312752.3	Sh3gl1	-1	21	IPI00555059.2	Prdx6	1	130
IPI00407425.2	Myo18a	-1.3	73	IPI00122826.1	Cend1	-1	12	IPI00135977.3	Clic4	1	10
IPI00137331.6	Cap1	-1.3	210	IPI00471372.2	Wasf1	-1	50	IPI00119035.1	Acan	1	49
IPI00403682.2	Mapre2	-1.3	15	IPI00330476.3	Cyfip1	-1	156	IPI00116134.1	Dpp3	1	98

Accession	Gene symbol	Log2 Ratio	Peptide number
IPI00139788.2	Trf	1	123
IPI00153400.2	H2afj	1.1	31
IPI00222228.5	4732456N10Rik	1.1	27
IPI00128973.1	Gap43	1.1	21
IPI00323592.2	Mdh2	1.1	1244
IPI00116192.1	Prdx3	1.1	182
IPI00308976.1	Me3	1.1	181
IPI00116074.1	Aco2	1.1	1609
IPI00132653.1	Oxct1	1.1	205
IPI00461964.3	Aldh6a1	1.1	56
IPI00330480.1	EG432987	1.2	169
IPI00113052.1	Tsfm	1.2	17
IPI00114241.2	Nefh	1.2	38
IPI00109169.1	Idh3g	1.2	95
IPI00116753.4	Etfa	1.2	140
IPI00330523.1	Pcca	1.2	111
IPI00121013.1	Pea15a	1.2	51
IPI00124692.1	Taldo1	1.2	69
IPI00127450.1	Man2c1	1.2	53
IPI00340165.5	21 kDa protein	1.2	16
IPI00230013.3	Cacna2d1	1.2	74
IPI00459279.2	Qdpr	1.2	90
IPI00130391.1	Tcrb-V20	1.3	208
IPI00229475.1	Jup	1.3	38
IPI00120045.1	EG628438	1.3	114
IPI00109109.1	Sod2	1.3	206
IPI00122971.1	Ncam1	1.3	313
IPI00122265.1	Sh3bgrl	1.3	41
IPI00170307.1	Apoa1bp	1.3	96
IPI00115620.1	Psat1	1.3	69
IPI00222515.5	Psmd11	1.3	61
IPI00759847.1	Ndrg2	1.4	15
IPI00169622.3	Phyhip	1.4	108
IPI00118825.2	Csl	1.4	10
IPI00121566.1	Gmpr	1.4	35
IPI00118011.6	Manba	1.5	13
IPI00229718.10	Gltp	1.5	15
IPI00121105.2	Hadh	1.5	29
IPI00120030.1	Crym	1.6	319
IPI00123014.1	Padi2	1.6	38
IPI00121534.11	Car2	1.6	215
IPI00222149.4	Chl1	1.7	75
IPI00123379.1	Hdlbp	2	35
IPI00114710.2	Pcx	2	459
IPI00112719.1	Alad	2.1	48
IPI00131830.1	Serpina3k	2.1	37
IPI00130640.5	Hrsp12	2.3	92
IPI00138274.1	Cryab	2.3	19
IPI00762198.2	Hbb-b1	4.2	123
IPI00454053.7	2010300C02Rik	5.1	12
IPI00118757.1	Phpt1	6.3	43
IPI00877236.1	Apoa1	-6.2	190
IPI00831484.1	382044	-4.4	76
IPI00177214.1	Igh-6	-4.3	63
IPI00116548.1	Reg3b	-3.8	12
IPI00855108.2	Hbb-b1	-3.5	75
IPI00113806.1	Reg3g	-3	85
IPI00118130.1	Orm1	-2.3	441
IPI00118455.1	Saa1	-2.1	87
IPI00309214.1	Apcs	-2	668
IPI00453488.1	Antxr2	-2	30
IPI00128484.1	Hpx	-1.8	5713
IPI00663742.3	Dnahc10	-1.8	40
IPI00122312.2	Fgg	-1.6	1416
IPI00279079.1	Fgb	-1.4	1439
IPI00115522.3	Fga	-1.4	1253
IPI00124725.2	Itih3	-1.4	1093
IPI00462363.1	BC026782	-1.4	71
IPI00468477.4	25 kDa protein	-1.4	26
IPI00129250.1	Lrg1	-1.3	183
IPI00222228.5	4732456N10Rik	-1.3	15
IPI00119299.1	Lifr	-1.2	247
IPI00314141.5	Serpina3n	-1.2	228
IPI00130010.4	Cfh	-1.1	2741
IPI00121055.1	EG214403	-1.1	116
IPI00378649.1	LOC63510	-1.1	38

Supplementary table 3. Proteins expressed differentially between HAB/LAB plasma (indirect comparison)

	1		
IPI00107952.2	Lyz2	-1.1	11
IPI00137599.2	Sepp1	-1	172
IPI00459201.1	Igh	-1	51
IPI00133751.1	Mfap4	-1	31
IPI00114099.2	Apoc3	1	317
IPI00109996.1	H2-Q2	1	62
IPI00468281.5	Rsad2	1.1	20
IPI00850317.1	LOC100044179	1.2	60
IPI00323571.1	Apoe	1.3	668
IPI00127560.1	Ttr	1.4	689
IPI00122429.1	Rbp4	1.4	463
IPI00111315.1	Apoa2	1.4	185
IPI00317356.10	Pon1	1.4	137
IPI00118994.1	Apoc4	1.4	54
IPI00119676.1	Apoc1	1.5	77
IPI00869381.1	Apoa2	1.6	190
IPI00666034.3	Apob	1.7	2182
IPI00138892.2	OTTMUSG00000004411	1.7	14
IPI00828873.1	Hbb	3.7	44
IPI00117910.3	Prdx2	5.7	36
IPI00621417.1	Hbb-b1	5.8	362
IPI00762198.2	Hbb-b1	6.4	556
IPI00230320.6	Car1	8.9	13

Supplementary table 4. Proteins expressed differentially between ^{14}N-HAB/^{15}N-HAB

Hippocampal cytosol (Isotope effect)

Accession	Gene symbol	Log2 Ratio	Peptide number
IPI00378172.2	Armc9	-7.3	13
IPI00338604.5	Myh10	-1.4	184
IPI00123181.3	Myh9	-1.3	112
IPI00229834.3	Copa	-1.1	10
IPI00114894.1	Myh11	-1.1	54
IPI00115363.2	Nhej1	-1	11
IPI00134344.6	Spnb3	-1	192
IPI00115827.1	Gbas	1	19
IPI00127560.1	Ttr	1	30
IPI00323800.6	Nefm	1	67
IPI00453777.2	Atp5d	1.1	11
IPI00221769.5	Ak3	1.1	12
IPI00129755.2	Serpina1b	1.1	18
IPI00131830.1	Serpina3k	1.1	145
IPI00121038.2	Vcan	1.2	17
IPI00153400.2	H2afj	1.2	17
IPI00122349.1	Dpysl3	1.2	204
IPI00122549.1	Vdac1	1.3	16
IPI00229598.4	Cnp	1.3	81
IPI00624192.3	Dpysl5	1.3	158
IPI00407425.2	Myo18a	1.7	17
IPI00117857.2	Serpina1c	1.7	47
IPI00224067.2	Hdgfrp3	1.9	10
IPI00221825.1	Clic6	1.9	21
IPI00403938.2	Tnc	1.9	68
IPI00621417.1	Hbb-b1	2	43
IPI00831055.2	Beta-globin	2.1	18

IPI00762198.2	Hbb-b1	2.4	116
IPI00128441.3	Hnrnpr	2.9	28
IPI00553419.3	Dsp	4.1	77
IPI00329998.3	11 kDa protein	4.7	10
IPI00222228.5	4732456N10Rik	5	17
IPI00117042.3	Gfap	5.5	78
IPI00118011.6	Manba	6	24
IPI00131674.3	2210010C04Rik	6	32
IPI00468203.3	Anxa2	6.3	20
IPI00229475.1	Jup	6.3	29
IPI00130391.1	Tcrb-V20	6.7	104
IPI00330480.1	EG432987	6.8	68

Supplementary table 5. Proteins expressed differentially between ^{14}N-HAB/^{15}N-HAB plasma (Isotope effect)

Accession	Gene symbol	Log2 Ratio	Peptide number
IPI00457439.1	Ssna1	-6.9	12
IPI00115553.2	BC005624	-2.1	23
IPI00411007.1	Man1c1	-2	50
IPI00230760.5	Mb	-1.9	18
IPI00112331.1	Gli1	-1.8	12
IPI00116105.1	Serpina6	-1.3	219
IPI00623506.3	Ank3	-1.2	15
IPI00118413.2	Thbs1	-1.2	37
IPI00881564.1	Serpina6	-1	22
IPI00222188.4	Col1a2	-1	34

Accession	Gene symbol	Log2 Ratio	Peptide number
IPI00119676.1	Apoc1	1	15
IPI00135547.1	Saa4	1.1	77
IPI00123924.1	Serpina1d	1.1	123
IPI00556721.1	Igfals	1.2	111
IPI00119299.1	Lifr	1.3	74
IPI00117857.2	Serpina1c	1.3	748
IPI00138892.2	OTTMUSG00000004411	1.5	11
IPI00648416.1	C8a	1.5	18
IPI00122122.1	C8g	1.5	54
IPI00118437.1	C8g	1.5	177
IPI00407657.2	C8a	1.5	303
IPI00121274.2	C8b	1.5	327
IPI00314270.3	C6	1.6	50
IPI00123223.2	Mug1	1.7	6074
IPI00890309.1	2610016E04Rik	1.9	22
IPI00621417.1	Hbb-b1	1.9	65
IPI00121190.1	Egfr	1.9	310
IPI00831055.2	Beta-globin	2	32
IPI00115241.1	Mup4	2.1	13
IPI00117910.3	Prdx2	2.1	22
IPI00762198.2	Hbb-b1	2.2	149
IPI00230718.3	C9	2.3	205
IPI00113996.7	Blvrb	2.4	20
IPI00120832.1	Mup3	2.5	67
IPI00330913.1	OTTMUSG00000000231	2.6	29
IPI00378649.1	LOC635101	2.7	17
IPI00230320.6	Car1	3.2	11
IPI00719897.1	Try10	3.6	13
IPI00115243.1	Mup5	4.1	22
IPI00131674.3	2210010C04Rik	5.1	39
IPI00132542.1	Mup2	5.1	125
IPI00468281.5	Rsad2	5.5	13
IPI00117042.3	Gfap	5.6	49
IPI00135701.3	Slco1a5	5.8	25
IPI00466399.1	Mup2	5.9	72
IPI00263313.1	Drg1	6.1	11
IPI00124590.3	Casp8ap2	6.4	19
IPI00118161.1	Usp26	6.8	15
IPI00458776.3	Irak1bp1	7.2	13
IPI00330480.1	EG432987	7.2	69
IPI00130391.1	Tcrb-V20	7.2	135

Supplementary table 6. Proteins expressed differentially between HAB/NAB hippocampal cotysol (Indirect comparison)

Accession	Gene symbol	Log2 Ratio	Peptide number
IPI00621417.1	Hbb-b1	-8.7	102
IPI00221825.1	Clic6	-5.4	23
IPI00474783.4	Acaca	-4.8	23
IPI00123379.1	Hdlbp	-4	30
IPI00135151.1	9030624J02Rik	-3.9	12
IPI00224067.2	Hdgfrp3	-2.9	13
IPI00221769.5	Ak3	-2.2	22
IPI00407425.2	Myo18a	-2.1	31
IPI00128071.7	Uso1	-2.1	13
IPI00115663.2	Dctn1	-2	61
IPI00228693.4	2310035C23Rik	-2	25
IPI00459177.6	Mtap7d2	-2	12
IPI00115824.1	Nipsnap1	-1.9	31
IPI00114241.2	Nefh	-1.9	28
IPI00119202.1	S100a11	-1.9	10
IPI00128319.1	Centg3	-1.9	10
IPI00125135.1	Ube2d2	-1.8	34
IPI00336281.1	Golga3	-1.8	30
IPI00420426.1	Ap3b2	-1.8	19
IPI00407835.2	Ubap2l	-1.7	26
IPI00115833.2	Mtap6	-1.6	197
IPI00120076.2	Ckmt2	-1.6	44
IPI00262349.2	Cpne7	-1.6	33
IPI00229483.3	Sec24c	-1.6	33
IPI00123709.1	Akap12	-1.5	61
IPI00469103.1	Kars	-1.5	47
IPI00222759.3	AI427515	-1.5	42
IPI00226872.1	Efhd2	-1.5	25
IPI00808550.1	B230112C05Rik	-1.5	25
IPI00129526.1	Hsp90b1	-1.4	510
IPI00762198.2	Hbb-b1	-1.4	249

IPI00320831.3	Nbea	-1.4	84	IPI00136054.1	Lsm2	-1.1	32	IPI00153144.3	Suox	1	11
IPI00128076.1	Serpina3c	-1.4	36	IPI00379625.2	Nova2	-1.1	31	IPI00656325.2	Nsf	1.1	488
IPI00785480.2	Inpp4a	-1.4	25	IPI00132539.3	Btf3l4	-1.1	28	IPI00115546.4	Gnao1	1.1	58
IPI00138089.4	Lrrc47	-1.4	13	IPI00308324.2	Rdx	-1.1	26	IPI00118011.6	Manba	1.1	36
IPI00229598.4	Cnp	-1.3	94	IPI00111876.2	Abhd14b	-1.1	11	IPI00132722.8	Anxa3	1.1	28
IPI00323800.6	Nefm	-1.3	90	IPI00308446.2	Ahcyl2	-1.1	11	IPI00229703.6	Vamp2	1.1	21
IPI00343557.1	Mapre3	-1.3	58	IPI00229080.7	Hsp90ab1	-1	996	IPI00352984.4	Xdh	1.1	16
IPI00468516.3	D6Wsu116e	-1.3	22	IPI00108150.1	Rock2	-1	147	IPI00308333.3	Ccdc128	1.1	15
				IPI00108388.1	Usp9x	-1	127	IPI00223060.1	Pck2	1.2	130
IPI00377609.2	Vcpip1	-1.3	19	IPI00111218.1	Aldh2	-1	108	IPI00129519.3	Basp1	1.2	103
IPI00465809.2	Kif3b	-1.3	12	IPI00453803.5	Ube2o	-1	84	IPI00221456.1	Sv2b	1.2	42
IPI00330862.5	Ezr	-1.2	114	IPI00127172.3	Ddx1	-1	75	IPI00132276.1	Vamp3	1.2	36
IPI00118120.1	Myo5a	-1.2	111	IPI00132080.1	Pgls	-1	64	IPI00281761.3	Prrt2	1.2	15
IPI00132762.1	Trap1	-1.2	102	IPI00119762.4	Dclk1	-1	43	IPI00116072.7	Ak5	1.2	15
IPI00331444.7	Ipo7	-1.2	93	IPI00128867.3	Purb	-1	38	IPI00121218.5	Fahd2a	1.3	77
IPI00381019.1	Smarcc2	-1.2	36	IPI00224151.5	Ap1g1	-1	34	IPI00316495.3	Rab3c	1.3	53
IPI00128341.1	Wasf3	-1.2	21	IPI00271905.2	Rabggta	-1	28	IPI00624175.1	Acp6	1.3	24
IPI00130555.1	Rasal1	-1.2	20	IPI00153400.2	H2afj	-1	27	IPI00227168.1	Nlgn3	1.3	20
IPI00312076.4	Kif3a	-1.2	15	IPI00116850.3	D10Wsu52e	-1	21	IPI00312058.5	Cat	1.5	78
IPI00458894.3	Tnfaip8	-1.2	14					IPI00670735.1	LOC677317	1.5	33
IPI00551348.1	Rapgef6	-1.2	13	IPI00464296.5	Epb4.1l3	-1	18				
IPI00420562.5	Cand1	-1.1	350	IPI00131873.1	Cops6	-1	13	IPI00470962.1	Camk2b	1.5	23
IPI00128296.1	Ckmt1	-1.1	246	IPI00130439.1	Camk1	-1	10	IPI00132506.3	Chac2	1.5	21
IPI00223253.1	Hnrnpk	-1.1	228	IPI00129451.1	Cpne6	1	461	IPI00762636.2	Acsf3	1.5	16
IPI00849505.1	LOC100043998	-1.1	114	IPI00136372.3	Syn1	1	332	IPI00133690.2	Tsta3	1.5	11
				IPI00134492.4	Syn2	1	272	IPI00162780.3	Gnb2	1.5	10
IPI00312128.3	Trim28	-1.1	92	IPI00117042.3	Gfap	1	105	IPI00230096.1	Camk2a	1.6	51
IPI00626501.3	Kif1a	-1.1	47	IPI00222833.1	Lsamp	1	27	IPI00113149.1	Stx1b	1.6	23
IPI00314153.4	Yars	-1.1	40	IPI00132087.1	Fdx1l	1	23	IPI00876208.1	Me3	1.6	15
IPI00399840.2	Ube3a	-1.1	35	IPI00337980.5	Rab21	1	20	IPI00318595.1	Erap1	1.6	12
IPI00331568.7	Hgs	-1.1	34	IPI00138406.1	Rap1a	1	17	IPI00283531.8	Gstp2	1.7	420

Accession	Gene symbol	Log2 Ratio	Peptide number
IPI00127558.3	Acox1	1.7	18
IPI00555023.2	Gstp1	1.8	148
IPI00120716.3	Gnb1	1.8	46
IPI00222228.5	4732456N10Rik	2	27
IPI00230408.2	Mapt	2.1	19
IPI00122069.1	Prkcc	2.2	258
IPI00109727.1	Thy1	2.4	42
IPI00117083.1	Grpel1	2.5	11
IPI00553419.3	Dsp	2.9	97
IPI00420725.4	Camk2a	2.9	32
IPI00831055.2	Beta-globin	3.4	24
IPI00648312.3	Nt5dc3	6.1	115

Supplementary table 7. Proteins expressed differentially between HAB/NAB plasma (Indirect comparison)

Accession	Gene symbol	Log2 Ratio	Peptide number
IPI00177214.1	Igh-6	-7.9	13
IPI00466399.1	Mup2	-6	239
IPI00480401.3	OTTMUSG00000007428	-6	23
IPI00890309.1	2610016E04Rik	-5.1	55
IPI00132542.1	Mup2	-4.9	261
IPI00115243.1	Mup5	-4.4	56
IPI00120832.1	Mup3	-3	136
IPI00378649.1	LOC635101	-2.9	28
IPI00330913.1	OTTMUSG00000000231	-2.3	32
IPI00381881.7	C7	-2.2	149
IPI00123411.1	Serpina3g	-2.1	59
IPI00402967.3	F13a1	-2	70
IPI00121190.1	Egfr	-1.7	565
IPI00119299.1	Lifr	-1.7	152
IPI00458159.1	Igh-VJ558	-1.7	56
IPI00459201.1	Igh	-1.7	39
IPI00648416.1	C8a	-1.6	45
IPI00131830.1	Serpina3k	-1.3	5633
IPI00121274.2	C8b	-1.3	432
IPI00553546.4	EG381806	-1.3	24
IPI00407657.2	C8a	-1.2	465
IPI00118437.1	C8g	-1.2	366
IPI00230718.3	C9	-1.2	331
IPI00137599.2	Sepp1	-1.2	143
IPI00272690.2	Ace	-1.2	98
IPI00123927.1	Serpina1e	-1.2	24
IPI00122272.1	Ecm1	-1.2	22
IPI00123223.2	Mug1	-1.1	13081
IPI00128076.1	Serpina3c	-1.1	1646
IPI00556721.1	Igfals	-1.1	198
IPI00115658.2	Igf1	-1.1	44
IPI00320239.1	Clec3b	-1.1	27
IPI00230320.6	Car1	-1.1	16
IPI00377351.2	Apoa4	-1	1160
IPI00113879.1	Il1rap	-1	58
IPI00222419.5	ENSMUSG00000058927	-1	16
IPI00109324.3	Retnla	-1	10
IPI00310049.3	Cpb2	1	69
IPI00762198.2	Hbb-b1	1.2	528
IPI00468477.4	25 kDa protein	1.2	26
IPI00119818.1	Itih4	1.3	1215
IPI00124725.2	Itih3	1.3	844
IPI00336324.11	Mdh1	1.3	13
IPI00312711.3	Itih4	1.4	98
IPI00850317.1	LOC100044179	1.4	26
IPI00666034.3	Apob	1.5	3348
IPI00323571.1	Apoe	1.7	671
IPI00663742.3	Dnahc10	1.9	26
IPI00309214.1	Apcs	2	447
IPI00230760.5	Mb	3.1	55
IPI00138860.3	Golga4	5.3	17
IPI00831055.2	Beta-globin	5.5	66
IPI00755694.1	LOC100045680	6.4	73

8 Abbreviations

1-DE	one-dimensional gel electrophoresis
2-DE	two-dimensional gel electrophoresis
5-HT	5-Hydroxytryptamine
AA	amino acid
ACTH	adrenocorticotrophic hormone
AD	Alzheimer's disease
AQUA	absolute quantification of proteins
CA2	carbonic anhydrase 2
CBG	corticosteroid-binding globulin
CRF	corticotropin-releasing factor
CRH	corticotropin-releasing hormone
DSM	diagnostic and statistical manual
DST	dexamethasone suppression test
ECS	electroconvulsive seizures
EGF	epidermal growth factor
EI	electron ionization
ELISA	enzyme-linked immunosorbent assay
EPM	elevated plus maze
ERK	extracellular signal-regulated kinase
ESI	electrospray ionization
FDR	false discovery rate
FSR	fractional synthesis rate
FST	forced swim test
FT-IR	fourier transform infrared spectroscopy
GABA	gamma amino butyric acid
GC-MS	gas chromatography-mass spectrometry
GDP	guanosine diphosphate
Glo1	glyoxalase-I
GO	gene ontology
GTP	guanosine-5'-triphosphate
HAB	high anxiety-related behavior
HCCA	4-hydroxy-α-cyano-cinnamic acid
HPA	hypothalamic-pituitary-adrenal
HPLC	high-performance liquid chromatography
ICAT	isotope-coded affinity tag
ICPL	isotope coded protein label
IEF	isoelectric focusing
IPG	immobilized pH gradient
iTRAQ	isotope tags for relative and absolute quantification
KEGG	Kyoto encyclopedia of genes and genomes
LAB	low anxiety-related behavior
LC	liquid chromatography
LC-MS	liquid chromatography-mass spectrometry

LTP	long-term synaptic potentiation
m/z	mass-to-charge
MALDI	matrix-assisted laser desorption ionization
MAO	monoamine oxidase
MAPK	mitogen-activated protein (MAP) kinases
MEK	mitogen-activated protein kinase kinase
MIDA	mass isotopomer distribution analysis
MRM	multiple reaction monitoring
MS	mass spectrometry
MSTFA	*N*-methyl-*N*-trimethylsilyltrifluoroacetamide
MUP	major urinary protein
Myh10	myosin, heavy polypeptide 10
NAB	normal anxiety-related behavior
Nefh	neurofilament heavy polypeptide
NIH	national institute of health
NMR	nuclear magnetic resonance
OCD	obsessive-compulsive disorder
PCA	principle component analysis
PD	Parkinson's disease
PLTP	phospholipid transfer protein
PMF	peptide mass fingerprinting
PND	postnatal day
PQD	pulsed q dissociation
PTM	post-translational modifications
PVDF	polyvinylidene fluoride
RIA	relative isotope abundance
RIA	radio immunoassay
RTK	receptor tyrosine kinases
SDS-PAGE	sodium dodecyl sulfate polyacrylamide gel electrophoresis
SILAC	Stable isotope labeling with amino acids in cell culture
SILAM	stable isotope labeling of amino acids in mammals
SILIP	stable isotope labeling *in planta*
SRM	selected reaction monitoring
SSRI	serotonin–selective reuptake inhibitor
TCA cycle	tricarboxylic acid cycle
TMT	tandem mass tags
TOF	time-of-flight
TST	tail suspension test
TTR	transthyretin
UPLC	ultra performance liquid chromatography
USV	ultrasonic vocalization test
WHO	world health organization

9 Acknowledgements

This dissertation would not have been possible without support and encouragement from many people near and far.

First, I would like to gratefully and sincerely thank Prof. Dr. Christoph W. Turck for giving me the opportunity to pursue my Ph.D. study in his team. Thanks to Chris for his supervision, understanding, patience, help, and most importantly, friendship during my stay with his group. I appreciate the freedom he always has given me in my academic research and his constructive suggestions. His faith in science and energetic attitude have influenced me greatly and will continue to do so in the future.

I also would like to thank Prof. Dr. Rainer Landgraf for being my doctoral supervisor. His excellent achievements in establishing the anxiety animal model are the foundation of this thesis. He always has been helpful, and I received a lot of generous encouragement and support from him in the years I spent working on this project.

Next, I would like to take the opportunity to thank all my colleagues and friends working in Chris Turck's research group. Thanks to Michaela Filiou for being such a wonderful co-worker on this project and for sharing so much joy and pain. Particular thanks to our bioinformatists, Stefan Reckow and Philipp Gormanns, whose intelligent algorithms made this thesis possible. I am thankful to Dr. Giuseppina Maccarrone and Christian Webhofer for their expertise in mass spectrometry, and I am also grateful to Dr. Jeeva Varadarajulu, Maria Lebar, Christiane Rewerts, and Larysa Teplytska for the pleasant way they managed the laboratory.

It gives me great pleasure to thank the people in Prof. Landgraf's group, especially Elisabeth Frank, Boris Hambsch, Melanie Keßler, Ludwig Czibere, and Markus Nußbaumer, who provided so much generous help on this project.

Finally, and most importantly, I owe my deepest gratitude to my beloved parents, twin brother Yaoguang in China, and girlfriend Bing Shan, who accompanied me to Munich. Without their love, concern, support, and strength, I would not have been able to complete this thesis.

10 Curriculum Vitae

Name: Yaoyang Zhang

Gender: Male

Nationality: Chinese

Date of Birth: 13-10-1981

Place of Birth: Henan, China

Education

2006 - 2010	Ph.D. student Department of Biology Ⅱ **Ludwig-Maximilians-Universität München**, Germany
2004 – 2006	M. Sc. (Molecular Biology & Biochemistry) School of Life Science and Technology **Beijing Institute of Technology**, China
2000 – 2004	B. Eng. (Bioengineering) School of Life Science and Technology **Beijing Institute of Technology**, China

Professional employment

2006 - 2010	Ph.D. student and postdoc scientist **Max Planck Institute of Psychiatry**, Germany Proteomics and Biomarkers (AG TURCK)

Publications

1. **Zhang, Y.**, Webhofer, C., Reckow, S., Filiou, M.D., Maccarrone, G., and Turck, C.W. (2009). A MS data search method for improved ^{15}N-labeled protein identification. Proteomics 9, 4265-4270.

2. Frank, E., Kessler, M.S., Filiou, M.D., **Zhang, Y.**, Maccarrone, G., Reckow, S., Bunck, M., Heumann, H., Turck, C.W., Landgraf, R., et al. (2009). Stable isotope metabolic labeling with a novel N-enriched bacteria diet for improved proteomic analyses of mouse models for psychopathologies. PLoS ONE 4, e7821.

3. Haegler, K., Mueller, N.S., Maccarrone, G., Hunyadi-Gulyas, E., Webhofer, C., Filiou, M.D., **Zhang, Y.**, and Turck, C.W. (2009). QuantiSpec--Quantitative mass spectrometry data analysis of

(15)N-metabolically labeled proteins. J Proteomics 71, 601-608.

4.   **Zhang, Y.**, Reckow, S., Webhofer, C., Boehme, M., Gormanns, P., Egge-Jacobsen, W.M., and Turck, C.W. Proteome scale turnover analysis in live animals using stable isotope metabolic labeling. (Submitted)

5   **Zhang, Y.**, Filiou, M.D., Reckow, S., Landgraf, R., and Turck, C.W. Proteomic and metabolomic brain and plasma profiling of a trait anxiety mouse model. (In preparation)

6.   Filiou, M.D., **Zhang, Y.**, Teplytska, L., Reckow, S., Gormanns, P., Maccarrone, G., Yassouridis, A., Bunck, M., Frank, E., Hambsch, B., et al. Biomarker pathway discovery in a trait anxiety mouse model: evidence for mitochondrial implication. (Submitted)

Academic presentations

1.   **Zhang, Y.**, Filiou, M.D., Bisle, B., Maccarrone, G., Landgraf, R., and Turck, C.W. (August 12-18, 2007). Biomarker discovery for trait anxiety using a ^{15}N metabolic labeling strategy. In 1st EU Summer School in Proteomic Basics (Brixen/Bressanone, Italy).

2.   Frank, E., Kessler, M., Filiou, M.D., **Zhang, Y.**, Haegler, K., Maccarrone, G., Hambsch, B., Landgraf, R., and Turck, C.W. (October 11-13, 2007). [15]N metabolic labeling of hyperanxious mice. In 6th World Congress on Stress (NH Danube City, Vienna, Austria).

3.   **Zhang, Y.**, Filiou, M.D., Bisle, B., Maccarrone, G., Landgraf, R., and Turck, C.W. (July 13-19, 2008). Biomarker discovery in a mouse model of trait anxiety using ^{15}N metabolic labeling. In 2nd EU Summer School in Proteomic Basics (Brixen/Bressanone, Italy).

4.   **Zhang, Y.**, Filiou, M.D., Bisle, B., Frank, E., Kessler, M., Haegler, K., Maccarrone, G., Landgraf, R., and Turck, C.W. (August 16-20, 2008). Biomarker discovery in brain and plasma of a mouse model of trait anxiety. In 7th HUPO Annual World Congress (Amsterdam, Netherlands).

5.   Filiou, M.D., **Zhang, Y.**, Bisle, B., Frank, E., Kessler, M., Haegler, K., Maccarrone, G., Hambsch, B., Landgraf, R., and Turck, C.W. (August 16-20, 2008). Biomarker discovery in a mouse model of trait anxiety. In 7th HUPO Annual World Congress (Amsterdam, Netherlands).

6.   **Zhang, Y.**, Webhofer, C., Reckow, S., Filiou, M.D., Maccarrone, G., and Turck, C.W. (March 29 - April 2, 2009). A database search method for improved ^{15}N-labeled protein identification. In Proteomic Forum (Berlin, Germany).

7.   **Zhang, Y.**, Filiou, M.D., Webhofer, C., Maccarrone, G., Reckow, S., and Turck, C.W. (August 30-September 4, 2009). Proteomic analysis of a stable isotope effect in a trait anxiety mouse model. In 18th International mass spectrometry conference (Bremen, Germany).

8.   Filiou, M.D., **Zhang, Y.**, Bisle, B., Frank, E., Kessler, M.S., Hambsch, B., Reckow, S., Haegler, K., Maccarrone, G., Landgraf, R., et al. (May 31 - June 4, 2009). Biomarker Discovery by Stable Isotope Labeling of Mouse Model. In 57th ASMS Conference on Mass Spectrometry and Allied Topics (Philadelphia, United States).

9   **Zhang, Y.**, Reckow, S., Filiou, M.D., Webhofer, C., Boehme, M., Gormanns, P., Maccarrone, G., Egge-Jacobsen, W.M., and Turck, C.W. (May 23-27, 2010). Expanding the biomarker discovery pipeline from protein expression to turnover. In 58th ASMS Conference on Mass Spectrometry and Allied Topics (Salt Lake City, Utah. United States). (Oral presentation)